A Quantitative Analysis of Chemotherapy-Induced Reactive Oxidative Species using Genetically Encoded Sensors and Generators

Beijing Kara Huang

B.S., California Institute of Technology, 2009

Submitted to the Department of Biological Engineering
in partial fulfillment of the requirements for the degree of

Doctor of Philosophy

at the

Massachusetts Institute of Technology

June, 2015 [September 2015]

Signature of Author: Signature redacted
Department of Biological Engineering
June 19th, 2015

Certified by: Signature redacted
Hadley D. Sikes
Assistant Professor of Chemical Engineering
Thesis Supervisor

Accepted by: Signature redacted
Forest M. White
Professor of Biological Engineering
Chairman, Committee for Graduate Students

This thesis has been examined by:

Professor Hadley D. Sikes
Thesis Supervisor
Assistant Professor of Chemical Engineering
Massachusetts Institute of Technology

Professor Bevin P. Engelward
Committee member and co-advisor
Professor of Biological Engineering
Deputy Director MIT Center for Environmental Health Sciences
Massachusetts Institute of Technology

Professor Gerald N. Wogan
Committee chair
Professor of Biological Engineering
Massachusetts Institute of Technology

A Quantitative Analysis of Chemotherapy-Induced Reactive Oxidative Species using Genetically Encoded Sensors and Generators

Beijing Kara Huang

Submitted to the Department of Biological Engineering on June 19, 2015

in partial fulfillment of the requirements of the degree of

Doctor of Philosophy in Biological Engineering

Abstract

Recent advances in chemotherapeutic development have targeted vital mechanisms that ensure survival of cancer cells; these include the ability to evade immune surveillance, undergo metabolic adaptations and form a defense mechanism against oxidative stress. Cancer cells often possess higher endogenous levels of reactive oxidative species (ROS) compared to normal cells due to the cumulative effects from genomic instability, inflammation and oncogene activation, and they become increasingly reliant on the cell antioxidant network to prevent this elevated oxidative stress from becoming toxic. Thus, chemotherapeutics that inhibit the antioxidant network and thereby elevating ROS are thought to be promising candidates that can selectively eliminate tumor cells. Despite the promises of these molecules, chemotherapeutics modulating ROS levels have mostly fallen short of their projected impact. We believe that a thorough understanding of the quantity, location and duration of ROS generation needed to cause tumor cell toxicity, will be important for understanding the mechanism of current successful chemotherapeutics and designing future ROS-based drug candidates. In this thesis, we explored the use of genetically encoded sensors and generators of ROS, H_2O_2 in particular, to answer these important redox biology questions.

We began by developing a deeper understanding of how to use these protein-based peroxide sensors in a quantitative manner. We created a technique quantifying intracellular peroxide levels by converting the fluorescence signal outputs from these sensors into more meaningful intracellular concentrations. This was accomplished via a combination of kinetic modeling, biochemical measurements and image analysis techniques. We also explored the cell to cell heterogeneity in sensor response to H_2O_2 stimulation, and found that the intracellular expression level of the sensor is correlated with the ratio-metric response of the probe. Further kinetic

modeling analysis showed that the slow recycling step of activated sensor was responsible for the correlation.

In the second part of the thesis, we used these sensors in combination with enzymatic generators that can produce H_2O_2 endogenously in a kinetically controlled manner. These tools allowed us to quantitatively determine that there are two toxicity thresholds, a total accumulation of H_2O_2, and intracellular concentration, that are needed for H_2O_2 -mediated cell death. We also applied these tools to investigate the mechanism of two ROS-based chemotherapeutics, phenethyl isocyanate (PEITC) and piperlongumine. We found that depletion of the glutathione antioxidant by these drugs was unimportant to the toxicity mechanism, and the amount of oxidative stress generated by these compounds was not enough to induce significant toxicity by itself.

The final part of the thesis involves technology development for a next generation enzymatic ROS generator. We explored the use of P450-BM3, an enzyme that can generate superoxide and hydrogen peroxide through a reaction that requires only NADPH and oxygen. While this reaction in the wild type protein is slow, it can be engineered to have much higher catalytic rates. We demonstrated through various protein engineering approaches that we could create P450-BM3 proteins with enhanced generation of H_2O_2. We also were able to express correctly folded, active enzymes inside mammalian cells that utilize intracellular NADPH and oxygen to produce H_2O_2.

Thesis supervisor: Hadley D. Sikes, Assistant Professor of Chemical Engineering

Acknowledgements

This PhD would not be possible without the love and support of my advisors, co-workers, friends and family. From the bottom of my heart, I truly thank each and every one of you.

To my advisor Hadley Sikes, thank you for taking a chance on me and accepting me into your lab. Learning from you have been a privilege and a pleasure, and you constantly push me to be a better, more independent scientist. Not only have you taught me how to think critically about the scientific problems, but you have also encouraged me to examine the bigger picture. You gave me the freedom to explore and answer the questions I'm interested in, and my explorations gave me the confidence I need to trust my scientific instincts. I appreciate your kindness and understanding towards your students, and I especially appreciate your constant optimism even when the projects are frustrating, I think it balances out my constant pessimism well. I hope I can be just as understanding and encouraging for anyone I mentor in the future.

To my committee members Bevin Engelward and Gerald Wogan, thank you for the care you've shown in your mentorship. I am lucky to have committee members who are so invested in my research and my career. Your insights are invaluable to the success of my projects.

To members of the Sikes Lab, it has been a pleasure working with such a talented group of graduate students and postdocs. I've been able to watch as this group grew from 4 members to the 9 members it is today. I especially want to acknowledge the original members of the ROS subgroup: Sohail Ali and Joseph Lim. It is not always easy being the first students on the project, but I believe we have come a long way in our understanding of the tools we are working with and the biology we are studying, and I couldn't have done it without your help. Thanks for commiserating with me when things aren't working, which is a lot of times. I'm extremely excited for future developments on this project, led by Troy Langford and Kassi Stein. There is so much left to be explored, and I believe the field is in good hands. Other lab members have also made my time here so enjoyable and entertaining. Kaja Kaastrup has become one of my closest friends, both in and out of the institute. It is nice to have someone who understands exactly what you are going through and provide the appropriate outrage and humor to accompany it all. I will miss our long talks in the office and I'm sure we will continue our Gchat conversations even after we leave MIT. Shefali Lathwal provided the much needed whimsy and listening ear as I navigated my projects and panicked about my future. I still owe her a tea date.

To my friends in the BE department, Boston and scattered around the country, thank you for being a constant source of support and encouragement. This journey hasn't been exactly smooth sailing, and I probably would've left with a master if you guys haven't convinced me to keep going for my PhD. Edgar Sanchez, Shannon Hughes, Caroline Chopko and Miles Miller gave me invaluable advice and comforted me through many crying sessions while I was switching labs. Josephine Shaw, Jing Ge, as well as the rest of my BE class, provided long dinners to new restaurants/bars and drunken parties to keep me sane and entertained throughout the years. I

would also like to thank Duc-Huy Nguyen, Jonathan and Stephanie Gilbert, Matthew Glassman and Shengchang Tang. I will miss our dinner parties and I promise I will stop yelling at all of you during Settlers of Catan. To my best friends from afar, Joy Sheng and Max G'Sell, thank you for checking in on me and worrying about me throughout graduate school, as well as flying across the country multiple times to visit the east coast. I promise I will not spend all my time in lab from now on ☺

To my parents, Baoquan Huang and Ping Zhu and my brother David Huang, there are no words to describe the depth of gratitude I feel for your support and everything you've done for me. I know what a sacrifice and hard work it was to provide me with the opportunities here in the states. I am extremely blessed to have parents that value their children's education above all else. Thank you for instilling in me discipline and perseverance, those traits were used frequently throughout my PhD. In addition, thank you for paying for my expensive Caltech undergraduate degree; I truly believe that it opened so many doors for me and I won't be here today if it hadn't been for the advantages it has given me. Finally, thank you for giving me a home-cooked meal and a comfortable bed whenever I needed it. Michigan will always be my home.

Last but not least, to my husband, Mitchell Wang, this thesis is dedicated to you. Being with you is the absolute highlight of my graduate school. Thank you for being my rock, my partner-in-crime, and obsessive co-owners of two adorable pet turtles. Thank you for believing in my abilities even when I don't believe in myself. You've made life here in Boston a joy for so many years. The best part of finishing my PhD is being able to come home to you again, and I can't wait for our next adventures to begin.

Table of Contents

List of Figures

List of Tables

Chapter 1: Introduction

Reactive oxidative species (ROS) is a family of molecules implicated in many functions important to cell survival and pathological problems related to aging, tumorigenesis and inflammatory diseases. Despite the apparent importance of these molecules, therapy involving the manipulation of ROS levels has fallen short of its promise. A thorough understanding ROS as discrete chemical entities with specific kinetic reaction rates will be important for the design of more effective ROS-based drugs in the future. To do so, we will need sensors that enable better quantification of specific molecules and ROS generators that investigate the biological role of these molecules in a controlled, systematic way. In this chapter, we will first provide background on where various ROS species are generated, what are their reaction targets, and the signaling and downstream phenotypic effects that have been studied. We will also discuss the success of previous ROS-based therapies for cancer. Finally, we will give an overview on the existing technologies for sensing and generating various ROS species for a more quantitative analysis of redox biology.

1.1 Reactive Oxidative Species: What are they and where do they come from?

Although molecular oxygen is a di-radical and rather unreactive, its univalent reduction leads to formation of more reactive species. Reactive oxidative species (ROS) are a family of chemical molecules that are formed during incomplete reduction of oxygen.[1,2] These molecules can include the initial species generated during the reduction, hydrogen peroxide (H_2O_2) and superoxide anion ($O_2^{\cdot-}$), along with their secondary reactive products such as hydroxyl radical ($HO^{\cdot}$) and hypochlorous acid (HOCl).[1] Biological systems are continually exposed to both

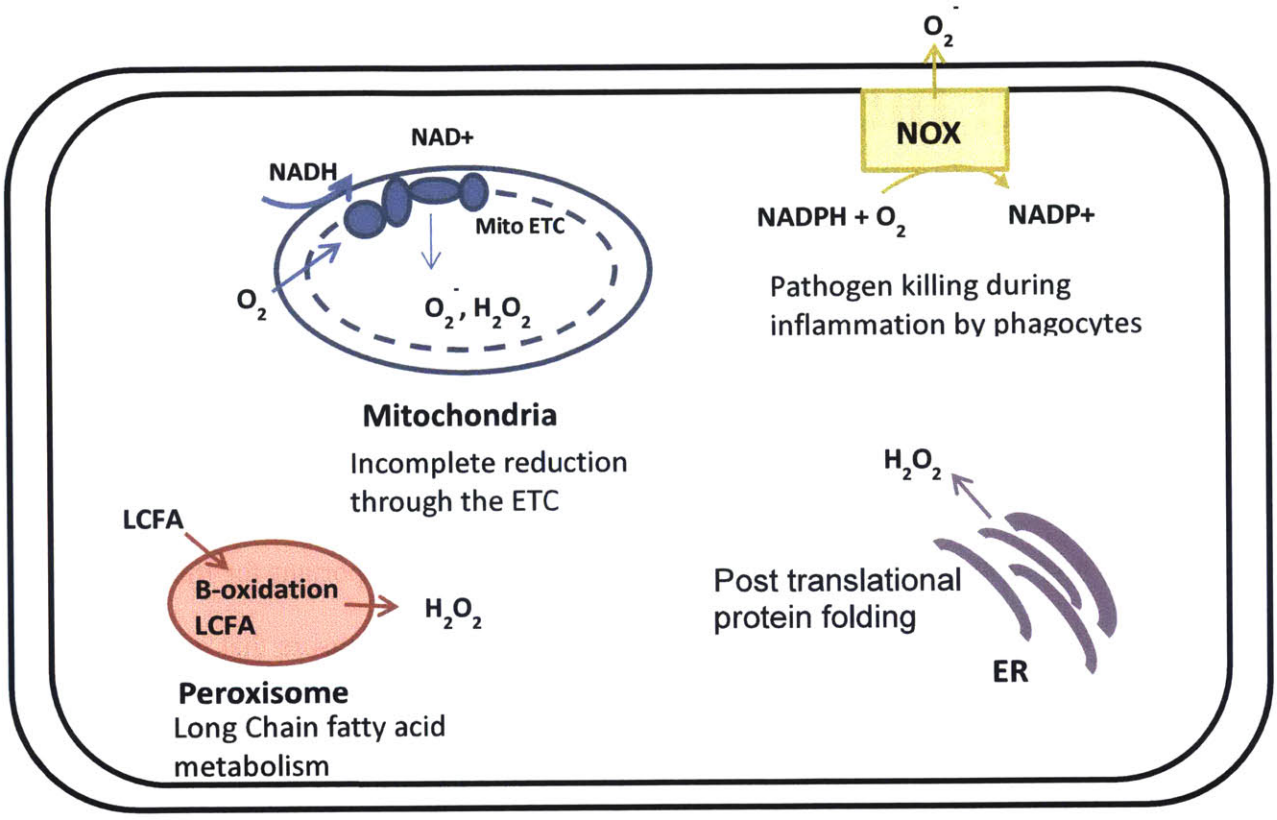

Figure 1.1: Sources of ROS generation inside the cell. ROS is generated through the electron transport chain, the NADPH oxidase enzymes, the ER and the peroxisome

extrinsic and intrinsic oxidative stress, and consideration needs to be given as to where a particular metabolite is generated, since microenvironment can dictate the targets these ROS molecules will potentially encounter.[3]

1.1.1 Mitochondria and respiration

The mitochondria houses the electron transport chain (ETC), which transfers electrons from NADH and succinate along a controlled redox path that ultimately results in a four-electron reduction of oxygen to water during aerobic respiration.[4] However, this reduction process is imperfect, and 1% of the time the oxygen exits from the reduction relay early to form H_2O_2 and superoxide, notably from complex I and III .[5] It is unclear whether the generation is by accident or for a purpose. The leakage, and especially the presence of H_2O_2, has been implicated in age-related decline in mitochondrial function, since it was found that mice overexpressing catalase in

the mitochondria live longer.[6] However, more recent studies suggest that ETC-generated H_2O_2 can be important for dopamine regulation and for activation of stress proteins for growth signaling.[7]

1.1.2 NADPH Oxidases (NOX) proteins

NADPH oxidases (NOX) are transmembrane proteins localized to various cellular membranes.[8] Family members of this protein transport electrons across biological membranes to reduce oxygen to superoxide, thus they are exclusive generators of ROS.[8] NOX2, the first member to be discovered, is implicated during inflammation mediated by phagocytes such as neutrophils and macrophages.[8,9] These cells express large amounts of NOX2 on the plasma surface and that generate copious amounts of superoxide upon activation and assembly of its co-factor subunits. The superoxide can be converted to H_2O_2 and reacts with myeloperoxidase to form oxidants such as HOCl, an effective killer of microbial pathogens.[10] The large amount of ROS released by these inflammatory cells can also affect the physiology of nearby cells, leading to environments conducive to tumorigenesis.[11] Other members of the family, NOX1 through NOX5, are found in various tissues such as the heart and lung endothelium, contributing to very different physiological roles.[8] NOX4, found exclusively in the endoplasmic reticulum, is constitutively active and only generates H_2O_2, not superoxide.[12] The role of these NOX proteins outside of inflammation is still an active area of research, since their activities and expression levels are often altered during other pathological phenomena, such as NOX4's role as a regulator of cardiovascular distress and NOX1's role as a promoter of neural growth.[13,14]

1.1.3 Post translational modifications and protein folding

Secreted proteins often undergo disulfide bond formation as a post-translational modification as they fold in the ER lumen.[15] These reactions are initiated by glycoprotein Ero1, which causes oxidation of thioredoxin protein disulfide isomerase (PDI), forming a disulfide bond.[15] This oxidation process requires a two-electron reduction of oxygen to H_2O_2, thus creating a flux of H_2O_2 every time PDI undergoes disulfide formation. The oxidized PDI then transfers its disulfide bond to the secreted protein via thiol-disulfide exchange.[3]

1.1.4 Other sources of generation

While ROS arising from the mitochondria, NOX proteins and the ER are thought to be the major producers, generation in other cellular compartments and by other enzymes is starting to be recognized as potentially important in recent years. The peroxisome is an organelle that carries out key metabolic functions in the cell including β-oxidation of fatty acids, a process which releases H_2O_2.[16] The ROS resulting from the peroxisome have been implicated in regulating mTORC1 signaling and causing autophagy in cells.[17] Other enzymes such as cytochrome P450, a superfamily of monooxygenases involved in heme-dependent oxidation of various metabolic intermediates, is thought to generate superoxide and hydrogen peroxide to regulate diurnal variation during corticosteroid production.[18]

1.2 Kinetic network and chemical targets of ROS

Since ROS encompasses a family of molecules and not a discrete chemical entity, different species can mediate a diverse array of modifications on biomolecules from proteins to lipids to nucleic acids. To achieve a better mechanistic understanding of redox biology, we would need to identify specific oxidants involved in a biological process and know what they react with as well

as the reaction rates. While some reactions are theoretically possible, the slow rate of reaction will render them physiologically irrelevant. To compare the reaction kinetics, we will have to consider both the second-order rate constant of the reaction and the amount of reactant target present. We also need to examine the reaction rates of intra-conversion between different ROS species compared to the rates of reaction of these reactive species with protein, lipids or DNA.

1.2.1 Intra-conversion between different ROS species

While superoxide and hydrogen peroxide are the two primary products resulting from the oxygen reduction process, they can react with enzymes to form other, more reactive ROS species and even reactive nitrogen species (RNS). Figure 1.2 shows the intra-conversion between different members of ROS and how RNS can arise from the presence of ROS. In particular, superoxide

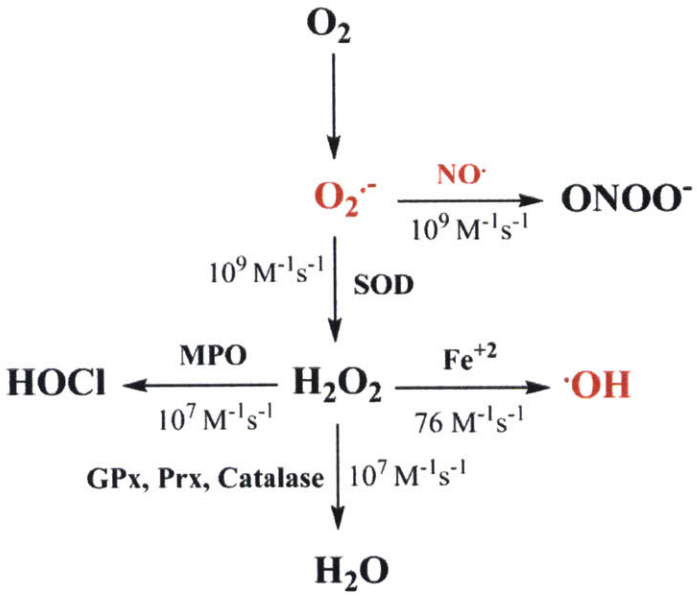

Figure 1.2. Intraconversion between different ROS species. While superoxide and hydrogen peroxide are the primary species of oxygen reduction, many secondary species can be generated from their reaction with peroxidases, dismutases and other radicals.

dismutase (SOD) is an enzyme found in different isoforms throughout cellular compartments that acts as a detox for the oxygen anion radical, reacting with $O_2^{\cdot -}$ with rate constants of $10^9\ M^{-1}s^{-1}$

(close to the diffusion limit) and converting it to H_2O_2.[19] Superoxide can also react with nitric oxide ($NO^{\cdot}$) to form peroxynitrite with similar second order rate constant to SOD.[20] Peroxynitrite ($ONOO^-$) is a powerful oxidant of the RNS family that can directly oxidize proteins and DNA via direct reaction or indirect radical-mediated mechanisms.[21] Hydrogen peroxide can participate in the fenton reaction with Fe^{+2} to yield the short-lived, highly reactive hydroxyl radical ($OH^{\cdot}$) with rate constant 76 $M^{-1}s^{-1}$. [22] It can also react with peroxidases with high reactivity, on the order of 10^7-10^8 $M^{-1}s^{-1}$.[1,23] Seleno and thiol peroxidases such as glutathione peroxidase (GPx) and peroxiredoxin (Prx) scavenge H_2O_2 by converting it into water. Heme-peroxidase myeloperoxidase (MPO) reacts with H_2O_2 to form the more reactive HOCl.[24] If we have information on the concentrations of reaction partners of superoxide and hydrogen peroxide, we can predict the dominant radical species for reaction with protein, lipids and DNA based on their lifetime.

One-electron		Two-electron	
Radical	**Reduction potential (V)**	**Oxidant**	**Rate constant with GSH ($M^{-1}s^{-1}$)**
$OH^{\cdot}$	2.31 [25]	HOCl	3×10^7 [26]
$O_2^{\cdot -}$	0.94 [25]	$ONOO^-$	700 [27]
		H_2O_2	0.9 [28]

Table 1.1 Reactivity of various ROS species, categorized by reduction potential and reaction rate with thiols.

The ROS/RNS species highlighted above can be divided into one-electron (radical) and two-electron (non-radical) oxidants, red and black in Fig 1.2, respectively. The oxidation strength (reactivity) of the one-electron radicals can be ranked based on the reduction potential, since the activation energy (kinetics) for radical reactions is low. The reactivity of two-electron (non-radical) oxidants is trickier, since the kinetics of the reaction is more important than the reduction potential, given the high activation energy barrier. Table 1.1 shows the relative reactivity of one-electron oxidants, based on the reduction potential, and the relative reactivity of two-electron oxidants, based their reaction rate constants with thiol protein glutathione (GSH). While

superoxide and hydrogen peroxide have lower reactivity compared to other oxidants in their class, they can rapidly convert into the more reactive species via the network described previously.

1.2.2 Major reaction targets of H_2O_2

Cysteines. Oxidation of the thiol side chains of cysteine through a two-electron oxidation mediated by H_2O_2 is the most commonly recognized and studied H_2O_2 modification of proteins. Due to the electrophilic nature of hydrogen peroxide, nucleophilic attack by deprotonated thiols releases H_2O to form a sulfenic acid, which can then go on to form internal or mixed-disulfides with GSH.[29] H_2O_2 is selectively reactive to cysteine residues depending on the protein environment. For example, the second order rate reaction of H_2O_2 with PTP1B is 20 $M^{-1}s^{-1}$ while the rate constant of H_2O_2 with antioxidant Prx-2 is 1.3 x 10^7 $M^{-1}s^{-1}$.[3] The reactivity of the cysteine residue is dictated by their solvent-exposed localization and ionization state, since thiolated anions ($-S^-$) are more nucleophilic than their protonated counterpart. Thus, the pKa of the residue relative to the intracellular pH is important for the second order rate constant.[28,30,31] The oxidized cysteine groups can be reduced in two different ways: internal disulfides can be reduced by thioredoxin (Trx), while mix-disulfides formed with GSH can be reduced by glutaredoxin (Grx).[32] Table 1.2 shows the reaction of H_2O_2 with various intracellular chemical targets in the cytoplasm, reported as a rate constant consist of second order rate constant x concentration of the analyte. The majority of H_2O_2 in the cytoplasm is scavenged by the thiol peroxidases peroxiredoxin I or II, due to their high activity and high abundance inside the cell. Many studies have shown that peroxiredoxin is important in H_2O_2-mediated signaling. Since actual signaling targets such as PTP1B or PTEN react with H_2O_2 very slowly, it is thought that a redox relay occurs where H_2O_2-oxidized Prx can transfer the oxidation to the desired signaling

molecule.[1,33] This phenomenon is shown during the oxidation of STAT3 by Prx-2, and the requirement of Prx-1 oxidation for the activation of p38 mitogen-activated protein kinase (MAPK).[34,35]

Selenols. A selenoprotein is any protein that includes a selenocysteine (Se-Cys) amino acid residue. They are structurally similar to that of cysteine, but with an atom of selenium in place of sulfur. Glutathione peroxidase (GPx) is a family of antioxidants with a reactive selenol, reacting with H_2O_2 with second order reaction rate of 10^7 $M^{-1}s^{-1}$ in the cytoplasm.[36] H_2O_2 causes oxidation of the selenocysteine to SeOH, which then forms a mix-disulfide with a glutathione molecule.[37] The mix-disulfide is transferred when another glutathione molecule comes in to reduce the enzyme. While GPx has the same second order reaction as Prx 1 or 2, it is present in much lower abundance in the cytoplasm (1:100 compared to Prx 1 and 2).[38] Thus, its reaction with H_2O_2 is secondary to that of Prx and only takes prominence when Prx is irreversibly over-oxidized or inactivated via phosphorylation.[39,40]

Iron-catalyzed reactions. In addition to cysteine thiols, various other amino acids can be oxidized by H_2O_2, although most of these oxidations are catalyzed by redox-cycling metal ions such as Fe^{+2} or Fe^{+3}.[41] An example of this is the conversion of histidine to 2-oxo-histidine, which has a second order rate constant of 10^2 $M^{-1}s^{-1}$.[33] H_2O_2 can also undergo Fe^{+2}-mediated decomposition known as fenton reaction, generating the highly reactive hydroxyl radical. However, the fastest iron-catalyzed reaction is the conversion of H_2O_2 to H_2O by catalase, with a second order rate constant of 2×10^7 $M^{-1}s^{-1}$.[36] While the complete mechanism of catalase is not entirely known, it is believed that the iron center of the heme group attached to the enzyme interacts with hydrogen peroxide, causing the oxidation of Fe^{+3} to Fe^{+4}.[42] Since catalase is

sequestered in the peroxisome, its apparent reaction rate in the cytoplasm is low.[37,43] However, H_2O_2 generated in the peroxisome will react predominately with catalase.

H_2O_2 Target Candidates	**Reaction rate s^{-1} (second order rate constant x concentration of analyte in cytoplasm)**
Prx-1 or 2	1300 [38]
GPx	10 [38]
Catalase	3 [38]
GSH	0.0045 [28]
Cdc25B	0.000016 [44]
PTP1B	0.000002 [45]

Table 1.2 Pseudo first order reaction rates with H_2O_2 with various intracellular targets including peroxidases and cellular signaling targets in the cytoplasm

As the most-studied ROS, the reaction partners of H_2O_2 are of intense interest. A summary of common targets of H_2O_2 is shown in Figure 1.3.

1.2.3 Major reaction targets of other ROS species

Superoxide. Despite the reduction potential of 0.9V, superoxide directly oxidizes few biological compounds because its anionic charge limits reaction with electron-rich centers. The majority of direct reactions with superoxide yield other, potentially more biologically reactive molecules. Superoxide dismutase reacts to convert superoxide to H_2O_2 with a rate constant close to the limit of diffusion. The detoxifying effect of this enzyme is extremely important, the loss of which causes mitochondrial depolarization and eventual apoptosis.[46,47] Nitric oxide, while having low reactivity by itself, can combine with superoxide to form peroxynitrite ($ONOO^-$), a molecule that can directly oxidize thiol protein groups or lead to secondary carbonate and nitrogen dioxide radicals.[21] These radicals can lead to significant DNA alterations. Due to the anionic charge, superoxide is highly attracted to iron-sulphur clusters, oxidizing the release of iron.[3,33]

HOCl. HOCl is a highly reactive species formed from reaction of H_2O_2 with myeloperoxidase (MPO), a heme-based peroxidase. HOCl is a key component during immune response since it is

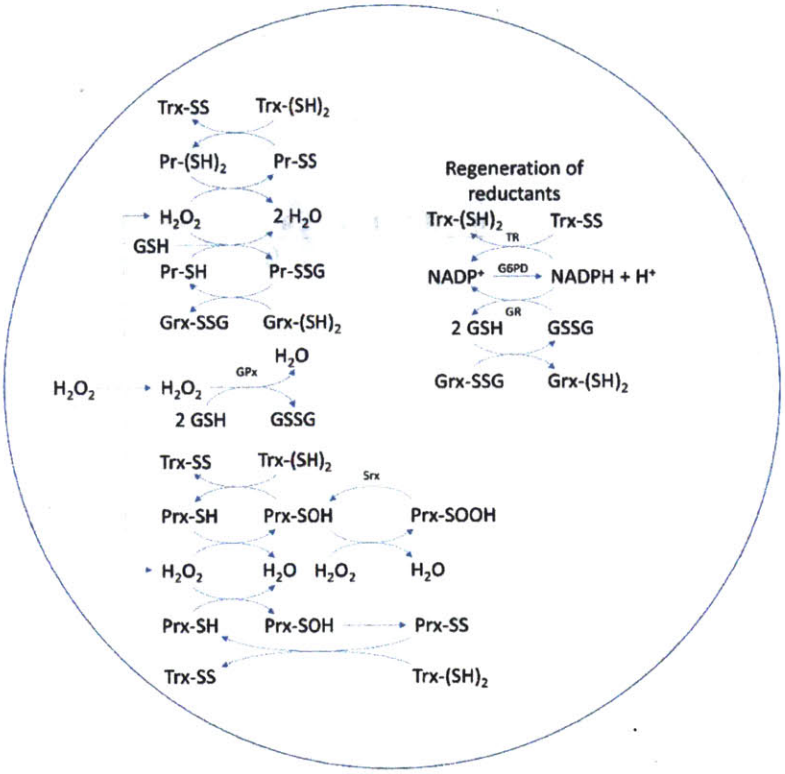

Figure 1.3 Mechanism of H2O2 interaction with peroxidases and protein thiols inside the cell. The mechanism of H2O2 interaction with peroxiredoxin, glutathione peroxidase and protein thiols are depicted, along with the re-generation mechanism of the reducing partners.

extremely toxic to bacteria, but it has been linked to several pathologies as a result of damage to host tissue.[10] HOCl can directly oxidize cysteine residues at a much faster rate than H_2O_2; the reaction rate constant of GSH with HOCl is 3 x 10^7 $M^{-1}s^{-1}$, compared to 0.9 $M^{-1}s^{-1}$ for H_2O_2.[1,3] HOCl can also react with tyrosine residues to form 3-chlorotyrosine, 5-chlorotyrosine and 3,5-chlorotyrosine, implicated in atherosclerosis and cystic fibrosis.[48]

$OH^{\cdot}$. Hydroxyl radical generated from H_2O_2 fenton reaction is extremely toxic and unstable. With a half-life of one nanosecond, hydroxyl radicals indiscriminately attack targets with rate constants typically in the 10^9 $M^{-1}s^{-1}$ range, making it difficult for any antioxidant to detoxify the molecule.[1] While most other ROS species cause modifications on proteins, oxidation of lipids and DNA is predominately due to $OH^{\cdot}$. Hydroxyl radical removes an electron from unsaturated

lipids, causing a free radical chain reaction mechanism that results in lipid peroxide (R-OOH).[49] It can also attack the deoxyribose DNA bases via addition to the electron-rich pi bonds. These pi bonds, located between C5-C6 of pyrimidines and N7-C8 of purines, can be converted to baseless sites subject to beta-elimination.[50]

1.2.4 Localization and kinetic targets

We would be remiss not to consider the effects of localization in a discussion of relevant kinetic targets of ROS. The second order rate constant is only one component of the overall kinetic rate, with the other important consideration being the concentration of the reactants. Less reactive substrates can become oxidized in the presence of more potent scavengers by considering site localization. This theory, known as the flood-gate model, proposes that low fluxes of ROS are quickly scavenged by the highest antioxidants, such as peroxiredoxin. However, higher fluxes of ROS can overwhelm the local peroxiredoxin by causing it over-oxidize and enable other less reactive proteins immediately outside the "scavenging zone" to be oxidized.[1,3,18,40,51,52] Another localization technique is to sequester the ROS and the target in the same cell compartment, as in the case of catalase and H_2O_2 in the peroxisome, or superoxide in the mitochondria, since it has low membrane permeability.[53] Manipulating the local concentration of the reactants is an alternative way for ROS molecules such as H_2O_2 to confer selectivity. For example, Nox proteins that influence receptor tyrosine kinase signaling via H_2O_2 are often colocalized with their phosphatase and kinase targets at the plasma membrane.[54] We should also consider that given the instability and short half-lives of certain ROS like hydroxyl radical, these species will only get the chance to react with what is in the immediate vicinity of their site of generation, so different ROS species can have very different localized effects.

1.3 Cell signaling and down-stream phenotypic effects related to H_2O_2 elevation

The previous section explored the different ROS and RNS that can arise from the primary species superoxide and hydrogen peroxide. Furthermore, we demonstrated that this family of molecules can have very different reaction targets due their chemistry and depending on their localization. While superoxide mostly participates in SOD-mediated dismutation to hydrogen peroxide or conversion to RNS, H_2O_2 and the secondary species generated from this molecule often participate in meaningful biological modifications leading to an array of cellular responses. Hydrogen peroxide itself has low second order rate constants with many signaling molecules; it overcomes this problem in one of three ways:

1. Conversion to more reactive molecules such as hydroxyl radical and HOCl
2. Using its high reactivity with peroxiredoxin (Prx) and glutathione peroxidase (GPx) to create a redox relay, allowing the oxidized Prx or the GPx to transfer the oxidation to the desired protein
3. Developing a large, highly localized flux of the molecule, temporarily overwhelming the local antioxidants to react with other less reactive proteins

There are many studies out there that connect H_2O_2 elevation to cell signaling leading to proliferation, apoptosis and necrosis. Without the proper tools, we don't know by which of the aforementioned mechanisms H_2O_2 is reacting, only that H_2O_2 and the oxidation of the phosphatases or kinases are correlated. The consensus in the field is that increasing intracellular H_2O_2 concentration cause a shift from pro-growth to pro-death response.[55–57] However, there is no consensus on what those concentrations are.

1.3.1 Role of H_2O_2 in pro-survival pathways and tumor formation

H_2O_2 has been long thought to play a role in neoplastic growth, since a variety of cell lines derived from human cancers demonstrate elevated oxidative stress.[58] Research in the past two decades has demonstrated that at most physiological levels, H_2O_2 serves as a second messenger in signaling, essential in maintaining the survival and homeostasis of the cell by regulating the MAPK and the PI3K pathway.[59–63] It does so by oxidizing tumor suppressors and apoptosis regulatory elements, and by causing genomic instability.[64,65] Molecules such as dual-specific phosphotase 3 (DUSP3), an inhibitor of the ERK molecule, results in sustained MAPK activation.[33,66] It can also inactivate other tyrosine phosphatases such as PTEN and Sph2, promoting the activation of proliferation/survival PI3K pathway.[66] The activation of these mitogenic pathways often leads to production of growth factors such as PDGF and VEGF, which drive the cell towards angiogenesis and cancer progression, while producing more reactive oxygen species.[67] The activation of the PI3K pathway also upregulates Akt, which prevents cells

H_2O_2 can promote proliferation, survival and tumorgenesis

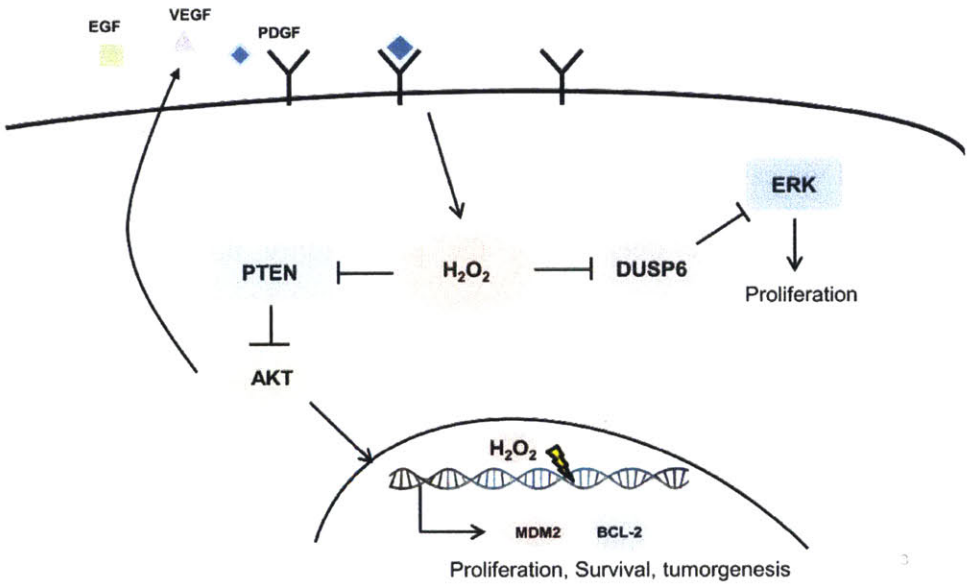

Figure 1.4 Signaling and interaction pathways for H_2O_2 to cause proliferation, survival and tumorigenesis. In particular, the AKT and the MAPK pathways are involved.

from programmable cell death and causes a transition from aerobic respiration to aerobic glycolysis, also known as the Warburg effect, a common phenomenon in advanced cancers.[68] Rather than oxidizing the protein signal molecules, H_2O_2, in its more reactive hydroxyl radical form, can also cause DNA mutation. Accumulation of these mutations leads to progressive genomic instability and tumor formation. The causal link between H_2O_2 and cancer progression is illustrated through experimental manipulation of the NOX proteins. NIH3T3 cells transfected with NOX1 increase the vascularity of tumors and induce angiogenesis when implanted in a mouse model.[59] More recently, specific NOX1 protein inhibitors have been able to block the formation of functional invadopodia in human DLD1, decreasing the metastatic potential of these colon cancer cells.[60]

1.3.2 Role of H_2O_2 in cell toxicity

Apoptosis. During highly elevated or persistent oxidative stress, H_2O_2 shifts from promoting growth to inducing apoptosis or necrotic cell death.[63] Apoptosis is a programmed cell death in which a cell breaks into several apoptotic bodies containing the organelles and releases them to the environment for digestion by the phagosomes, minimizing damage to the surrounding cells.[69] It is usually activated via caspases. There are two caspase-dependent pathways to apoptosis: the intrinsic pathway involves the opening of the permeability transition pore complex in mitochondria and the release of cytochrome c, culminating in caspase-3 cleavage, and the extrinsic pathway involves the Fas ligand and TNFR activating the caspase 8 pathway to induce apoptosis.[57,69,70] H_2O_2 can participate in the intrinsic pathway by inhibiting phosphatases that would interfere with ASK signaling molecule, leading to JNK and p38 activation. The activation of these known pro-death pathways causes the mitochondrial membrane to activate pore-

destabilizing proteins (Bax/Bak). [71] The p38 pathway is also found to be specific to H_2O_2-induced activation, as only oncogenes that increase H_2O_2 production cause the activation of the p38 pathway and caspase mediated cell death.[72] However, apoptosis signaling via H_2O_2 does not necessarily require caspase-3 cleavage. Continuous, low generation of H_2O_2 using extracellular enzymes such as glucose oxidase can lead to translocation of AIF, a key mitochondrial death factor, to the nucleus and subsequent mitochondrial disassembly.[73] H_2O_2-mediated apoptosis also does not have to occur through oxidative manipulation of signaling pathways. Generation of high enough concentrations of H_2O_2 and other ROS in the mitochondria can cause oxidation of membrane lipids in mitochondria, leading to depolarization of membrane potential.[47,74,75] Finally, excessive presence of DNA damage by hydroxyl radicals can alert p53, a tumor suppressor gene that will activate ATM (ataxia telangiectasia mutated), signaling the beginning of programmed cell death.[76]

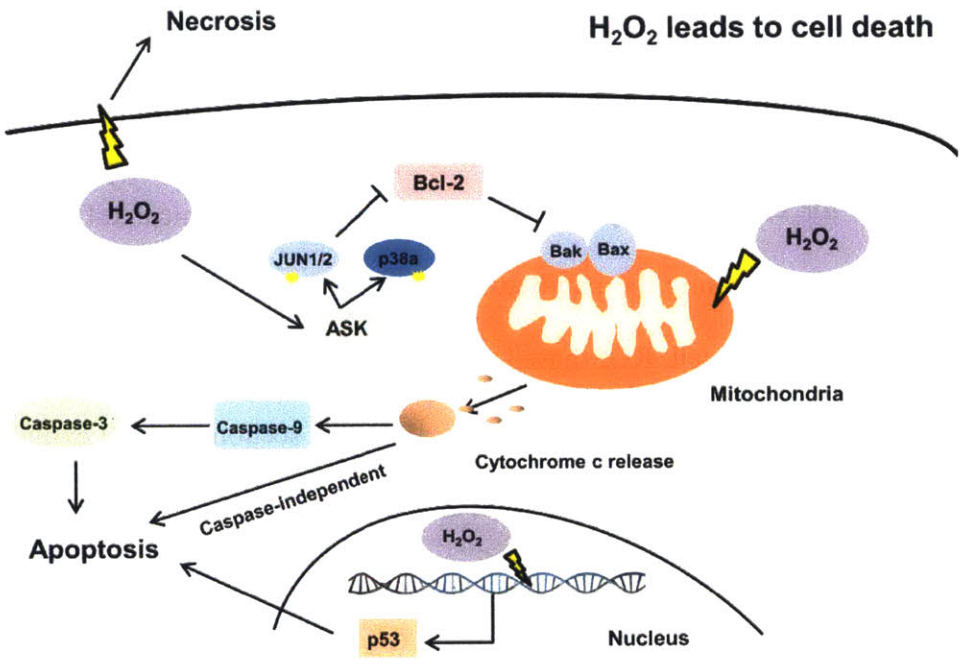

Figure 1.5: Pathways and interaction with H_2O_2 that lead to cellular apoptosis or necrosis. H_2O_2 can induce depolarization of the mitochondria by ASK signaling, lipid modifications through hydroxyl radical, and DNA-damage-triggered p53 activation

Necrosis. Necrotic cell death lacks the pre-programmed and organized disassembling of cellular organelles of apoptosis since the cell membrane ruptures to release the cell's content, unpackaged.[69] Necrosis is an undesired cell death process since the release of cellular content is toxic to surrounding cells and often is accompanied by inflammation. Instead, it is thought of as a backup cell death pathway when the caspases or caspase-dependent pathways cannot be properly activated. High, acute H_2O_2 insults have been shown to cause necrotic cell death.[77] However, little is known about the mechanism by which cells switch from an apoptotic to a necrotic mode of death. It is likely that necrosis occurs when the excessive H_2O_2, some of which converts to hydroxyl radical, causes massive, sudden lipid peroxidation, rupturing the plasma membrane before the cell can activate the appropriate mechanism to form apoptotic bodies.

1.4 ROS-based cancer chemotherapeutics

The use of cancer chemotherapeutics have always been limited by dose toxicity, the concentration above which both normal cells and tumor cells are affected by the drug.[76] Thus, it is an ultimate goal for chemotherapy to be able to exploit biochemical differences between normal and tumor cells, widening the gap between which the drug is harmful to the tumor cell and not harmful to the normal cell. ROS-based cancer chemotherapeutics in particular exploit the redox state differences between tumor and normal cell. In this section, we will explain the theory and give examples of this new class of drugs that are purported to selectively kill cancer cells by causing excessive oxidative stress.

1.4.1 The theory behind ROS-based chemotherapeutics

As mentioned in the previous section, oxidative stress contributes to progression of tumor formation. Both intrinsic and extrinsic oxidative stress cause a wide variety of protein and genomic instability in the cell, and accumulation of these mistakes are a central part of malignancy. Intrinsic factors such as oncogene activation, aberrant metabolism, mitochondrial dysfunction and loss of p53 are known to increase ROS production in cancer cells.[78,79] Expression of genes associated with tumor transformation, such as H-Ras^{v12}, causes a large amount of superoxide to be generated through the NOX protein.[80,81] Besides oncogenic transformation, ROS-induced genetic mutations in the mitochondrial DNA lead to leakage of electrons in the ETC.[82] Finally, at later stages of cancer development, p53 inactivation via accumulated mutations prevent the aberrant cells from regulating genetic instability through p53-mediated DNA repair or apoptosis.[83] In addition to the intrinsic factors, the microenvironment around tumor cells is often conducive to elevation of oxidative stress. Tumors are often found in the same locale as immune cells, since the oxidative burst released from macrophages and neutrophils during pathogen combat can impact nearby, otherwise healthy cells.[84] The microenvironment surrounding tumors are also hypoxic. Hypoxia is known to stimulate the production of mitochondrial ROS, activating hypoxia-inducible transcription factor 1 (HIF-1), a known factor that promotes angiogenesis, survival and glycolysis (Warburg effect).[85]

Measurement of oxidative stress markers, such as oxidized DNA base (8OHdG) and lipid peroxidation, is much more elevated in tumor cells than their normal counterparts.[86–88] To combat the endogenous elevated ROS level, cancer cells have evolved stronger antioxidant systems to keep the stress from becoming overly toxic. Cells adapted to increasing level of oxidative stress show elevation of catalase and glutathione peroxidase activity *in vitro*, and the

same can be observed *in vivo*.[89–91] Tumor cells often activate redox-sensitive transcription factors such as nuclear factor-kB (NF-kB) and NRF-2. These transcription factors are typically bound and inactive in the cytoplasm until oxidation of their binding partner allows them to translocate to the nucleus, leading to increased expression of SOD, catalase, thioredoxin and GSH to combat the elevated stress.[92] Thus, cancer cells have characteristically high antioxidant capacity that regulates ROS to levels that are compatible with cellular biological functions, but still higher than in normal cells. Thus, a strategy to treat tumor cells is to manipulate the ROS level inside the tumor cells.

The first strategy is to scavenge the excess ROS produced by the cancer cells, bringing them back to a normal oxidative state. Several antioxidants, including vitamin E for free radicals and

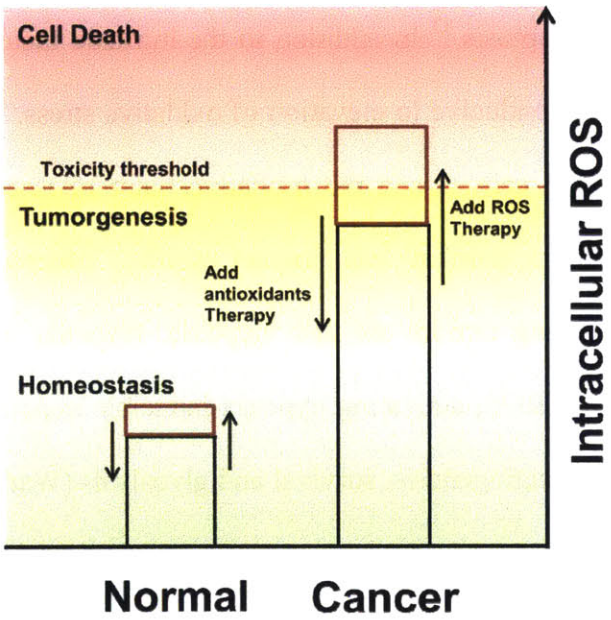

Figure 1.6 Strategies to eliminate tumors through ROS-based therapies. Cancer cells have elevated endogenous ROS compared to normal cells. We can either add antioxidants to bring that level down, or we can add more ROS to selectively push tumor cells over the toxicity threshold.

selenium for glutathione peroxidase, have been used in this context.[93,94] However, the success of these antioxidants is varied. In many cases, the use the vitamin E and selenium actually increased

the progression of cancer.[95,96] This is because the concentration of the ROS matters, as we described in the previous section. If the antioxidant is not successful in bringing the cancer cell completely down to normal physiological levels and instead lingers at concentrations of associated with onset of disease, the antioxidants would actually be helping the cell survive in persistent oxidative stress. Using antioxidant-based therapy would require very careful monitoring of intracellular ROS level.

The second, more clinically successful strategy is to actually increase the ROS level inside the cell (Figure 1.6). As the previous section describes, high levels of oxidative stress can induce cell apoptosis. Since cancer cells have an elevated ROS level compared to normal cells, addition of more ROS can selectively propel these cells over the toxicity threshold, while leaving the normal cells unharmed. These can be drugs that directly cause more production of ROS from various cellular sources, such as arsenic trioxide's inhibition of mitochondrial respiratory chain, or they can be compounds that take advantage of cancer cell's higher dependence of antioxidants by depleting these ROS detoxifiers.[65] The next section details this antioxidant depletion strategy with actual examples of ROS-based chemotherapeutics currently being developed.

1.4.2 Examples of ROS-based chemotherapeutics for tumor elimination

Many of ROS-elevating chemotherapy strategies involve knocking down the antioxidant system that tumor cells rely on for survival. Three main antioxidants have been targeted with current chemotherapy: glutathione, thioredoxin and superoxide dismutase.

GSH metabolism. GSH metabolism appears to be actively involved in protecting cancer cells from apoptosis, as well as in mechanisms of multidrug and radiation resistance. In particular, elevated GSH in tumor cells has been associated with resistance to platinum-containing anti-

cancer compounds such as cisplatin.[97] GSH participates in H_2O_2 elimination as a reducing partner for glutathione peroxidase; it is also used during protein oxidation as a protectant of the –SOH group, targeting it for reduction via glutaredoxin.[29,98,99] Finally, GSH, via its thiol group, can bind to toxic, electrophilic compounds and export them from the cytoplasm.[99]

Glutamate cysteine ligase (GCL) is the rate-limiting enzyme in the synthesis of GSH, thus it is a target for drug therapy. The classical drug used to inhibit GCL activity is buthionine sulphoximine (BSO), the only known inhibitor of de novo GSH synthesis in clinical use.[100] Two other more recent drug candidates employing supposedly the same mechanism include phenethyl isothiocyanate (PEITC)[74,81,101], which has shown promise in preclinical mouse models of ovarian cancer[102], and piperlongumine, which suppresses tumor growth in mouse xenografts of bladder, breast and lung, possibly due to its interaction with GSTP-1.[103,104] Incubation of tumor cells with these drugs is linked to substantial decrease in total GSH level, and increase in ROS measured by DCFH fluorescence dye.[105] The ROS increase is selectively more magnified in tumor cells than normal cells, causing tumor cells to undergo apoptosis while leaving the normal cells unharmed.

Thioredoxin metabolism. Similar to GSH, thioredoxin is central to one of the major redox systems in animal cells. Thioredoxin is important for catalyzing the reduction of protein di-sulfide bonds, making it an integral part of the H_2O_2 scavenging mechanism via peroxiredoxin 1 and 2.[106,107] Auranofin is a gold compound that is clinically used as an antirheumatic agent and functions as a specific thioredoxin inhibitor.[108,109] Ovarian cancer cells treated with Auranofin undergo cytochrome-c mediated cell death.[109] Furthermore, co-treatment of Auranofin and BSO, which knocks down both GSH and thioredoxin, is extremely effective against head and neck squamous cell carcinomas.[108]

Superoxide dismutase. Since mitochondrial dysregulation is a common pathology associated with cancer cells, production of superoxide is an integral part of tumorigenesis. An unbiased small molecule screen identified superoxide dismutase 1, or SOD1, as a target for inhibitors of growth in many lung adenocarcinoma cells *in vitro*.[110,111] A copper chelating agent, ATN-224, has been shown to specifically inhibit SOD1 by binding and removing copper from the active site of the enzyme. This SOD-1 inhibition has led to steady state increases in ROS level via DCFH, and also increased mitochondrial membrane depolarization, leading to release of cytochrome c and apoptosis.[46,111,112] In particular, ATN-224 has been demonstrated *in vitro* to be effective for non-small-cell lung cancer (NSCLCs), a class of tumors that have poor prognosis and few therapeutic targets.[112]

1.4.3 Shortcomings of ROS-based chemotherapeutics

Although ROS-based chemotherapeutics, as described above, show great promise for advancement of tumor treatment, the use of these chemotherapeutics is still fraught with complications, and many of these chemotherapy candidates never make it past clinical trials. One aspect limiting the effectiveness of these drugs, as well as many other chemotherapeutics, is the development of chemo-resistance.[65] Tumor cells are constantly evolving to adapt to oxidative stress. Some tumor cells have evolved strong overexpression of cyto-protective genes that make them resistant to the ROS-elevating effects of these drugs. An example of gene-related adaptation is the up-regulation of NRF-2 found in many chemo-resistant tumor cells.[113–115] In normal cells, NRF-2 is usually bound to KEAP1 and subject to degradation. Since KEAP1 contains many reactive thiol groups, it acts as a "sensor" for the presence of H_2O_2; oxidation of these thiol groups lead to de-coupling of NRF-2 from KEAP1 and translocation of NRF-2 to the nucleus to activate antioxidant response elements (ARE).[116] However, some cancers have

evolved somatic mutations in KEAP1 or KEAP1 binding domain to NRF-2, and consequently NRF-2 is constitutively active in the nucleus.[114] Gradual treatment of breast cancer cells with doxorubicin at sub-lethal levels over a period of a few weeks leads to consistent up-regulation of nuclear NRF-2, and certain difficult-to-treat lung adenocarcinomas often have an oncogene-mediated increase in nuclear NRF-2 via KRAS, or deletion of KEAP1.[114,117,118] Thus, it is important to consider genomic regulation of ROS-mediating transcription factors before suggesting ROS-based chemotherapy treatments for a particular tumor.

There has been a lack of thorough investigation into the mechanisms of these chemotherapeutics due to lack of appropriate, quantitative tools and proper ROS-generating controls. For example, while many previous studies indicated the correlative effects between GSH depletion and ROS-elevation with subsequent apoptosis for BSO, PEITC and piperlongumine, it has never been fully tested whether the depletion of GSH, or elevation of ROS, is necessary for toxicity, and it is unclear which reactive species is responsible and where it is being generated. As a result, high-throughput screens identifying "ROS-elevating" small molecules show that there is no dosage correlation between ROS elevation and toxicity of the compound.[105,119,120] These shortcomings can be addressed with better, more species-specific measurement tools, along with protein tools that provide spatial and temporal generation of the desired oxidative species. Only with a systematic investigation into the ROS mechanism of these chemotherapeutics can we begin to apply these compounds most effectively to treating tumors.

1.5 Sensors and generators of hydrogen peroxide and superoxide

To enable mechanistic understanding of ROS-based chemotherapeutics and to inspire their future design, we need to develop a better understanding of how individual ROS species and their generation affect phenotypic outcome. Tools that can measure locally-produced ROS and

enzyme generators that can produce spatially and temporally controlled oxidants will be important in that goal. In this section, we discuss the currently available sensors and generators for studying redox biology. While we will discuss tools available to study both superoxide and hydrogen peroxide, there is an emphasis on tools tailored to H_2O_2, due to its longer lifetime and more interesting biological implication.

1.5.1 Colorimetric and dye-based sensors for H_2O_2

Colorimetric assays. Although H_2O_2 has a distinct UV absorbance measureable at 240 nm, its sensitivity is poor and requires millimolar concentrations, well outside the physiological range found in biological systems.[37] Therefore, the majority of extracellular peroxide measurements are done using horseradish peroxidase (HRP) based assays with substrates such as azino-bis(3-ethylbenzthiazoline-6-sulfonic acid) (ABTS) or 10-acetyl-3,7-dihydroxyphenoxazin (Amplex Red).[38,121,122] Both of these compounds, colorless to begin with, act as electron donors when in contact with H_2O_2, with their oxidation catalyzed by HRP. The oxidized product from this reaction is a soluble green compound in the case of ABTS, and a red compound called resorufin in the case of Amplex Red, the color of which can be quantified using a UV-Vis. The dynamic range of this reaction, amplified by HRP, is between 2 – 50 μM for ABTS and between 250 nM – 10 μM for Amplex Red (data not shown). Since the reaction between the reagent and H_2O_2 is irreversible, these assays are useful for end-point signal collection and measurement of cumulative H_2O_2. They cannot follow the real-time fluctuations in H_2O_2 concentration.

Fluorescent-based dyes. While colorimetric assays are sufficient for extracellular measurement, the compounds cannot diffuse across the plasma membrane to record intracellular peroxide concentrations. About 30 years ago, a fluorescent dye called 2',7'-dichlorodihydrofluorescein

($DCFH_2$) was invented. $DCFH_2$ is able to penetrate cells as its esterified derivative, DCFH-DA.[123] Once inside the cell, the acetate groups are hydrolyzed to form $DCFH_2$, which is polar and unable to diffuse out. Upon oxidation, $DCFH_2$ forms the fluorescent product DCF. Although often touted to be a measurement of H_2O_2, $DCFH_2$ does not actually get oxidized directly by H_2O_2. Instead, it is directly oxidized by one-electron free radicals, and the intermediate radical species gets subsequently converted to a fluorescent product (Figure 1.7).[124] In order for a reaction between H_2O_2 and $DCFH_2$ to take place, a metal catalyst would be required. Thus increases in $DCFH_2$ could simply be a measure of an increase in metal ions inside the cell.[125] The direct reactants of $DCFH_2$ are radical species, therefore it is a non-specific probe for many ROS or even RNS. Finally, the intermediate radical species of $DCFH_2$ can be scavenged with radical capturing antioxidants. Thus, signal output from $DCFH_2$ is riddled with caveats. Despite all this, it is still the most commonly used sensor for H_2O_2 measurement in redox biology.

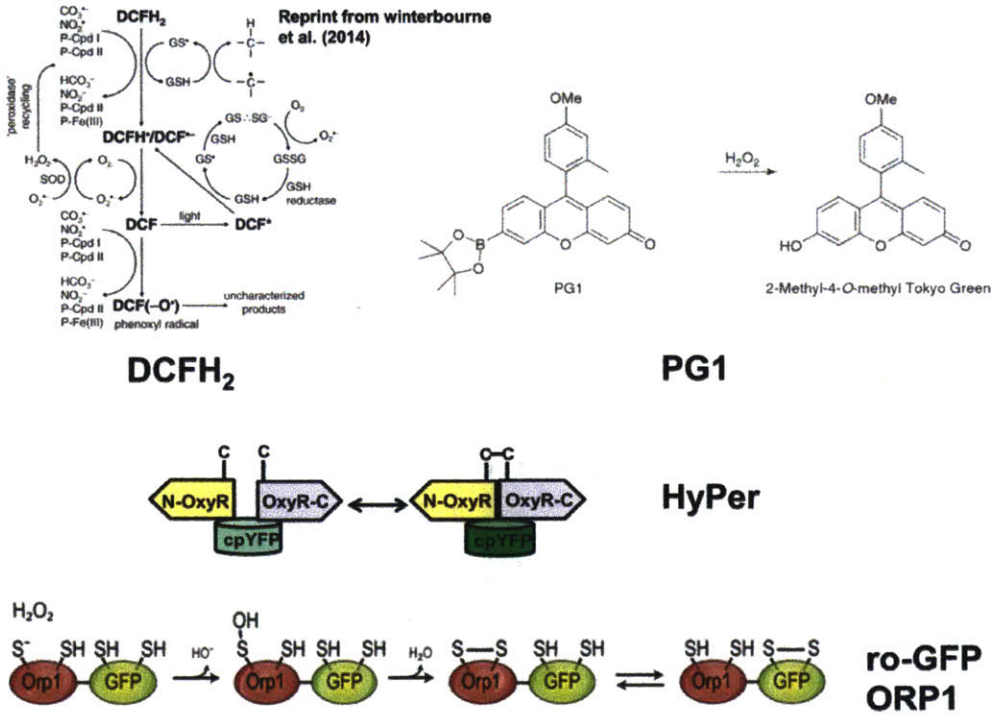

Figure 1.7: Different methodology for intracellular quantification of H_2O_2/other ROS. $DCFH_2$ and PG1 are membrane-permeable dye-based methods of measuring ROS. HyPer and ro-GFP ORP1 are protein-based sensors that are genetically expressed

Building on the repertoire of chemical-based sensors, an intracellular dye using boronate deprotection reaction of H_2O_2 called Peroxy Green 1 (PG1) was invented as a more specific sensor for H_2O_2.[126] Briefly, 2-methyl-4-O-methyl Tokyo Green is treated with N-phenyl bis(trifluoromethanesfulonamide) and palladium-catalyzed borylation, the end product produced, as shown Figure 1.7, is essentially Toyko Green with a boronate group. When H_2O_2 comes in contact with PG1, a marked increase in green fluorescence occurs as the boronate deprotection reaction regenerates the 2-methyl-4-O-methyl Tokyo Green. This deprotection reaction is specific to H_2O_2, as incubation with other members of the ROS family such as superoxide and hydroxyl radical did not cause a change in signal.

While PG1 is an improvement in specificity from $DCFH_2$, use of fluorescent dyes for detection of H_2O_2, or ROS in general, is problematic. First of all, the reaction of the dye with the oxidants is irreversible, so the probes can only measure total accumulated H_2O_2, rather than a real-time concentration. Secondly, experimental variability with dye uptake into the cell can be confounded with an actual difference in H_2O_2 level, and there is no control for it due to the fact that it is a single feature measurement. The probe cannot be selectively localized to different cellular compartments, and finally, its H_2O_2 sensitivity of 10 -100 μM can miss pathological intracellular concentrations that are of interest.[56,127,128]

1.5.2 Intracellular protein-based sensors for H_2O_2

In recent years, genetic engineering has been used to produce fusions of fluorescent proteins with bacterial and yeast proteins that react specifically with hydrogen peroxide. Fusions are constructed such that changes in the spectrum of the fluorescent protein occur when hydrogen

peroxide oxidizes a cysteine of the microbial or yeast protein, causing it to subsequently form a disulfide bond with a neighboring cysteine.[129–131] Two examples of this type of fusion are the bacterial-based HyPer sensor and the yeast-based ro-GFP Orp1 sensor (Figure 1.7). In the case of HyPer, a circular-permutated YFP was inserted in between the cysteine groups of the OxyR H_2O_2 sensor domain of bacteria, and upon H_2O_2 oxidation, the cysteine groups form a disulfide bond and change the conformation of the entire fusion protein.[132,133] In the case of ro-GFP Orp1, the ro-GFP fluorescent protein, with cysteines engineered on the β-barrel of EGFP, is fused downstream of Orp1, a yeast sensor specific for H_2O_2 oxidation sensing. The oxidation by H_2O_2 causes a disulfide bond formation on Orp-1, which is subsequently transferred to the ro-GFP.[134] The conformational changes involving the fluorescent proteins affect two spectral features: an excitation peak at one wavelength decreasing and an excitation peak at a second wavelength increasing in a dose-dependent manner upon stimulation with hydrogen peroxide.[131,133] For HyPer, the 500 nm wavelength increases while the 420 nm wavelength decreases, and the opposite trend occurs for ro-GFP Orp1. The dynamic ranges of both sensors are similar and very sensitive, detecting intracellular changes in the nanomolar range.[38,135]

Besides the specificity and sensitivity in response to H_2O_2, genetically encoded protein sensors have a huge advantage in terms of the ability to localize to specific cellular compartments or locale when an appropriate targeting sequence is attached, or when the sensor is fused to the source of generation. Furthermore, the oxidation of these probes is reversible by intracellular glutaredoxin or thioredoxin, enabling measurements of fluctuations in intracellular H_2O_2 rather than a cumulative output. However, these measurements are not exactly real-time, since these sensors suffer from slow reduction kinetics, causing them to lag behind the actual cellular concentration.[130] Another caveat of using HyPer, in particular, is the pH sensitivity of the YFP

protein. Small changes in pH have shown large shifts in ratiometric fluorescent response. Thus a control protein, SypHer, where one of the cysteine residues of the OxyR is mutated to serine, needs to be used with every experiment to ensure that the effects were due to H_2O_2 and not environmental artifacts.[136]

1.5.3 Sensors for superoxide

Over the past 20 years, hydroethidine (HE) has become the gold standard for detecting superoxide. The oxidation product of the HE and superoxide reaction, 2-Hydroxyethidium, is unique to superoxide and peroxynitrite; H_2O_2 and hydroxyl radical do not form the same product upon reaction with HE.[137] However, the current detection method using fluorescence cannot distinguish 2-hydroxyethidium from the products formed by other oxidants.[138,139] The only accurate method of detecting this compound is via HPLC or mass spectrometry, making the detection method too cumbersome to be effectively employed.

1.5.4 Generators of hydrogen peroxide and superoxide

Bolus H_2O_2 addition. Researchers have historically used bolus addition to perturb intracellular levels of H_2O_2 and study its effects. However, bolus treatment can only add H_2O_2 to the extracellular medium, requiring H_2O_2 to diffuse through the cell membrane, which results in a gradient.[37,38,140] While generation of H_2O_2 external to the cell is relevant to certain cellular processes, such as inflammation and the respiratory burst, this is not the case with respect to many other diseases that produce oxidative stress.[141,142] Furthermore, bolus addition of H_2O_2 has non-physiological kinetics: while bolus addition is expected to produce a sudden increase in intracellular H_2O_2 concentration followed by exponential decay due to antioxidant scavengers, realistic H_2O_2 production is gradual over a more prolonged period of time. These differences in

kinetics may result in effects not seen when H_2O_2 is produced using endogenous cellular sources.[141,143,144] Continuous generation of H_2O_2 in localized settings within the cell may better reflect physiological processes with respect to spatiotemporal changes in H_2O_2 levels during the actions of certain drugs and pathologies, making this a preferred method of perturbation. Both enzymes and small molecules have been used in this capacity, as discussed below.

Enzymes for ROS generation. The three main enzymes that have been used in past studies to perturb H_2O_2 levels are oxidases: xanthine oxidase (XO), glucose oxidase (GO), and D-amino acid oxidase (DAAO). While xanthine oxidase and glucose oxidase have been predominately used for continuous ROS generation outside the cell, D-amino acid oxidase has been used as a genetically encoded generator.

Enzyme	Source	ROS generation rate (min^{-1})	Intracellular versus extracellular	Substrates	Products
Xanthine oxidase	Bovine milk	~550 [148]-630 [149]	Extracellular	Xanthine/hypo xanthine + O_2	Uric acid/xanthine + $H_2O_2/O_2^{\cdot-}$
Glucose oxidase	*Aspergillus niger*	~56000 [150]	Extracellular	β-D-glucose + O_2	Gluconic acid + H_2O_2
D-amino acid oxidase	*Rhodotorula gracilis*	~20000 [151]	Intracellular	D-amino acid + H_2O + O_2	α-keto acid + NH_4^+ + H_2O_2

Table 1.3 Key characteristics of existing enzymatic ROS generators. Xanthine oxidase, Gluocse oxidase and D-amino acid oxidase are enzymatic generators that can produce H_2O_2 and superoxide.

While XO purportedly generates $O_2^{\cdot-}$, it actually generates both $O_2^{\cdot-}$ and H_2O_2, and was recently found to predominantly produce H_2O_2 under physiologically relevant conditions.[145] Furthermore, while extracellular $O_2^{\cdot-}$ can diffuse across the membrane through anion channels to enact intracellular effects, it may also dismutate to H_2O_2, either outside or inside the cell.[146] It is thus inappropriate to label XO solely as a superoxide-generating agent, and it is important to determine the stoichiometry of the products from a reaction catalyzed by XO in a given set of

experimental conditions. Because XO is given to catalyzing production of a mixture of H_2O_2 and $O_2^{\cdot-}$, along with other byproducts such as uric acid, it is difficult to pinpoint any resulting biological effects to a particular species. While XO could theoretically be genetically encoded for intracellular perturbation, its promiscuous activity with a wide range of endogenous substrates would add another undesirable complication.[147]

GO is an enzyme that oxidizes glucose to D-glucono-δ-lactone, and produces H_2O_2 as a by-product. The H_2O_2 produced from GO has often been used in conjunction with catalase, an H_2O_2 scavenger, to modulate steady state levels of H_2O_2.[144] It thus offers product specificity that is difficult to control in reactions catalyzed by XO. However, GO has only ever been used for extracellular generation, likely because it requires use of a valuable metabolite, glucose, that would greatly perturb cellular metabolism and obfuscate any resulting effects that could be attributed to either H_2O_2 or glucose consumption. While this may be relevant for studying inflammatory processes,[142] this may not be the case for processes involving only intracellular generation.

DAAO is an enzyme that is predominately found in the peroxisome. It enables the oxidation of a D-amino acid to the corresponding imino acid with a FAD co-factor, producing ammonia and hydrogen peroxide as by-products.[152] By altering the peroxisomal targeting sequence, DAAO from yeast can be expressed in the cytosol.[153,154] The production of H_2O_2 is initiated when D-alanine is added extracellularly, with increasing D-alanine concentration causing an increase in the kinetics of generation. DAAO has been used in this manner in numerous other studies,[153,155–157] giving insights into the effects of endogenously produced H_2O_2.

The properties of the enzymatic generators are summarized in Table 1.3.

Small molecule generators. Miller et al. developed a photocaged H_2O_2 generator termed Caged Peroxide Generator 1 (CPG1) that produces superoxide as an intermediate species and hydrogen peroxide via dismutation upon activation by light.[158] CPG1 was able to produce H_2O_2 on the order of tens of micromolar, with the total amount and kinetic rate modulated by the amount of CPG1 loaded into the cell. In a similar system, Cheong et al. used a photosensitizer, hematoporphyrin, and light to activate intracellular ROS generation in dendritic cells.[159] It is noted that hematoporphyrin produces singlet oxygen (1O2), hydroxyl radical ($OH^{\cdot}$), and O_2-, in addition to H_2O_2. Both probes were loaded into the cytosol of cells, as they currently do not have any tag to direct them to a particular subcellular compartment. The lack of localizability and specific species generation make it difficult to use these tools to pinpoint with more precise spatial resolution the effects of a particular ROS.

1.6 Conclusion and purpose of thesis work

This chapter provides an overview of reactive oxidative species in terms of where they come from, what are the reaction kinetics of the protein, lipid and DNA targets of each member, and how the concentration of the ROS is implicated in signal transduction and downstream phenotypic effects. This dual life-versus-death role of ROS, depending on the intracellular concentration, is exploited by ROS-based cancer chemotherapeutics to selectively eliminate tumor cells, but the use of these drugs is fraught with complications and falls short of its promise. Therefore, a quantitative, systematic study of specific ROS and their phenotypic effects will inform better design of these therapies in the future. These studies require state-of-the-art tools that can provide species-specific measurements, as well as spatially and temporally relevant generation.

In this thesis work, we explored quantitative use of genetically encoded sensors for H_2O_2. We did so by developing an assay that converts the signal generated from the sensors into an intracellular concentration change. We also explored the massive heterogeneity in the sensor response to an identical stimulant, understanding how we should interpret the sensor output in context of this heterogeneity. We then used these genetically encoded sensors together with generators of H_2O_2 to quantitatively study H_2O_2-induced toxicity, and also applied them to better understand the ROS mechanism of the chemotherapeutics PEITC and piperlongumine. Finally, we engaged in our own technology development, creating a new enzymatic generator based on P450-BM3, an easily engineer-able protein that can produce hydrogen peroxide and superoxide with controlled kinetics. Taken together, our findings yielded greater quantitative insight into how we use these genetically encoded sensors, and how these sensors and generators can be used to elucidate H_2O_2-mediated cell death in cancer chemotherapeutics. Finally, our work inspired the development of next generation sensor and generators for study of reactive oxidative species.

1.7 Bibliography

(1) Winterbourn, C. C. (2008) Reconciling the chemistry and biology of reactive oxygen species. *Nat. Chem. Biol. 4*, 278–86.
(2) Murphy, M. P., Holmgren, A., Larsson, N.-G., Halliwell, B., Chang, C. J., Kalyanaraman, B., Rhee, S. G., Thornalley, P. J., Partridge, L., Gems, D., Nyström, T., Belousov, V., Schumacker, P. T., and Winterbourn, C. C. (2011) Unraveling the biological roles of reactive oxygen species. *Cell Metab. 13*, 361–6.
(3) Dickinson, B. C., and Chang, C. J. (2011) Chemistry and biology of reactive oxygen species in signaling or stress responses. *Nat. Chem. Biol. 7*, 504–11.
(4) Singh, M., Sharma, H., and Singh, N. (2007) Hydrogen peroxide induces apoptosis in HeLa cells through mitochondrial pathway. *Mitochondrion 7*, 367–73.
(5) Weinberg, S. E., Sena, L. a, and Chandel, N. S. (2015) Mitochondria in the Regulation of Innate and Adaptive Immunity. *Immunity 42*, 406–417.
(6) Schriner, S. E., Linford, N. J., Martin, G. M., Treuting, P., Ogburn, C. E., Emond, M., Coskun, P. E., Ladiges, W., Wolf, N., Van Remmen, H., Wallace, D. C., and Rabinovitch, P. S. (2005) Extension of murine life span by overexpression of catalase targeted to mitochondria. *Science 308*, 1909–11.
(7) Bao, L., Avshalumov, M. V, Patel, J. C., Lee, C. R., Miller, E. W., Chang, C. J., and Rice, M. E. (2009) Mitochondria are the source of hydrogen peroxide for dynamic brain-cell signaling. *J. Neurosci. 29*, 9002–9010.
(8) Bedard, K., and Krause, K.-H. (2007) The NOX family of ROS-generating NADPH oxidases: physiology and pathophysiology. *Physiol. Rev. 87*, 245–313.
(9) Lambeth, J. D. (2007) Nox enzymes, ROS, and chronic disease: an example of antagonistic pleiotropy. *Free Radic. Biol. Med. 43*, 332–47.
(10) Lambeth, J. D. (2004) NOX enzymes and the biology of reactive oxygen. *Nat. Rev. Immunol. 4*, 181–189.
(11) Lu, H., Ouyang, W., and Huang, C. (2006) Inflammation, a key event in cancer development. *Mol. Cancer Res. 4*, 221–233.
(12) Kuroda, J., Ago, T., Matsushima, S., Zhai, P., Schneider, M. D., and Sadoshima, J. (2010) NADPH oxidase 4 (Nox4) is a major source of oxidative stress in the failing heart. *Proc. Natl. Acad. Sci. U. S. A. 107*, 15565–15570.
(13) Weyemi, U., Lagente-Chevallier, O., Boufraqech, M., Prenois, F., Courtin, F., Caillou, B., Talbot, M., Dardalhon, M., Al Ghuzlan, a, Bidart, J.-M., Schlumberger, M., and Dupuy, C. (2012) ROS-generating NADPH oxidase NOX4 is a critical mediator in oncogenic H-Ras-induced DNA damage and subsequent senescence. *Oncogene 31*, 1117–1129.
(14) Brown, D. I., and Griendling, K. K. (2009) Nox proteins in signal transduction. *Free Radic. Biol. Med. 47*, 1239–1253.
(15) Gross, E., Sevier, C. S., Heldman, N., Vitu, E., Bentzur, M., Kaiser, C. a, Thorpe, C., and Fass, D. (2006) Generating disulfides enzymatically: reaction products and electron acceptors of the endoplasmic reticulum thiol oxidase Ero1p. *Proc. Natl. Acad. Sci. U. S. A. 103*, 299–304.
(16) Holmström, K. M., and Finkel, T. (2014) Cellular mechanisms and physiological consequences of redox-dependent signalling. *Nat. Rev. Mol. Cell Biol. 15*, 411–21.
(17) Zhang, J., Kim, J., Alexander, A., Cai, S., Tripathi, D. N., Dere, R., Tee, A. R., Tait-Mulder, J., Di Nardo, A., Han, J. M., Kwiatkowski, E., Dunlop, E. a, Dodd, K. M., Folkerth, R. D., Faust, P. L., Kastan, M. B., Sahin, M., and Walker, C. L. (2013) A tuberous sclerosis complex signalling node at the peroxisome regulates mTORC1 and autophagy in response to ROS. *Nat. Cell Biol. 15*, 1186–96.
(18) Rhee, S. G., Woo, H. A., Kil, I. S., and Bae, S. H. (2012) Peroxiredoxin functions as a peroxidase and a regulator and sensor of local peroxides. *J. Biol. Chem. 287*, 4403–10.
(19) Weydert, C. J., and Cullen, J. J. (2010) Measurement of superoxide dismutase, catalase and glutathione peroxidase in cultured cells and tissue. *Nat. Protoc. 5*, 51–66.
(20) Estévez, A. G., and Jordán, J. (2002) Nitric oxide and superoxide, a deadly cocktail. *Ann. N. Y. Acad. Sci. 962*, 207–211.
(21) Lancaster, J. R. (2006) Nitroxidative, nitrosative, and nitrative stress: kinetic predictions of reactive nitrogen species chemistry under biological conditions. *Chem. Res. Toxicol. 19*, 1160–74.
(22) Woodmansee, A. N., and Imlay, J. a. (2002) Reduced flavins promote oxidative DNA damage in non-respiring Escherichia coli by delivering electrons to intracellular free iron. *J. Biol. Chem. 277*, 34055–34066.
(23) Manta, B., Hugo, M., Ortiz, C., Ferrer-Sueta, G., Trujillo, M., and Denicola, A. (2009) The peroxidase and peroxynitrite reductase activity of human erythrocyte peroxiredoxin 2. *Arch. Biochem. Biophys. 484*, 146–54.

(24) Furtmuller, P. O., Obinger, C., Hsuanyu, Y., and Dunford, H. B. (2000) Mechanism of reaction of myeloperoxidase with hydrogen peroxide and chloride ion. *Eur. J. Biochem. 267*, 5858–5864.
(25) Buettner, G. R. (1993) The pecking order of free radicals and antioxidants: lipid peroxidation, alpha-tocopherol, and ascorbate. *Arch. Biochem. Biophys.*
(26) Pattison, D. I., and Davies, M. J. (2001) Absolute Rate Constants for the Reaction of Hypochlorous Acid with Protein Side Chains and Peptide Bonds. *Chem. Res. Toxicol. 14*, 1453–1464.
(27) Bonini, M. G., and Augusto, O. (2001) Carbon Dioxide Stimulates the Production of Thiyl, Sulfinyl, and Disulfide Radical Anion from Thiol Oxidation by Peroxynitrite. *J. Biol. Chem. 276*, 9749–9754.
(28) Winterbourn, C. C., and Metodiewa, D. (1999) Reactivity of biologically important thiol compounds with superoxide and hydrogen peroxide. *Free Radic. Biol. Med. 27*, 322–328.
(29) Grek, C. L., Zhang, J., Manevich, Y., Townsend, D. M., and Tew, K. D. (2013) Causes and consequences of cysteine S-glutathionylation. *J. Biol. Chem. 288*, 26497–504.
(30) Poole, L. B. (2014) The Basics of Thiols and Cysteines in Redox Biology and Chemistry. *Free Radic. Biol. Med.* 1–10.
(31) Poole, L. B., Karplus, P. A., and Claiborne, A. (2004) Protein sulfenic acids in redox signaling. *Annu. Rev. Pharmacol. Toxicol. 44*, 325–347.
(32) Holmgren, a, Johansson, C., Berndt, C., Lönn, M. E., Hudemann, C., and Lillig, C. H. (2005) Thiol redox control via thioredoxin and glutaredoxin systems. *Biochem. Soc. Trans. 33*, 1375–7.
(33) D'Autréaux, B., and Toledano, M. B. (2007) ROS as signalling molecules: mechanisms that generate specificity in ROS homeostasis. *Nat. Rev. Mol. Cell Biol. 8*, 813–24.
(34) Sobotta, M. C., Liou, W., Stöcker, S., Talwar, D., Oehler, M., Ruppert, T., Scharf, A. N. D., and Dick, T. P. (2014) Peroxiredoxin-2 and STAT3 form a redox relay for H_2O_2 signaling. *Nat. Chem. Biol. 11*, 64–70.
(35) Conway, J. P., and Kinter, M. (2006) Dual role of peroxiredoxin I in macrophage-derived foam cells. *J. Biol. Chem. 281*, 27991–28001.
(36) Adimora, N. J., Jones, D. P., and Kemp, M. L. (2010) A Model of Redox Kinetics Implicates the Thiol Proteome in Cellular Hydrogen Peroxide Responses. *Antioxid. Redox Signal. 13*, 731–743.
(37) Antunes, F., and Cadenas, E. (2000) Estimation of H_2O_2 gradients across biomembranes. *FEBS Lett. 475*, 121–6.
(38) Huang, B. K., and Sikes, H. D. (2014) Quantifying intracellular hydrogen peroxide perturbations in terms of concentration. *Redox Biol. 2*, 955–962.
(39) Nelson, K. J., Parsonage, D., Karplus, P. A., and Poole, L. B. (2013) Evaluating peroxiredoxin sensitivity toward inactivation by peroxide substrates. *Methods Enzymol. 527*, 21–40.
(40) Woo, H. A., Yim, S. H., Shin, D. H., Kang, D., Yu, D.-Y., and Rhee, S. G. (2010) Inactivation of peroxiredoxin I by phosphorylation allows localized H(2)O(2) accumulation for cell signaling. *Cell 140*, 517–28.
(41) Stadtman, E. R. (2006) Protein oxidation and aging. *Free Radic. Res. 40*, 1250–8.
(42) Alfonso-Prieto, M., Biarnés, X., Vidossich, P., and Rovira, C. (2009) The molecular mechanism of the catalase reaction. *J. Am. Chem. Soc. 131*, 11751–61.
(43) Purdue, P. E., and Lazarow, P. B. (1996) Targeting of human catalase to peroxisomes is dependent upon a novel COOH-terminal peroxisomal targeting sequence. *J. Cell Biol. 134*, 849–862.
(44) Sohn, J., and Rudolph, J. (2003) Catalytic and chemical competence of regulation of cdc25 phosphatase by oxidation/reduction. *Biochemistry 42*, 10060–70.
(45) Denu, J. M., and Tanner, K. G. (1998) Specific and reversible inactivation of protein tyrosine phosphatases by hydrogen peroxide: evidence for a sulfenic acid intermediate and implications for redox regulation. *Biochemistry 37*, 5633–42.
(46) Lee, K., Briehl, M. M., Mazar, A. P., Batinic-Haberle, I., Reboucas, J. S., Glinsmann-Gibson, B., Rimsza, L. M., and Tome, M. E. (2013) The copper chelator ATN-224 induces peroxynitrite-dependent cell death in hematological malignancies. *Free Radic. Biol. Med. 60*, 157–167.
(47) Papa, L., Hahn, M., Marsh, E. L., Evans, B. S., and Germain, D. (2014) SOD2 to SOD1 switch in breast cancer. *J. Biol. Chem.* C113.526475–.
(48) Winterbourn, C. C., and Kettle, A. J. (2000) Biomarkers of myeloperoxidase-derived hypochlorous acid. *Free Radic. Biol. Med. 29*, 403–409.
(49) Yoon, J. H., Lee, M. S., and Kang, J. H. (2010) Reaction of ferritin with hydrogen peroxide induces lipid peroxidation. *BMB Rep. 43*, 219–224.
(50) Cadet, J., Delatour, T., Douki, T., Gasparutto, D., Pouget, J. P., Ravanat, J. L., and Sauvaigo, S. (1999) Hydroxyl radicals and DNA base damage. *Mutat. Res. - Fundam. Mol. Mech. Mutagen. 424*, 9–21.

(51) Jarvis, R. M., Hughes, S. M., and Ledgerwood, E. C. (2012) Peroxiredoxin 1 functions as a signal peroxidase to receive, transduce, and transmit peroxide signals in mammalian cells. *Free Radic. Biol. Med. 53*, 1522–30.
(52) Wood, Z. a, Poole, L. B., and Karplus, A. (2003) Peroxiredoxin Evolution and the Signaling. *Science (80-.). 300*, 650–653.
(53) Hawkins, B. J., Madesh, M., Kirkpatrick, C. J., and Fisher, A. B. (2007) Superoxide flux in endothelial cells via the chloride channel-3 mediates intracellular signaling. *Mol. Biol. Cell 18*, 2002–12.
(54) Ushio-Fukai, M. (2006) Localizing NADPH oxidase-derived ROS. *Sci. STKE 2006*, re8.
(55) Laurent, A., Nicco, C., Chéreau, C., Goulvestre, C., Alexandre, J., Alves, A., Lévy, E., Goldwasser, F., Panis, Y., Soubrane, O., Weill, B., and Batteux, F. (2005) Controlling tumor growth by modulating endogenous production of reactive oxygen species. *Cancer Res. 65*, 948–956.
(56) Antunes, F., and Cadenas, E. (2001) Cellular titration of apoptosis with steady state concentrations of H(2)O(2): submicromolar levels of H(2)O(2) induce apoptosis through Fenton chemistry independent of the cellular thiol state. *Free Radic. Biol. Med. 30*, 1008–18.
(57) Gough, D. R., and Cotter, T. G. (2011) Hydrogen peroxide: a Jekyll and Hyde signalling molecule. *Cell Death Dis. 2*, e213.
(58) Szatrowski, T. P., and Nathan, C. F. (1991) Production of Large Amounts of Hydrogen Peroxide by Human Tumor Cells. *Cancer Res. 51*, 794–798.
(59) Arbiser, J. L., Petros, J., Klafter, R., Govindajaran, B., McLaughlin, E. R., Brown, L. F., Cohen, C., Moses, M., Kilroy, S., Arnold, R. S., and Lambeth, J. D. (2002) Reactive oxygen generated by Nox1 triggers the angiogenic switch. *Proc. Natl. Acad. Sci. U. S. A. 99*, 715–720.
(60) Gianni, D., Taulet, N., Zhang, H., DerMardirossian, C., Kister, J., Martinez, L., Roush, W. R., Brown, S. J., Bokoch, G. M., and Rosen, H. (2010) A novel and specific NADPH oxidase-1 (Nox1) small-molecule inhibitor blocks the formation of functional invadopodia in human colon cancer cells. *ACS Chem. Biol. 5*, 981–93.
(61) Groeger, G., Quiney, C., and Cotter, T. G. (2009) Hydrogen peroxide as a cell-survival signaling molecule. *Antioxid. Redox Signal. 11*, 2655–71.
(62) Youle, R. J., and Strasser, A. (2008) The BCL-2 protein family: opposing activities that mediate cell death. *Nat. Rev. Mol. Cell Biol. 9*, 47–59.
(63) Circu, M. L., and Aw, T. Y. (2010) Reactive oxygen species, cellular redox systems, and apoptosis. *Free Radic. Biol. Med. 48*, 749–762.
(64) Gorrini, C., Harris, I. S., and Mak, T. W. (2013) Modulation of oxidative stress as an anticancer strategy. *Nat. Rev. Drug Discov. 12*, 931–47.
(65) Trachootham, D., Alexandre, J., and Huang, P. (2009) Targeting cancer cells by ROS-mediated mechanisms: a radical therapeutic approach? *Nat. Rev. Drug Discov. 8*, 579–91.
(66) Trachootham, D., Lu, W., Ogasawara, M. a, Nilsa, R.-D. V., and Huang, P. (2008) Redox regulation of cell survival. *Antioxid. Redox Signal. 10*, 1343–1374.
(67) Finkel, T. (2011) Signal transduction by reactive oxygen species. *J. Cell Biol.*
(68) Cairns, R. a, Harris, I. S., and Mak, T. W. (2011) Regulation of cancer cell metabolism. *Nat. Rev. Cancer 11*, 85–95.
(69) Vanden Berghe, T., Van Loo, G., Saelens, X., Van Gurp, M., Brouckaert, G., Kalai, M., Declercq, W., and Vandenabeele, P. (2004) Differential Signaling to Apoptotic and Necrotic Cell Death by Fas-associated Death Domain Protein FADD. *J. Biol. Chem. 279*, 7925–7933.
(70) Porter, a G., and Jänicke, R. U. (1999) Emerging roles of caspase-3 in apoptosis. *Cell Death Differ. 6*, 99–104.
(71) Bhat, N. R., and Zhang, P. (1999) Hydrogen peroxide activation of multiple mitogen-activated protein kinases in an oligodendrocyte cell line: role of extracellular signal-regulated kinase in hydrogen peroxide-induced cell death. *J. Neurochem. 72*, 112–9.
(72) Dolado, I., Swat, A., Ajenjo, N., De Vita, G., Cuadrado, A., and Nebreda, A. R. (2007) p38alpha MAP kinase as a sensor of reactive oxygen species in tumorigenesis. *Cancer Cell 11*, 191–205.
(73) Son, Y.-O., Jang, Y.-S., Heo, J.-S., Chung, W.-T., Choi, K.-C., and Lee, J.-C. (2009) Apoptosis-inducing factor plays a critical role in caspase-independent, pyknotic cell death in hydrogen peroxide-exposed cells. *Apoptosis 14*, 796–808.
(74) Chen, G., Chen, Z., Hu, Y., and Huang, P. (2011) Inhibition of Mitochondrial Respiration and Rapid Depletion of Mitochondrial Glutathione by β-Phenethyl Isothiocyanate: Mechanisms for Anti-Leukemia Activity. *Antioxid. Redox Signal. 15*, 2911–2921.
(75) Ryter, S. W., Kim, H. P., Hoetzel, A., Park, J. W., Nakahira, K., Wang, X., and Choi, A. M. K. (2006) Mechanisms of Cell Death in Oxidative Stress.

(76) Morandell, S., and Yaffe, M. B. (2012) Exploiting synthetic lethal interactions between DNA damage signaling, checkpoint control, and p53 for targeted cancer therapy. *Prog. Mol. Biol. Transl. Sci. 110*, 289–314.
(77) Gardner, A. M., Xu, F. H., Fady, C., Jacoby, F. J., Duffey, D. C., Tu, Y., and Lichtenstein, A. (1996) Apoptotic vs. nonapoptotic cytotoxicity induced by hydrogen peroxide. *Free Radic. Biol. Med. 22*, 73–83.
(78) Waris, G., and Ahsan, H. (2006) Reactive oxygen species: role in the development of cancer and various chronic conditions. *J. Carcinog. 5*, 14.
(79) Liou, G.-Y., and Storz, P. (2010) Reactive oxygen species in cancer. *Free Radic. Res. 44*, 479–96.
(80) Irani, K. (1997) Mitogenic Signaling Mediated by Oxidants in Ras-Transformed Fibroblasts. *Science (80-.). 275*, 1649–1652.
(81) Trachootham, D., Zhou, Y., Zhang, H., Demizu, Y., Chen, Z., Pelicano, H., Chiao, P. J., Achanta, G., Arlinghaus, R. B., Liu, J., and Huang, P. (2006) Selective killing of oncogenically transformed cells through a ROS-mediated mechanism by beta-phenylethyl isothiocyanate. *Cancer Cell 10*, 241–52.
(82) Ishikawa, K., Takenaga, K., Akimoto, M., Koshikawa, N., Yamaguchi, A., Imanishi, H., Nakada, K., Honma, Y., and Hayashi, J.-I. (2008) ROS-generating mitochondrial DNA mutations can regulate tumor cell metastasis. *Science 320*, 661–4.
(83) Bourdon, J.-C. (2007) P53 and Its Isoforms in Cancer. *Br. J. Cancer 97*, 277–282.
(84) Grivennikov, S. I., Greten, F. R., and Karin, M. (2010) Immunity, Inflammation, and Cancer. *Cell 140*, 883–899.
(85) Semenza, G. L. (2011) Oxygen Sensing, Homeostasis, and Disease 537–547.
(86) Patel, B. P., Rawal, U. M., Dave, T. K., Rawal, R. M., Shukla, S. N., Shah, P. M., and Patel, P. S. (2007) Lipid peroxidation, total antioxidant status, and total thiol levels predict overall survival in patients with oral squamous cell carcinoma. *Integr. Cancer Ther. 6*, 365–72.
(87) Kumar, B., Koul, S., Khandrika, L., Meacham, R. B., and Koul, H. K. (2008) Oxidative stress is inherent in prostate cancer cells and is required for aggressive phenotype. *Cancer Res. 68*, 1777–85.
(88) Tsao, S.-M., Yin, M.-C., and Liu, W.-H. (2007) Oxidant stress and B vitamins status in patients with non-small cell lung cancer. *Nutr. Cancer 59*, 8–13.
(89) Onul, A., Elseth, K. M., Vitto, H., Paradise, W. a., Vesper, B. J., Tarjan, G., Haines, G. K., Rumjanek, F. D., and Radosevich, J. a. (2012) Long-term adaptation of the human lung tumor cell line A549 to increasing concentrations of hydrogen peroxide. *Tumor Biol. 33*, 739–748.
(90) Choi, J., Liu, R.-M., and Forman, H. J. (1997) Adaptation to oxidative stress: Quinone-mediated protection of signaling in rat lung epithelial L2 cells. *Biochem. Pharmacol. 53*, 987–993.
(91) Diehn, M., Cho, R. W., Lobo, N. A., Kalisky, T., Dorie, M. J., Kulp, A. N., Qian, D., Lam, J. S., Ailles, L. E., Wong, M., Joshua, B., Kaplan, M. J., Wapnir, I., Dirbas, F. M., Somlo, G., Garberoglio, C., Paz, B., Shen, J., Lau, S. K., Quake, S. R., Brown, J. M., Weissman, I. L., and Clarke, M. F. (2009) Association of reactive oxygen species levels and radioresistance in cancer stem cells. *Nature 458*, 780–3.
(92) Ganesh Yerra, V., Negi, G., Sharma, S. S., and Kumar, A. (2013) Potential therapeutic effects of the simultaneous targeting of the Nrf2 and NF-??B pathways in diabetic neuropathy. *Redox Biol. 1*, 394–397.
(93) Wang, J., and Yi, J. (2014) Cancer cell killing via ROS: To increase or decrease, that is the question. *Cancer Biol. Ther. 7*, 1875–1884.
(94) Blot, W. J., Li, J. Y., Taylor, P. R., Guo, W., Dawsey, S., Wang, G. Q., Yang, C. S., Zheng, S. F., Gail, M., and Li, G. Y. (1993) Nutrition intervention trials in Linxian, China: supplementation with specific vitamin/mineral combinations, cancer incidence, and disease-specific mortality in the general population. *J. Natl. Cancer Inst. 85*, 1483–92.
(95) Sayin, V. I., Ibrahim, M. X., Larsson, E., Nilsson, J. a, Lindahl, P., and Bergo, M. O. (2014) Antioxidants accelerate lung cancer progression in mice. *Sci. Transl. Med. 6*, 221ra15.
(96) Klein, E. A., Thompson, I. M., Tangen, C. M., Crowley, J. J., Lucia, M. S., Goodman, P. J., Minasian, L. M., Ford, L. G., Parnes, H. L., Gaziano, J. M., Karp, D. D., Lieber, M. M., Walther, P. J., Klotz, L., Parsons, J. K., Chin, J. L., Darke, A. K., Lippman, S. M., Goodman, G. E., Meyskens, F. L., and Baker, L. H. (2011) Vitamin E and the risk of prostate cancer: the Selenium and Vitamin E Cancer Prevention Trial (SELECT). *JAMA 306*, 1549–56.
(97) Hayden, A., Douglas, J., Sommerlad, M., Andrews, L., Gould, K., Hussain, S., Thomas, G. J., Packham, G., and Crabb, S. J. (2014) The Nrf2 transcription factor contributes to resistance to cisplatin in bladder cancer. *Urol. Oncol. 32*, 806–14.
(98) Lillig, C. H., and Berndt, C. (2013) Glutaredoxins in thiol/disulfide exchange. *Antioxid. Redox Signal. 18*, 1654–65.
(99) Circu, M. L., and Aw, T. Y. (2012) Glutathione and modulation of cell apoptosis. *Biochim. Biophys. Acta 1823*, 1767–77.

(100) Griffith, O. W. (1982) Mechanism of Action, Metabolism, and Toxicity of Buthionine Sulfoximine and. *J. Biol. Chem. 257*, 13704–13712.
(101) Chen, Y.-R., Han, J., Kori, R., Kong, a-N. T., and Tan, T.-H. (2002) Phenylethyl isothiocyanate induces apoptotic signaling via suppressing phosphatase activity against c-Jun N-terminal kinase. *J. Biol. Chem.*
(102) Loganathan, S., Kandala, P. K., Gupta, P., and Srivastava, S. K. (2012) Inhibition of EGFR-AKT axis results in the suppression of ovarian tumors in vitro and in preclinical mouse model. *PLoS One 7*, e43577.
(103) Raj, L., Ide, T., Gurkar, A. U., Foley, M., Schenone, M., Li, X., Tolliday, N. J., Golub, T. R., Carr, S. A., Shamji, A. F., Stern, A. M., Mandinova, A., Schreiber, S. L., and Lee, S. W. (2011) Selective killing of cancer cells by a small molecule targeting the stress response to ROS. *Nature 475*, 231–4.
(104) Dhillon, H., Chikara, S., and Reindl, K. M. (2014) Piperlongumine induces pancreatic cancer cell death by enhancing reactive oxygen species and DNA damage. *Toxicol. Reports 1*, 309–318.
(105) Zhu, C., Hu, W., Wu, H., and Hu, X. (2014) No evident dose-response relationship between cellular ROS level and its cytotoxicity--a paradoxical issue in ROS-based cancer therapy. *Sci. Rep. 4*, 5029.
(106) Hall, A., Karplus, P. A., and Poole, L. B. (2009) Typical 2-Cys peroxiredoxins--structures, mechanisms and functions. *FEBS J. 276*, 2469–77.
(107) Berndt, C., Lillig, C. H., and Holmgren, A. (2008) Thioredoxins and glutaredoxins as facilitators of protein folding. *Biochim. Biophys. Acta - Mol. Cell Res. 1783*, 641–650.
(108) Sobhakumari, A., Love-Homan, L., Fletcher, E. V. M., Martin, S. M., Parsons, A. D., Spitz, D. R., Knudson, C. M., and Simons, A. L. (2012) Susceptibility of human head and neck cancer cells to combined inhibition of glutathione and thioredoxin metabolism. *PLoS One 7*, e48175.
(109) Marzano, C., Gandin, V., Folda, A., Scutari, G., Bindoli, A., and Rigobello, M. P. (2007) Inhibition of thioredoxin reductase by auranofin induces apoptosis in cisplatin-resistant human ovarian cancer cells. *Free Radic. Biol. Med. 42*, 872–881.
(110) Juarez, J. C., Betancourt, O., Pirie-Shepherd, S. R., Guan, X., Price, M. L., Shaw, D. E., Mazar, A. P., and Doñate, F. (2006) Copper binding by tetrathiomolybdate attenuates angiogenesis and tumor cell proliferation through the inhibition of superoxide dismutase 1. *Clin. Cancer Res. 12*, 4974–82.
(111) Juarez, J. C., Manuia, M., Burnett, M. E., Betancourt, O., Boivin, B., Shaw, D. E., Tonks, N. K., Mazar, A. P., and Doñate, F. (2008) Superoxide dismutase 1 (SOD1) is essential for H_2O_2-mediated oxidation and inactivation of phosphatases in growth factor signaling. *Proc. Natl. Acad. Sci. U. S. A. 105*, 7147–52.
(112) Glasauer, A., Sena, L. A., Diebold, L. P., Mazar, A. P., and Chandel, N. S. (2013) Targeting SOD1 reduces experimental non-small-cell lung cancer. *J. Clin. Invest.*
(113) Solis, L. M., Behrens, C., Dong, W., Suraokar, M., Ozburn, N. C., Moran, C. A., Corvalan, A. H., Biswal, S., Swisher, S. G., Bekele, B. N., Minna, J. D., Stewart, D. J., and Wistuba, I. I. (2010) Nrf2 and Keap1 abnormalities in non-small cell lung carcinoma and association with clinicopathologic features. *Clin. Cancer Res. 16*, 3743–53.
(114) Kansanen, E., Kuosmanen, S. M., Leinonen, H., and Levonen, A.-L. (2013) The Keap1-Nrf2 pathway: Mechanisms of activation and dysregulation in cancer. *Redox Biol. 1*, 45–9.
(115) Jaramillo, M. C., and Zhang, D. D. (2013) The emerging role of the Nrf2-Keap1 signaling pathway in cancer. *Genes Dev. 27*, 2179–91.
(116) Ma, Q., and He, X. (2012) Molecular basis of electrophilic and oxidative defense: promises and perils of Nrf2. *Pharmacol. Rev. 64*, 1055–81.
(117) Shim, G., Manandhar, S., Shin, D., Kim, T.-H., and Kwak, M.-K. (2009) Acquisition of doxorubicin resistance in ovarian carcinoma cells accompanies activation of the NRF2 pathway. *Free Radic. Biol. Med. 47*, 1619–31.
(118) DeNicola, G. M., Karreth, F. a, Humpton, T. J., Gopinathan, A., Wei, C., Frese, K., Mangal, D., Yu, K. H., Yeo, C. J., Calhoun, E. S., Scrimieri, F., Winter, J. M., Hruban, R. H., Iacobuzio-Donahue, C., Kern, S. E., Blair, I. a, and Tuveson, D. a. (2011) Oncogene-induced Nrf2 transcription promotes ROS detoxification and tumorigenesis. *Nature 475*, 106–9.
(119) Adams, D. J., Boskovic, Z. V, Theriault, J. R., Wang, A. J., Stern, A. M., Wagner, B. K., Shamji, A. F., and Schreiber, S. L. (2013) Discovery of small-molecule enhancers of reactive oxygen species that are nontoxic or cause genotype-selective cell death. *ACS Chem. Biol. 8*, 923–9.
(120) Adams, D. J., Dai, M., Pellegrino, G., Wagner, B. K., Stern, A. M., Shamji, A. F., and Schreiber, S. L. (2012) Synthesis, cellular evaluation, and mechanism of action of piperlongumine analogs. *Proc. Natl. Acad. Sci. U. S. A. 109*, 15115–20.
(121) Mishin, V., Gray, J. P., Heck, D. E., Laskin, D. L., and Laskin, J. D. (2010) Application of the Amplex red/horseradish peroxidase assay to measure hydrogen peroxide generation by recombinant microsomal enzymes. *Free Radic. Biol. Med. 48*, 1485–1491.

(122) Rhee, S. G., Chang, T.-S., Jeong, W., and Kang, D. (2010) Methods for detection and measurement of hydrogen peroxide inside and outside of cells. *Mol. Cells 29*, 539–49.
(123) Balce, D. R., and Yates, R. M. (2013) Redox-sensitive probes for the measurement of redox chemistries within phagosomes of macrophages and dendritic cells. *Redox Biol. 1*, 467–474.
(124) Winterbourn, C. C. (2014) The challenges of using fluorescent probes to detect and quantify specific reactive oxygen species in living cells. *Biochim. Biophys. Acta 1840*, 730–8.
(125) Tetz, L. M., Kamau, P. W., Cheng, A. A., Meeker, J. D., and Loch-Caruso, R. Troubleshooting the dichlorofluorescein assay to avoid artifacts in measurement of toxicant-stimulated cellular production of reactive oxidant species. *J. Pharmacol. Toxicol. Methods 67*, 56–60.
(126) Miller, E. W., Albers, A. E., Pralle, A., Isacoff, E. Y., and Chang, C. J. (2005) Boronate-based fluorescent probes for imaging cellular hydrogen peroxide. *J. Am. Chem. Soc. 127*, 16652–9.
(127) Malinouski, M., Zhou, Y., Belousov, V. V, Hatfield, D. L., and Gladyshev, V. N. (2011) Hydrogen peroxide probes directed to different cellular compartments. *PLoS One* (Kowaltowski, A. J., Ed.) *6*, e14564.
(128) Stone, J. R., and Yang, S. Hydrogen peroxide: a signaling messenger. *Antioxid. Redox Signal. 8*, 243–70.
(129) Meyer, A. J., and Dick, T. P. (2010) Fluorescent protein-based redox probes. *Antioxid. Redox Signal. 13*, 621–50.
(130) Lukyanov, K. a, and Belousov, V. V. (2014) Genetically encoded fluorescent redox sensors. *Biochim. Biophys. Acta 1840*, 745–56.
(131) Ezeriņa, D., Morgan, B., and Dick, T. P. (2014) Imaging dynamic redox processes with genetically encoded probes. *J. Mol. Cell. Cardiol. 73*, 43–9.
(132) Belousov, V. V, Fradkov, A. F., Lukyanov, K. A., Staroverov, D. B., Shakhbazov, K. S., Terskikh, A. V, and Lukyanov, S. (2006) Genetically encoded fluorescent indicator for intracellular hydrogen peroxide. *Nat. Methods 3*, 281–6.
(133) Mishina, N. M., Markvicheva, K. N., Bilan, D. S., Matlashov, M. E., Shirmanova, M. V, Liebl, D., Schultz, C., Lukyanov, S., and Belousov, V. V. (2013) Visualization of intracellular hydrogen peroxide with HyPer, a genetically encoded fluorescent probe. *Methods Enzymol.* 1st ed. Copyright © 2013 Elsevier, Inc. All rights reserved.
(134) Gutscher, M., Sobotta, M. C., Wabnitz, G. H., Ballikaya, S., Meyer, A. J., Samstag, Y., and Dick, T. P. (2009) Proximity-based protein thiol oxidation by H_2O_2-scavenging peroxidases. *J. Biol. Chem. 284*, 31532–40.
(135) Bilan, D. S., Pase, L., Joosen, L., Gorokhovatsky, A. Y., Ermakova, Y. G., Gadella, T. W. J., Grabher, C., Schultz, C., Lukyanov, S., and Belousov, V. V. (2013) HyPer-3: A Genetically Encoded H(2)O(2) Probe with Improved Performance for Ratiometric and Fluorescence Lifetime Imaging. *ACS Chem. Biol. 8*, 535–542.
(136) Roma, L. P., Duprez, J., Takahashi, H. K., Gilon, P., Wiederkehr, A., and Jonas, J.-C. (2012) Dynamic measurements of mitochondrial hydrogen peroxide concentration and glutathione redox state in rat pancreatic β-cells using ratiometric fluorescent proteins: confounding effects of pH with HyPer but not roGFP1. *Biochem. J. 441*, 971–8.
(137) Zielonka, J., Vasquez-Vivar, J., and Kalyanaraman, B. (2008) Detection of 2-hydroxyethidium in cellular systems: a unique marker product of superoxide and hydroethidine. *Nat. Protoc. 3*, 8–21.
(138) Zielonka, J., and Kalyanaraman, B. (2010) Hydroethidine- and MitoSOX-derived red fluorescence is not a reliable indicator of intracellular superoxide formation: Another inconvenient truth. *Free Radic. Biol. Med. 48*, 983–1001.
(139) Zhao, H., Kalivendi, S., Zhang, H., Joseph, J., Nithipatikom, K., Vásquez-Vivar, J., and Kalyanaraman, B. (2003) Superoxide reacts with hydroethidine but forms a fluorescent product that is distinctly different from ethidium: potential implications in intracellular fluorescence detection of superoxide. *Free Radic. Biol. Med. 34*, 1359–1368.
(140) Miller, E. W., Dickinson, B. C., and Chang, C. J. (2010) Aquaporin-3 mediates hydrogen peroxide uptake to regulate downstream intracellular signaling. *Proc. Natl. Acad. Sci. U. S. A. 107*, 15681–6.
(141) Sobotta, M. C., Barata, A. G., Schmidt, U., Mueller, S., Millonig, G., and Dick, T. P. (2013) Exposing cells to H_2O_2: a quantitative comparison between continuous low-dose and one-time high-dose treatments. *Free Radic. Biol. Med. 60*, 325–35.
(142) De Oliveira-Marques, V., Cyrne, L., Marinho, H. S., and Antunes, F. (2007) A quantitative study of NF-kappaB activation by H_2O_2: relevance in inflammation and synergy with TNF-alpha. *J. Immunol. 178*, 3893–902.
(143) Barbouti, A., Amorgianiotis, C., Kolettas, E., Kanavaros, P., and Galaris, D. (2007) Hydrogen peroxide inhibits caspase-dependent apoptosis by inactivating procaspase-9 in an iron-dependent manner. *Free Radic. Biol. Med. 43*, 1377–87.

(144) Mueller, S., Millonig, G., and Waite, G. N. (2009) The GOX/CAT system: a novel enzymatic method to independently control hydrogen peroxide and hypoxia in cell culture. *Adv. Med. Sci. 54*, 121–35.
(145) Kelley, E. E., Khoo, N. K. H., Hundley, N. J., Malik, U. Z., Freeman, B. A., and Tarpey, M. M. (2010) Hydrogen peroxide is the major oxidant product of xanthine oxidase. *Free Radic. Biol. Med. 48*, 493–8.
(146) Fisher, A. B. (2009) Redox signaling across cell membranes. *Antioxid. Redox Signal. 11*, 1349–56.
(147) Massey, V. (1973) Iron-Sulfur Flavoprotein Hydroxylases, in *Iron-Sulfur Proteins* (Lovenberg, W., Ed.) 1st ed., pp 301–85. Academic Press Inc., London.
(148) Mangino, M. E., and Brunner, J. R. (1977) Isolation and Partial Characterization of Xanthine Oxidase Associated with the Milk Fat Globule Membrane of Cows' Milk. *J. Dairy Sci. 60*, 841–850.
(149) Sawa, T., Wu, J., Akaike, T., and Maeda, H. (2000) Tumor-targeting Chemotherapy by a Xanthine Oxidase-Polymer Conjugate That Generates Oxygen-free Radicals in Tumor Tissue. *Cancer Res. 60*, 666–671.
(150) Van Stroe-Biezen, S. A. M., Janssen, A. P. M., and Janssen, L. J. J. (1994) A kinetic study of soluble glucose oxidase using a rotating-disc electrode. *Bioelectrochemistry Bioenerg. 33*, 55–60.
(151) Pollegioni, L., Langkau, B., Tischer, W., Ghisla, S., and Pilone, M. (1993) Kinetic mechanism of D-amino acid oxidases from Rhodotorula gracilis and Trigonopsis variabilis. *J. Biol. Chem. 268*, 13850–13857.
(152) Ryuichi, K., and Yosihiro, Y. (1992) d-Amino-Acid oxidase and its physiological function. *Int. J. Biochem. 24*, 519–524.
(153) Stegman, L. D., Zheng, H., Neal, E. R., Ben-Yoseph, O., Pollegioni, L., Pilone, M. S., and Ross, B. D. (1998) Induction of cytotoxic oxidative stress by D-alanine in brain tumor cells expressing Rhodotorula gracilis D-amino acid oxidase: a cancer gene therapy strategy. *Hum. Gene Ther. 9*, 185–93.
(154) Haskew-Layton, R. E., Payappilly, J. B., Smirnova, N. A., Ma, T. C., Chan, K. K., Murphy, T. H., Guo, H., Langley, B., Sultana, R., Butterfield, D. A., Santagata, S., Alldred, M. J., Gazaryan, I. G., Bell, G. W., Ginsberg, S. D., and Ratan, R. R. (2010) Controlled enzymatic production of astrocytic hydrogen peroxide protects neurons from oxidative stress via an Nrf2-independent pathway. *Proc. Natl. Acad. Sci. U. S. A. 107*, 17385–90.
(155) El Sayed, S. M., Abou El-Magd, R. M., Shishido, Y., Chung, S. P., Sakai, T., Watanabe, H., Kagami, S., and Fukui, K. (2012) D-amino acid oxidase gene therapy sensitizes glioma cells to the antiglycolytic effect of 3-bromopyruvate. *Cancer Gene Ther. 19*, 1–18.
(156) Matlashov, M. E., Belousov, V. V, and Enikolopov, G. (2014) How much H(2)O(2) is produced by recombinant D-amino acid oxidase in mammalian cells? *Antioxid. Redox Signal. 20*, 1039–44.
(157) Halvey, P. J., Hansen, J. M., Johnson, J. M., Go, Y.-M., Samali, A., and Jones, D. P. (2007) Selective oxidative stress in cell nuclei by nuclear-targeted D-amino acid oxidase. *Antioxid. Redox Signal. 9*, 807–16.
(158) Miller, E. W., Taulet, N., Onak, C. S., New, E. J., Lanselle, J. K., Smelick, G. S., and Chang, C. J. (2010) Light-activated regulation of cofilin dynamics using a photocaged hydrogen peroxide generator. *J. Am. Chem. Soc. 132*, 17071–3.
(159) Cheong, T.-C., Shin, E. P., Kwon, E.-K., Choi, J.-H., Wang, K.-K., Sharma, P., Choi, K. H., Lim, J.-M., Kim, H.-G., Oh, K., Jeon, J.-H., So, I., Kim, I.-G., Choi, M.-S., Kim, Y. K., Seong, S.-Y., Kim, Y.-R., and Cho, N.-H. (2014) Functional Manipulation of Dendritic Cells by Photoswitchable Generation of Intracellular Reactive Oxygen Species. *ACS Chem. Biol.*

Chapter 2: Quantifying intracellular hydrogen peroxide perturbations in terms of concentration

Molecular level, mechanistic understanding of the roles of reactive oxygen species (ROS) in a variety of pathological conditions is hindered by the difficulties associated with determining the concentration of various ROS species. Here, we present an approach that converts fold-change in the signal from an intracellular sensor of hydrogen peroxide into changes in absolute concentration. The method uses extracellular additions of peroxide and an improved biochemical measurement of the gradient between extracellular and intracellular peroxide concentrations to calibrate the intracellular sensor. By measuring peroxiredoxin activity, we found that this gradient is 650-fold rather than the 7-10-fold that is widely cited. The resulting calibration is important for understanding the mass-action kinetics of complex networks of redox reactions, and it enables meaningful characterization and comparison of outputs from endogenous peroxide generating tools and therapeutics across studies.

2.1 Introduction

Redox reactions underlie a number of signaling pathways within cells, causing a variety of observable cellular responses ranging from homeostasis to proliferation to death [1–4]. Understanding the molecular mechanisms that make one of these responses more likely than another is an active area of current research, and such an understanding has far-reaching practical significance since several pathological states are characterized by altered redox biology [5]. As one example of a class of pathological states, cancerous cells are thought to function in the presence of higher levels of oxidative species than noncancerous cells [6]. Redox therapeutics are

hypothesized to act by causing the intracellular oxidant level of cancer cells to rise above the upper limit that is compatible with survival [7–9]. For safety, it is important that the perturbation induced by the therapeutic stays within the limits of the defense networks of healthy cells [10]. This hypothesis and approach are inherently quantitative and success would depend on the magnitudes of the changes to oxidant levels in healthy and diseased cells and how the final levels relate to the threshold for survival. However, facile measurement of perturbations to the intracellular levels of oxidants in terms of concentration and as a function of time has been a long-standing challenge in the field.

Hydrogen peroxide is a particularly interesting oxidant because of its stability; its longer lifetime allows it to participate either as a secondary messenger molecule or a lethal oxidant [11]. Most phenotypic and signaling studies of cellular responses to peroxide are done using extracellular addition, either with a bolus or with sustained generation using glucose oxidase [12,13]. However, hydrogen peroxide has limited permeability across the plasma membrane [14]. When peroxide is added to the outside of cells, fast consumption by antioxidant enzymes inside the cell creates a gradient across the plasma membrane, making the intracellular concentration lower than the extracellular concentration. Antunes, et al. were the first to move from simply reporting external concentrations to estimating intracellular concentrations by building a compartmental model that estimates the gradient using experimentally determined kinetics of known antioxidants and of the hydrogen peroxide adsorption rate across the membrane [15]. A gradient of ~7- to 10-fold results from their analysis, meaning for a given extracellular concentration, the corresponding change to the intracellular concentration is about 7- to 10-fold lower. Using this method, changes to intracellular concentrations have been correlated with cellular responses indirectly by observing the effects of extracellular hydrogen peroxide perturbations [13,16].

However, since these publications appeared, other antioxidants have been discovered as important in scavenging hydrogen peroxide [17]. These were not included in the original kinetic calculations and therefore, depending on the magnitude of their contribution, the original gradient estimate may be lower than the actual gradient across the membrane, leading to incorrect intracellular associations for different phenotypes. Furthermore, the study of cellular response to hydrogen peroxide is shifting from using extracellular perturbation to endogenous generators, with the reasoning that endogenous generators better mimic physiological conditions during the action of drugs and for some disease states in terms of the location and kinetics of peroxide generation [12,18–20]. It is currently difficult to assess the hydrogen peroxide concentrations generated by these endogenous tools.

To address this need, we developed a quantification approach, demonstrated here as we correlate fold-change in signal from a genetically encoded peroxide sensor to change in intracellular concentration. HyPer, the particular probe used herein, is derived from the OxyR transcription factor found in bacteria with YFP inserted between two reactive thiol groups to provide a fluorescent readout of OxyR's oxidation state [21]. The sensor is expressed by the cell and emits a ratiometric fluorescence change upon reaction with hydrogen peroxide only; it is unresponsive to other oxidants. Unlike the readouts in other intracellular peroxide sensing strategies [22], the signal of HyPer is reversible due to the activity of intracellular reductases, and this feature allows peroxide to be monitored as a function of time. To convert fold-change in HyPer's signal to a change in absolute intracellular concentration, we first added various known amounts of peroxide to the outside of HeLa cells expressing HyPer and measured the resulting fluorescence using methodology established in previous work [23]. Then, we modified the compartmental model from Antunes, et al. to include peroxiredoxin, and devised methodology for experimentally

determining the kinetic parameters required for calculation of an improved peroxide gradient across the plasma membrane. Using the new gradient, we are able to interpret changes in HyPer fluorescence resulting from the known, external bolus additions in terms of absolute intracellular concentration (Fig 2.1a), and the resulting calibration accomplished using extracellular addition of peroxide can be then used to quantify peroxide produced by intracellular generators.

2.2 Methods and Materials

Materials

Hydrogen peroxide, horseradish peroxidase (HRP), neomycin, penicillin-streptomycin, glucose oxidase, catalase, L-glutathione, glutathione reductase, digitonin, triton X-100, were purchased from Sigma (St. Louis, MS, USA). 2, 2'-Azino-bis(3-ethylbenzothiazoline-6-sulfonic acid) diammonium salt (ABTS) was purchased from Tokyo Chemical Industry Co (Portland, OR, USA). D(+)-Glucose was purchased from Macron Fine Chemicals (Center Valley, PA, USA). NADPH was purchased from Roche (Basel, Switzerland). HeLa cells were a gift from the Wittrup Lab at MIT (Cambridge, MA, USA). The Modified Eagle's medium (EMEM) and fetal bovine serum were purchased from ATCC (Manassas, VA, USA). Trypsin was purchased from Lonza (Walkerville, MD, USA). Lipofectamine 2000 was purchased from Invitrogen (Carlsbad, CA, USA). A plasmid encoding HyPer-cyto plasmid was purchased from Evrogen (Moscow, Russia). Q HP FF, Phenyl HP and Superdex75 FPLC purification columns were purchased from GE Healthcare (Fairfield, CT, USA). Other common chemicals to make buffer solutions were purchased from VWR International (USA).

Cell culture and transfection

HeLa cells were cultured in EMEM with 10% FBS at 37°C, 95% air and 5% CO_2. A stable cell line of HeLa cells expressing HyPer was created by transfecting HeLa cells with a mixture of plasmid DNA and Lipofectamine for 24 hours, and a single colony was gradually selected over a period of six weeks using neomycin at 1 mg/mL. The plasmid was maintained in the cell with neomycin at 0.2 mg/mL.

Fluorescence spectroscopy for HyPer readings in intact HeLa cells

HeLa cells expressing HyPer were trypsinized, washed once in phosphate buffer saline (PBS), pH 7.4 and re-suspended in the same buffer at a concentration of 250,000 cells/mL. Excitation spectra of HyPer expressed in cells were recorded using a Tecan M200 microplate reader with excitation at 410-510 nm, 9 nm bandwidth, and emission at 545 nm, 20 nm bandwidth. A baseline excitation spectrum was taken, then a bolus of hydrogen peroxide was added to the suspension and kinetics were followed for a period of 10 minutes. HyPer's ratiometric fluorescent response was obtained by dividing the emission reading for excitation at 500 nm by the emission reading for excitation at 420 nm, then dividing the peak of the ratiometric fluorescence by the baseline to obtain a fold change. The fold change data is normalized to a control case where no hydrogen peroxide was added to the system (i.e. an equal volume of buffer only was added).

Consumption of hydrogen peroxide by intact HeLa cells

HeLa cells containing HyPer were grown in 10 cm BD Falcon dishes (VWR International, USA) until confluent. The cells were trypinized, washed once in PBS, pH 7.4, and re-suspended in PBS with 2 g/L D-glucose at a concentration of 10^6 cells/mL, 10 mL total. A bolus of hydrogen peroxide was then mixed into the dish, making it a total of 80-100 μM in cell suspension. Every

two minutes, a 200 μL sample of the cell suspension was inactivated with 13 μL 5 N HCl to prevent further antioxidant scavenging. The samples were incubated for 10 minutes in HCl, then centrifuged at 14,000 x ***g***. 160 μL of the supernatant was removed, mixed with 70 μL of 1 M Kpi (pH 8.0), followed by 50 μL of 2.5 mM of 2,2'-azino-bis(3-ethylbenzothiazoline-6-sulphonic acid) (ABTS) solution and 10 μL of 3 mg/mL horse-radish peroxidase. The samples were read at an absorbance wavelength of 405 nm. A standard curve between 0 μM and 50 μM for hydrogen peroxide was done with each set of data.

Exposure of HeLa cells to steady state levels of hydrogen peroxide

If the first order rate constant of hydrogen peroxide consumption by intact HeLa cells is correct, then we can do a steady state balance between the consumption of hydrogen peroxide and the generation of hydrogen peroxide by a glucose oxidase system [13]. Glucose oxidase was diluted in PBS (pH 7.4) with 2 g/L D(+)-glucose to concentrations of ~5 mU/mL. The rate of hydrogen peroxide generation for the diluted stock was determined using the ABTS assay. Then, 10 μM of hydrogen peroxide mixed with 0.8 million cells/mL and an appropriate amount of glucose oxidase (generates 2.8 μM hydrogen peroxide/min) in the PBS + glucose solution, and the concentration of hydrogen peroxide outside the cell was measured for a period of 60 minutes using the ABTS assay.

Consumption of hydrogen peroxide by catalase

Trypinized HeLa cells expressing HyPer (10^6 cells/mL) were lysed by re-suspending the cells in 50 mM potassium phosphate buffer (pH 7.4) containing digitonin. Digitonin concentration was varied from 0.01 to 1 mg/mL. For each lysate sample, hydrogen peroxide depletion was measured in the presence of 10 mM hydrogen peroxide and kinetics were followed at 37°C for 5

minutes at 240 nm (extinction coefficient 43.6 $M^{-1}cm^{-1}$). At digitonin concentrations of less 0.1 mg/mL, only the plasma membrane was affected, yielding depletion kinetics due to catalase acting on H_2O_2 that diffused across an intact peroxisomal membrane.

Consumption of hydrogen peroxide by glutathione peroxidase

HyPer HeLa cells expressing HyPer (5million cells/mL) were lysed in 50 mM potassium phosphate (pH 7.4), 1mM DPTA buffer containing 0.1% Triton solution. The lysate mixture was then pre-incubated at 37°C with a range of 1 to 3 mM of GSH, 1.1 U/mL glutathione reductase, 0.3 mM NADPH and 1 mM NaN_3 to reduce any oxidized GPx for 10 minutes. Then, a bolus of 35 μM hydrogen peroxide was added to the mixture and NADPH depletion at 340 nm (extinction coefficient 6.22 $mM^{-1}cm^{-1}$) was followed for a period of 5 minutes. For kinetic analysis, the part of the curve corresponding to 2 to 15 μM hydrogen peroxide remaining was used for fitting to the integrated rate equation shown below:

$$\frac{t-t_0}{[H_2O_2]_0-[H_2O_2]_t} = \frac{\frac{1}{k_2'}+\frac{1}{k_3'}}{GPx_{total}[GSH]} + \frac{1}{k_1'*GPx_{total}}\left(\frac{Ln\left(\frac{[H_2O_2]_0}{[H_2O_2]_t}\right)}{[H_2O_2]_0-[H_2O_2]_t}\right)$$

where t is the time since the addition of a bolus of hydrogen peroxide to the lysate system, k_1', k_2', k_3' are rate constants associated with GPx redox reaction as indicated in SI, and $[GPx]_{total}$ is the total concentration of GPx enzyme. $k_{Gpx} = k_1' * [GPx]_{total}$ and was obtained by the inverse slope of linear fitting $\left(\frac{Ln\left(\frac{[H_2O_2]_0}{[H_2O_2]_t}\right)}{[H_2O_2]_0-[H_2O_2]_t}\right)$ *to* $\frac{t-t_0}{[H_2O_2]_0-[H_2O_2]_t}$.

Consumption of hydrogen peroxide by 2-cys Peroxiredoxin

HeLa cells expressing HyPer (5.8 million/mL) were lysed in 20 mM Hepes (pH 7.4), 1 mM EDTA buffer containing 0.1% Triton solution. The lysate mixture was pre-incubated at 37°C

with a range of 20-50 μM yeast Trx, 2 μM yeast TrxR, 0.4 mM NADPH and 1 mM NaN_3 for a period of 10 minutes. Then, a bolus of hydrogen peroxide between 20 to 25 μM was added to the mixture and NADPH depletion was followed by monitoring absorbance at 340 nm (extinction coefficient 6.22 $mM^{-1}cm^{-1}$) for a period of 5 minutes. For kinetic analysis, the experimental data was fitted to a model simulation using root-mean square deviation and the pseudo first order rate constant k_{prx} was extracted.

Purification of yeast-thioredoxin and thioredoxin-reductase

Plasmids for yeast Trx/TrxR (pET17b-yTrx1 and pET17b0yTrxR) were a gift from Dr. Sang Won Kang (Ewha Woman's University, Seoul, Korea) [24]. To purify the recombinant proteins, E.coli BL21 (DE3) transformed with the plasmids were was grown until OD 0.6 (λ=600 nm) in 250mL of Terrific Broth, at which point expression was induced by addition of 1 mM isopropyl-1-thio-B-d-galatoside (IPTG), cells are harvest after shaking for 4 hours at 250 rpm. The cells are lysed, on ice, for 20 minutes, 1 min interval in 10 mL of buffers specified in [24], then spun at 12,000 x ***g*** for 15 minutes. The supernatant was filtered through a 0.22 μm Acrodisc Syringe Filter (Pall Corporation, USA). For TrxR, the crude extract was loaded onto a Q HP fast-flow anionic exchange FPLC column. The protein was eluted with a linear gradient of 0-500 mM NaCl in 20 mM Tris-HCl (pH 7.5), and the fraction containing yTrxR protein was verified through SDS-PAGE gel and used for a subsequent purification. After dialyzing the fraction against 20 mM Hepes-NaOH (pH 7.0), the protein was equilibrated with 1M ammonium sulfate (pH 7.0) and loaded onto a Phenyl HP FPLC column. The protein of interest came out in the flow-through before the elution step, and the pool of purified proteins were dialyzed against buffer containing 20 mM Hepes (pH 7.4) and stored at -70C until required. For Trx, the crude extract was heat-treated for 30min at 75°C and centrifuged to remove denatured protein. The

soluble supernatant was loaded onto the Q-HP fast flow anionic exchange and eluted with the same linear NaCl gradient as TrxR. The fractions containing Trx were then loaded onto Superdex 75 gel filtration column equilibrated with 20 mM Tris-HCl, 1mM EDTA and 150 mM NaCl (pH 7.0). Protein purities for both Trx/TrxR were confirmed through SDS-Page gel and UV spectra (Appendix). The reducing potential of yTrxR was measured by pre-oxidizing yTrx with equimolar hydrogen peroxide for 10 minutes, then incubating with yTrxR and NADPH to measure the reduction kinetics [24]. An activity of 2.4 ± 0.3 μmol/min/mg was found, indicating active yTrxR was produced that couples with the yTrx redox state.

Statistical analysis

For kinetics analyses at least three technical replicates and two biological replicates were performed for each rate constant. The experimental values are reported as the mean ± standard error of mean (SEM). For the HyPer standard curve, the data points represent the mean over 4 trials (2 technical and 2 biological replicates), and the error bars are the 95% confidence intervals.

To determine k_{prx}, a parameter sweep from 0.1 to 100, step size 0.1 was performed using Matlab2013, and for each value of k_{prx}, the root mean square deviation (RMSD) is calculated between the simulation kinetic curve and the experimental kinetic curve. The k_{prx} value that gives the minimum of the RMSD function is the estimated k_{prx}. This fitting was performed for various Trx and hydrogen peroxide concentrations, and the overall k_{prx} reported is the mean from all of the fittings.

$$\text{RMSD} = \sqrt{\frac{\sum_1^n (x^s - x^e)^2}{n}}$$

where n is the number of data points, x^s is the value of the simulation data, and x^e is the value of the experimental data.

2.3 Results

2.3.1 Determining the hydrogen peroxide gradient across the HeLa biomembrane

We determined the peroxide gradient across the HeLa biomembrane by adapting Antunes' model (Fig 2.1b). Since intracellular concentrations of hydrogen peroxide are generally thought to be sub-micromolar, most of the antioxidant pool is expected to exist in the reduced form, resulting in a pseudo-first order reaction [15,25,26]. Thus, at equilibrium, the rate of absorption of hydrogen peroxide across the plasma membrane will equal the rate of consumption of hydrogen peroxide by the antioxidants inside the cell:

$$k_{intact}[H_2O_2]_{outside} = k_{antioxidants}[H_2O_2]_{cell} \quad (1)$$

where k_{intact} is the pseudo-first order rate constant for absorption of peroxide across the membrane of intact cells and $k_{antioxidants}$ is the sum of pseudo first-order rate constants for all intracellular antioxidants. Re-arranging these terms yields an equation for the gradient, R, across the plasma membrane.

$$\frac{[H_2O_2]_{outside}}{[H_2O_2]_{cell}} = \frac{k_{antioxidants}}{k_{intact}} = R \quad (2)$$

This gradient is independent of peroxide concentration and is only dependent on the first order rate constants of hydrogen peroxide adsorption by the intact cell and by the intracellular antioxidants.

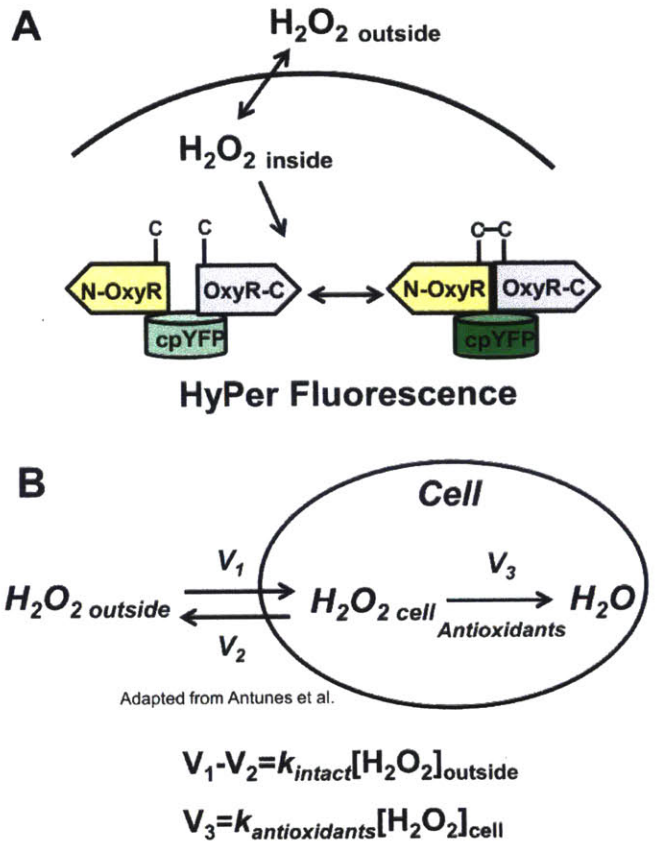

Figure 2.1: Schematics for quantification assay and gradient measurement. *(A)* Schematic of a quantification assay for hydrogen peroxide. We measured the gradient of hydrogen peroxide across the plasma membrane of HeLa cells and the fluorescent response of a genetically encoded sensor, HyPer, to known added amounts of extracellular peroxide. Knowledge of the gradient provides a correlation between intracellular concentration and HyPer fold change. *(B)* Kinetic model of hydrogen peroxide absorption across the plasma membrane and scavenging within the cell. A gradient is established across the plasma membrane due to the rapid consumption of hydrogen peroxide by intracellular antioxidants. The magnitude of this gradient depends on the relative value of the rate constant for intracellular consumption ($k_{antioxidants}$) and the rate constant for transport across the membrane (k_{intact})

The pseudo first order rate constants for the rate of adsorption of hydrogen peroxide across the plasma membrane (k_{intact}) and consumption by antioxidants catalase ($k_{catalase}$) and glutathione peroxidase (k_{GPx}) in the cytoplasm were determined using methodology similar to that outlined in [15]. To determine k_{intact}, we tracked the extracellular concentration of hydrogen peroxide as a function of time using an absorbance-based horseradish peroxidase assay in place of an oxygen electrode, and we verified the value using steady state generation of peroxide by an extracellular glucose oxidase system (Appendix). $k_{catalase}$ and k_{GPx} were determined using the experimental protocol and data analysis methods of the original Antunes paper. We found a k_{intact} *of 5.9±0.2*

$x10^{-12}$ $s^{-1}cell^{-1}L$ (N=6), $k_{catalase}$ of $8.5 \pm 0.3\ x10^{-13}$ $s^{-1}cell^{-1}L$ *(N=8)* and a k_{GPx} $3.4 \pm 0.08\ x10^{-11}$ s^{-1} $s^{-1}cell^{-1}L$ *(N=12)* (Fig 2.2).

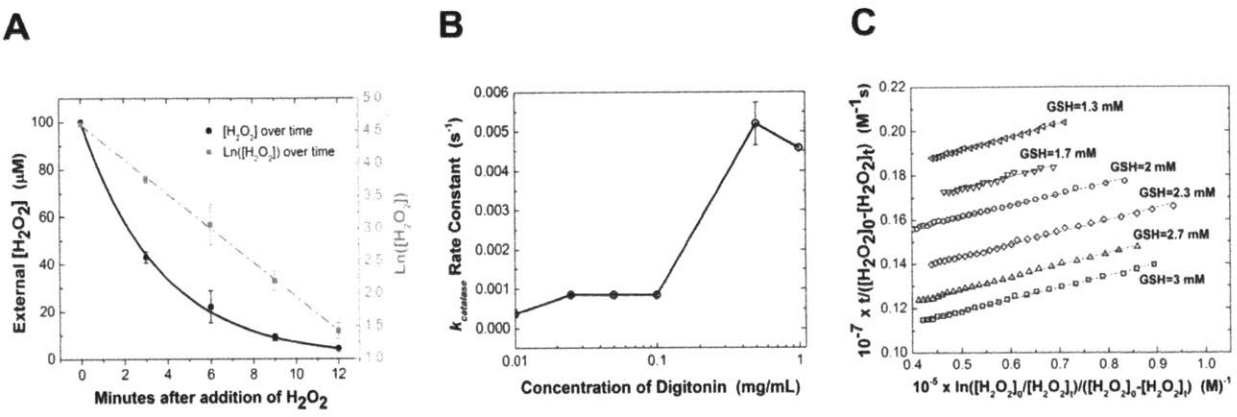

Figure 2.2: Finding k_{intact}, $k_{catalase}$ and k_{GPx} *(A)* Finding k_{intact}. The rate constant of hydrogen peroxide diffusion across the membrane was determined by adding hydrogen peroxide to a suspension of HeLa cells and measuring the extracellular concentration of peroxide using 2,2'-azino-bis(3-ethylbenzothiazoline-6-sulphonic acid) (ABTS) absorbance based assay. *(B)* Finding $k_{catalase}$. HeLa cells were permeabilized with increasing concentrations of digitonin and lysates were incubated with 10 mM H_2O_2. Depletion of peroxide was measured at 240 nm and the first order rate constant was determined. The plateau before the rise in kinetic activity indicates conditions where the peroxisome is not disrupted. *(C)* Finding k_{GPx}. HeLa cells lysed with 0.1% Triton were incubated with 1.3 mM to 3 mM of GSH, 1.1 U/mL of glutathione reductase, 1 mM NaN_3, 0.3 mM NADPH and 35 μM hydrogen peroxide. NADPH depletion, as an indicator of hydrogen peroxide depletion, was measured at 340nm. Hydrogen peroxide depletion kinetics between 2-15 μM were then fitted to an integrated rate equation and k_{GPx} was determined.

Since the time of Antunes' widely cited gradient estimations, a class of antioxidants called peroxiredoxins (Prx) has been hypothesized to play a major role in scavenging hydrogen peroxide in mammalian cells. Though pseudo-first order rate constants are not yet available in the literature, second order oxidation rate constants the same order of magnitude as that of glutathione peroxidase (GPx) have been reported for purified 2-cysteine forms of the protein [17,27]. The 2-cysteine Prx (2-cys-Prx) that react with peroxide are largely localized in the cytoplasm, and in HeLa cells, cytoplasmic Prx I and II account for over 90% of these isoforms found throughout the cell [28]. Following reaction with peroxide, thioredoxins are responsible for returning oxidized form of Prx to its reduced state. We believe that the contribution of this class of antioxidants cannot be ignored in determining the gradient across the plasma membrane.

One interesting and potentially complicating feature of 2-cys-Prx is that the redox active thiol group can be hyper-oxidized to sulfinic or sulfonic acid groups under sufficient hydrogen peroxide concentrations, rendering it inactive. These species are then very slowly reduced to -SOH by sulfiredoxins (Fig 2.3a) [29]. However, hyper-oxidation of 2-cys-Prx has been detected only for cells exposed to high concentrations of extracellular hydrogen peroxide (>100 μM) and is generally not detected during hydrogen peroxide mediated signaling events [26,30,31]. Below the hyper-oxidation detection threshold, the abundant thioredoxin system in most cell lines rapidly recycles any oxidized 2-cys-Prx, so we can approximate that the majority of the active cytoplasmic 2-cys Prxs are in the reduced form [26,32]. Thus under most *in vivo* hydrogen peroxide conditions, the Prx scavenging activity can be estimated as pseudo first order, where the rate constant k_{prx} is a function of the second-order rate constant of the oxidation step, and the total active intracellular 2-cys-Prx concentration, $[Prx_{active}]$.

The reaction scheme of 2-cys Prx oxidation, hyperoxidation and reduction is shown below:

$$H_2O_2 + Prx-(SH)_2 + H^+ \xrightarrow{k_1} Prx-(SOH) + H_2O \quad (3)$$

$$Prx-SOH \xrightarrow{k_2} Prx-(SS) + H_2O \quad (4)$$

or

$$H_2O_2 + Prx-(SOH) + H^+ \xrightarrow{k_3} Prx-(SO_2H) + H_2O \quad (5)$$

$$Prx-(SO_2H) \xrightarrow{k_4} Prx-SOH + H^+ + H_2O \quad (6)$$

$$Prx-(SS) + Trx_{red} \xrightarrow{k_5} Prx-(SH)_2 + Trx_{Ox} \quad (7)$$

$$Trx_{Ox} + NADPH \xrightarrow{k_6} NADP^+ + Trx_{red} + H^+ \quad (8)$$

Writing these reactions as ordinary differential equations yield:

$$\frac{\partial[H_2O_2]}{\partial t} = -k_1[H_2O_2][Prx_{reduced}] - k_3[H_2O_2][Prx-(SOH)] \quad (9)$$

$$\frac{\partial[Prx_{reduced}]}{\partial t} = -k_1[H_2O_2][Prx_{reduced}] + k_5[Prx-SS][Trx_{reduced}] \quad (10)$$

$$\frac{\partial[\text{Prx}-\text{SOH}]}{\partial t} = k_1[H_2O_2][Prx_{reduced}] - k_3[H_2O_2][Prx-(SOH)] - k_2[Prx-(SOH)] + k_4[\text{Prx}-(\text{SO}_2\text{H})] \quad (11)$$

$$\frac{\partial[\text{Prx}-(\text{SO}_2\text{H})]}{\partial t} = k_3[H_2O_2][Prx-(SOH)] - k_4[\text{Prx}-(\text{SO}_2\text{H})] \quad (12)$$

$$\frac{\partial[\text{Prx}-\text{SS}]}{\partial t} = k_2[Prx-(SOH)] - k_5[Prx-SS][Trx_{reduced}] \quad (13)$$

$$\frac{\partial[Trx_{reduced}]}{\partial t} = -k_5[Prx-SS][Trx_{reduced}] + k_6[Trx_{Ox}][NADPH] \quad (14)$$

$$\frac{\partial[Trx_{ox}]}{\partial t} = k_5[Prx-SS][Trx_{reduced}] - k_6[Trx_{Ox}][NADPH] \quad (15)$$

We added known initial concentrations of hydrogen peroxide and excess thioredoxin/thioredoxin reductase to reduce the 2-cys Prx present in lysates of HeLa cells, and tracked the hydrogen peroxide depletion via NADPH consumption. To determine k_{prx}, we extracted the value of k_1*[$\text{Prx}_{\text{active}}$] from our kinetic data of peroxide concentration as a function of time. We did so by fitting the experimental kinetic data to a simulation of the experimental system, built from the system of ODEs above with the appropriate rate constants and initial conditions (Equations 9-15, SI) [17,24,33–35]. Fitting using a root-mean square deviation method, we found a k_{prx} of $3.8 \pm 0.03 \times 10^{-9}\ s^{-1}cell^{-1}L$ *(N=6),* meaning 2-cys-Prx scavenges peroxide 100 times faster than GPx under most physiological conditions (Fig 2.3b). As shown in the appendix, it is important to consider hyper-oxidation effects for our experimental set-up since we added a significant peroxide bolus to cell lysate in order to get a measurable kinetic curve.

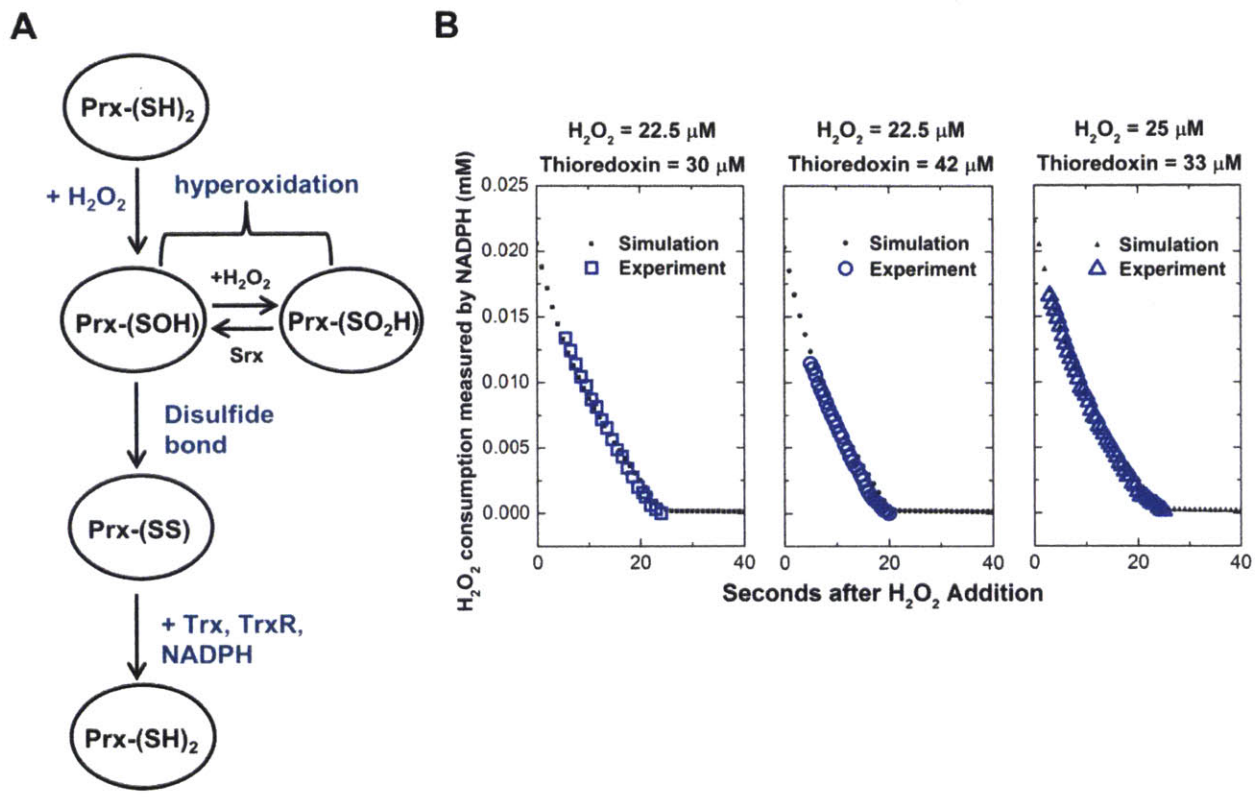

Figure 2.3: Measuring k_{Prx} using a combination of simulation and experimental fitting. *(A)* Schematic of 2-cys peroxiredoxin oxidation and reduction cycle through reactions with hydrogen peroxide and thioredoxin. Peroxide oxidizes 2-cys Prx to form Prx-SOH. Prx-SOH can then either react with a second hydrogen peroxide to form a hyper-oxidized state, or it can interact with another Prx to form a disulfide bond, which can then be reduced through the thioredoxin/thioredoxin reductase system. *(B)* Finding k_{Prx}. HeLa cells lysed with 0.1% Triton were incubated with 30 μM-50 μM yTrx, 2 μM of yTrxR, 1 mM NaN_3, 0.3 mM NADPH and 20-25 μM hydrogen peroxide. NADPH depletion, as an indicator of hydrogen peroxide depletion, was measured at 340nm. The kinetic data were then fitted by minimizing the root mean square deviation to a simulated model of the experimental system. The rate constant k_{Prx} was determined for several peroxide and thioredoxin (Trx) concentrations. For the case of hydrogen peroxide=22.5 μM and Trx=30 μM, we obtained a k_{Prx} value of 3.7×10^{-9} $s^{-1}cell^{-1}L$ (N=2). For hydrogen peroxide=22.5 μM and Trx=42 μM, k_{Prx} was 3.8×10^{-9} $s^{-1}cell^{-1}L$ (N=2), and with hydrogen peroxide=25 μM and Trx=33 μM, k_{Prx} was 3.9×10^{-9} $s^{-1}cell^{-1}L$ *(N=2)*. The k_{Prx} value reported in the text is the average of all six trials.

Substituting the pseudo first order rate constants for intact cells and for the various antioxidants into Equation 2, we obtain a gradient of ~650 fold across the plasma membrane. This value is significantly higher than the gradient of 7- to 10- fold calculated by Antunes et al., and we note that the inclusion of 2-cys-Prx in our calculations is crucial in obtaining the higher value. Typical, non-pathogenic intracellular H_2O_2 perturbations have been given as between 1 to 700 nM [36]. This widely cited information is based on the gradient calculated by Antunes et al, combined with data in a subsequent paper showing that a steady concentration of less than 5 μM

extracellular hydrogen peroxide does not affect Jurkat cell morphology, but a concentration above this threshold causes these cells to undergo apoptosis [16]. Our new gradient suggests that the perturbation to the average intracellular concentration before the onset of cell death is less than 7.5 nM, and for perturbations between 7.5 nM and 10.5 nM, induction of apoptosis would be expected. Thus, changes to the level of intracellular hydrogen peroxide that lead to the onset of apoptosis appear to be in the low nanomolar range.

2.3.2 Quantifying Intracellular [H_2O_2] with HyPer and the H_2O_2 Membrane Gradient

With the improved membrane gradient, we now demonstrate a quantitative approach to calibrate the HyPer sensor such that we can translate its signal output into a change in concentration. We made a standard curve that relates HyPer signals to extracellular peroxide concentrations by adding known boluses of hydrogen peroxide to a suspension of HeLa cells expressing HyPer. We followed the kinetics of HyPer fluorescence over a period of 10 minutes and extracted the peak ratiometric fluorescence for each bolus addition, and divided that ratio by the baseline ratiometric fluorescence to obtain a fold-change in HyPer response. To account for potential pH effects, buffer without hydrogen peroxide was added to an identical sample of HeLa cells, and fold-change for every hydrogen peroxide bolus is normalized to this control case. The intracellular sensor responded dynamically to 2 to7 μM of hydrogen peroxide added externally to a suspension containing $2.5x10^5$ cells/mL (Fig 2.4). Using our experimentally determined hydrogen peroxide gradient, we can calculate the corresponding intracellular peroxide change for each different external hydrogen peroxide concentration added. This analysis suggests HyPer responds to 3 to 10 nM changes in intracellular peroxide concentrations (Fig 2.4). Now, independent of the method of hydrogen peroxide perturbation, we can measure the intracellular

fold-change in HyPer signal and use the standard curve in Fig. 4 to determine the change in terms of an absolute concentration.

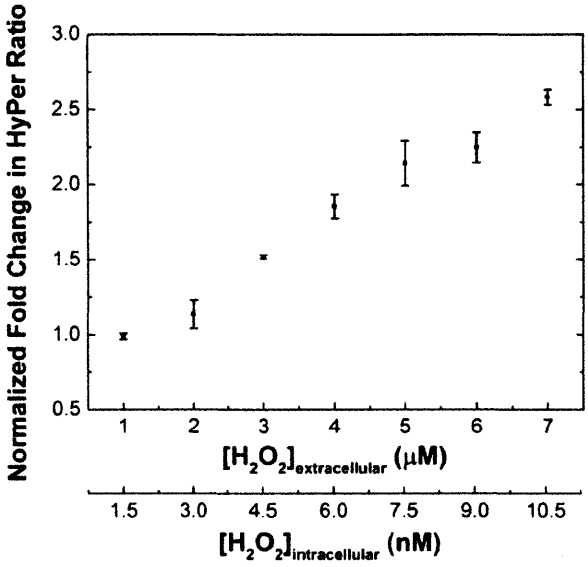

Figure 2.4: Calibrating HyPer's ratiometric fluorescent response to hydrogen peroxide. The excitation spectra of cell suspensions containing $2.5x10^5$ cells/mL treated with 0-7 μM hydrogen peroxide were measured at 2-minute intervals with excitation from 410 nm-510 nm and emission monitored at 545 nm. The peak of the response was noted. Ratiometric responses (500nm/420nm) were calculated at the peak. This ratio was divided by the baseline ratio before addition of hydrogen peroxide, and normalized to the case where an equal amount of buffer without hydrogen peroxide was added to obtain the normalized fold change values. The error bars for each data point represent 95% confidence intervals. In order to determine the corresponding intracellular hydrogen peroxide concentration for each HyPer response, the extracellular concentration is divided by 650, the estimated gradient of hydrogen peroxide across the plasma membrane.

2.4 Discussion and Conclusion

Peroxiredoxins have been proposed as the dominant hydrogen peroxide elimination enzyme in mammalian cells, and our experimental results support this hypothesis as we found that the pseudo first-order rate constant for the oxidation of Prx by hydrogen peroxide is about 100 times faster than that of GPx. This finding suggests that antioxidant-based therapeutics should focus on targeting Prx isoforms and their reduction partners, thioredoxin and glutathione. Another implication of peroxiredoxin activity is the much higher hydrogen peroxide gradient we

measured across the plasma membrane. The new gradient estimates the switch between non-pathological to pathological perturbations to the intracellular concentration of peroxide to be in the low nanomolar range. This lower intracellular concentration means that the rate of cytoplasmic hydrogen peroxide reacting with a protein thiol is even slower than previously thought. Direct action of hydrogen peroxide on its target may require very close proximity of the target to the source of generation, as suggested by the flood-gate model [27,31,37]. Another possibility is that hydrogen peroxide acts on the downstream signaling targets in an indirect manner, through oxidation of more abundant Prx/Gpx antioxidants or conversion to a more reactive radical species such as hydroxyl radical [1,30,38]. Improving our quantitative understanding of these concentration parameters can establish more powerful mathematical models of biological redox systems. Specifically, knowledge of actual intracellular concentrations is important for allowing evaluation of the likelihood of mass-action interactions of various oxidants with their supposed targets, yielding better predictions of fundamental redox processes. Furthermore, concentrations associated with phenotypic responses establish design criteria for future ROS-therapeutics as to how much of a perturbation to the intracellular hydrogen peroxide level is needed to switch from proliferation to apoptosis or another mechanism of cell death [6,7].

Our calibration of an intracellular peroxide sensor using a gradient measurement is an important advance that supports and parallels the development of physiologically relevant intracellular ROS-generators. The gradient can be used for intracellular quantification with a known amount of exogenous addition, but it alone cannot give any concentration information for intracellular generator tools. For this task, an intracellular sensor must be paired with knowledge of the gradient. As Fig. 2.4 indicates, the response of HyPer to hydrogen peroxide, like that of many popular redox sensors, is non-linear [22]. As a result, it is difficult to interpret the common

approach of reporting sensor signal as fold-change, since an increase in signal between a 1.5x-fold change and a 2x-fold change, versus a 2x-fold change and a 2.5x-fold change are not necessary the same. The calibration approach detailed herein will be important in providing real-time verification, visualization and quantification of the perturbations produced by intracellular peroxide generators.

Accuracy in measuring perturbations to the intracellular peroxide concentration depends in part on the choice of sensor. We chose HyPer to demonstrate our quantification approach because it is an intracellular sensor specific for peroxide, and it is reversible and ratio-metric [23]. These characteristics offer an advantage over the dye-based sensors such as DCFH or PG-1 since HyPer measures real-time concentrations rather than a cumulative effect [39], and HyPer provides greater specificity and sensitivity than other fluorescent genetically-encoded sensors such as roGFP [40]. However, using the sensor is not without its caveats. First, the probe is pH sensitive, so proper controls are required to ensure the results are not artifacts of the external environment [41]. We addressed this issue by including a control where buffer without hydrogen peroxide was added to a suspension of HeLa cells, and fold-change for every hydrogen peroxide bolus was normalized to this control case. Secondly, the OxyR domain has a second order rate constant of 10^5 M^{-1} s^{-1} with hydrogen peroxide [42], while 2-cys Prx interacts with hydrogen peroxide with a second order rate constant of 10^7 M^{-1} s^{-1}. Thus, in the kinetic competition for reaction with intracellular peroxide, HyPer does not effectively compete with Prx. It follows that in lining up our standard curve with the results of the biochemical gradient measurement, we are slightly over-estimating the intracellular concentration of hydrogen peroxide for each HyPer fold-change. We should note that our quantitative approach generalizes to probes other than HyPer, and

accuracy and responsive regions will improve as improved hydrogen peroxide sensors are developed.

The accuracy of this quantification is also dependent on the accuracy of the gradient across the plasma membrane. In fitting our kinetic data for cytoplasmic 2-cys-Prx activity in HeLa cells, where Prx I and II are predominant, we were able to obtain second order rate constants for Prx II but not for Prx I for use in our numerical model. Thus, our experimental data is an average activity of both Prx isoforms in the cytoplasm, but our theoretical fit assumes Prx I have the same rate constants as Prx II. It has been observed that Prx I is less susceptible to hyper-oxidation than Prx II, and is rather inactivated by phosphorylation, however these kinetic rates are unknown and so could not be included in our model [31]. In addition, a recent kinetic model suggests the inclusion of an inhibitor of Prx II as a plausible way to obtain the correct oxidation/reduction kinetics for the antioxidant in red blood cells, and this modeling approach predicts that only a small fraction of the total Prx II protein is active in these cells [43]. Since our kinetic experiments are done under dilute, lysed cell conditions, it is possible that any inhibitor function may be disrupted under these experimental conditions and we over-estimate the concentration of active Prx II. The identity of molecular species that may act as inhibitors and whether this theory applies in HeLa cells remain open questions. Finally, discovery of new antioxidants and targets that react with hydrogen peroxide at a rate similar to that of Prx would further increase the value of the gradient. The model and analysis can easily be updated as more information becomes available. It should be noted that the current calculation as it stands is already a vast improvement over the previous gradient measurement. A combined effort of intracellular quantification and generation tools will allow physiologically relevant and systematic studies of the role of hydrogen peroxide in determining cellular phenotypes. In

addition to promoting fundamental, mechanistic understanding of human redox biology, such studies hold promise for determining quantitative design criteria for future ROS-based therapeutics.

2.5 Bibliography

(1) D'Autréaux, B., and Toledano, M. B. (2007) ROS as signalling molecules: mechanisms that generate specificity in ROS homeostasis. *Nat. Rev. Mol. Cell Biol. 8*, 813–24.

(2) Burdon, R. H., and Rice-Evans, C. (1989) Free radicals and the regulation of mammalian cell proliferation. *Free Radic. Res. Commun. 6*, 345–58.

(3) Winterbourn, C. C. (2008) Reconciling the chemistry and biology of reactive oxygen species. *Nat. Chem. Biol. 4*, 278–86.

(4) Singh, M., Sharma, H., and Singh, N. (2007) Hydrogen peroxide induces apoptosis in HeLa cells through mitochondrial pathway. *Mitochondrion 7*, 367–73.

(5) Lambeth, J. D. (2007) Nox enzymes, ROS, and chronic disease: an example of antagonistic pleiotropy. *Free Radic. Biol. Med. 43*, 332–47.

(6) Laurent, A., Nicco, C., Chéreau, C., Goulvestre, C., Alexandre, J., Alves, A., Lévy, E., Goldwasser, F., Panis, Y., Soubrane, O., Weill, B., and Batteux, F. (2005) Controlling tumor growth by modulating endogenous production of reactive oxygen species. *Cancer Res. 65*, 948–956.

(7) Trachootham, D., Alexandre, J., and Huang, P. (2009) Targeting cancer cells by ROS-mediated mechanisms: a radical therapeutic approach? *Nat. Rev. Drug Discov. 8*, 579–91.

(8) Schumacker, P. T. (2006) Reactive oxygen species in cancer cells: live by the sword, die by the sword. *Cancer Cell 10*, 175–6.

(9) Gorrini, C., Harris, I. S., and Mak, T. W. (2013) Modulation of oxidative stress as an anticancer strategy. *Nat. Rev. Drug Discov. 12*, 931–47.

(10) Raj, L., Ide, T., Gurkar, A. U., Foley, M., Schenone, M., Li, X., Tolliday, N. J., Golub, T. R., Carr, S. A., Shamji, A. F., Stern, A. M., Mandinova, A., Schreiber, S. L., and Lee, S. W. (2011) Selective killing of cancer cells by a small molecule targeting the stress response to ROS. *Nature 475*, 231–4.

(11) Gough, D. R., and Cotter, T. G. (2011) Hydrogen peroxide: a Jekyll and Hyde signalling molecule. *Cell Death Dis. 2*, e213.

(12) Forman, H. J. (2007) Use and abuse of exogenous H2O2 in studies of signal transduction. *Free Radic. Biol. Med. 42*, 926–32.

(13) De Oliveira-Marques, V., Cyrne, L., Marinho, H. S., and Antunes, F. (2007) A quantitative study of NF-kappaB activation by H2O2: relevance in inflammation and synergy with TNF-alpha. *J. Immunol. 178*, 3893–902.

(14) Miller, E. W., Dickinson, B. C., and Chang, C. J. (2010) Aquaporin-3 mediates hydrogen peroxide uptake to regulate downstream intracellular signaling. *Proc. Natl. Acad. Sci. U. S. A. 107*, 15681–6.

(15) Antunes, F., and Cadenas, E. (2000) Estimation of H2O2 gradients across biomembranes. *FEBS Lett. 475*, 121–6.

(16) Antunes, F., and Cadenas, E. (2001) Cellular titration of apoptosis with steady state concentrations of H(2)O(2): submicromolar levels of H(2)O(2) induce apoptosis through Fenton chemistry independent of the cellular thiol state. *Free Radic. Biol. Med. 30*, 1008–18.

(17) Peskin, A. V, Low, F. M., Paton, L. N., Maghzal, G. J., Hampton, M. B., and Winterbourn, C. C. (2007) The high reactivity of peroxiredoxin 2 with H(2)O(2) is not reflected in its reaction with other oxidants and thiol reagents. *J. Biol. Chem. 282*, 11885–92.

(18) Dickinson, B. C., and Chang, C. J. (2011) Chemistry and biology of reactive oxygen species in signaling or stress responses. *Nat. Chem. Biol. 7*, 504–11.

(19) Miller, E. W., Taulet, N., Onak, C. S., New, E. J., Lanselle, J. K., Smelick, G. S., and Chang, C. J. (2010) Light-activated regulation of cofilin dynamics using a photocaged hydrogen peroxide generator. *J. Am. Chem. Soc. 132*, 17071–3.

(20) Haskew-Layton, R. E., Payappilly, J. B., Smirnova, N. A., Ma, T. C., Chan, K. K., Murphy, T. H., Guo, H., Langley, B., Sultana, R., Butterfield, D. A., Santagata, S., Alldred, M. J., Gazaryan, I. G., Bell, G. W., Ginsberg, S. D., and Ratan, R. R. (2010) Controlled enzymatic production of astrocytic hydrogen peroxide protects neurons from oxidative stress via an Nrf2-independent pathway. *Proc. Natl. Acad. Sci. U. S. A. 107*, 17385–90.

(21) Belousov, V. V, Fradkov, A. F., Lukyanov, K. A., Staroverov, D. B., Shakhbazov, K. S., Terskikh, A. V, and Lukyanov, S. (2006) Genetically encoded fluorescent indicator for intracellular hydrogen peroxide. *Nat. Methods 3*, 281–6.

(22) Kalyanaraman, B., Darley-Usmar, V., Davies, K. J. A., Dennery, P. A., Forman, H. J., Grisham, M. B., Mann, G. E., Moore, K., Roberts, L. J., and Ischiropoulos, H. (2012) Measuring reactive oxygen and nitrogen species with fluorescent probes: challenges and limitations. *Free Radic. Biol. Med. 52*, 1–6.

(23) Malinouski, M., Zhou, Y., Belousov, V. V, Hatfield, D. L., and Gladyshev, V. N. (2011) Hydrogen peroxide probes directed to different cellular compartments. *PLoS One* (Kowaltowski, A. J., Ed.) *6*, e14564.

(24) Kim, J.-A., Park, S., Kim, K., Rhee, S. G., and Kang, S. W. (2005) Activity assay of mammalian 2-cys peroxiredoxins using yeast thioredoxin reductase system. *Anal. Biochem. 338*, 216–23.

(25) Chance, B., Sies, H., and Boveris, A. (1979) Hydroperoxide metabolism in mammalian organs. *Physiol. Rev. 59*, 527–605.

(26) Low, F. M., Hampton, M. B., Peskin, A. V, and Winterbourn, C. C. (2007) Peroxiredoxin 2 functions as a noncatalytic scavenger of low-level hydrogen peroxide in the erythrocyte. *Blood 109*, 2611–7.

(27) Hall, A., Karplus, P. A., and Poole, L. B. (2009) Typical 2-Cys peroxiredoxins--structures, mechanisms and functions. *FEBS J. 276*, 2469–77.

(28) Chae, H. Z., Kim, H. J., Kang, S. W., and Rhee, S. G. (1999) Characterization of three isoforms of mammalian peroxiredoxin that reduce peroxides in the presence of thioredoxin. *Diabetes Res. Clin. Pract. 45*, 101–112.

(29) Nelson, K. J., Parsonage, D., Karplus, P. A., and Poole, L. B. (2013) Evaluating peroxiredoxin sensitivity toward inactivation by peroxide substrates. *Methods Enzymol. 527*, 21–40.

(30) Marinho, H. S., Real, C., Cyrne, L., Soares, H., and Antunes, F. (2014) Hydrogen peroxide sensing, signaling and regulation of transcription factors. *Redox Biol. 2*, 535–562.

(31) Woo, H. A., Yim, S. H., Shin, D. H., Kang, D., Yu, D.-Y., and Rhee, S. G. (2010) Inactivation of peroxiredoxin I by phosphorylation allows localized H(2)O(2) accumulation for cell signaling. *Cell 140*, 517–28.

(32) Hofmann, B., Hecht, H., and Flohé, L. (2002) Birgit Hofmann 1 , Hans-Jürgen Hecht 2 and Leopold Flohé 1, * 1 *383*, 347–364.

(33) Arnér, E. S. J., Zhong, L., and Holmgren, A. (1999) Oxidants and Antioxidants Part B. *Methods Enzymol.* Elsevier.

(34) Peskin, A. V, Dickerhof, N., Poynton, R. A., Paton, L. N., Pace, P. E., Hampton, M. B., and Winterbourn, C. C. (2013) Hyperoxidation of peroxiredoxins 2 and 3: rate constants for the reactions of the sulfenic acid of the peroxidatic cysteine. *J. Biol. Chem. 288*, 14170–7.

(35) Chang, T.-S., Jeong, W., Woo, H. A., Lee, S. M., Park, S., and Rhee, S. G. (2004) Characterization of mammalian sulfiredoxin and its reactivation of hyperoxidized peroxiredoxin through reduction of cysteine sulfinic acid in the active site to cysteine. *J. Biol. Chem. 279*, 50994–1001.

(36) Stone, J. R., and Yang, S. Hydrogen peroxide: a signaling messenger. *Antioxid. Redox Signal. 8*, 243–70.

(37) Rhee, S. G., Woo, H. A., Kil, I. S., and Bae, S. H. (2012) Peroxiredoxin functions as a peroxidase and a regulator and sensor of local peroxides. *J. Biol. Chem. 287*, 4403–10.

(38) Jarvis, R. M., Hughes, S. M., and Ledgerwood, E. C. (2012) Peroxiredoxin 1 functions as a signal peroxidase to receive, transduce, and transmit peroxide signals in mammalian cells. *Free Radic. Biol. Med. 53*, 1522–30.

(39) Murphy, M. P., Holmgren, A., Larsson, N.-G., Halliwell, B., Chang, C. J., Kalyanaraman, B., Rhee, S. G., Thornalley, P. J., Partridge, L., Gems, D., Nyström, T., Belousov, V., Schumacker, P. T., and Winterbourn, C. C. (2011) Unraveling the biological roles of reactive oxygen species. *Cell Metab. 13*, 361–6.

(40) Lukyanov, K. a, and Belousov, V. V. (2014) Genetically encoded fluorescent redox sensors. *Biochim. Biophys. Acta 1840*, 745–56.

(41) Roma, L. P., Duprez, J., Takahashi, H. K., Gilon, P., Wiederkehr, A., and Jonas, J.-C. (2012) Dynamic measurements of mitochondrial hydrogen peroxide concentration and glutathione redox state in rat pancreatic β-cells using ratiometric fluorescent proteins: confounding effects of pH with HyPer but not roGFP1. *Biochem. J. 441*, 971–8.

(42) Kóna, J., and Brinck, T. (2006) A combined molecular dynamics simulation and quantum chemical study on the mechanism for activation of the OxyR transcription factor by hydrogen peroxide. *Org. Biomol. Chem. 4*, 3468–78.

(43) Benfeitas, R., Selvaggio, G., Antunes, F., Coelho, P. M. B. M., and Salvador, A. (2014) Hydrogen peroxide metabolism and sensing in human erythrocytes: A validated kinetic model and reappraisal of the role of peroxiredoxin II. *Free Radic. Biol. Med. 74*, 35–49.

(44) Jones, D. P., and Kemp, M. L. (2010) A Model of Redox Kinetics Implicates the Thiol Proteome in Cellular Hydrogen Peroxide Responses *13*.

2.6 Appendix

Hydrogen peroxide production by glucose oxidase. Glucose oxidase was diluted to concentrations between 3-5 mU/mL in in PBS (pH 7.4) + 2 g/L glucose. The production of peroxide by the enzyme was measured using the ABTS assay. (B) A steady-state hydrogen peroxide level obtained using external glucose oxidase as a generator and Hyper HeLa cells as scavengers. HyPer HeLa cells were re-suspended at 0.8 million cells/mL in PBS + 2 g/L glucose. The amount of glucose oxidase producing 2.8 μM hydrogen peroxide/min was added simultaneously with 10 μM of hydrogen peroxide. The extracellular peroxide concentration was monitored for a period of 1 hour using the ABTS assay. A constant extracellular concentration verifies the k_{intact} value.

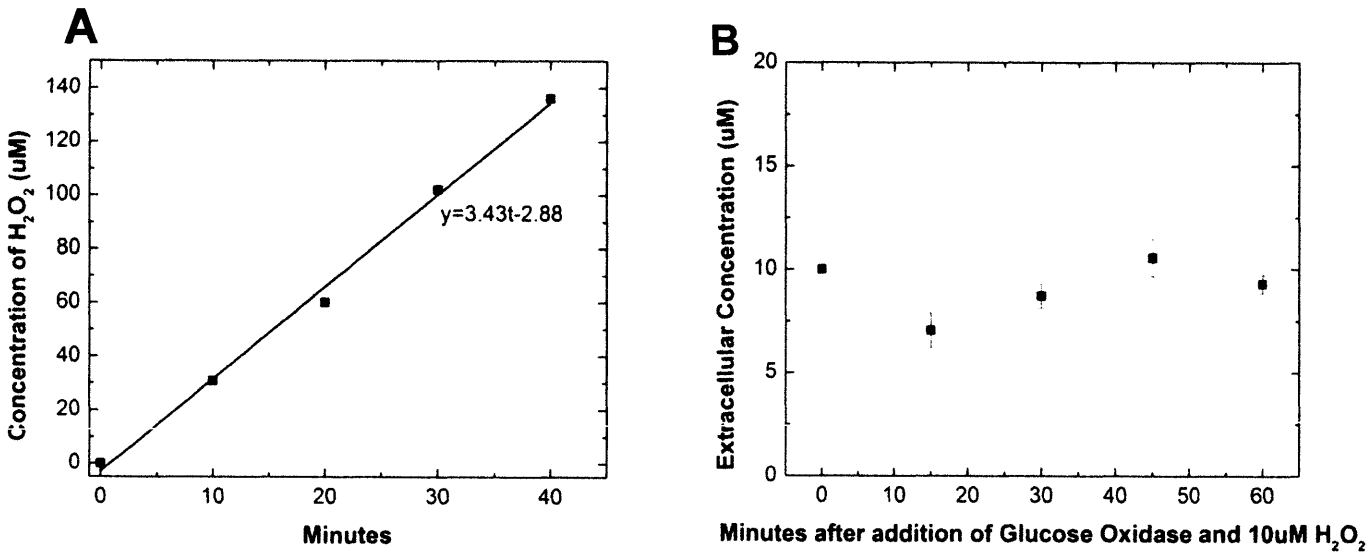

Depletion of hydrogen peroxide due to 2-cys Prx activity in cell lysates with and without hyper-oxidation effects. While hyper-oxidation of 2-cys Prx in intact cells has only been detected for extracellular additions of >100 μM, it is important to consider hyper-oxidation effects for lower peroxide concentrations when the sample consists of cell lysates rather than intact cells.

The kinetics of Prx activity in the experimental system was modeled using a system of ODEs implemented using Matlab (SI). The situation where Prx can undergo hyper-oxidation (solid) versus without hyper-oxidation (dotted) was compared for bolus additions of 20 μM (black) and 35 μM (blue) hydrogen peroxide to a solution of HeLa cell lysate. The possibility of hyper-oxidation changes the kinetics of hydrogen peroxide depletion significantly, and this effect is greater for the 35 μM addition in comparison with the 20 μM addition. From this simulation, we conclude that for both concentrations, hyper-oxidation needs to be taken into account when fitting the Prx kinetic data to a rate equation. Other parameters used in the simulation were Trx=30 μM, k_1*[Prx_{active}]= $3.8s^{-1}x10^{-9}$ $s^{-1}cell^{-1}L$ and a cell density of 5.8 million cells/mL.

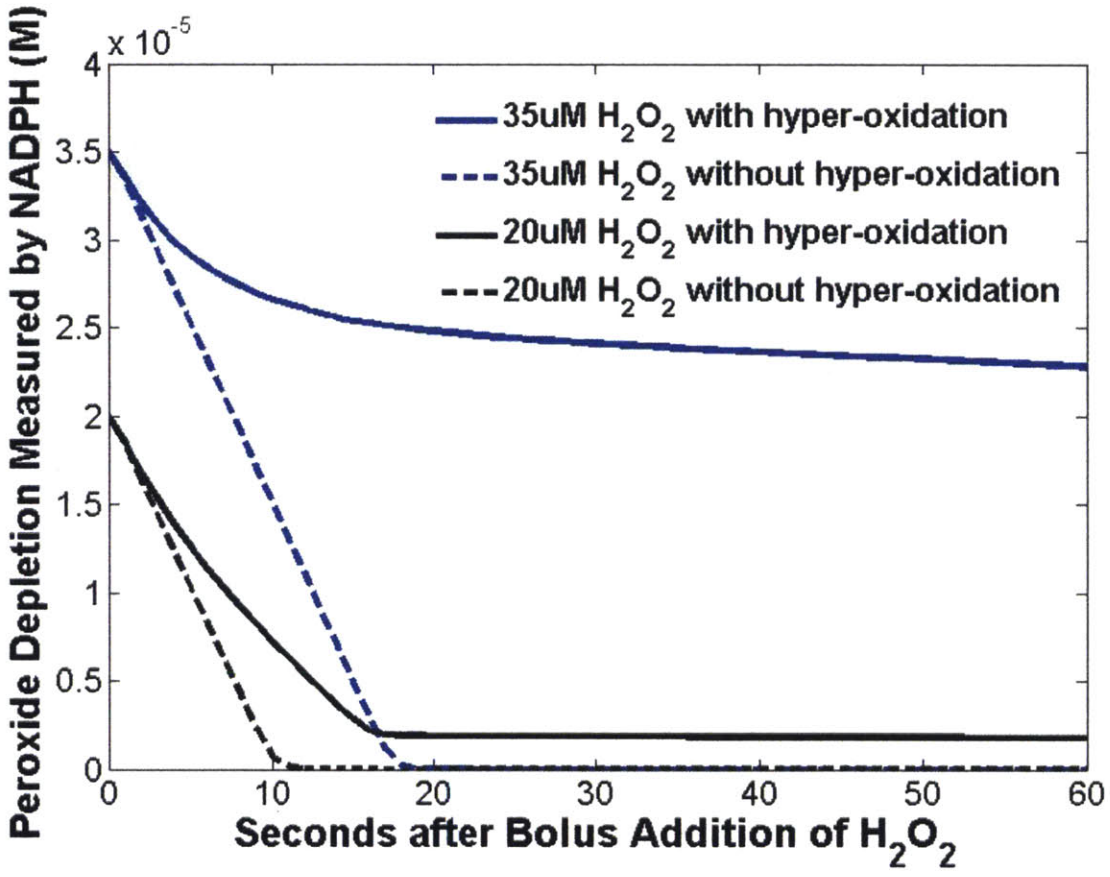

Expression and purification of yTrx and TrxR. After induction with IPTG and expression for 4 hours, Trx and TrxR overexpression was detected in the lysate fractions. After chromatographic separations with anionic (Q) and gel filtration (Superdex75) columns using an AKTA FPLC, a single 11kD fragment for Trx was observed using SDS PAGE. Similarly, TrxR was also purified using Q and Phenyl hydrophobic columns, and a strong band of 35 kD was detectable. The UV-spectra for the purified TrxR showed the correct peaks at 280 nm, 359 nm and 452 nm.

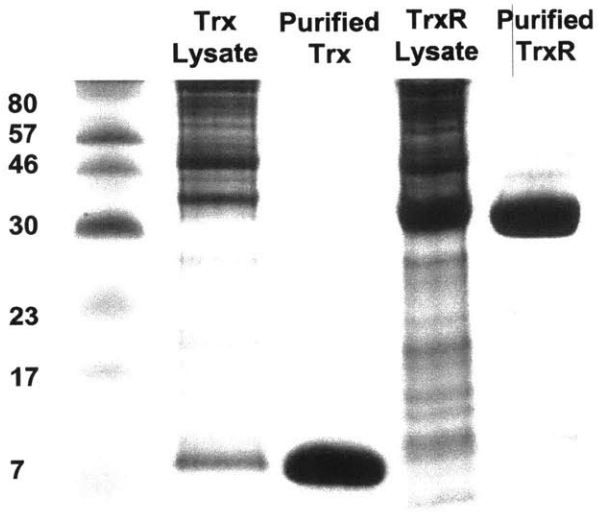

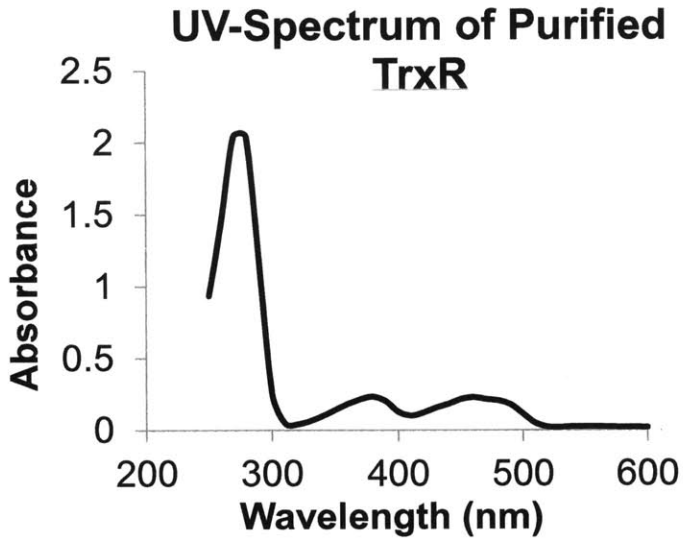

Calculations and model parameters for the GPx and Prx kinetic measurements

GPx kinetics

The reaction mechanism of GPx consists of an oxidation-reduction cycle where GPx is oxidized by H_2O_2 and reduced by GSH:

$$H_2O_2 + GPx_{red} + H^+ \xrightarrow{k_1'} GPx_{ox} + H_2O$$
$$GPx_{ox} + GSH \xrightarrow{k_2'} GS - GPx + H_2O$$
$$GS - GPx + GSH \xrightarrow{k_3'} GPx_{red} + GSSG + H^+$$

The GSSG is then reduced using electrons supplied by NADPH inside the cell. By adding excess NADPH to cell lysate, we can indirectly track the consumption of H_2O_2 by GPx. These depletion kinetics are fitted to the integrated rate law reported in *Materials and Methods.*

2-Cys Prx kinetics

Similar to GPx, 2-cys Prx requires a partner, Trx, to return it to the reduced form after oxidation by hydrogen peroxide. The difference between GPx and Prx is that Prx can react with a second hydrogen peroxide molecule to form sulfinic or sulfonic acid. This over-oxidized form reverts very slowly back to Prx-SOH through reaction with sulfiredoxin. The competing reaction to hyper-oxidation is the formation of a disulfide bond between the –SOH and –SH groups of adjacent 2-cys Prx molecules to form Prx-SS. This disulfide bond is reduced by thioredoxin/thioredoxin reductase back to the Prx-$(SH)_2$ form.

In order to obtain an analytic solution, we make a quasi-steady state assumption of the intermediate species $Prx-SOH$, $Prx-(SO_2H)$ and $Prx-SS$, and by adding excess yeast $Trx_{reduced}$ and TrxR to the system, we can assume that concentration to be constant. Since the conversion of $Prx-(SO_2H)$ back to $Prx-SOH$ is very slow [44], we can also assume that the oxidation reaction k_5 is irreversible for the kinetic time frame we are considering. Furthermore, at hydrogen peroxide of less than < 62 μM, only 1% of the mammalian 2-cys Prx enzymes are over-oxidized per cycle [29]. This allowed us to simply the expression $\frac{k_1[H_2O_2]}{k_3[H_2O_2]+k_2}$ to $\frac{k_1[H_2O_2]}{k_2}$. Solving the system of ODEs (equations 9-15) give us an implicit equation of hydrogen peroxide related to time:

$$(k_1 Prx_{active}\left(\frac{1}{k_2}+\frac{1}{k_5[Trx]}\right)-\frac{k_3}{k_2})\ln(\frac{Prx_{active}+\frac{k_3}{k_2}[H_2O_2]_0}{Prx_{active}+\frac{k_3}{k_2}[H_2O_2]_1})+\frac{k_3}{k_2}\ln(\frac{[H_2O_2]_0}{[H_2O_2]_1})=\Delta t$$

What is notable about the equation is that the rate constants k_1, k_2, k_3 and k_4 are needed in order to fit the $[H_2O_2]$ against Δt, since the implicit form is not as elegant as GPx that allow us to determine k_1'*[GPx_{total}] from the slope of expression involving only hydrogen peroxide terms and time. Thus, the most accurate way of determining k_1*[Prx_{active}] will be to numerically simulate a model with the system of ordinary differential equations as shown above, with rate

constants and initial values as shown in the table below, and fit our experimental data to the model.

Reaction	Rate Constant
k_1	$1.3*10^{7}$ M^{-1} s^{-1} [17]
k_2	$2\ s^{-1}$ [34]
k_3	$1.2*10^{4}$ M^{-1} s^{-1} [34]
k_4	$3*10^{-3}$ s^{-1} [35]
k_5	$1*10^{5}$ M^{-1} s^{-1} [24]
k_6	$2*10^{7}$ M^{-1} s^{-1} [33]
Species	**Initial Concentration**
H_2O_2	20-25 μM
Prx_{active}	Parameter to fit
Prx-SOH	1e-14 M
Prx-SO_2H	1e-14 M
Prx-SS	1e-14 M
$Trx_{reduced}$	20-50 μM
$Trx_{oxidized}$	1e-14 M
NADPH	300 μM

The system of ODEs was simulated using MatLab2013, time step size of 1s. k_1=$1.3*10^{7}$ M^{-1} s^{-1}, k_5= $2\ s^{-1}$ and k_3=$1.2*10^{4}$ M^{-1} s^{-1} were obtained from *in vitro* data with 2-cys Prx II [17,34], a close homolog of Prx I that also exists in the cytoplasm. k_4 =$3*10^{-3}$ s^{-1} was obtained from experimental data with purified human Prx I protein interaction with human Srx [35]. k_5=$1*10^{5}$ M^{-1} s^{-1} comes from experimental data with human Prx I and a yeast Trx/TrxR system [24]. k_6=$2*10^{7}$ M^{-1} s^{-1} is derived from experimental data measuring mammalian Trx reduction with the mammalian Trx [33]. The initial conditions for hydrogen peroxide and $Trx_{reduced}$ are given as experimental inputs.

NADPH initial condition is 300 μM. The variable to fit is the initial concentration of active reduced 2-cys peroxiredoxin in the system. k_{prx} is equal to k_1*[Prx_{active}].

Chapter 3: Interpreting heterogeneity in cellular response to H_2O_2 protein biosensors

Fluorescent, genetically encoded sensors of hydrogen peroxide have enabled visualization of perturbations to the intracellular level of this signaling molecule with sub-cellular and temporal resolution. Ratiometric sensors hold the additional promise of meaningful quantification of intracellular hydrogen peroxide levels as a function of time, a longstanding goal in the field of redox signaling. To date, studies that have connected the magnitudes of observed ratios with peroxide concentrations have either examined suspensions of cells or small numbers of adherent cells (~10). In the present work, we examined the response of all cells in several microscopic fields of view to an identical perturbation and observed a striking degree of heterogeneity of fluorescence ratios from individual cells. The expression level of the probe and phase within the cell cycle were each examined as potential contributors to the observed heterogeneity. Higher ratiometric responses correlated with greater expression levels of the probe, and phase in the cell cycle was also shown to influence the magnitude of response. To aid in the interpretation of experimental observations, we incorporated the reaction of the reduced probe with peroxide and the reactions of the oxidized probe with glutathione and glutaredoxin into a larger kinetic model of peroxide metabolism. The predictions of the kinetic model suggest possible explanations for the experimental observations. This work highlights the importance of a systems-level approach to understanding the output of genetically encoded sensors that function via redox reactions involving thiol and disulfide groups.

3.1 Introduction

Hydrogen peroxide is a signaling molecule important for normal cellular function [123] and implicated in pathological conditions such as inflammation and cancer [456] as well as neurodegenerative [7] and cardiovascular [89] disorders. It acts as a signaling molecule by oxidizing particular cysteine residues of particular proteins[10], and discovering the identities of these proteins is an intense focus of research [1112]. Whether hydrogen peroxide is associated with normal function or pathology is hypothesized to depend on its spatiotemporal concentration within the cell.[13] Due to limitations in methods for measuring intracellular peroxide concentrations reliably [14151617], it has been difficult to definitively test this reasonable hypothesis and, more importantly, establish a quantitative understanding of the signaling networks that characterize particular biological processes. For example, without reliable measurement tools, it is not possible to ask how these networks compare quantitatively across cell types within an organism, different malignant tumors, or even cells within the same tumor.

Knowledge of bacterial and yeast proteins that react specifically with hydrogen peroxide exceeds knowledge of the same within mammalian systems.[2] In recent years, genetic engineering has been used to produce fusions of fluorescent proteins with bacterial and yeast proteins that react specifically with hydrogen peroxide.[181920] Fusions are constructed such that changes in the spectrum of the fluorescent protein occur when hydrogen peroxide oxidizes a cysteine of the microbial protein, causing it to subsequently form a disulfide bond with a neighboring cysteine.[2122] Two spectral features are affected, with an excitation peak at one wavelength decreasing and an excitation peak at a second wavelength increasing in a dose-dependent manner upon stimulation with hydrogen peroxide. The ability to examine the ratio of two spectral features, in contrast with measuring changes in fluorescence intensity for only one feature,

enables measurements unbiased by the amount of sensor within the cell or the number of cells within a sample.

As part of an on-going effort to connect the magnitudes of fluorescent, ratiometric responses from a sensor with intracellular concentrations of hydrogen peroxide [23], we have noted with interest the cell-to-cell heterogeneity, captured in part by standard deviations of signals measured from several cells, that has been reported when populations of adherent cells expressing genetically encoded peroxide sensors are stimulated with an identical amount of hydrogen peroxide.[1920] In this work, we explore several hypotheses regarding factors that may underlie this heterogeneity. To do so, we examine larger sample sizes than were typical in past work, and we use a systems model of hydrogen peroxide metabolism within HeLa cells to aid in the interpretation of experimental results. Insights from this analysis support future efforts toward a quantitative understanding of redox signaling in physiological and pathological processes.

3.2 Methods and Materials

Materials

EMEM and FBS were sourced from ATCC (Manassas, VA). Penicillin-streptomycin was from EMD Millipore (Gibbstown, NJ). HyPer plasmid (pHyPer-cyto) was from Evrogen (Moscow, Russia). Lipofectamine was from Life Technologies (Carlsbad, CA). PBS, thymidine and G418 were from Sigma-Aldrich (St. Louis, MO). H_2O_2 was from BDH Chemicals (West Chester, PA). HRP and ABTS were from Alfa Aesar (Ward Hill, MA) and Tokyo Chemicals (Tokyo, Japan), respectively.

Cell Culture and Transfection

HeLa cells were cultured in EMEM supplemented with 10% FBS and 1% penicillin-streptomycin. The cell cultures were maintained in a 37°C humidified incubator in the presence of 5% CO_2. Media was changed every 3 days and cells were passaged every 5-6 days.

HeLa cells were stably transfected with pHyPer-cyto vector containing the HyPer gene under CMV promoter. Cells were first transiently transfected with Lipofectamine following supplier's protocol. Twenty-four hours after transfection, media was changed and supplemented with 700 μg/mL of G418. After two weeks, stable clones were selected by picking fluorescent colonies using an Olympus widefield fluorescence camera (IX81). The selected colonies were expanded in medium containing 200 μg/mL G418 in 96-well plates. The best fluorescing colony was kept for subsequent experiments. The stable HyPer-HeLa cell line was cultured in 200 μg/mL G418 to maintain selection pressure and remove non-fluorescing cells.

For imaging, HyPer-HeLa cells were plated at a density of 2 x 10^4 cells per well for approximately 42 hours in 96-well plate without G418. Before imaging, each well was washed with pre-warmed PBS (pH 7.4), and incubated with 150 μL of 20 μM H_2O_2 in PBS for 10 minutes at room temperature.

Cell Cycle Synchronization

For G1 synchronization, HyPer-HeLa cells were grown as described above in the presence of 2 mM thymidine [24]. Control cultures were grown similarly in absence of thymidine. For G0 synchronization, cells were plated at a density of 1 x 10^4 cells per well in EMEM with 10% FBS. After culturing for 24 hours, cells were washed with PBS (pH 7.4) and placed in serum-free media for additional 24 hours before imaging [25]. Control cultures were grown similarly except the replaced media contained 10% FBS.

Imaging

HyPer imaging was done using an Olympus widefield fluorescence microscope (IX81) and Prior Lumen2000 lamp. Images were acquired with a 20X Olympus objective. The 96-well plate was clamped on the stage to obtain same view-field images before and after the incubation with H_2O_2. HyPer fluorescence images were taken using Chroma D415/30x and Semrock FF01-488/6-25 excitation filters while emission was collected using a Semrock FF02-525/40-25 filter. Both images have 1600 x 1200 pixel density at 16-bit resolution. Exposure time was set at 300ms with the lamp intensity at 25%. Images were taken using a Retiga 2000R camera. The microscope, lamp and camera settings were kept constant throughout this study.

Image Analysis

HyPer images were background subtracted using the rolling ball algorithm (radius=200 pixels) in ImageJ. These images were then used to identify cell regions in CellProfiler software based on intensity thresholding. The thresholding algorithm used was 'Mixture of Gaussian Adaptive.' The regions determined were filtered using a size criterion of 30-125 pixels and eccentricity of 0-0.9. HyPer ratio for a particular region was calculated as the average pixel intensity in HyPer-long channel divided by the average pixel intensity in HyPer-short channel in that region.

Measuring Cellular Scavenging of H_2O_2 as a Function of Time Using an HRP-ABTS Assay

HyPer-HeLa cells, seeded at $1x10^6$ cells in 10 cm^2 dishes, were grown as described above in the absence of G418 for 48 hours. Cells were washed with PBS (pH 7.4) and placed in contact with 10 mL of 20 μM H_2O_2 in PBS (pH 7.4). Over a period of ten minutes, 150 μL samples were withdrawn every two minutes and placed in a 96 well plate. 50 μL of 2.5 mM ABTS and 10 μl of

3 mg/mL HRP were added to each well. Absorbance was measured at 405 nm using a Tecan M200 plate reader.

Mathematical Modeling of the Kinetics of Reactions of HyPer with H_2O_2 and Reductants

The basic framework of the model has been previously reported by Admiora, et al [26]. It includes a system of 28 species and ordinary differential equations (ODEs) that describe the kinetics of the network of reactions between H_2O_2, antioxidants, and thiols of proteins within Jurkat cells. We modified certain kinetic parameters and initial conditions of the original model to better represent our cells of interest, HeLa cells. We added a set of redox reactions that describes HyPer's reactivity within this network. All parameters that we modified or added are listed in the tables in the appendix. The system of equations governing the rates of reaction of HyPer with H_2O_2 and disulfide reductase species that we added to the model is as follows:

$$\frac{\partial HyPer-(SH)_2}{\partial t} = -k_{ox}[H_2O_2][HyPer-(SH)_2] + k_{red}[Grx][HyPer-SS] + k_{GRssg}[Grx][HyPer-SSG] \quad (1)$$

$$\frac{\partial HyPer-(SOH)}{\partial t} = k_{ox}[H_2O_2][HyPer-(SH)_2] - k_s[HyPer-SOH] - k_{ssg}[GSH][HyPer-SOH] \quad (2)$$

$$\frac{\partial HyPer-SS}{\partial t} = k_s[HyPer-SOH] - k_{red}[Grx][HyPer-SS] \quad (3)$$

$$\frac{\partial HyPer-SSG}{\partial t} = k_{ssg}[GSH][HyPer-SOH] - k_{GRssg}[Grx][HyPer-SSG] \quad (4)$$

$$\frac{\partial Grx-SS}{\partial t} = k_{red}[Grx][HyPer-SS] - k_{GSHssg}[GSH][Grx] \quad (5)$$

Where k_{ox} is the rate constant for the reaction of HyPer with H_2O_2, k_{red} is the rate constant of the reduction of HyPer-SS by Grx, k_s is the rate constant of the formation of the disulfide bond

resulting in HyPer-SS, k_{ssg} is the rate constant of the reaction of GSH with HyPer-SOH, k_{GRssg} is the rate constant of the reduction of HyPer-SSG by Grx, and k_{GSHssg} is the rate constant of the reduction of Grx-SS by GSH. We modified the ODEs for H_2O_2, GSH, GSSG, Grx and Grx-SSG using the appropriate mass balances.

3.3 Results

3.3.1 Analysis of fluorescence images

As in past studies[1822], the genetically encoded sensor HyPer was stably expressed by HeLa cells and these cells were stimulated with peroxide via extracellular bolus addition. Most prior studies that included microscopic image analysis of cells expressing peroxide sensors used small sample sizes (~10 cells) [19202728](29-30). To facilitate analysis of larger sample sizes, we automated the image analysis process, using a combination of ImageJ (U.S. National Institutes of Health) and Cell Profiler software (Broad Institute, Cambridge, MA). Figure 3.1 shows the image processing steps that were used to quantify the HyPer signal from the HeLa cells. A set of two images were obtained for each field of view per time point, using excitation filters centered at 488 nm and 415 nm, with emission collected at 525 nm for both measurements (Figures 3.1A and 3.1B). Images were corrected for uneven illumination using the rolling ball algorithm in Image J with a radius of 200 pixels [31]. Figures 3.1C and 3.1D demonstrate that the algorithm allows the elimination of background signal in both excitation channels, and that the level of background signal is quite different in the two channels. Following background correction, we aligned each set of images of the same field of view and used CellProfiler to identify individual cells expressing HyPer. Cells were identified using a combination of object diameter, eccentricity, and Mixture of Gaussian intensity-thresholding algorithms, and cells in a cluster are distinguished from one another from

based on the intensity profile around the cell border [32]. (Figure 3.1E). Once each cell expressing HyPer was identified, fluorescence ratios within each were calculated by dividing the mean intensity of all pixels within the cell in the 488 nm excitation image by the mean of all pixels within the cell in the 415 nm excitation image. This methodology facilitates rapid analysis of 200-300 cells from multiple sets of images.

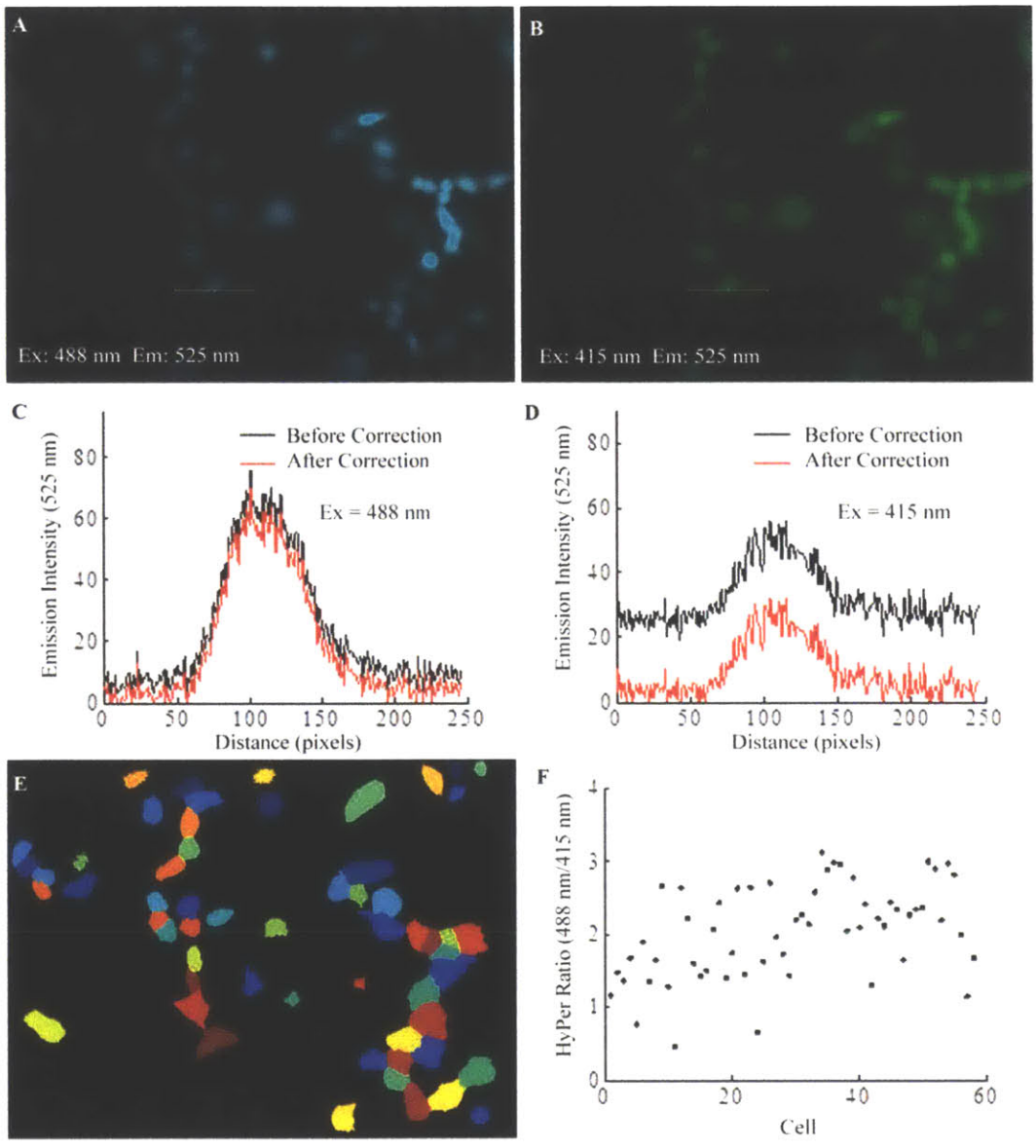

Figure 3.1: Images processing before calculating the ratiometric HyPer readout. (A) Fluorescent image (λ_{ex}=488 nm, λ_{em}=525 nm) of HeLa cells stably expressing the HyPer sensor protein under control of the CMV promoter. (B) Fluorescent image of the same field of view (λ_{ex}=415 nm, λ_{em}=525 nm). Images shown in (A) and (B) were taken 10 minutes after stimulation with 20 μM

H_2O_2. (C, D) Intensity as a function of distance plots for the line shown in panels A and B before (black) and after (red) correction for background signal using the rolling ball algorithm (radius = 200 pixels) in Image J. (E) Cells expressing HyPer are identified in an automated fashion (CellProfiler) using the background-subtracted image acquired using λ_{ex}=488 nm, λ_{em}=525 nm. (F) Calculated HyPer ratio for the cells identified in (E). The HyPer ratio is defined as the average emission intensity upon excitation with 488 nm light divided by the average emission intensity upon excitation with 415 nm light. Each data point represents the average HyPer ratio within one cell.

3.3.2 Heterogeneity in cellular response to H_2O_2

Figure 3.2 shows a representative dose-response experiment when cells are stimulated with hydrogen peroxide and imaged after ten minutes. Without exogenous addition of peroxide, all of the cells are characterized by similar fluorescence ratios near 0.5. When bolus additions of 5-20 μM H_2O_2 are used to stimulate the cells, increased HyPer ratios are observed, and above 20 μM H_2O_2, the ratios remain at saturated values and do not increase further. The degree of heterogeneity in the sensor's response in a population of cells to an identical stimulus is striking. For example, a bolus addition of 20 μM H_2O_2 leads to observations of the full range of possible ratios from 0.5 to 3 within the population of cells. We investigated several possible explanations for these drastically different apparent responses.

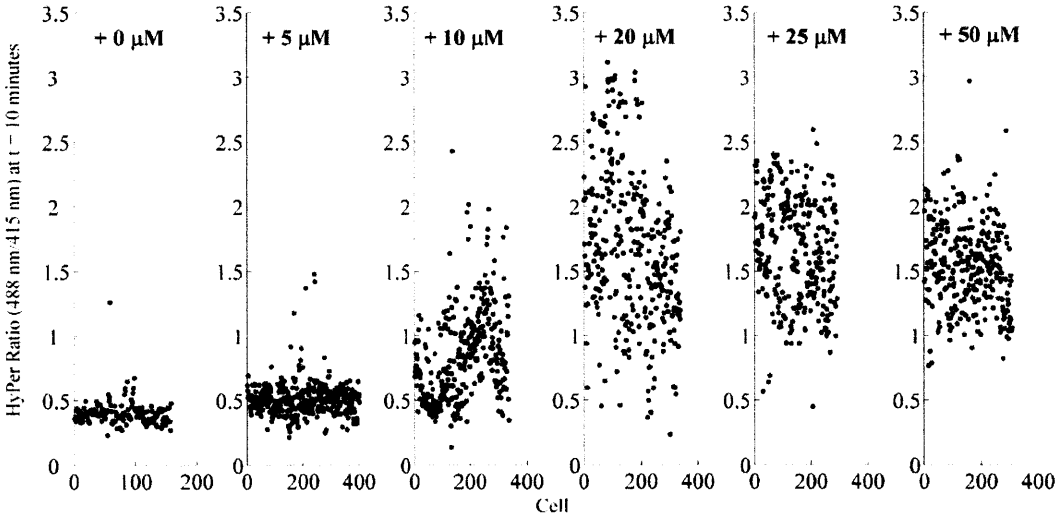

Figure 3.2: The ratiometric response of HyPer to H_2O_2. HyPer-HeLa cells were stimulated with 0-50 μM H_2O_2 and imaged after 10 minutes. Fluorescence images were obtained using excitation filters centered at 488 and 415 nm. Emission was measured at 525 nm. Each data point represents the HyPer ratio within one cell. Sample sizes are as follows: 0 μM (158 cells); 5 μM (431 cells); 10 μM (337 cells); 20 μM (338 cells); 25 μM (292 cells); 50 μM (307 cells).

3.3.3 Dependence of HyPer response on expression level of the probe and cell cycle

Though HyPer's response is assumed to be independent of expression level, this has not been tested. We tested this assumption by examining the same field of view before and after stimulation by H_2O_2. Figure 3.3A shows that though in the basal state, a representative 300 cells in addition to those shown in Figure 3.2 exhibited HyPer ratios near 0.5. Figure 3.3B shows though the ratios in all cells are similar, the expression level of the sensor in all cells is not. Emission intensity upon excitation centered at 415 nm varies up to 20-fold from the highest expressing cell to the lowest, while emission intensity upon excitation centered at 488 nm varies up to 10-fold.

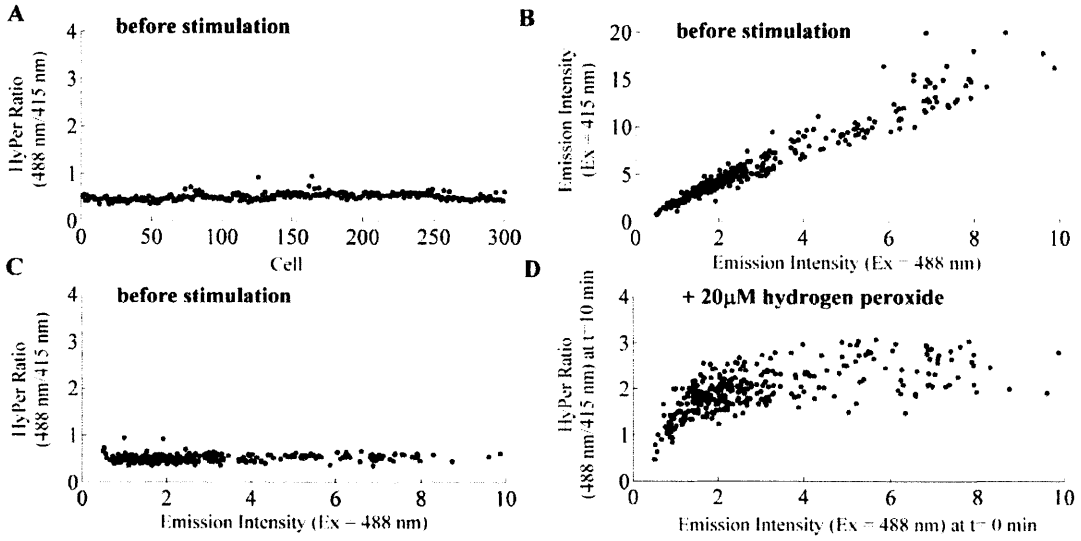

Figure 3.3: HyPer's ratiometric response to H_2O_2 correlates with its expression level. Images of HyPer-HeLa cells were obtained using excitation filters centered at 488 and 415 nm and emission was measured at 525 nm. The same fields of view were imaged prior to stimulation and 10 minutes after stimulation with hydrogen peroxide. Each data point represents one cell. (A) HyPer ratios within individual cells prior to stimulation with hydrogen peroxide are relatively uniform. (B) Prior to stimulation, the range of emission intensities within cells indicates expression level of the fluorescent sensor protein, and emission intensity at each of the excitation wavelengths is positively correlated. Emission intensity at either excitation wavelength prior to stimulation can be used to indicate expression level. (C) Prior to stimulation, the HyPer ratio within each cell does not correlate with the expression level of the sensor. (D) Ten minutes after stimulation with 20 μM H_2O_2, the observed HyPer ratio (y-axis) correlates with the expression level of the sensor within the cell as measured by the emission intensity upon excitation centered at 488 nm prior to stimulation (x-axis). All emission intensities were scaled by a factor of 10^4.

As expected, given that the ratios in all cells are nearly identical, high emission from a cell in one channel correlates with high emission from that cell in the other channel. Thus, emission from either channel prior to simulation can be used as a measure of the expression level of the fluorescent sensor. Figure 3.3C plots the HyPer ratio of 300 cells prior to stimulation with hydrogen peroxide as a function of expression level of the sensor, as indicated by emission upon excitation at 488 nm. Figure 3.3D shows the HyPer ratio within these same cells 10 minutes after stimulation with 20 μM H_2O_2, plotted as a function of emission intensity prior to stimulation, and it is clear that the magnitude of the observed HyPer response correlates with the expression level of the probe. The Spearman correlation between the emission intensity at time zero and the ratiometric response at 10 minutes was determined to be 0.70 ($p<0.05$), signifying that 70% of the variability in the HyPer ratio could be attributed to variation in the expression level of the probe.

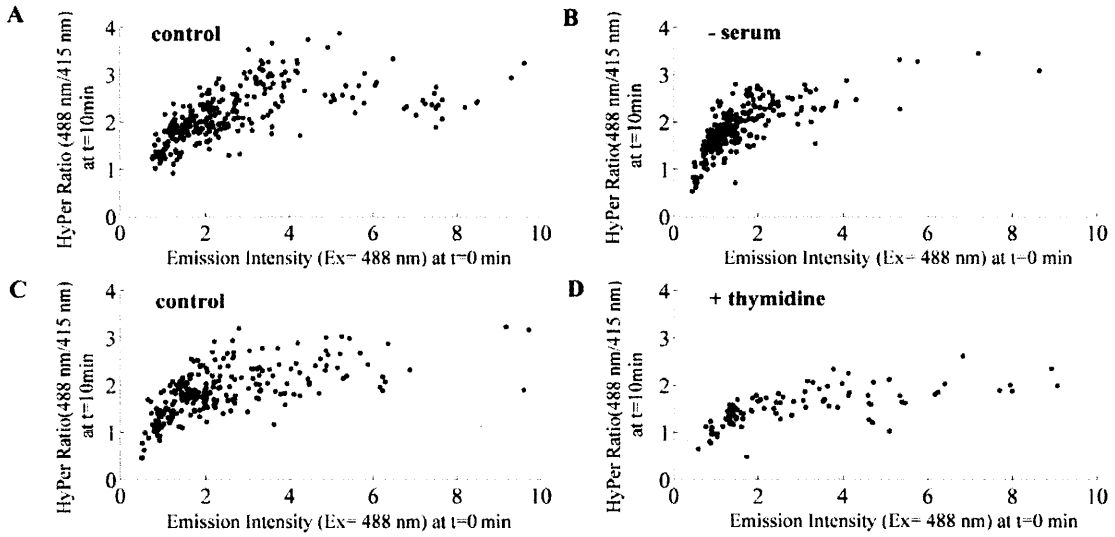

Figure 3.4: Phase within the cell cycle affects HyPer's response. HyPer-HeLa cells were synchronized in G0 phase using serum starvation or in G1 phase using 2 mM thymidine. Unsynchronized control cells cultured using complete medium (A) and synchronized cells cultured using serum-free medium were each identically stimulated with 20 μM H_2O_2 and imaged after 10 minutes. Similarly, unsynchronized control cells cultured in complete medium without thymidine (C) were compared with cells synchronized in G1 via culture using medium containing 2 mM thymidine (D). All emission intensities were scaled by a factor of 10^4.

We examined phase within the cell cycle as an additional factor that may contribute to the observed heterogeneity. We synchronized cells in different stages of the cell cycle to determine whether there is a difference in HyPer's response to H_2O_2 as a function of this variable. HeLa cells expressing HyPer were blocked in the G0 phase using serum starvation and in the G1 phase using 2 mM thymidine [24]. Figure 3.4 shows that, upon stimulation with 20 μM of H_2O_2, there was a subtle difference in the distribution of HyPer responses from cells that were blocked in the G0 phase (Figure 3.4B) compared to the unsychronized cell population (Figure 3.4A). The difference between HyPer responses of cells that were treated with thymidine and those that were not was more readily apparaent. Figure 3.4D shows that thymidine-blocked cells exhibited muted responses in comparison to cells that were unsychronized (Figure 3.4C).

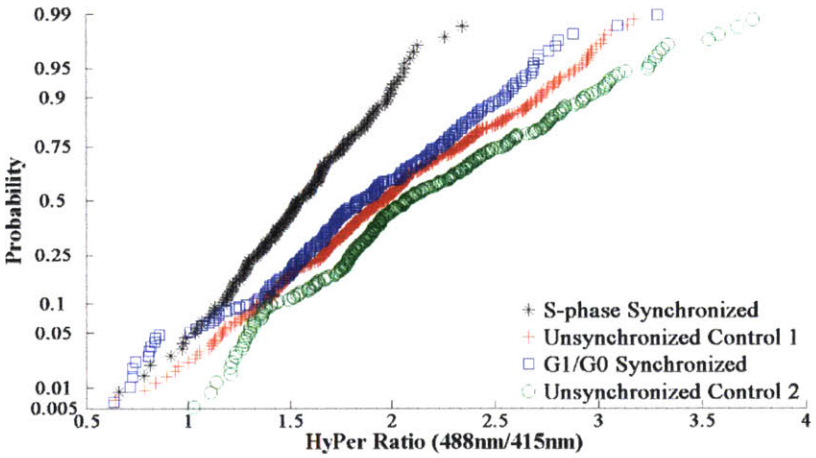

Figure 3.5: A normal probability plot of the cell cyle and its effect on HyPer signal. Phase within the cell cycle has an effect on the magnitude of the response of the fluorescent biosensor. All cells were stimulated with 20 μM H_2O_2 and imaged after 10 minutes. The HyPer ratio is a ratio of emission intensity at 525 nm upon excitation at two different wavelengths, 488 nm and 415 nm.

These differences are quantitatively elaborated by Figure 3.5, a normal probability plot. For cells that were blocked in the G1 phase using thymidine, the probability of the HyPer ratio within a cell being under 2.5 was 0.99, while for cells that were blocked using serum starvation this probability was 0.9. In contrast, this measure was 0.75-0.8 for unsychronized cells. In addition,

cells that were exposed to media containing thymidine do not have markedly lower expression levels of HyPer as evidenced by the magnitudes of emission intensities prior to stimulation, so a factor other than expression level of the sensor must be responsible for the observed differences in HyPer responses.

The levels of antioxidant enzymes have been reported to vary with phase within the cell cycle for some cell types [33]. We reasoned, on the basis of typical expression levels and second order rate constants for reaction with hydrogen peroxide, that upregulation of these enzymes may reduce the effectiveness of HyPer in the kinetic competion for reaction with hydrogen peroxide, resulting in lower observed HyPer signals. To measure the scavenging capacity of the G1 phase cells versus the unsynchronized cells, we compared the rates at which the two cultures removed hydrogen peroxide from the extracellular media. After adding 20 μM H_2O_2 to the cultures, we followed the H_2O_2 concentration remaining in the medium for 10 minutes. Fitting to a first order kinetic equation, we compared the decay rates obtained with G1 synchronized cells with those obtained using unsynchronized cells (Appendix). G1 cells (117±22 cells per field of view, n=4 fields) and unsynchronized cells (227±24 cells per field of view, n=6 fields) each removed H_2O_2 from the media at the same rate, with a decay constant for the entire dish of 0.1 min^{-1}. Since fewer cells in the case of the thymidine-blocked sample contributed to this rate of removal, the data suggest that these cells have a greater capacity for scavenging hydrogen peroxide. One of the ways the decay rate per cell can be increased is if the antioxidant levels inside each cell are up-regulated. Therefore, variations in phase within the cell cycle may contribute to hetereogenity in HyPer response, with higher antioxidant levels leading to lower observed ratiometric responses.

3.3.4 Mathematical model of metabolism of hydrogen peroxide by HeLa cells expressing HyPer

In order to better understand why variations in the expression level of the probe and antioxidant levels within individual cells might cause variation in HyPer's response, we implemented an ODE-based network model simulating the redox reactions of H_2O_2, HyPer, antioxidants and other proteins within a cell. The network model for H_2O_2 elimination by Jurkat cells reported by Adimora et al. served as a base template, since it included the reactivity of catalase, glutathione peroxidase, peroxiredoxin and glutaredoxin, the redox reactions of thioredoxin and glutathione, the pseudo-enzymatic oxidative turnover of protein thiols, and the diffusion of H_2O_2 across the plasma membrane [26]. We adjusted the model for HeLa cells using rate constants and other parameters that we measured in previous work [23]. We added reactions of HyPer with H_2O_2, glutathione and glutaredoxin to the basic framework (Figure 3.6A).

The oxidation of HyPer by H_2O_2 occurs at cysteine 199 of the OxyR domain [34]. As a result of this reaction, HyPer in its reduced state (HyPer-$(SH)_2$) converts to a sulfenic acid form (HyPer-SOH) that can react with cysteine 208 on the same domain to form a disulfide bond [34]. This fully oxidized form of HyPer (HyPer-SS) differs significantly in conformation from the reduced form, as evidenced by a change in the excitation spectrum [18]. Alternatively, glutathione can react with HyPer-SOH to form a mixed-disulfide form of HyPer (HyPer-SSG) that can be reduced by glutaredoxin [35]. For the reduction of the fully oxidized HyPer (HyPer-SS), it has been shown that the disulfide bonds of OxyR are preferentially reduced by the glutaredoxin (Grx)/glutathione (GSH) system [16,36,37]. Glutaredoxin can attack the disulfide bond via a dithiol mechanism similar to thioredoxin, resulting in the transfer of the disulfide bond to glutaredoxin and the reduction of HyPer [35,38]. The oxidized glutaredoxin (Grx-SS) can then be reduced by GSH [35,38,39].

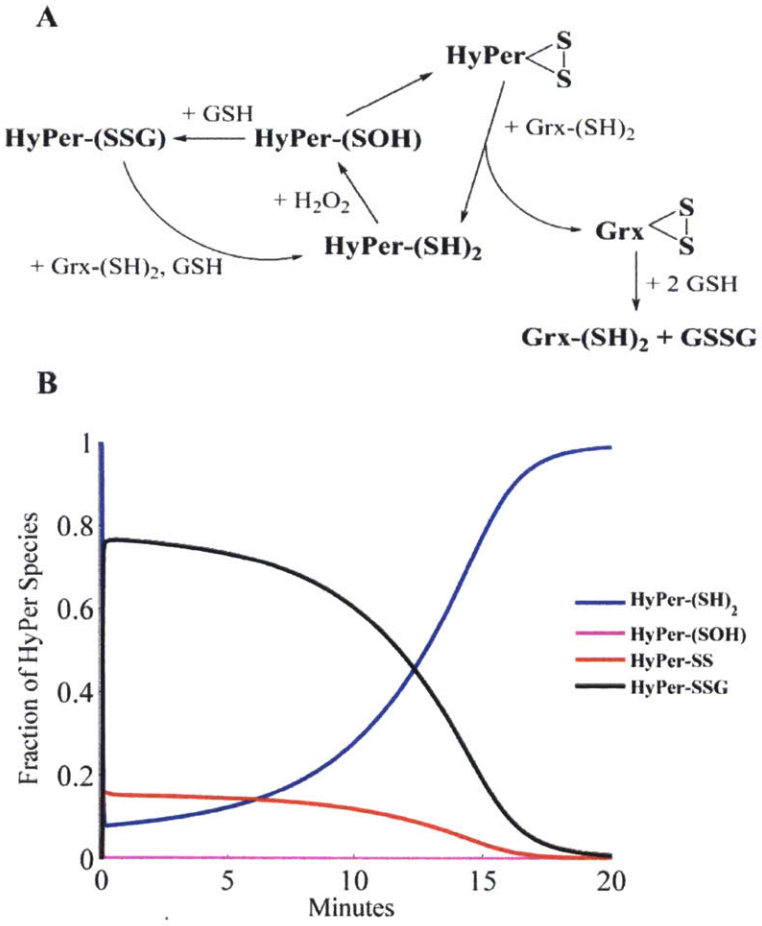

Figure 3.6: Network of HyPer's reactions with H_2O_2 and cellular disulfide reductase species and simulated reaction kinetics. (A) Schematic of the HyPer oxidation and reduction through H_2O_2. The reduced form of HyPer (HyPer-$(SH)_2$) is oxidized to the sulfenic form, HyPer-(SOH), through cysteine oxidation at the 199 position. This intermediate species can then form a mix-disulfide bond with glutathione (GSH) to form HyPer-SSG, or it can form a disulfide bond with a nearby cysteine (HyPer-SS), causing a conformational change in HyPer that leads to a different excitation spectrum. Both HyPer-SSG and HyPer-SS are reduced by glutaredoxin (Grx) and GSH back to HyPer-$(SH)_2$. (B) Representative figure showing the predicted fraction of each of HyPer's oxidation states over time after stimulation with 20 μM of H_2O_2 bolus. Total HyPer concentration = 0.1 μM. A majority of the HyPer proteins convert to HyPer-SSG almost immediately upon oxidation due to rapid reactions with abundant GSH in the cytoplasm. Slightly less than 20% convert to the HyPer-SS form. A negligible fraction of the HyPer proteins are in the HyPer-SOH form since it reacts very quickly with a cysteine or a GSH. Over time, the Grx/GSH reduction cycle converts the various oxidized forms of HyPer back to HyPer-$(SH)_2$. We assume that HyPer-SS is the only species that has a different excitation spectrum. Thus changes in the overall HyPer ratio can be represented by fraction of HyPer-SS.

The measured excitation spectrum from a cell expressing HyPer at a particular time point reflects contributions from all of the various oxidation states that are present at that time. Thus, the overall HyPer ratio in a cell is determined by

$$f_{hyper-ss} * R_{hyper-ss} + f_{hyper-ssG} * R_{hyper-ssG} + f_{hyper-(SH)_2} * R_{hyper-(SH)_2} + f_{hyper-SOH} * R_{hyper-SOH}$$

where f is the fraction of the total HyPer that is in a particular oxidation state, and R is the ratio of emission upon excitation at 488 nm to emission upon excitation at 415 nm for that particular state. From the equation, it is evident that changes in the average HyPer ratio is determined by the changes in the fraction of HyPer in each oxidation state. In our model, we simulated the experimental addition of a 20 μM bolus of H_2O_2 outside the cell and followed the kinetics of the HyPer subspecies distributions over time (Figure 3.6B), assuming that all of the HyPer are initially in the reduced form [40]. Immediately after the addition of H_2O_2, about 80% of the HyPer molecules convert to the HyPer-SSG state while about 20% react to form HyPer-SS. Over a period of 20 minutes, the fraction of HyPer in these two states decreases as glutaredoxin and glutathione reduces the disulfide bonds and the fraction of HyPer-$(SH)_2$ rises (Figure 3.6B). HyPer-SOH represents a negligible fraction of the total HyPer concentration since it is quickly converted to the disulfide or mixed disulfide form. For the purposes of this analysis, we assume that HyPer-$(SH)_2$, HyPer-SOH and HyPer-SSG have similar excitation spectra since the modifying groups are small and limited to one thiol group, and only HyPer-SS has a significantly different spectrum than that of the reduced form. Thus, changes in the fraction of HyPer in the fully oxidized state are an indirect indication of changes in the overall HyPer ratio.

Typical heterologous expression levels of fluorescent proteins appropriate for detection using fluorescence microscopy result in intracellular, cytosolic concentrations in the range of 0.1-1 μM [41,42]. We varied the intracellular concentration of HyPer from 0.1-0.5 μM in our model, and plotted the predicted fraction of HyPer-SS as a function of time following the addition of a 20 μM bolus of H_2O_2 (Figure 3.7A). We found that increasing the expression level of HyPer increases the fraction of HyPer-SS, and the differences in the fractional value for each expression

level becomes more significant with time. One hypothesis we investigated is that an increased expression level of HyPer would make it a more effective competitor with the antioxidants inside

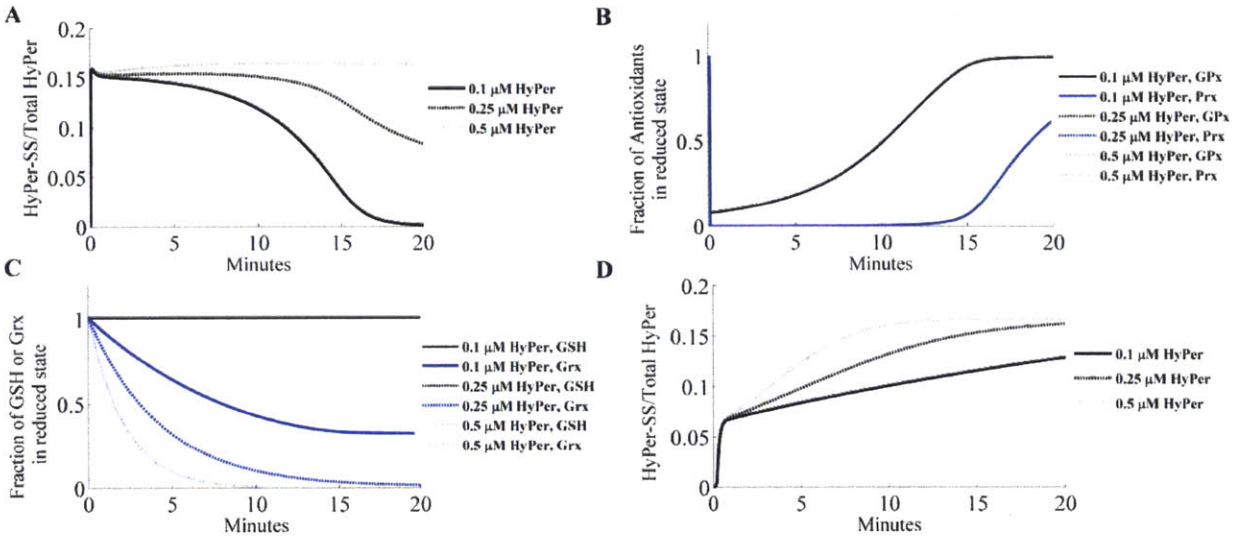

Figure 3.7: Predictions of the impact of variations in HyPer's expression level on the expected oxidation states of HyPer and several antioxidant species as a function of time following stimulation with an extracellular bolus of 20 μM H_2O_2 (A-C) or stimulation with continuous, endogenously generated H_2O_2 (D). (A) Increasing the expression level of HyPer from 0.1 to 0.5 μM changes the fraction of HyPer in the disulfide bond form significantly. (B) The effect of increased expression levels of HyPer on the fraction of glutathione peroxidase (GPx) and peroxiredoxin (Prx) in the reduced form over time. Coincident curves show that the expression level of HyPer has no effect on either. (C) Effects of an increased expression level of HyPer on the concentrations of GSH and reduced Grx over time. While the GSH concentration did not change, the amount of reduced Grx decreased significantly with higher HyPer expression level. (D) The effect of increased expression levels of HyPer on the fraction of HyPer in the disulfide bond for endogenous generation of H_2O_2. Elevating the internal generation of H_2O_2 to 1.1 x 10^{-5} M/s causes a continuous increase in the fraction of HyPer-SS, and the magnitude of this increase varies with HyPer expression level. Depending on the total HyPer present inside each cell, different HyPer ratios might be measured upon an identical stimulation to all cells.

the cell for H_2O_2. However, when we examined glutathione peroxidase (GPx) and peroxiredoxin (Prx), two of the dominant H_2O_2 scavengers inside the cell, there is no effect on the magnitude of their interaction with H_2O_2 as measured by the fraction of the GPx and Prx proteins that are in the reduced form in response to the 20 μM bolus (Figure 3.7B). Since the expression level of HyPer does not affect the competition at the oxidation step, we examined the effect of HyPer's expression level on the two reduction agents, Grx and GSH. While increasing the concentration of HyPer within the cell does not affect the concentration of GSH in response to the H_2O_2 bolus, it significantly depletes the level of reduced Grx (Figure 3.7C). This prediction implies that the

reduction of oxidized HyPer is slowed in response to the increased expression of the sensor. Increasing the total expression level of HyPer means proportionally more HyPer molecules can be oxidized, however, the limited amount of reduced glutaredoxin means only certain number of the disulfide bonds can be reduced at a time, causing an accumulation of HyPer in the oxidized HyPer-SS states, and therefore elevating the overall HyPer ratio. This bottleneck at the reduction step due to Grx causes differences in the fraction of HyPer-SS to become more significant with increased time, since the sensor is more rapidly reduced for lower concentrations of HyPer while at higher concentrations, HyPer remains trapped in the disulfide form.

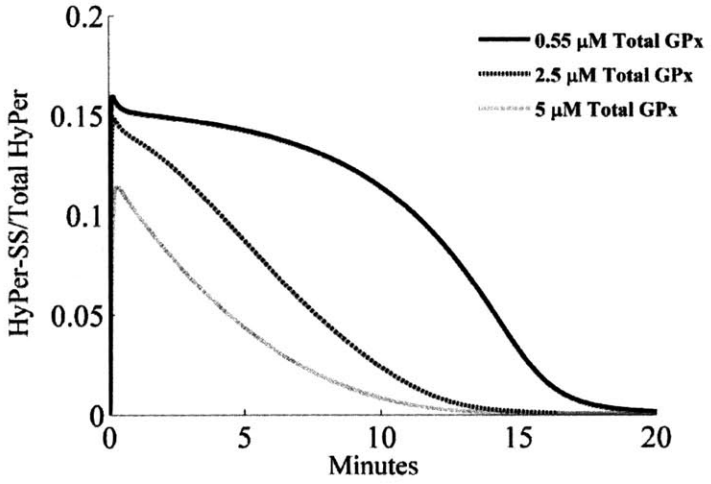

Figure 3.8: The effect of variation in antioxidant expression level on HyPer's oxidation state following stimulation with an extracellular bolus of 20 μM H_2O_2. An increase in glutathione peroxidase (GPx) concentration in the range of 0.55 μM to 5 μM causes a decrease in the fraction of HyPer-SS.

For the bolus addition of H_2O_2, Figure 3.7A suggests that reading the signal at earlier time points may minimize the response differences as a function of HyPer expression levels, before the kinetics of the reduction step play a significant role. However, in many cases of interest, the elevation of H_2O_2 levels is continuous, and following the signal from the sensor over a longer period of time is desirable. In this case, the reduction kinetics becomes important as shown in Figure 3.7D. We simulated the case of internal generation of H_2O_2 and predicted the signal

development over a period of twenty minutes. In this case, the rise in fraction of HyPer-SS is significantly different depending on the expression level of HyPer in the cell.

We also wanted to use our model to investigate whether changes in the antioxidant levels of the cell can impact the HyPer ratio, since we found that thymidine-blocked cells had enhanced H_2O_2 scavenging capacity. As we increased the expression level of glutathione peroxidase, we saw a decrease in the fraction of HyPer-SS (Figure 3.8). This prediction is consistent with our observation that these synchronized cells exhibited a muted response compared to the unsynchronized cells. The increase in antioxidants decreases the amount of H_2O_2 available to react with HyPer, resulting in a lower overall signal.

3.4 Discussion and Conclusion

The ratiometric property of HyPer and other disulfide redox sensors have long been touted as a way of circumventing problems interpreting data since variations in the expression level of the sensor are not expected to affect the response. However, we found that the expression level of the genetic sensor does affect its ratiometric response to H_2O_2. The higher the expression level of the probe, the higher its percentage residing in the oxidized rather than the reduced form, resulting in a higher ratio. Contrary to our initial intuition, the model predicts that an increased expression level of HyPer does not significantly alter its competition with the antioxidant network inside for reaction with H_2O_2, likely because of the slow second order rate constant of HyPer compared to that of the antioxidants. Instead, our model suggests that there is an imbalance between a rapid oxidation reaction of the sensor by hydrogen peroxide and a slow reduction step once the sensor is oxidized, with glutaredoxin as the limiting reagent for reduction. This imbalance results in an accumulation of HyPer in a disulfide form that increases

with the expression level of the probe, while the active depletion of glutaredoxin prevents a proportionate amount of HyPer from being effectively recycled. Following this logic, the magnitude of the ratiometric signal at the level of the individual cell from other genetic H_2O_2 sensors such as the ro-GFP family may also show a similar dependence on expression level since the disulfide bond of the ro-GFP interacts preferentially with glutaredoxin [16,37]. We should note that at the extreme ends of the dose-response curve, this dependence on the expression level is minimized: for H_2O_2 concentrations less than 1 μM, not enough of the sensor is oxidized to create a kinetic bottleneck during recycling; for H_2O_2 concentrations greater than 200 μM, the residence time of H_2O_2 in the cell is long enough such that much of the sensor is being continually oxidized for a long period of time, and recycling to the reduced state is extremely slow regardless of the sensor expression level. However, these concentrations are outside of the detectable or dynamic range of HyPer.

Furthermore, we found that HyPer-expressing cells blocked in the G1 of the cell cycle respond to H_2O_2 with a muted ratiomentric signal in comparison to cells expressing similar levels of HyPer in other phases of the cell cycle. These cells also showed higher H_2O_2 scavenging ability, implying that they have a higher antioxidant capacity. It is possible that the muted HyPer response to H_2O_2 in G1 phase synchronized cells was due to the presence of higher antioxidant levels. We tested this explanation using our model by increasing the concentration of glutathione peroxidase (GPx), an enzyme that catalyzes the elimination of H_2O_2, and found that an increase in the intracellular concentration of this antioxidant caused a decrease in the fraction of HyPer molecules predicted to be found in the oxidized form (HyPer-SS).

An alternative hypothesis for the heterogeneity in HyPer's response from cell to cell that we have not explored is that the redox states of the HeLa cells are in reality vastly different from one

another at the basal state, even though differences are undetectable by HyPer. These differences may manifest when H_2O_2 is added to the cells, putting the overall intracellular concentration in the detection range of HyPer. This explanation would suggest that the cell-to-cell variation in H_2O_2 level is on the same order of magnitude as that of the dynamic range of the sensor and a large quantity of valuable information could potentially lie outside of what the probe can measure and detect. Intracellular probes that respond to even lower levels of hydrogen peroxide are not currently available; thus, a test of this hypothesis is not feasible at present.

We showed that the expression level of the sensor and the antioxidant variations among cells at different stages of the cycle can yield very different HyPer ratios in response to the same H_2O_2 stimulus. This heterogeneity suggests that, for questions that are quantitative in nature, caution must be exercised in comparing the responses of small numbers of cells to one another. The automated image processing technique we described allows for unbiased analysis of hundreds of cells from different fields of view, while previous literature that used HyPer for microscopic studies have analyzed typically on the order of 10 cells. We must be careful making inferences based on a few cells, taking into account sensor expression level and cell cycle phase as potential experimental artifacts that can be misinterpreted as indicators of differing magnitudes of change in intracellular peroxide concentration. A quantitative understanding of hydrogen peroxide's role as a cellular signaling molecule will contribute to mechanistic understanding of how networks of reactions control phenotype. To achieve this understanding using genetic sensors, it is important that we measure their outputs with an awareness of the caveats of using these tools to monitor dynamic concentrations of redox-active analytes.

3.5 Bibliography

(1) Finkel, T. (2011) Signal transduction by reactive oxygen species. *J. Cell Biol.*

(2) Marinho, H. S., Real, C., Cyrne, L., Soares, H., and Antunes, F. (2014) Hydrogen peroxide sensing, signaling and regulation of transcription factors. *Redox Biol. 2*, 535–562.

(3) Sies, H. (2014) Role of metabolic H2O2 generation: redox signaling and oxidative stress. *J. Biol. Chem. 289*, 8735–41.

(4) Wiseman, H., and Halliwell, B. (1996) Inflammatory Disease and Progression To Cancer *29*, 17–29.

(5) Trachootham, D., Alexandre, J., and Huang, P. (2009) Targeting cancer cells by ROS-mediated mechanisms: a radical therapeutic approach? *Nat. Rev. Drug Discov. 8*, 579–91.

(6) Gorrini, C., Harris, I. S., and Mak, T. W. (2013) Modulation of oxidative stress as an anticancer strategy. *Nat. Rev. Drug Discov. 12*, 931–47.

(7) Barnham, K. J., Masters, C. L., and Bush, A. I. (2004) Neurodegenerative diseases and oxidative stress. *Nat. Rev. Drug Discov. 3*, 205–214.

(8) Gao, L., and Mann, G. E. (2009) Vascular NAD(P)H oxidase activation in diabetes: a double-edged sword in redox signalling. *Cardiovasc. Res. 82*, 9–20.

(9) Al Ghouleh, I., Khoo, N. K. H., Knaus, U. G., Griendling, K. K., Touyz, R. M., Thannickal, V. J., Barchowsky, A., Nauseef, W. M., Kelley, E. E., Bauer, P. M., Darley-Usmar, V., Shiva, S., Cifuentes-Pagano, E., Freeman, B. a., Gladwin, M. T., and Pagano, P. J. (2011) Oxidases and peroxidases in cardiovascular and lung disease: New concepts in reactive oxygen species signaling. *Free Radic. Biol. Med. 51*, 1271–1288.

(10) García-Santamarina, S., Boronat, S., and Hidalgo, E. (2014) Reversible cysteine oxidation in hydrogen peroxide sensing and signal transduction. *Biochemistry 53*, 2560–2580.

(11) Sobotta, M. C., Liou, W., Stöcker, S., Talwar, D., Oehler, M., Ruppert, T., Scharf, A. N. D., and Dick, T. P. (2014) Peroxiredoxin-2 and STAT3 form a redox relay for H2O2 signaling. *Nat. Chem. Biol. 11*, 64–70.

(12) Rhee, S. G., Woo, H. A., Kil, I. S., and Bae, S. H. (2012) Peroxiredoxin functions as a peroxidase and a regulator and sensor of local peroxides. *J. Biol. Chem. 287*, 4403–10.

(13) Gough, D. R., and Cotter, T. G. (2011) Hydrogen peroxide: a Jekyll and Hyde signalling molecule. *Cell Death Dis. 2*, e213.

(14) Winterbourn, C. C. (2014) The challenges of using fluorescent probes to detect and quantify specific reactive oxygen species in living cells. *Biochim. Biophys. Acta 1840*, 730–8.

(15) Ezeri, D., Morgan, B., and Dick, T. P. NOTICE WARNING CONCERNING The copyright law of the United States [Title 17 , United States Code] governs the making of photocopies or other reproductions of copyrighted material Under certain conditions specified in the law , libraries and archives are .

(16) Lukyanov, K. a, and Belousov, V. V. (2014) Genetically encoded fluorescent redox sensors. *Biochim. Biophys. Acta 1840*, 745–56.

(17) Rhee, S. G., Chang, T. S., Jeong, W., and Kang, D. (2010) Methods for Detection and Measurement of Hydrogen Peroxide Inside and Outside of Cells. *Mol. Cells 29*, 539–549.

(18) Belousov, V. V, Fradkov, A. F., Lukyanov, K. A., Staroverov, D. B., Shakhbazov, K. S., Terskikh, A. V, and Lukyanov, S. (2006) Genetically encoded fluorescent indicator for intracellular hydrogen peroxide. *Nat. Methods 3*, 281–6.

(19) Gutscher, M., Sobotta, M. C., Wabnitz, G. H., Ballikaya, S., Meyer, A. J., Samstag, Y., and Dick, T. P. (2009) Proximity-based protein thiol oxidation by H2O2-scavenging peroxidases. *J. Biol. Chem. 284*, 31532–40.

(20) Enyedi, B., Zana, M., Donkó, Á., and Geiszt, M. (2013) Spatial and temporal analysis of NADPH oxidase-generated hydrogen peroxide signals by novel fluorescent reporter proteins. *Antioxid. Redox Signal. 19*, 523–34.

(21) Breckwoldt, M. O., Pfister, F. M. J., Bradley, P. M., Marinković, P., Williams, P. R., Brill, M. S., Plomer, B., Schmalz, A., St Clair, D. K., Naumann, R., Griesbeck, O., Schwarzländer, M., Godinho, L., Bareyre, F. M., Dick, T. P., Kerschensteiner, M., and Misgeld, T. (2014) Multiparametric optical analysis of mitochondrial redox signals during neuronal physiology and pathology in vivo. *Nat. Med. 20*, 555–60.

(22) Malinouski, M., Zhou, Y., Belousov, V. V, Hatfield, D. L., and Gladyshev, V. N. (2011) Hydrogen Peroxide Probes Directed to Different Cellular Compartments. *PLoS One 6*.

(23) Huang, B. K., and Sikes, H. D. (2014) Quantifying intracellular hydrogen peroxide perturbations in terms of concentration. *Redox Biol. 2*, 955–962.

(24) Bootsma, D., Budke, L., and Vos, O. (1964) Studies on Synchronous Division of Tissue Culture Cells Initiated By Excess Thymidine. *Exp. Cell Res. 33*, 301–309.

(25) Lafontaine, J., Rodier, F., Tchakarska, G., and Mes-Masson, A.-M. (2012) Necdin modulates proliferative cell survival of human cells in response to genotoxic stress. *BMC Cancer 12*, 234.

(26) Adimora, N. J., Jones, D. P., and Kemp, M. L. (2010) A Model of Redox Kinetics Implicates the Thiol Proteome in Cellular Hydrogen Peroxide Responses. *Antioxid. Redox Signal. 13*, 731–743.

(27) Matlashov, M. E., Belousov, V. V, and Enikolopov, G. (2014) How much H(2)O(2) is produced by recombinant D-amino acid oxidase in mammalian cells? *Antioxid. Redox Signal. 20*, 1039–44.

(28) Miller, E. W., Taulet, N., Onak, C. S., New, E. J., Lanselle, J. K., Smelick, G. S., and Chang, C. J. (2010) Light-activated regulation of cofilin dynamics using a photocaged hydrogen peroxide generator. *J. Am. Chem. Soc. 132*, 17071–3.

(29) Espinosa, A., García, A., Härtel, S., Hidalgo, C., and Jaimovich, E. (2009) NADPH oxidase and hydrogen peroxide mediate insulin-induced calcium increase in skeletal muscle cells. *J. Biol. Chem. 284*, 2568–2575.

(30) Weyemi, U., Lagente-Chevallier, O., Boufraqech, M., Prenois, F., Courtin, F., Caillou, B., Talbot, M., Dardalhon, M., Al Ghuzlan, a, Bidart, J.-M., Schlumberger, M., and Dupuy, C. (2012) ROS-generating NADPH oxidase NOX4 is a critical mediator in oncogenic H-Ras-induced DNA damage and subsequent senescence. *Oncogene 31*, 1117–1129.

(31) Hartig, S. M. (2013) Basic image analysis and manipulation in imageJ. *Curr. Protoc. Mol. Biol.* 1–12.

(32) Carpenter, A. E., Jones, T. R., Lamprecht, M. R., Clarke, C., Kang, I. H., Friman, O., Guertin, D. a, Chang, J. H., Lindquist, R. a, Moffat, J., Golland, P., and Sabatini, D. M. (2006) CellProfiler: image analysis software for identifying and quantifying cell phenotypes. *Genome Biol. 7*, R100.

(33) Li, N., and Oberley, T. D. (1998) Modulation of antioxidant enzymes, reactive oxygen species, and glutathione levels in manganese superoxide dismutaseoverexpressing NIH/3T3 fibroblasts during the cell cycle. *J. Cell. Physiol. 177*, 148–160.

(34) Tao, K. (1999) In vivo oxidation-reduction kinetics of OxyR, the transcriptional activator for an oxidative stress-inducible regulon in Escherichia coli. *FEBS Lett. 457*, 90–92.

(35) Berndt, C., Lillig, C. H., and Holmgren, A. (2007) Thiol-based mechanisms of the thioredoxin and glutaredoxin systems: implications for diseases in the cardiovascular system. *Am. J. Physiol. Heart Circ. Physiol. 292*, H1227–36.

(36) Aslund, F., Zheng, M., Beckwith, J., and Storz, G. (1999) Regulation of the OxyR transcription factor by hydrogen peroxide and the cellular thiol-disulfide status. *Proc. Natl. Acad. Sci. U. S. A. 96*, 6161–6165.

(37) Meyer, A. J., and Dick, T. P. (2010) Fluorescent protein-based redox probes. *Antioxid. Redox Signal. 13*, 621–50.

(38) Lillig, C. H., and Berndt, C. (2013) Glutaredoxins in thiol/disulfide exchange. *Antioxid. Redox Signal. 18*, 1654–65.

(39) Østergaard, H., Tachibana, C., and Winther, J. R. (2004) Monitoring disulfide bond formation in the eukaryotic cytosol. *J. Cell Biol. 166*, 337–345.

(40) Malinouski, M., Zhou, Y., Belousov, V. V, Hatfield, D. L., and Gladyshev, V. N. (2011) Hydrogen peroxide probes directed to different cellular compartments. *PLoS One* (Kowaltowski, A. J., Ed.) *6*, e14564.

(41) Tsien, R. Y. (1998) The green fluorescent protein. *Annu. Rev. Biochem. 67*, 509–544.

(42) Patterson, G. H., Knobel, S. M., Sharif, W. D., Kain, S. R., and Piston, D. W. (1997) Use of the green fluorescent protein and its mutants in quantitative fluorescence microscopy. *Biophys. J. 73*, 2782–2790.

(43) Low, F. M., Hampton, M. B., Peskin, A. V, and Winterbourn, C. C. (2007) Peroxiredoxin 2 functions as a noncatalytic scavenger of low-level hydrogen peroxide in the erythrocyte. *Blood 109*, 2611–7.

(44) Peskin, A. V, Dickerhof, N., Poynton, R. A., Paton, L. N., Pace, P. E., Hampton, M. B., and Winterbourn, C. C. (2013) Hyperoxidation of peroxiredoxins 2 and 3: rate constants for the reactions of the sulfenic acid of the peroxidatic cysteine. *J. Biol. Chem. 288*, 14170–7.

(45) Kemp, M., Go, Y.-M., and Jones, D. P. (2008) Nonequilibrium thermodynamics of thiol/disulfide redox systems: a perspective on redox systems biology. *Free Radic. Biol. Med. 44*, 921–937.

(46) Lundberg, M., Fernandes, A. P., Kumar, S., and Holmgren, A. (2004) Cellular and plasma levels of human glutaredoxin 1 and 2 detected by sensitive ELISA systems. *Biochem. Biophys. Res. Commun. 319*, 801–809.

(47) Kóna, J., and Brinck, T. (2006) A combined molecular dynamics simulation and quantum chemical study on the mechanism for activation of the OxyR transcription factor by hydrogen peroxide. *Org. Biomol. Chem. 4*, 3468–78.

(48) Holmgren, a, Johansson, C., Berndt, C., Lönn, M. E., Hudemann, C., and Lillig, C. H. (2005) Thiol redox control via thioredoxin and glutaredoxin systems. *Biochem. Soc. Trans. 33*, 1375–7.

(49) Holmgren, A. (1985) Thioh.edoxin.

(50) Fernandes, A. P., and Holmgren, A. (2004) Glutaredoxins: glutathione-dependent redox enzymes with functions far beyond a simple thioredoxin backup system. *Antioxid. Redox Signal. 6*, 63–74.

3.6 Appendix

HRP-ABTS assay is used to measure antioxidant capacity by following the H_2O_2 decay kinetics in thymidine blocked (A) and unsynchronized cells (B). 20 μM H_2O_2 was added in the extracellular medium. Samples were withdrawn every 2 minutes to measure the remaining H_2O_2 concentration. Each data point is the average of three measurements. Error bars represent one standard deviation about the mean. The exponential decay constants calculated from the kinetic data in (A) and (B) were 0.1 min^{-1} for each case. In order to meaningfully compare the peroxide scavenging capacities of thymidine blocked cells (A) with unsynchronized cells (B), it is essential to consider the number of cells in each sample. Cells were counted in brightfield images obtained using a 20X magnification lens. The average cell count was 117 ± 22 (n=4 images) in thymidine blocked samples and 227 ± 24 (n=6 images) in unsynchronized samples. Since fewer cells in (A) than in (B) led to the same decay constant, these data suggest that the thymidine blocked cells had a greater capacity for reducing hydrogen peroxide.

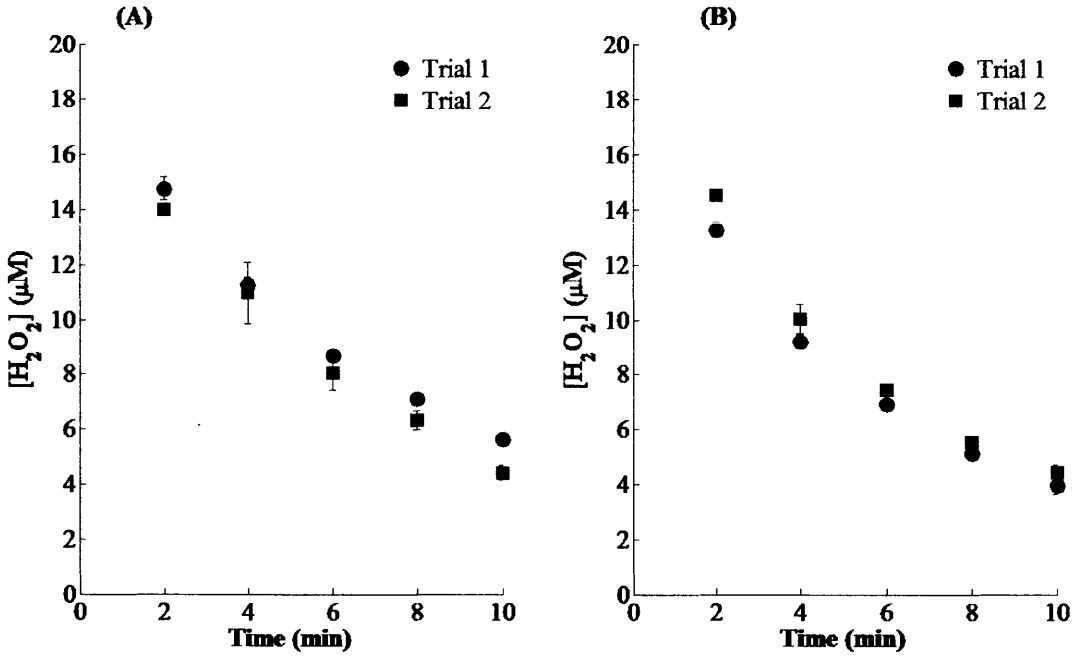

Parameters values for HeLa cells (this work) that differ from those used in Adimora et al.'s model of Jurkat cells (26).

Reaction	**Rate Constant**
k_1	1×10^{-3} cm/s**
k_8	1.3×10^{7} M^{-1} s^{-1} [43]
k_9	1.2×10^{4} M^{-1} s^{-1} [44]
k_{11}	2 s^{-1} [44]
k_{14}	1×10^{2} M^{-1} s^{-1} [2]
k_{18}	1×10^{2} M^{-1} s^{-1} [2]
k_{24}	3.84×10^{-7} M/s [45]
Species	**Initial Concentration**
H_2O_2	20 μM
GPx reduced	0.55 μM [23]
Catalase cytoplasm	0.1 μM [23]
Prx reduced	100 μM [23]
Grx-SH	0.8 μM [46]
Cell density	0.4 million/mL

** fitted to the experimental H_2O_2 decay data in S1

Added parameters for HyPer mechanism

Reaction	Rate Constant
k_{ox}	1.1×10^5 M^{-1} s^{-1} [47]
k_{s}	9.7 s^{-1} [47]
k_{red}	1.0×10^5 M^{-1} s^{-1} [48–50]**
k_{GSHssg}	1.2×10^5 M^{-1} s^{-1} [39]
k_{ssg}	1.2×10^5 M^{-1} s^{-1} [26]
k_{GRssg}	9.1×10^4 M^{-1} s^{-1} [26]
Species	**Initial Concentration**
HyPer-$(SH)_2$	0.1-0.5 μM [41,42]
HyPer-(SOH)	1×10^{-14} M
HyPer-SS	1×10^{-14} μM
HyPer-SSG	1×10^{-14} μM
Grx-SS	1×10^{-14} μM

**based on the similarity in structure and in function at the active site of dithiol reduction mechanism of glutaredoxin and thioredoxin

Chapter 4: Using peroxide sensors and generators for quantitative analysis of H_2O_2-induced toxicity

4.1 Introduction

Hydrogen peroxide is an often-studied member of a class of molecules called reactive oxidative species (ROS) due to its stability, longer life-time and involvement in a number of signaling pathways within the cell, causing a variety of observable cellular responses. [1–3] Depending on the intracellular level of H_2O_2, these responses can be a part of normal cellular homeostasis, or associated with pathological outcomes.[4,5] It is hypothesized that low level elevation of hydrogen peroxide promotes survival, proliferation and differentiation, while increasing peroxide beyond that level lead to increase DNA and lipid injury, eventually leading to apoptosis.[4,6,7] Despite the importance of peroxide level in controlling phenotype outcome, there are very few studies putting quantitative numbers on these levels in a physiologically relevant way. The few studies that do exist are often done with a bolus addition or extracellular enzymatic generation, when many examples of oxidative elevation are intracellular processes.[6,8,9] The lack of quantitative information about H_2O_2 has led to many conflicting reports on mechanisms of H_2O_2-mediated pathways involving cell apoptosis.[10,11]

Mounting evidence suggests that cancer cells in particular have elevated levels of H_2O_2 compared to their normal counterparts.[12,13] As a method of combating the toxicity effects of elevated oxidative stress, tumor cells often have higher levels of antioxidants and are extremely reliant on these molecules for survival.[14–16] Thus, it is believed that targeting these antioxidant

defenses and subsequently raising of the oxidative stress level above the toxicity threshold might be a viable option for selectively eliminating tumor cells while sparing normal cells.[12,16–18] Many cancer chemotherapeutics have been designed around this principle.[17,19–21] However, the success rate of these ROS-based chemotherapeutics is low due to use of non-specific, non-quantitative probes.[22,23] We believe that with a better quantitative understanding of the oxidative stress threshold leading to apoptosis, we will enable design of more effective ROS-based chemotherapeutics in the future.

We used a genetically encoded protein sensor is specific to H_2O_2 called HyPer that can quantify the intracellular production. HyPer is derived from the OxyR transcription factor found in bacteria with YFP inserted between two reactive thiol groups to provide a fluorescent readout of OxyR's oxidation state.[24,25] The sensor is expressed by the cell and emits a ratiometric fluorescence change upon reaction with hydrogen peroxide. Unlike the readouts in other intracellular peroxide sensing strategies, the signal of HyPer is reversible due to the activity of intracellular reductases, and this feature allows real-time monitoring of peroxide level.[26] In conjunction with HyPer, we generated hydrogen peroxide in a kinetically and spatially controlled fashion using two different enzymes. Glucose oxidase, an enzyme that can be added externally to the cell media, catalyzes the conversion of glucose and production of H_2O_2.[27] D-amino acid oxidase, an enzyme that can be expressing inside many different cellular compartments and the cytoplasm, and produces hydrogen peroxide as a by-product when D-alanine is added as a substrate in the media.[28,29] We want to explore the caveats and limitations of using HyPer for detection of continuous peroxide generation, investigate the differences in using an external versus internal generator, and develop better quantitative metrics for determining the threshold necessary to cause H_2O_2-mediated apoptosis in cancer cells. This systematic study of hydrogen

peroxide using physiologically and kinetically relevant generator tools will allow us direct the desired phenotypic outcome from ROS-based chemotherapeutics in the future.

4.2 Methods and Materials

Materials used

Glucose oxidase, D-alanine, Flavin adenine dinucleotide (FAD), methyl methanethiosulfonate (MMTS), horse radish peroxidase (HRP), puromycin, polybrene and H_2O_2 were all purchased from Sigma. 2, 2'-Azino-bis(3-ethylbenzothiazoline-6-sulfonic acid) diammonium salt (ABTS) was purchased from Tokyo Chemical Industry Co. The RPMI 1640 no-phenol red for generation experiments was purchased from Invitrogen. DMEM media was purchased from Lonza. FBS was purchased from ATCC. Staining reagents Annexin V-APC and propidium iodide were purchased from BioLegends. Prx-2 antibody was purchased from R&D Systems. HeLa cells were a gift from the Dane Wittrup (Massachusetts Institute of Technology, USA). The cytoplasmic HyPer plasmid was purchased from Evrogen. SypHer plasmid was a gift from Nicolas Demaurex (Addgene plasmid # 48250). The PLJM-EGFP plasmid was a gift from David Sabatini (Addgene plasmid #19319). The DAAO plasmid was a gift from Brian Ross (University of Michigan, USA).

Cell culture

HeLa cells were cultured in DMEM media supplemented with 10% fetal bovine serum (FBS). The cultures were maintained in 37°C humidified incubator in the presence of 5% CO2. Media was changed every 3 days and cells were passaged every 5-6 days. HeLa cells virally infected

with plasmids containing HyPer, catalase and DAAO were maintained in the same DMEM media containing 2ug/mL of puromycin.

Lentiviral infection of HyPer, SypHer, DAAO

HyPer, SypHer and DAAO were re-cloned from their original vector into a lenti-viral transfer plasmid PLJM-EGFP, cutting out the EGFP portion of the plasmid. HeK FT cells were seeded at $7.5x10^5$ cells/35mm well and grown for 2 days until 90% confluence. The PLJM transfer vector with the appropriate gene insert was co-transfected with the packaging plasmids PAX2 and pMD2.G at 3:2:1 ratio for a total of 5ug of plasmid and 10ug of Lipofectamine 2000 for a period of 18 hours in OptiMEM media. Subsequently, 1 mL of 10% FBS + DMEM media was used to replace the transfection media. This media containing lentiviruses was collected every 24 hours for a period of 2 days. The media was centrifuged at 500g for 5 minutes and the supernatant was collected.

The 1mL of the supernatant, along with 6ug/mL of polybrene, was then added to an 80-90% confluent 35mm well of HeLa cells. Three days post infection, media containing 5ug/mL of puromycin was used for selection of HeLa cells containing the plasmid for a period of 10 days for HyPer and SypHer. For the DAAO plasmid, the plasmid was incubated for 4 days post infection and used immediately.

Glucose oxidase H_2O_2 *generation*

A stock solution of glucose oxidase from *Aspergillus niger* was formed by diluting 0.1 mg of the powder in 1 mL of PB, kept on ice and made fresh every day. Immediately prior to use, the stock solution was diluted further 1:50 to 1:250 in 5 mL of PBS. For experiments involving studying the caveats of the HyPer signal, 20 μL of the diluted stock solution was added to 1 mL total

volume of RPMI 1640 media no phenol red (already containing glucose) and added to HeLa cells expressing HyPer seeded at 1 x 10^5 cells/well in a 24 well plate. For experiments involving phenotypic effects of glucose oxidase generation, 100 μL of the diluted stock solution was added to 2 mL of RPMI 1640 media no phenol red, then added to HeLa cells seeded at 3.5 x 10^5 cells/well in a 6-well plate. HyPer signal was followed over the desired period of time using microscopy. For phenotypic assays, media containing glucose oxidase was replaced with DMEM media containing 10% FBS after the peroxide generation period, and the assays were performed 48 hours later.

D-amino acid oxidase H_2O_2 *generation*

HeLa cells co-infected with HyPer (or SypHer) and DAAO plasmids were seeded at 1 x 10^5 cells/well on a 24 well plate for experiments studying caveats of the HyPer sensor signal, and 3.5 x 10^5 cells/well on a 6 well plate for experiments requiring phenotypic assays. The substrate for the DAAO enzyme, D-alanine, was added at 0-10 mM to the 1 mL of extracellular media (RPMI 1640, no phenol red), along with co-factor substrate FAD at 5 μM for the 24-well plate experiments. For the 6-well plate phenotypic experiments, the D-alanine was added at 0-24 mM to 2 mL of extracellular media, along with 5 μM FAD co-factor. Four microscopy images per well of the cells were taken with the HyPer wavelengths every 30 min to 1 hour for the desired H_2O_2 generation period. For phenotypic assays, media containing glucose oxidase was replaced with DMEM media containing 10% FBS after the peroxide generation period, and the assays were performed 48 hours later.

Microscope quantification of HyPer or SypHer signal

The excitation wavelengths of HyPer were captured using a Nikon x81 epi-fluorescence microscope on 10x objective setting. Images were excited at 415 nm/30 nm and 488 nm/25 nm and emission was recorded at 525 nm/40 nm, on 10% lamp intensity and 300ms exposure. Four to five fields of view are captured per condition, and the images were exported to ImageJ for post-processing. All images were background subtracted using the rolling ball algorithm with radius of 200 pixels, and then the mean pixel intensity for each image was measured [30]. The HyPer ratio for each field of view was calculated by dividing the mean pixel intensity at 488 nm by the mean pixel intensity at 415 nm. The baseline HyPer ratio is around 0.45-0.5, and the maximum ratio for the probe is 0.85-0.9.

ABTS assay for extracellular H_2O_2 *measurement*

2 mM stock solution of ABTS and 3 mg/mL of HRP were prepared in RPMI 1640 no phenol red media prior to start of the experiment. Extracellular media samples containing hydrogen peroxide were dilute 1:2 and 150 µL of the sample was added to 50 µL of 2 mM ABTS and 10 µL of 3 mg/mL HRP stock. The samples were mixed via shaking and read immediately at absorbance wavelength of 405 nm. A standard curve between 0uM and 100uM for hydrogen peroxide was done with each set of data.

Annexin V/PI Apoptosis assay

48 hours after generator treatment, the extracellular media and HeLa cells remaining on the dish were collected and centrifuged at 500 x g for 5 minutes. The pellet was re-suspended in 1 mL PBS and a cell count was performed. Following a second centrifugation, the cells were resuspended at a concentration of 1 million cells / mL in annexin V binding buffer containing 10 mM HEPES/NAOH, 150 mM NaCl and 2.5mM $CaCl_2$ (pH 7.4). 100 µL of the sample was

incubated with 5 μL of Annexin V- APC conjugate antibody and 10 μL of propidium iodide stain for 15 minutes in the dark. Afterwards, 400 μL of annexin V binding buffer was added to the mixture and the fluorescent reading in the APC and PE-Cy5 channels were read immediately via flow cytometry. Cells that were stained positive with PI or Annexin V antibody were considered apoptotic and a percentage of cell death was calculated based on a an analysis of 20,000 cells per condition.

Growth inhibition assay

48 hours after removal of peroxide generator, the remaining live cells on the dish were trypinized and quantified using Beckman Coulter Vi-Cell Counter (courtesy of Doug Lauffenburger, MIT), the fraction of live cells remaining was calculated by dividing by the number of live cells in the control case without H_2O_2 generation.

Immunoblot for Prx-2 oxidation

HeLa cells were exposed to 24 hours of continuous H_2O_2 generation via DAAO, below the detection limit of HyPer. After 24 hours, the cells were trypinized, washed once with 1x PBS, followed by re-suspension in 2 mL of 100mM MMTS to convert sulfhydryl groups to $-S-CH_3$. This is to prevent artificial oxidation during the cell lysis step.[9] The MMTS cell suspension was placed on ice for 20 minutes, followed by 2 more 1x PBS washes. The cell pellet was lysed using 100 μL of 1% Triton x-100, spun at 12,000g for 10 minutes and the supernatant cell lysate was collected and stored at -20 C until needed.

To immunoblot for monomer and dimer form of peroxiredoxin-2 (Prx-2), we denatured the cell lysate sample using non-reducing sample buffer, then loaded 25 ug of cell lysate per lane to run on a tris-tricine gel/buffer system. After transferring the proteins to a PDVF membrane, the blot is blocked using Licor blocking buffer for an hour, followed by overnight incubation in goat

primary antibody (1:1000 in PBS-blocking buffer-Tween20) against Prx-2 at 4C. After washing with PBS + 0.1% tween-20, licor anti-goat secondary antibody IR 688 was added at 1:10000 dilution and incubated for 1 hour. Blots are visualized on Odyssey CLx Infrared Imaging System (Koch Institute, Cambridge, MA).

4.3 Results

4.3.1 Interpreting signals from HyPer used in conjunction with a continuous peroxide generator

In order for us to gain better quantitative information about the amount of hydrogen peroxide that correlates with a particular phenotype, we need to accurately interpret the HyPer signal

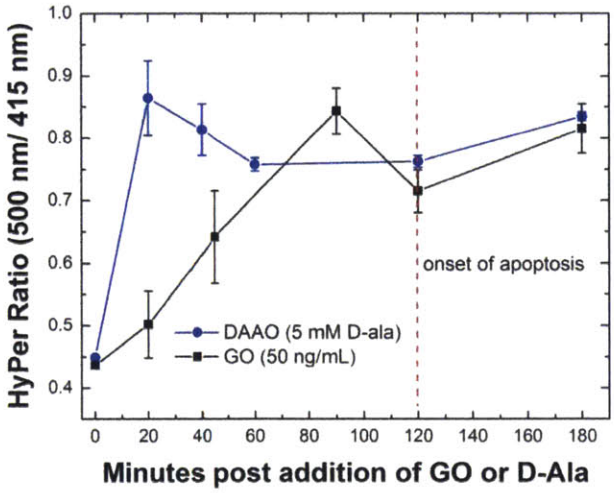

Figure 4.2: Sample kinetic profile of HyPer signal over time in response to DAAO or GO peroxide generators. 5 mM D-alanine or 50 ng/mL glucose oxidase was added to the extracellular media of HeLa cells expressing HyPer. The HyPer ratio was followed for a period of 3 hours. The HyPer ratio decreased upon reaching the maximum possible HyPer ratio at 0.85, and increased again after the cells began to show visible signs of apoptosis.

stemming from the presence of a continuous peroxide generator. We were able to generate H_2O_2 both extracellularly and intracellularly in HeLa cells expressing the HyPer sensor using two different enzymes. Glucose oxidase (GO) from *Aspergillus niger* was added to RPMI cell media

at concentrations from 0-50 ng/mL. The enzyme catalyzes the oxidation of glucose present in the RPMI media to H_2O_2 and D-glucono-lactone. This externally generated peroxide can then diffuse across the plasma membrane and cause a change in the HyPer ratiometric reading in the cytoplasm. Alternatively, D-amino acid oxidase (DAAO) from *R. gracilis* was co-expressed in HeLa cell cytoplasm with HyPer. Adding 0-10 mM D-alanine as substrate and 5 μM FAD as co-factor to the external media allow the two compounds to diffuse across the membrane and react with DAAO to produce intracellular H_2O_2 with tunable kinetics. We tracked the HyPer signal over a period of three hours for a range of substrate/enzyme concentrations. While most kinetic curves showed a steady increase HyPer signal over period measured, we noticed an interesting trend at the higher substrate or enzyme concentrations. A sample HyPer signal kinetic curve in response to each generator, 50 ng/mL of GO and 5 mM D-Alanine is shown in Figure 4.1. Two interesting inflection points stood out about the kinetic curves: first, after the HyPer ratio reached a peak at around 0.85, the signal subsequently decreased; secondly, the ratio started to rise again after 2 hours of generation, corresponding to the onset of apoptosis (Appendix) in the peroxide treated HeLa cells. We want to determine if these fluctuations in HyPer signal is reflective of actual changes in intracellular peroxide concentration.

The first inflection point at a HyPer ratio of 0.85 corresponded to the maximum possible ratio achievable by the sensor, since adding additional peroxide beyond that ratio did not result in increase in HyPer signal (Appendix). We wanted to test if the subsequent decrease in HyPer after the maximum was reached was an artifact from generating excessive peroxide beyond the limit of the probe. Using 40 ng/mL of GO as external generator, we followed the intracellular HyPer signal over a period of 3 hours. We also measured the H_2O_2 concentration outside the cell during the same period of time, using ABTS horseradish peroxidase assay. While the HyPer ratio

decreased upon reaching the maximum possible sensor ratio after the first 30 minutes, the actual concentration outside steadily increased for the entire 3 hour period of measurement (Figure 4.2).

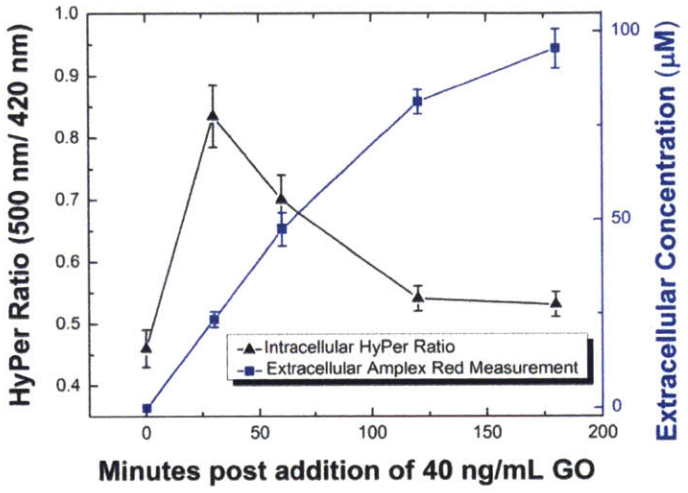

Figure 4.3: Intracellular HyPer signal compared to extracellular H2O2 concentration generated by glucose oxidase. HyPer signal was followed for 3 hours after addition of 40 ng/mL GO to the extracellular media. At the same time, the extracellular H2O2 concentration was measured using ABTS-Hrp assay. While HyPer signal decrease after reaching the peak ratio, the extracellular measurement showed that there was no decrease in H2O2 produced by the glucose oxidase enzyme.

Thus, the decrease in the HyPer ratio was not a function of actual decrease in H_2O_2, rather a consequence of prolonged peroxide generation beyond the limit of the sensor. We also tested whether the sensor was still functional and responding to H_2O_2 after the decrease in sensor signal. After the 3 hour generation period, the HeLa cells expressing HyPer were allowed to return back to the baseline for a period of 30 minutes, and then a bolus of 75 μM peroxide was added to the cells. The subsequent ratiometric increase of HyPer treated with 40 ng/mL of GO for 3 hours was un-impaired (Appendix).

We wanted to determine whether the subsequent rise in Hyper signals (second inflection point) following the onset of apoptosis is due to production from the H_2O_2 generator increasingly overcoming the antioxidants inside the cell. We tuned intracellular peroxide production using DAAO and D-alanine substrate at 1.5 mM, 2.5 mM and 5 mM. The second inflection point for

these three substrate concentrations occurred between 1-2 hours after the initiation of generation, and Hyper signal continued to rise for the rest of the 3 hour generation period. After 3 hours, the D-alanine substrate was removed, stopping the generator production, and the HyPer signal was followed for an additional hour post removal. We found that while the HyPer signal after the

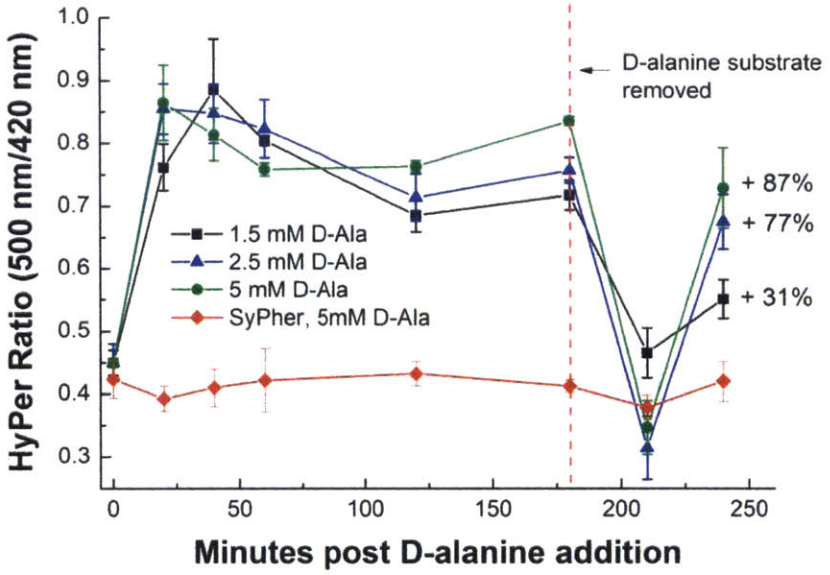

Figure 4.4: HyPer kinetics before and after removal of H2O2 generator DAAO. D-alanine was added at 1.5 mM, 2.5 mM and 5mM concentrations and HyPer kinetics was followed over a period of 4 hours. 3 hours after addition of D-ala, the substrate was removed and the kinetic was continually measured for another hour. After removal of the generator, the signal initially decreased, but then increased again after 30 minutes. The degree of increase was correlated with the % increase in apoptosis, measured via Trypan Blue exclusion assay after 24 hours.

generator removal decrease towards baseline initially, it begin to rise again after 30 minutes, independent of presence of a generator (Figure 4.3). The degree of increase was correlated with the toxicity of the generation, as measured by apoptosis 24 hours post removal of the D-alanine substrate. To confirm that this rise was due to peroxide elevation, and not an artifact of the fluorescence sensor or pH effects, we employed a mutant form of HyPer called SypHer, which had cysteine 199 of HyPer mutated to a serine to prevent di-sulfide bond formation following H_2O_2 oxidation. HeLa cells expressing SypHer did not experience a rise in the ratiometric fluorescent signal post 5 mM D-ala generation treatment. We can conclude that onset of

apoptosis in HeLa produces a secondary source of hydrogen peroxide independent of the H_2O_2 generator, possibly contributing to this second increase in HyPer signal at later times

4.3.2 Low continuous generation of hydrogen peroxide below the detection limit of HyPer

While previous studies have explored the phenotypic effects of peroxide in the dynamic range of HyPer, little has been done to address whether concentrations below the detection limit of HyPer

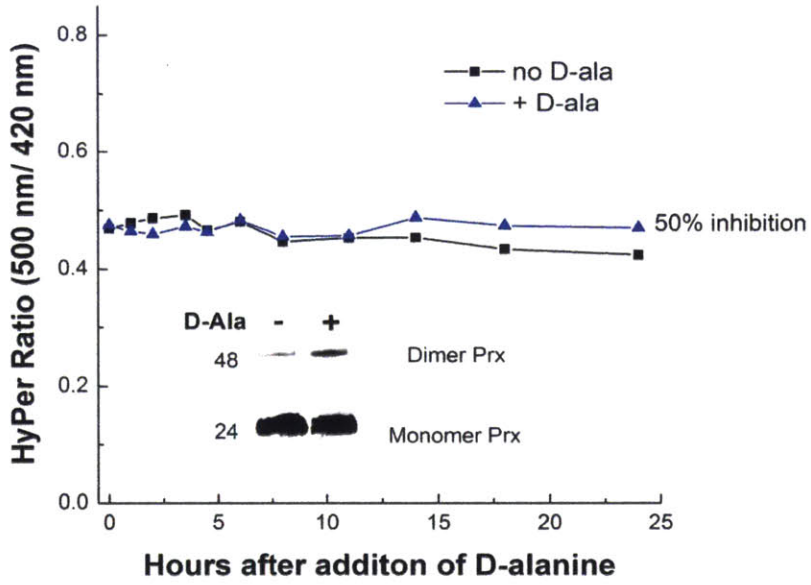

Figure 4.5: Phenotypic and Prx-2 oxidation effects of generating H2O2 below the detection limit of HyPer. Hydrogen peroxide was produced using 14 mM D-alanine substrate for HeLa cells expressing HyPer and DAAO seeded on a 6-well plate. The peroxide was produced for a period of 24 hours and HyPer signal was measured during the time course. The generation never caused an increase in HyPer signal. The number of cells on the dish after 24 hours of peroxide generation was measured and compared to the control case with no D-alanine added. Peroxiredoxin-2 oxidation was also measured by immunoblotting for the presence of dimer Prx-2. The generator caused an increase in dimerized Prx-2.

lead to interesting effects on the cell biology. Using DAAO, we tuned the D-alanine substrate to produce low concentrations of peroxide un-detectable by HyPer for a period of 24 hours. To verify that hydrogen peroxide was being produced, we looked for the presence of peroxiredoxin II (Prx-2) oxidation for these low generators. Prx-2 is an antioxidant found in the mammalian cytoplasm at hundreds of micromolar abundance and reacts specifically with H_2O_2 at rate

constants greater than 10^7 $M^{-1}s^{-1}$. Thus its reaction with peroxide is much more sensitive than that of HyPer. When Prx-2 comes in contact with H_2O_2, a cysteine on the Prx-2 is oxidized to –SOH, which can then form a disulfide bond with a nearby thiol group of another Prx-2 to form a dimer. Elevated presence of this dimer-form of Prx-2 is evidence of H_2O_2-derived oxidative stress. Figure 4.4 showed that while the peroxide generated by DAAO was undetectable via HyPer over a period of 24 hours, there was a clear elevation in Prx-2 dimer due to generator presence. This elevation in turn caused a 50% growth inhibition compared to the control without H_2O_2 generation. Thus, long, continuous peroxide concentrations generated below the detection limit of HyPer can have important pathological consequences, and using HyPer quantitatively at these longer periods of time (24 hours and greater) comes with the caveat that we can be missing important amounts of undetectable peroxide.

4.3.3 Establishing a new quantitative metric for studying H_2O_2-induced toxicity

The previous sections demonstrated the need for careful interpretation of HyPer signal in response to peroxide generators. Generation of H_2O_2 past the maximum HyPer signal cause inexplicable decrease in the ratiometric fluorescence, even if the actual concentration intracellular concentration is not decreasing. Using the sensor beyond the onset of apoptosis to quantify contribution from a particular generation source can be marred by the secondary intracellular peroxide production during cell death. Finally, the limit of detection prevents the probe from capturing pathological amounts of low oxidative stress during generation periods greater than 24 hours.

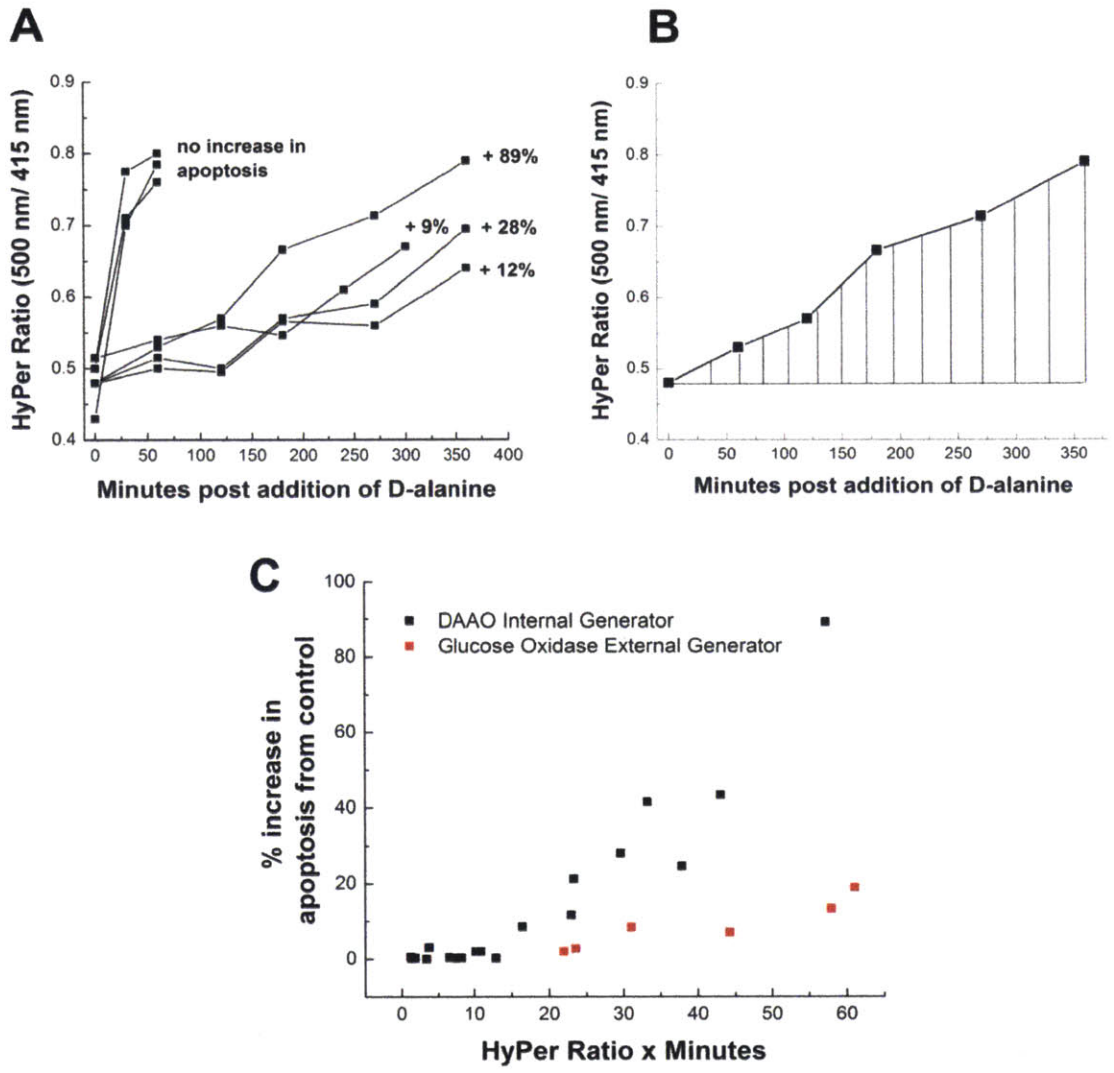

Figure 4.6: Development of a new quantitative metric for correlating HyPer signal with cell apoptosis. A) Using DAAO generator to produce H_2O_2 kinetic curves with different durations and end point signals. While some short, 1 hour generation resulted in HyPer signals with higher end point concentrations, kinetic curves with longer but lower end point signal can result in much greater apoptotic effects. B) Measurement of area under the curve for each kinetic profile. Using the ratio at t=0 as the base, the area under the kinetic curve was measured using trapezoid rule. This resulted in a new quantity, HyPer ratio x time, which captures both the time and the concentration characteristics of the generation. C) Correlating HyPer x time versus HeLa cell apoptosis after 48 hours for DAAO and GO generator. HyPer x time correlated positively with % apoptosis. DAAO generator caused more cellular damage than GO generator for the same intracellular accumulation of H_2O_2.

With these caveats in mind, we want to use HyPer in combination with the two H_2O_2 generators to develop a quantitative understanding of peroxide-induced apoptosis. The information from the study will be important for establishing design criteria for ROS-based cancer-elimination agents, and making meaningful comparison across different oxidative stress generating conditions. We

tuned the generation kinetics in HeLa cells by varying the concentration of D-alanine or GO, and allowing the generator to run for periods of time between 1 – 12 hours while recording the HyPer signal every hour. Only kinetics curves where the HyPer signal remained below the maximum possible ratio for the entire generation duration were used in our analysis so we can extract meaningful quantitative information. For each of the kinetic curve, we determined the percentage of apoptotic cell 48 hours post generation using Annexin V/ PI double staining and subtract the percent apoptosis for the control case with no H_2O_2 generation from the result. The delta of the two values represents the percent cell death incurred by the elevated oxidative stress. As a control for HyPer artifact such as pH fluctuations, HeLa cell line expressing SypHer was also used for the same generation conditions. We found that the SypHer cell line did not show increase in signal in response to generation by DAAO or GO (Appendix).

Much of the quantitative efforts on correlating peroxide with specific phenotype have focused on the intracellular concentration, and few very studies have considered the impact of both concentration and kinetics on the phenotypic effects. In Figure 4.5a, we juxtaposed some kinetic curves where the total DAAO generation time was an hour, with kinetic curves where the total generation time was 5-6 hours. We detected no increase in apoptosis for the one hour generation time, even though the ending HyPer ratio of these kinetic curves were higher than some of the more toxic 5-6 hour generation ones. Thus, the duration of the generation, along with the concentration, need to be considered simultaneously for the most accurate quantitative metric of peroxide production. To capture the full characteristics of the kinetic curve, we took the area under the curve (Figure 4.5b) using the trapezoid rule, giving us a value with units HyPer ratio x time. Plotting HyPer ratio x minutes against the toxicity of the generation (measured in % increase in cell death), we found an expected increasing trend (Figure 4.5c). The one hour

generation kinetic curves, when converted to HyPer ratio x minutes, had values between 0 – 12.5, putting them in the beginning parts of the scatter plot where there were no toxicity effects, and also no proliferation or growth inhibition effects (Appendix). The 5-6 hour kinetic curves were found with HyPer ratio x minutes values between 15 – 55, and increasing apoptosis up to 90% cell death.

With our new metric, HyPer x minutes, we did a quantitative comparison of different generation conditions. In particular, we were interested in whether the localization of the generation was important for the toxicity outcome. We used GO for a generation period of 5-6 hours to plot a similar toxicity curve of HyPer x minutes versus apoptosis as the DAAO. Surprisingly, even though the same intracellular concentrations were reached in both scenarios, the peroxide generated outside by GO was much less toxicity than peroxide generated inside by DAAO (Figure 4.5c). While DAAO showed almost 90% apoptosis for HyPer x minutes of 55, the same area under the kinetic curve for GO led to less than 20% apoptosis. Our quantitative approach allowed us to make controlled comparisons between inside and outside peroxide generation to discover localization bias for cell toxicity.

4.3.4 Validity of HyPer x time as an appropriate metric for capturing design criteria related to H_2O_2-induced apoptosis

We demonstrated that measuring the area under the curve captured the generation of hydrogen peroxide better than looking at the concentration alone. We want to evaluate whether calculating the area is sufficient in capturing the peroxide dosage necessary to induce apoptosis. A thoroughly understanding of how to calculate this threshold is important for designing effective chemotherapeutics. We compared the cell apoptosis for kinetic curves of different DAAO

generation duration, but the same area under the curve (same Hyper x minute value), three examples are shown in Figure 4.6. If the area metric was sufficient for capturing the design criteria for inducing apoptosis, then the kinetic curves with controlled area should show similar apoptosis. However, we found that longer generations at lower end-point HyPer ratio were consistently less toxic than the shorter generations at higher end-point HyPer ratio. We hypothesize that the concentration, in addition to the area under the curve, were important for determining the toxicity. Thus, there are two threshold criteria associated with H_2O_2-induced apoptosis: a cumulative amount is needed, and a certain concentration has to be reached for the cell to undergo apoptosis.

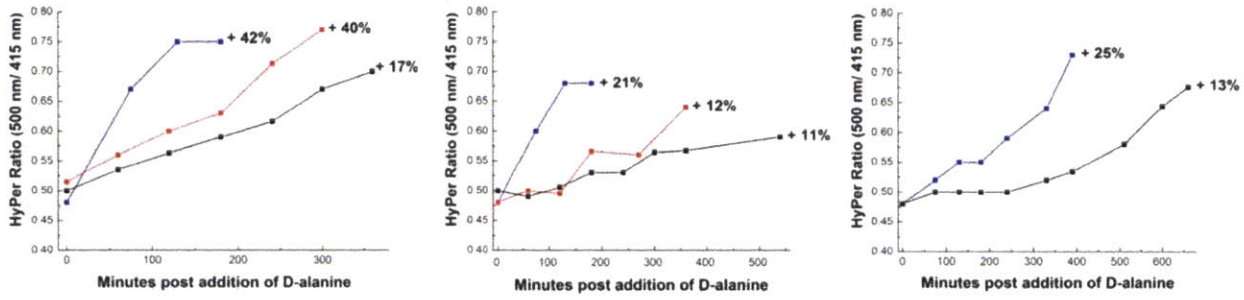

Figure 4.7: Comparing the toxicity of kinetic curves with the same area HyPer x time but different generation duration. A set of three different kinetic curves that have the same area but DAAO peroxide generation times ranging from 3 hours to 11 hours. Longer generations that reached lower end-point HyPer signal were consistently less toxic than the shorter generation with higher end-point HyPer signal. We hypothesize that while the area under the curve is important, there is a second concentration threshold that also need to be reached in order for cells to undergo H_2O_2 induced apoptosis.

4.4 Discussion and Conclusion

Our study showed the caveats of interpreting HyPer signal from produced from a continuous peroxide generator. HyPer signals after the maximum possible fluorescence ratio has been reached is unreliable, and using HyPer past the onset of apoptosis means a secondary peroxide generation during cell death is also included along with what is being produced by the generator. These findings indicate the importance of looking at the kinetics of peroxide generation over

time, since these features were only discovered when we followed the HyPer signal over the course of the entire generation period. The kinetic profile was also important in the new quantitative metric we employed for measuring peroxide dosage. The cumulative peroxide dosage, HyPer x time, helped captured many more subtleties of the peroxide generation than simply looking at the end point concentrations, and is a necessary component in determining the threshold for cell apoptosis.

HyPer, in combination with peroxide generators could be used for a controlled study of the quantity of oxidative stress in phenotypic outcomes. In particular, many chemotherapeutics are thought to produce ROS, but it is unclear what, if any effects the amount generated contribute to the overall toxicity of the compound. The use of intracellular sensor and appropriate generator mimicking the physiological condition is important for evaluating these existing chemotherapeutics, and also sets quantitative design criteria for future ROS-based chemotherapeutics. We found that the previous notions of correlating intracellular concentration of peroxide alone with different phenotypic outcomes to be too limiting.[4] Instead, phenotype such as apoptosis is determined by two different thresholds: a cumulative amount of peroxide needs to be generated, as measured by Hyper x time, and a intracellular concentration also need to be reached before significant apoptosis occurs. This dual threshold concept had been previous observed in nitric oxide: steady state extracellular delivery of nitric oxide results in toxicity only above a certain concentration and duration.[31]

Our study also showed the importance of localization on the phenotypic outcome. Comparing generation via GO (extracellular) versus DAAO (intracellular), similar kinetic curves in intracellular HyPer increase, show vastly different levels of HeLa cell apoptosis. The intracellular antioxidant network is very powerful and scavenges H_2O_2 very quickly, thus

hydrogen peroxide has a limited effective radius before being consumed by these enzymes.[32] Furthermore, previous work have shown that by fusing DAAO with HyPer, higher ratiometric response can be obtained than if the sensor and generator were to be expressed separately.[33] It is perhaps unsurprising that generating peroxide outside versus inside the cell causes localized, specific responses. Our finding emphasizes the need to mimic the physiological conditions of our problem of interest. While using glucose oxidase is a suitable model for studying oxidative stress during inflammation, it will not accurate portray H_2O_2 effects from intracellular perturbations.

Finally, there has been very little previous investigation into the detection capabilities of HyPer in terms of measureable phenotypic effects. It was unclear whether phenotypes related to low levels of oxidative stress, such as proliferation, can be studied using HyPer. Using the DAAO for 24 hour, continuous generation below the detection limit of HyPer, we found that H_2O_2 generation at these sub-HyPer concentrations can lead to significant growth inhibition effects on the HeLa cells. Thus, there are interesting pathological phenomena to be studied at these low, chronic H_2O_2 elevations, outside the quantitative capability of HyPer. However, we found that by measuring peroxiredoxin-2 oxidation via western blot, we can detect these low H_2O_2 elevations. Thus, designing a peroxide sensor around using peroxiredoxin as the reacting component may be a worthwhile pursuit to study chronic oxidative stress.

Our work provides guidelines for using an intracellular peroxide sensor with continuous H_2O_2 generators for quantitative analysis of H_2O_2-related phenotypes. We showed the caveats of interpreting HyPer signals from these generators, the limitations in what is measurable by the HyPer probe and the new quantitative metrics to capture the concentration as well as the kinetics of the peroxide generation. Furthermore, we applied the results from these tools to establish design criteria for inducing apoptosis in HeLa cells. By considering both H_2O_2 concentration and

cumulative Hyper x time thresholds, we can direct the desired phenotypic outcome from chemotherapeutics in the future that eliminate cancer cells via oxidative stress. An interesting next step might be to compare the toxicity thresholds of different cancer cell lines. This can inform us whether ROS-based chemotherapeutics will be an effective strategy against a particular type of cancer. We can also compare the toxicity thresholds of a tumor line with its normal counterpart. Ideally, a chemotherapeutic will selectively eliminate the tumor cells while sparing the normal cells to prevent excessive unwanted side-effects.[34] Thus, designing a drug that produces H_2O_2 in the therapeutic window where the tumor cells are selectively eliminated will require quantitative knowledge of peroxide dosage and expected phenotypic effects. A quantitative understanding of hydrogen peroxide's role as a cellular signaling molecule will contribute to mechanistic understanding of how networks of reactions control phenotype. To achieve this understanding, we need to use genetic sensors and generators in a physiologically relevant manner, and interpret their outputs in a meaningful way.

4.5 Bibliography

(1) D'Autréaux, B., and Toledano, M. B. (2007) ROS as signalling molecules: mechanisms that generate specificity in ROS homeostasis. *Nat. Rev. Mol. Cell Biol. 8*, 813–24.

(2) Murphy, M. P., Holmgren, A., Larsson, N.-G., Halliwell, B., Chang, C. J., Kalyanaraman, B., Rhee, S. G., Thornalley, P. J., Partridge, L., Gems, D., Nyström, T., Belousov, V., Schumacker, P. T., and Winterbourn, C. C. (2011) Unraveling the biological roles of reactive oxygen species. *Cell Metab. 13*, 361–6.

(3) Winterbourn, C. C. (2008) Reconciling the chemistry and biology of reactive oxygen species. *Nat. Chem. Biol. 4*, 278–86.

(4) Laurent, A., Nicco, C., Chéreau, C., Goulvestre, C., Alexandre, J., Alves, A., Lévy, E., Goldwasser, F., Panis, Y., Soubrane, O., Weill, B., and Batteux, F. (2005) Controlling tumor growth by modulating endogenous production of reactive oxygen species. *Cancer Res. 65*, 948–956.

(5) Gough, D. R., and Cotter, T. G. (2011) Hydrogen peroxide: a Jekyll and Hyde signalling molecule. *Cell Death Dis. 2*, e213.

(6) Antunes, F., and Cadenas, E. (2001) Cellular titration of apoptosis with steady state concentrations of H(2)O(2): submicromolar levels of H(2)O(2) induce apoptosis through Fenton chemistry independent of the cellular thiol state. *Free Radic. Biol. Med. 30*, 1008–18.

(7) Arbiser, J. L., Petros, J., Klafter, R., Govindajaran, B., McLaughlin, E. R., Brown, L. F., Cohen, C., Moses, M., Kilroy, S., Arnold, R. S., and Lambeth, J. D. (2002) Reactive oxygen generated by Nox1 triggers the angiogenic switch. *Proc. Natl. Acad. Sci. U. S. A. 99*, 715–720.

(8) Vanden Berghe, T., Van Loo, G., Saelens, X., Van Gurp, M., Brouckaert, G., Kalai, M., Declercq, W., and Vandenabeele, P. (2004) Differential Signaling to Apoptotic and Necrotic Cell Death by Fas-associated Death Domain Protein FADD. *J. Biol. Chem. 279*, 7925–7933.

(9) Sobotta, M. C., Barata, A. G., Schmidt, U., Mueller, S., Millonig, G., and Dick, T. P. (2013) Exposing cells to H2O2: a quantitative comparison between continuous low-dose and one-time high-dose treatments. *Free Radic. Biol. Med. 60*, 325–35.

(10) De Oliveira-Marques, V., Cyrne, L., Marinho, H. S., and Antunes, F. (2007) A quantitative study of NF-kappaB activation by H2O2: relevance in inflammation and synergy with TNF-alpha. *J. Immunol. 178*, 3893–902.

(11) Son, Y.-O., Jang, Y.-S., Heo, J.-S., Chung, W.-T., Choi, K.-C., and Lee, J.-C. (2009) Apoptosis-inducing factor plays a critical role in caspase-independent, pyknotic cell death in hydrogen peroxide-exposed cells. *Apoptosis 14*, 796–808.

(12) Trachootham, D., Alexandre, J., and Huang, P. (2009) Targeting cancer cells by ROS-mediated mechanisms: a radical therapeutic approach? *Nat. Rev. Drug Discov. 8*, 579–91.

(13) Fang, J., Seki, T., and Maeda, H. (2009) Therapeutic strategies by modulating oxygen stress in cancer and inflammation. *Adv. Drug Deliv. Rev. 61*, 290–302.

(14) Sporn, M. B., and Liby, K. T. (2012) NRF2 and cancer: the good, the bad and the importance of context. *Nat. Rev. Cancer 12*, 564–71.

(15) Kansanen, E., Kuosmanen, S. M., Leinonen, H., and Levonen, A.-L. (2013) The Keap1-Nrf2 pathway: Mechanisms of activation and dysregulation in cancer. *Redox Biol. 1*, 45–9.

(16) Gorrini, C., Harris, I. S., and Mak, T. W. (2013) Modulation of oxidative stress as an anticancer strategy. *Nat. Rev. Drug Discov. 12*, 931–47.

(17) Xiao, D., Powolny, A. A., Moura, M. B., Kelley, E. E., Bommareddy, A., Kim, S.-H., Hahm, E.-R., Normolle, D., Van Houten, B., and Singh, S. V. (2010) Phenethyl isothiocyanate inhibits oxidative phosphorylation to trigger reactive oxygen species-mediated death of human prostate cancer cells. *J. Biol. Chem. 285*, 26558–69.

(18) Raj, L., Ide, T., Gurkar, A. U., Foley, M., Schenone, M., Li, X., Tolliday, N. J., Golub, T. R., Carr, S. A., Shamji, A. F., Stern, A. M., Mandinova, A., Schreiber, S. L., and Lee, S. W. (2011) Selective killing of cancer cells by a small molecule targeting the stress response to ROS. *Nature 475*, 231–4.

(19) Raj, L., Ide, T., Gurkar, A. U., Foley, M., Schenone, M., Li, X., Tolliday, N. J., Golub, T. R., Carr, S. a, Shamji, A. F., Stern, A. M., Mandinova, A., Schreiber, S. L., and Lee, S. W. (2011) Selective killing of cancer cells by a small molecule targeting the stress response to ROS. *Nature 475*, 231–4.

(20) Glasauer, A., Sena, L. A., Diebold, L. P., Mazar, A. P., and Chandel, N. S. (2013) Targeting SOD1 reduces experimental non-small-cell lung cancer. *J. Clin. Invest.*

(21) Marzano, C., Gandin, V., Folda, A., Scutari, G., Bindoli, A., and Rigobello, M. P. (2007) Inhibition of thioredoxin reductase by auranofin induces apoptosis in cisplatin-resistant human ovarian cancer cells. *Free Radic. Biol. Med. 42*, 872–881.

(22) Adams, D. J., Boskovic, Z. V, Theriault, J. R., Wang, A. J., Stern, A. M., Wagner, B. K., Shamji, A. F., and Schreiber, S. L. (2013) Discovery of small-molecule enhancers of reactive oxygen species that are nontoxic or cause genotype-selective cell death. *ACS Chem. Biol. 8*, 923–9.

(23) Zhu, C., Hu, W., Wu, H., and Hu, X. (2014) No evident dose-response relationship between cellular ROS level and its cytotoxicity--a paradoxical issue in ROS-based cancer therapy. *Sci. Rep. 4*, 5029.

(24) Belousov, V. V, Fradkov, A. F., Lukyanov, K. A., Staroverov, D. B., Shakhbazov, K. S., Terskikh, A. V, and Lukyanov, S. (2006) Genetically encoded fluorescent indicator for intracellular hydrogen peroxide. *Nat. Methods 3*, 281–6.

(25) Lukyanov, K. a, and Belousov, V. V. (2014) Genetically encoded fluorescent redox sensors. *Biochim. Biophys. Acta 1840*, 745–56.

(26) Lee, C., Lee, S. M., Mukhopadhyay, P., Kim, S. J., Lee, S. C., Ahn, W.-S., Yu, M.-H., Storz, G., and Ryu, S. E. (2004) Redox regulation of OxyR requires specific disulfide bond formation involving a rapid kinetic reaction path. *Nat. Struct. Mol. Biol. 11*, 1179–85.

(27) Van Stroe-Biezen, S. A. M., Janssen, A. P. M., and Janssen, L. J. J. (1994) A kinetic study of soluble glucose oxidase using a rotating-disc electrode. *Bioelectrochemistry Bioenerg. 33*, 55–60.

(28) Haskew-Layton, R. E., Payappilly, J. B., Smirnova, N. A., Ma, T. C., Chan, K. K., Murphy, T. H., Guo, H., Langley, B., Sultana, R., Butterfield, D. A., Santagata, S., Alldred, M. J., Gazaryan, I. G., Bell, G. W., Ginsberg, S. D., and Ratan, R. R. (2010) Controlled enzymatic production of astrocytic hydrogen peroxide protects neurons from oxidative stress via an Nrf2-independent pathway. *Proc. Natl. Acad. Sci. U. S. A. 107*, 17385–90.

(29) Matlashov, M. V, Belousov, V. V, and Enikolopov, G. (2013) How Much H2O2 Is Produced by Recombinant D-Amino Acid Oxidase in Mammalian Cells? *Antioxid. Redox Signal. 00*.

(30) Hartig, S. M. (2013) Basic image analysis and manipulation in imageJ. *Curr. Protoc. Mol. Biol.* 1–12.

(31) Li, C.-Q., Pang, B., Kiziltepe, T., Trudel, L. J., Engelward, B. P., Dedon, P. C., and Wogan, G. N. (2006) Threshold effects of nitric oxide-induced toxicity and cellular responses in wild-type and p53-null human lymphoblastoid cells. *Chem. Res. Toxicol. 19*, 399–406.

(32) Huang, B. K., and Sikes, H. D. (2014) Quantifying intracellular hydrogen peroxide perturbations in terms of concentration. *Redox Biol. 2*, 955–962.

(33) Matlashov, M. E., Belousov, V. V, and Enikolopov, G. (2014) How much H(2)O(2) is produced by recombinant D-amino acid oxidase in mammalian cells? *Antioxid. Redox Signal. 20*, 1039–44.

(34) Morandell, S., and Yaffe, M. B. (2012) Exploiting synthetic lethal interactions between DNA damage signaling, checkpoint control, and p53 for targeted cancer therapy. *Prog. Mol. Biol. Transl. Sci. 110*, 289–314.

4.6 Appendix

HeLa cells undergo visible apoptosis 2 hours into H_2O_2 generation via DAAO or Glucose oxidase. SypHer is expressed in the cells. Fluorescent images are taken on Excitation 415 nm/Emission 525 nm

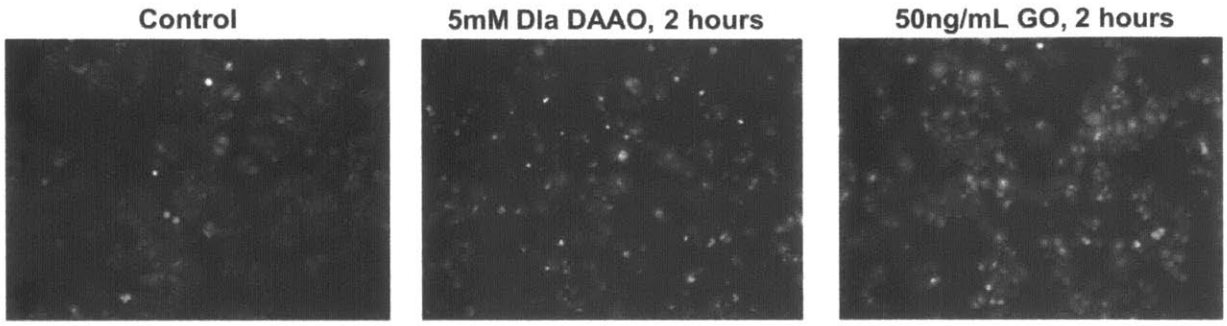

Peak HyPer ratio in response to external bolus addition of hydrogen peroxide between 0-75 μM. HeLa cells expressing HyPer were plated at 1 x 10^5/well on a 24 well plate. 1 mL of RPMI 1640 media containing H_2O_2 was added and HyPer ratio was followed for a period of 10 minutes.

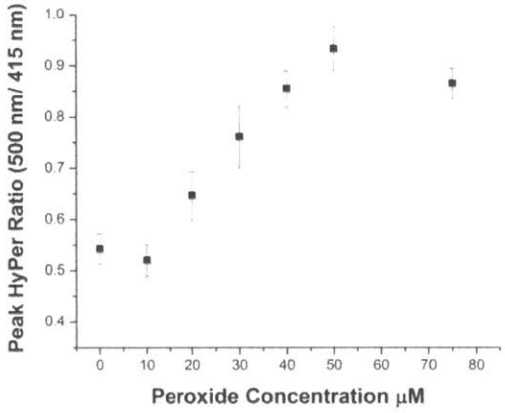

Bolus testing for 40 ng/mL GO after the 3 hour generation period. After the GO media was removed, HeLa cells were allowed to return to baseline for a period of 30 minutes. Then, a bolus of 75 μM H_2O_2 is added to the dish. HyPer was not impaired by GO generation.

Glucose oxidase	Before bolus	After 75 μM bolus
0 ng/mL	0.5	0.84
40 ng/mL	0.49	0.84

SypHer signal over a period of 12 hours. D-alanine concentrations from 0 mM – 24 mM were added to the extracellular RPMI media. The fluorescence ratio (500 nm/ 420 nm) were followed for a period of 12 hours. No elevation in SypHer signal was detected.

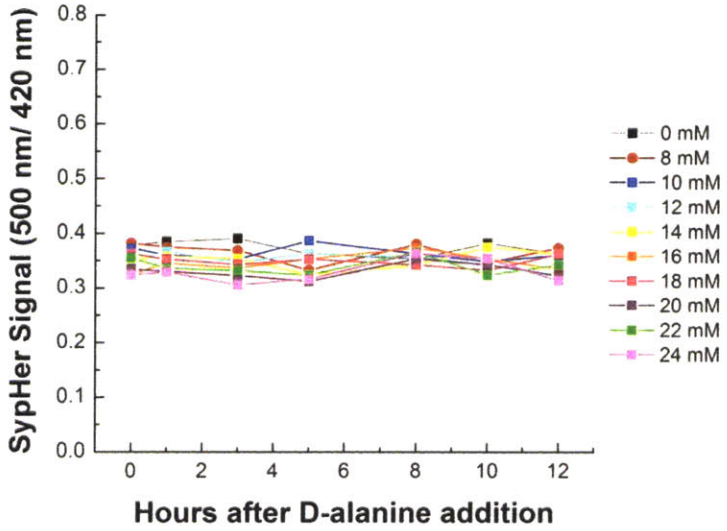

Percent increase or decrease in proliferation, as measured via BRDU staining, and % growth inhibition, as measured by counting live cells remaining on the dish and comparing to the no generator control case. D-alanine or GO was added to the dish at different concentrations and the kinetics was followed for a period of 1 hour. The area under the curve was determined for each kinetic curve. Proliferation or growth inhibition was determined 48 hours post removal of the generator.

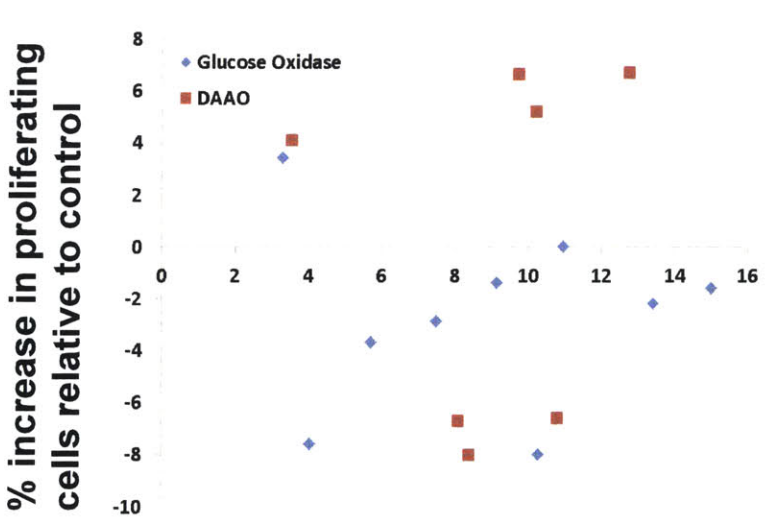

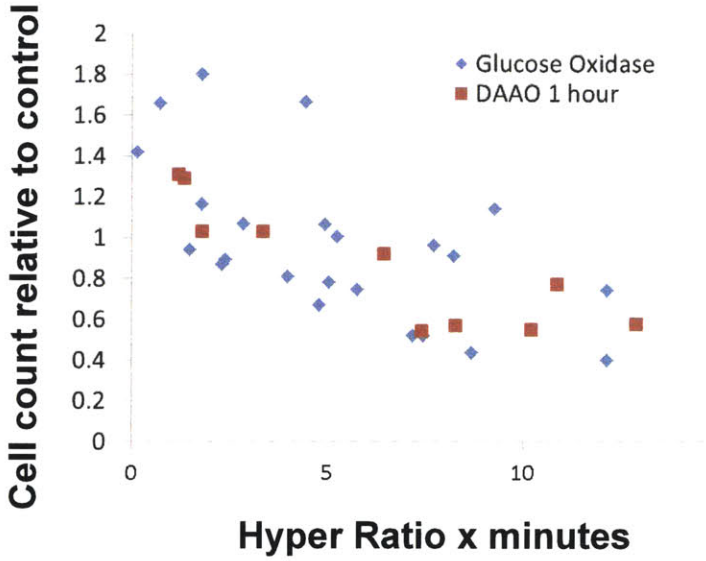

Chapter 5: Using sensors and generators for H_2O_2 to elucidate the toxicity mechanism of ROS-based cancer chemotherapeutics

5.1 Introduction

Reactive oxygen species (ROS) are formed as a byproduct of intracellular processes involving respiration, protein folding or signaling, and as an inflammatory response against pathogens [1,2]. These molecules are found to cause a variety of observable cellular responses from promoting growth and proliferation at lower concentrations, to causing lethal oxidative damages to lipids and DNA when present in excess [3,4]. Mounting evidence suggest that many types of cancer cells have increased levels of ROS compared to their normal counterpart [5,6]. This elevated ROS is the cumulative result of intrinsic factors such as activation of oncogene, aberrant metabolism, mitochondrial dysfunction through genetic instability, along with extrinsic factors such as inflammatory signals from nearby immune cells [5–7]. As a method of combating the toxicity effects of elevated oxidative stress, tumor cells often have higher levels of antioxidants and are extremely reliant on these molecules for survival [8]. Thus, it is believed that targeting these antioxidant defenses and subsequently raising of the oxidative stress level above the toxicity threshold might be a viable option for selectively eliminating tumor cells while sparing normal cells [7–9]. Many cancer chemotherapeutics have been designed around this principle. In particular, electrophilic small molecules piperlongumine (PL) and phenethyl isothiocynate (PEITC) are thought to cause depletion of glutathione (GSH), an important regulator of peroxide scavenging

[10–14]. Both of these drugs have been shown to be selectively toxic to certain *in vitro* and *in vivo* tumor models and are under clinical trials for various cancers.

However, while some ROS-elevating compounds have shown success as chemotherapeutics, a good majority of other small molecules that also show apparent increase in ROS are in fact non-toxic. A high-throughput screening of small molecules using dichlorofluorescin (DCFH), a cell permeable fluorescent dye, as an indicator of ROS yielded mostly unsuccessful candidates that are non-toxic as well as non-selective for cancer versus normal cells [15]. Furthermore, studies on several ROS-based chemotherapeutics show that there does not seem to be a dose-response correlation between the signal from DCFH and drug toxicity [16]. These studies suggest that our understanding of ROS, and how these drugs utilize ROS to cause toxic effects is incomplete. One way to improve our understanding is to use quantitative, species specific sensors for studying oxidative stress produced by these chemotherapeutics. While DCFH is commonly used by many redox biology studies, it indiscriminately detects ROS, RNS and a wide variety of artifacts [17]. Furthermore, its quantitative capability is limited by the variability in dye uptake between cells [18]. In recent years, genetic engineering has allowed us to produce fusions of fluorescent proteins with bacterial and yeast proteins that react specifically with hydrogen peroxide [19,20]. Fusions are constructed such that changes in the spectrum of the fluorescent protein occur when hydrogen peroxide oxidizes a cysteine of the microbial or yeast protein, causing it to subsequently form a disulfide bond with a neighboring cysteine [21]. Two spectral features are affected, with an excitation peak at one wavelength decreasing and an excitation peak at a second wavelength increasing in a dose-dependent manner upon stimulation with hydrogen peroxide. The ability to examine the ratio of two spectral features, in contrast with

measuring changes in fluorescence intensity for only one feature like DCFH, enables better intracellular quantification of H_2O_2 [22,23].

Complementary to better measurement efforts, we can improve our understanding of these ROS-based chemotherapeutics by incorporating additional controls relating to the hypothesized mechanism of action. Using different methods of knocking down the antioxidant pathway that is thought to be involved, whether by siRNA or alternative small molecules, we can determine whether the changes we see is important to the drug toxicity, or just a secondary effect [24]. We can also test if the oxidative stress at the amount generated is enough to induce toxicity using genetically encoded generators of particular ROS species. D-amino acid oxidase (DAAO) from *R. gracilis* has been previously shown to be a powerful intracellular enzyme that can produce tunable endogenous H_2O_2 levels depending on the concentration of D-alanine substrate added [25–27]. Using DAAO give spatial and temporal control over the production of H_2O_2, we can mimic the oxidative stress generation by these chemotherapeutics.

In this study, we focused on understanding the mechanism of piperlongumine (PL) and phenethyl isothiocynate (PEITC). Previous studies have shown that incubation of tumor cells with both of these compounds result in depletion of GSH and elevation of DCFH signal [10,11,13,14]. The toxicity of the compound is attributed to oxidative stress elevation due to the lowered quantity of GSH, an important antioxidant involved in protecting cells from electrophilic compounds, H_2O_2 accumulation and protein oxidation [28,29]. We aimed to study the role of oxidative stress from these compounds more quantitatively using HyPer, a genetically encoded sensor for H_2O_2, along with DAAO, the intracellular generator for H_2O_2. We also used another glutathione synthesis inhibitor, buthionine sulfoxmine (BSO) as a control to understand the effects of GSH depletion on cell toxicity. Finally, we used both human tumor cells HeLa and

A549, along with knockout variants of lung tumor model cell line, $p53^{fl}/Kras^{G12D}$ to understand the biochemical difference that contribute to why non-small cell carcinoma A549 is more resistant to these chemotherapeutics than other tumors [24,30]. The insights from our investigation will aid application and design of future ROS-based chemotherapeutics to improve their success rate.

5.2 Methods and Materials

Materials used

Piperlongumine (PL) and buthionine sulfoxmine (BSO), GSH assay kit and S-glutathionylation kit were purchased from Cayman Chemicals. Phenethyl isothiocynate (PEITC), DMSO, Triton X-100, D-Alanine, Flavin adenine dinucleotide (FAD), methyl methanethiosulfonate (MMTS), puromycin, were purchased from Sigma. DMEM media was purchased from Lonza. Fetal bovine serum (FBS) and pCAT10 catalase plasmid were purchased from ATCC. HyPer plasmid was obtained from Evrogen. DAAO plasmid was a gift from Brian Ross (University of Michigan). The lentiviral transfer plasmid PLJM-EGFP was a gift from David Sabatini (Addgene plasmid #19319). The HeLa cell line was a gift from Dane Wittrup (Massachusetts Institute of Technology, USA). The A549 cell line was a gift from Doug Lauffenburger (Massachusetts Institute of Technology. USA). The $p53^{fl}/Kras^{G12D}$, $p53^{fl}/Kras^{G12D}/Nrf\text{-}2^{-}$, $p53^{fl}/Kras^{G12D}/Keap\text{-}1^{-}$ cell lines were a gift from Tyler Jacks (Massachusetts Institute of Technology, USA). The HeKFT cell line and the PAX2 and pMD2.G viral packaging plasmids were a gift from Christopher Chen (Boston University, USA). Cell Tracker Deep Red, Opti-MEM and Lipofectamine 2000 were purchased from Invitrogen. Primary goat antibody for Prx-2 was purchased from R&D systems. Primary rabbit antibodies for alpha tublin and GADPH were purchased from Cell Signaling. Primary mouse antibody against protein-GSH conjugates was

purchased from Abcam. Secondary licor antibodies against goat and rabbit were purchased from Licor Biosciences. Secondary FITC antibody against mouse was purchased from Jackson ImmunoResearch.

Cell culture

HeLa, A549, $p53^{fl}$/Kras ^{G12D}, $p53^{fl}$/Kras ^{G12D}/Nrf-2^{-}, $p53^{fl}$/Kras ^{G12D}/Keap-1^{-} were cultured in DMEM media supplemented with 10% fetal bovine serum (FBS). The cultures were maintained in 37°C humidified incubator in the presence of 5% CO2. Media was changed every 3 days and cells were passaged every 5-6 days. HeLa cells virally infected with plasmids containing HyPer, catalase and DAAO were maintained in the same DMEM media containing 2ug/mL of puromycin.

Molecular cloning for HyPer, catalase and DAAO

The coding sequence for HyPer (1.5kb) and DAAO (1.2kb) was amplified and re-inserted in lenti-viral transfer vector PLJM-EGFP at cloning sites Nhe1 and BamH1, removing the EGFP. The relevant coding sequence of human catalase (1.6kb) was amplified from the pCAT10 vector with a point mutation in the reverse primer, changing the penultimate amino acid from asparagine (N) to aspartic acid (D). The primers used to amplify the sequence were 5' primer: AAAA GCTAGC GCA GTG TTC CGC ACA GCA AAC and 3' primer: AAAA GGCGCGCC TCA CAG ATC TGC CTT CTC CCT TGC (the underlined part being the point mutation), and inserted between the Nhe1 and Asc1 sites on the PLJM-EGFP vector.

Lentiviral infection for HyPer, catalase and DAAO plasmids

HeK FT cells were seeded at $7.5x10^5$ cells/35mm well and grown for 2 days until 90% confluence. The PLJM transfer vector with the appropriate gene insert was co-transfected with the packaging plasmids PAX2 and pMD2.G at 3:2:1 ratio for a total of 5ug of plasmid and 10ug of Lipofectamine 2000 for a period of 18 hours in OptiMEM media. Subsequently, 1 mL of 10% FBS + DMEM media was used to replace the transfection media. This media containing lentiviruses was collected every 24 hours for a period of 2 days. The media was centrifuged at 500g for 5 minutes and the supernatant was collected.

The 1mL of the supernatant, along with 6ug/mL of polybrene, was then added to an 80-90% confluent 35mm well of HeLa cells. Three days post infection, media containing 5ug/mL of puromycin was used for selection of HeLa cells containing the plasmid for a period of 10 days.

Growth inhibition assay

Cells were seeded at 1.5 x 10^5 cells/well in a 12-well plate. The next day, 1mL of 10% FBS + DMEM media with the appropriate combination of chemotherapeutic cocktail were added to each well and incubated for a period of 48 hours. Afterwards, the remaining live cells on the dish were trypinized and quantified using Beckman Coulter Vi-Cell Counter (courtesy of Doug Lauffenburger, MIT), the fraction of live cells remaining was calculated by dividing by the number of live cells in the control case with DMSO only.

Total GSH measurement

Cells were seeded at 3.5 x 10^5 cells/well in a 6 well dish. The next day, 2.5mL of 10% FBS + DMEM media with the appropriate combination of chemotherapeutic cocktail were added to each well and incubated for a period of 10 hours. Afterwards, the cells were trypinized and lysed with 100 μL of 1% triton X-100 for 20 minutes on ice, followed by 10min of centrifugation at

12,000g. The supernatant collected was de-proteinated using equal volume of 0.1g/mL of metaphosphoric acid, re-spun at 12,000g to separate the liquid from the precipitate. The pH was readjusted by adding 4 M triethanolamine at 1:20 dilution to the supernatant. Both oxidized and reduced glutathione were measured by using glutathione reductase to reduce the GSSG, followed by reaction with DTNB (Ellman's Reagent) as dictated by the glutathione quantification kit from Cayman Chemicals.

Using DAAO enzyme for controlled peroxide production

HeLa cells co-infected with HyPer and DAAO plasmids were seeded at 3.5 x 10^5 cells/well on a 6 well plate. The substrate for the DAAO enzyme, D-alanine, was added at various millimolar concentrations to the 2mL of extracellular media (10% FBS + DMEM), along with co-factor substrate FAD at 5 μM. 4-5 images per well of the cells were taken with the HyPer wavelengths every 30 minutes for a period of 12.5 hours.

Microscopy quantification of HyPer fluorescence

The excitation wavelengths of HyPer were captured using a Nikon x81 epi-fluorescence microscope on 10x objective setting. Images were excited at 415 nm/30 nm and 488 nm/25 nm and emission was recorded at 525 nm/40 nm, on 10% lamp intensity and 300ms exposure. Four to five fields of view are captured per condition, and the images were exported to ImageJ for post-processing. All images were background subtracted using the rolling ball algorithm with radius of 200 pixels, and then the mean pixel intensity for each image was measured [31]. The HyPer ratio for each field of view was calculated by dividing the mean pixel intensity at 488 nm by the mean pixel intensity at 415 nm. The baseline HyPer ratio is around 0.5, and the maximum ratio for the probe is 0.9.

Immunoblotting for peroxiredoxin-2 oxidation

Cells were seeded at 3.5 x 10^5 cells per well in a 6 well plate. The wells were treated with 2.5 mL of 10 μM PL, PEITC or 100 μM of BSO for a period of 10 hours. After treatment, the cells were trypinized, washed once with 1x PBS, followed by re-suspension in 2 mL of 100mM MMTS to convert sulfhydryl groups to $-S-CH_3$. This is to prevent artificial oxidation during the cell lysis step [32]. The MMTS cell suspension was placed on ice for 20 minutes, followed by 2 more 1x PBS washes. The cell pellet was lysed using 100 μL of 1% Triton x-100, spun at 12,000g for 10 minutes and the supernatant cell lysate was collected and stored at -20 C until needed.

To immunoblot for monomer and dimer form of peroxiredoxin-2 (Prx-2), we denatured the cell lysate sample using non-reducing sample buffer, then loaded 25 ug of cell lysate per lane to run on a tris-tricine gel/buffer system. After transferring the proteins to a PDVF membrane, the blot is blocked using Licor blocking buffer for an hour, followed by overnight incubation in goat primary antibody (1:1000 in PBS-blocking buffer-Tween20) against Prx-2 at 4C. After washing with PBS + 0.1% tween-20, licor anti-goat secondary antibody IR 688 was added at 1:10000 dilution and incubated for 1 hour. Blots are visualized on Odyssey CLx Infrared Imaging System (Koch Institute, Cambridge, MA).

Detection of protein-GSH conjugation

By immunofluorescence: HeLa cells seeded at 1.0 x 10^4 cells/well in a 24-well plate were incubated for 10 hours with 10 μM PL, PEITC or 100 μM of BSO. After incubation, the cells were fixed in plate with 4% paraformaldehyde for 30 minutes, washed 3 times with PBS, and followed by permeabilization with 0.5% triton x-100 (PBST) for 30 minutes. The cells were then blocked for 30 minutes in PBST + 2% BSA, then primary mouse antibody against glutathione-

protein conjugates at 1:200 dilution in PBST + 2% BSA overnight at 4C. After 3 washes with PBST, secondary anti-mouse FITC antibody was incubated at 1:250 dilution in PBST + 2% BSA. The images were taken on NIKON x81 epi-fluorescence microscope at 10% lamp intensity and 200ms exposure.

By flow cytometry: HeLa and A549 cells seeded at 2 x 10^5 cells/well in a 6-well plate were incubated for 10 hours with 10 μM PL, or DMSO control. After incubation, the cells were trypinized, washed with PBS, and re-suspended in 4% paraformaldehyde for 30 minutes. After fixation and washing, the cells were permeabilized with 0.5% triton x-100 for 30 minutes, then blocked with 2% BSA for an hour on a rocker. The cells pellets were re-suspended in 100 μL of 1:100 primary mouse antibody, rocked for 2 hours at room temperature. After washes, cells were re-suspended in secondary anti-mouse FITC antibody at 1:100 dilution and incubated for 30 minutes on ice. The labeled cells were analyzed on BD LSR II at the Flow Cytometry Core Facility (Koch Institute, Cambridge, MA).

Immunofluorescence quantification of S-glutathionylation

HeLa cells were seeded at 7500 cells/well in a 24-well plate, then treated for 10 hours with 10 μM PL, or DMSO control. After incubation, the cells were fixed on the dish with 4% paraformaldehyde for 30 minutes, followed by PBS washes. Afterwards, cells were labeled with Cell Tracker Deep Red for 1 hour at RT. Cells were permeabilized and protein free-thiols were blocked with 100 mM MMTS. The reduction and detection steps were carried out according to the S-Glutathionylation kit from Cayman Chemicals. 8 images were taken per condition (N=200) on the microscope for the FITC channel (bio-tinylated reduced thiol groups) and the Cy5 channel (cell tracker label) at 400 ms exposure, 10% lamp intensity. Using a pipeline we built in

CellProfiler (Broad Institute, Cambridge, MA) [33], the cell tracker images were used to determine the outline of the cell objects, create a mask which was then superimposed onto the FITC images and the total pixel intensity per cell was determined.

5.3 Results

5.3.1 Differential response of HeLa and A549 cells to Piperlongumine and Phenethyl Isothiocynate

We exposed two different tumor cell lines, HeLa and A549, to increasing concentrations of electrophilic chemotherapeutics piperlongumine (PL) and phenethyl isothiocynate (PEITC) for a period of 48 hours. Since cancer cell growth inhibition and apoptosis are both potential desired outcomes of these small molecules drugs, we measure the efficacy by counting the live cells

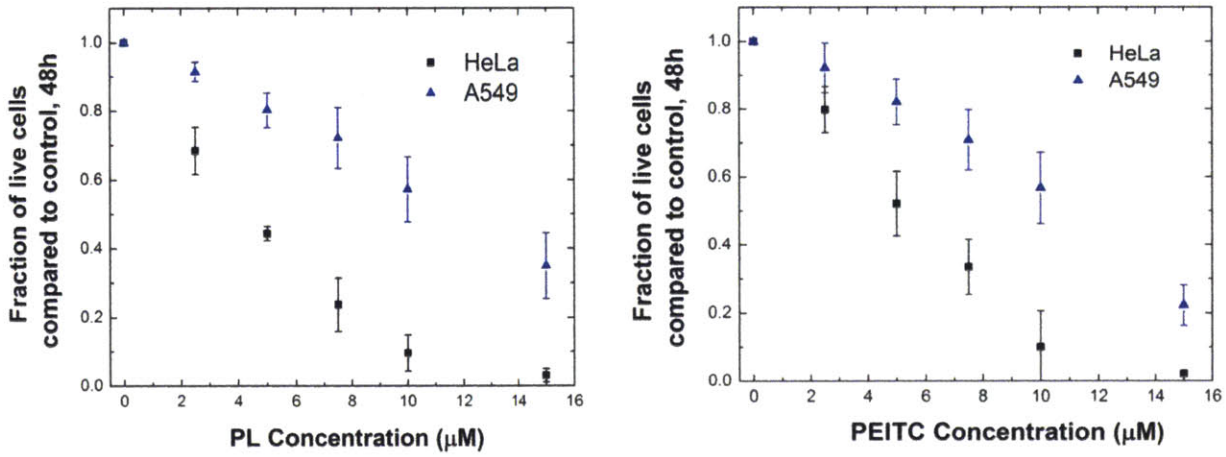

Figure 5.1: Growth inhibition curves of PL and PEITC for HeLa and A549 cells. 1.5 x 10^5 cells are seeded. After 24 hours, PL and PEITC concentrations from 0-15 μM were added and incubated for 48 hours. Number of live cells remaining on the dish were counted and compared to the DMSO control. Blue triangle: A549, black squares: HeLa.

remaining on the dish after a period of 48 hours and comparing it to the DMSO control. We found that for both compounds, the A549 cells are more resistant than the HeLa cells. In the case of PL, the concentration needed to inhibit tumor cell population by 50% is 4.4 ± 0.1 μM for HeLa and 11.7 ± 2.0 μM for the A549, for PEITC it is 5 μM and 10.2 ± 1.1μM, respectively

(Figure 5.1). We want to understand how the differential responses arise in context of the redox biochemistry of the cell lines so we apply these drugs more effectively to tumor treatments.

5.3.2 The role of glutathione in PL and PEITC mediated tumor inhibition

One of the main mechanisms of PL and PEITC toxicity suggested by the original papers is the depletion of intracellular glutathione (GSH) level and the subsequent rise of oxidative stress. We used another glutathione synthesis inhibitor, buthionine sulfoxmine (BSO) to determine whether

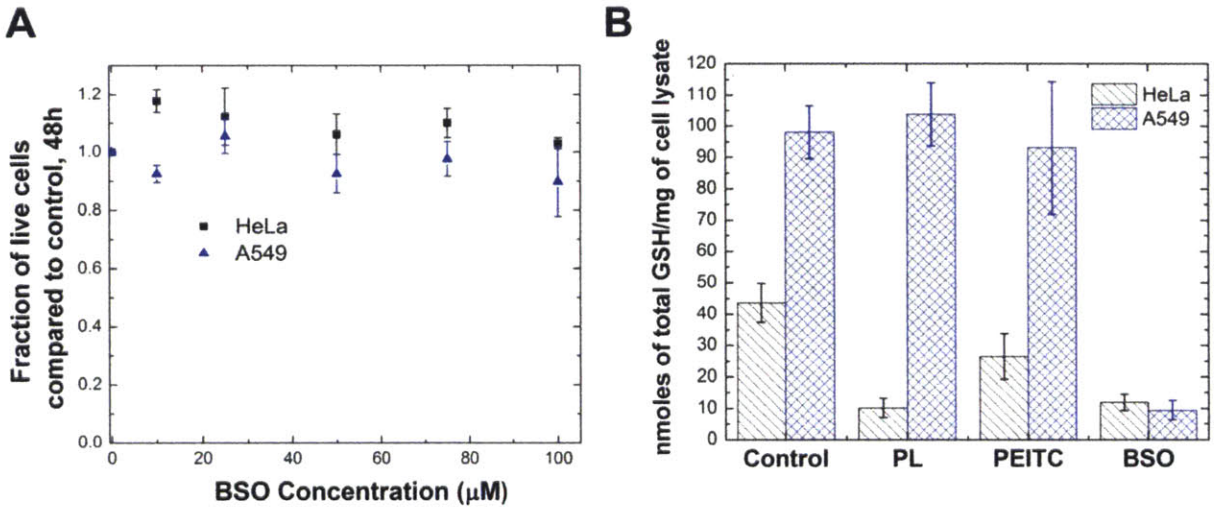

Figure 5.2: Toxicity and glutathione depletion effects of PL, PEITC and BSO. A) Incubations of HeLa and A549 cells with BSO concentrations 0-100 μM. Fraction of live cells remaining after 48 hours was counted and compared to the control. BSO did not induce toxicity in either cell line at the tested concentrations. B) Measurement of total GSH concentration in the cell lysate. Cells are incubated with 10 μM PL, 10 μM PEITC or 100 μM BSO for a period of 10 hours, then cells are lysed and total glutathione level is measured and normalized to the amount of cell lysate. Cells incubated with BSO show the most depletion in GSH level. A549 cells show the least depletion of GSH in response to the drugs.

this depletion is an important contributor to the tumor inhibition [16]. We found that BSO did not cause any significant tumor growth inhibition in either the HeLa or the A549 cell lines (Figure 5.2a). When we measured the intracellular GSH level of both cell lines after 10 hour exposure to BSO, PL and PEITC, we found that BSO depleted intracellular GSH level more significantly than PEITC and at the same level as PL for HeLa (Figure 5.2b). A549 cells did not experience a

decrease in the glutathione level in response to either drug. This suggests that the GSH depletion is not the main toxicity mechanism of the PL or PEITC.

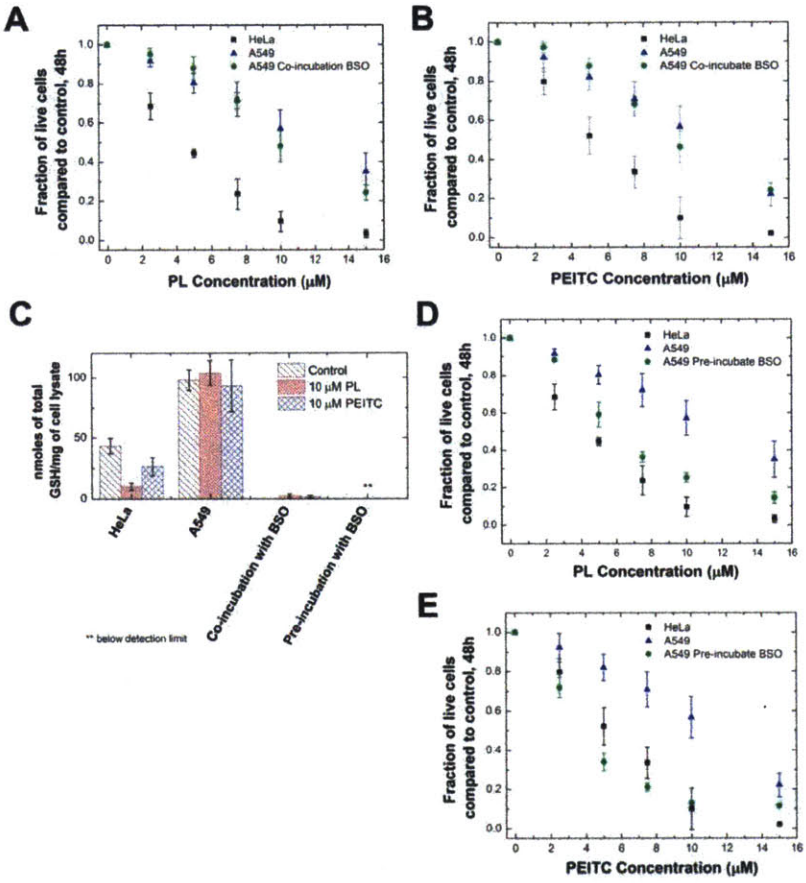

Figure 5.3: Toxicity and glutathione depletion effects of PL + BSO, or PEITC + BSO co-treatments A) Co-incubations of A549 cells with 75 μM BSO and 10 μM of PL. Fraction of live cells remaining after 48 hours was counted and compared to the control. The co-incubation did not cause an increase in sensitivity of A549s to the PL B) Co-incubations of A549 cells with 75 μM BSO and 10 μM of PEITC. Fraction of live cells remaining after 48 hours was counted and compared to the control. The co-incubation did not cause an increase in sensitivity of A549s to the PEITC. C) Total GSH concentration of HeLa, A549 after 10h incubation with PL or PEITC, and A549 cells co-incubated or pre-incubated with BSO (10 hours). A549 co-incubation and pre-incubation with BSO, along with PL or PEITC, causes more GSH depletion than HeLa cells treated with PL or PEITC. D) Pre-incubation of A549 cells with 100 μM BSO for 10 hours, followed by treatment with 10 μM PL for 48 hours. E) Pre-incubation of A549 cells with 100 μM BSO for 10 hours, followed by treatment with 10 μM PEITC for 48 hours.

However, we noticed that the A549 cells were more resistant to GSH depletion through PL and PEITC compared to the HeLa cells. The addition of PL to these lung carcinoma cells actually increased the overall GSH concentration, while PEITC had no effect on the GSH level. On the other hand, the HeLa cells saw two-fold decrease in GSH level in response to PEITC, and four-fold decrease in response to PL. One hypothesis might be that the extra GSH in the A549 cells is

important for detoxifying either secondary effects from the compounds, or conjugating to these electrophiles themselves and export them from the cell, conferring resistance for the A549s over the HeLas. We tested this hypothesis by co-treating A549 cells with BSO and PL, or BSO and PEITC, then measuring the subsequent GSH concentration and growth inhibition and comparing it to the HeLa cells incubated with just PL or PEITC. Co-incubating A549s with 75 μM of BSO and various concentrations of PL and PEITC did not change the efficacy of the two drugs compared to treatment with the drugs by themselves (Figure 5.3a,b). However, the co-incubation depleted the A549 GSH level to below that of HeLas treated with PL or PEITC (Figure 5.3c). Thus, the sensitivity of the HeLa cells to PL and PEITC compared to the A549 cells is not due to the selective depletion of GSH in these cells.

We then increased the concentration of BSO to 100 μM and pre-incubated the A549 cells with the compound, followed by addition of different concentrations of PL or PEITC after 10 hours. The pre-incubation and the higher BSO concentration had a dramatic effect on the sensitivity of the A549s to the electrophilic compounds (Figure 5.3d,e). The concentration of GSH concentration 10 hours post PL or PEITC addition is below the detection limit of the assay for this pre-treatment protocol (Figure 5.3c). It is likely that the increased sensitivity is due to the fact that some amount of GSH, however small compared to the control pool, is necessary for combating the toxicity effects of PL and PEITC. A way to increase the potency of the two chemotherapeutic compounds to these more resistant A549 cells would be to pre-treat the tumors with BSO to deplete all or almost all of the GSH, followed by treatment with the compounds.

5.3.3 The role of oxidative stress generated by PL and PEITC

In previous studies, the measured increase in DCFH signal from both PL and PEITC was used as an indicator of elevated oxidative stress, commonly thought to be associated with the depletion of GSH. Here, we pioneered a new approach towards studying the oxidative stress generated by these compounds using both sensors and generators for a particular oxidative species. This new

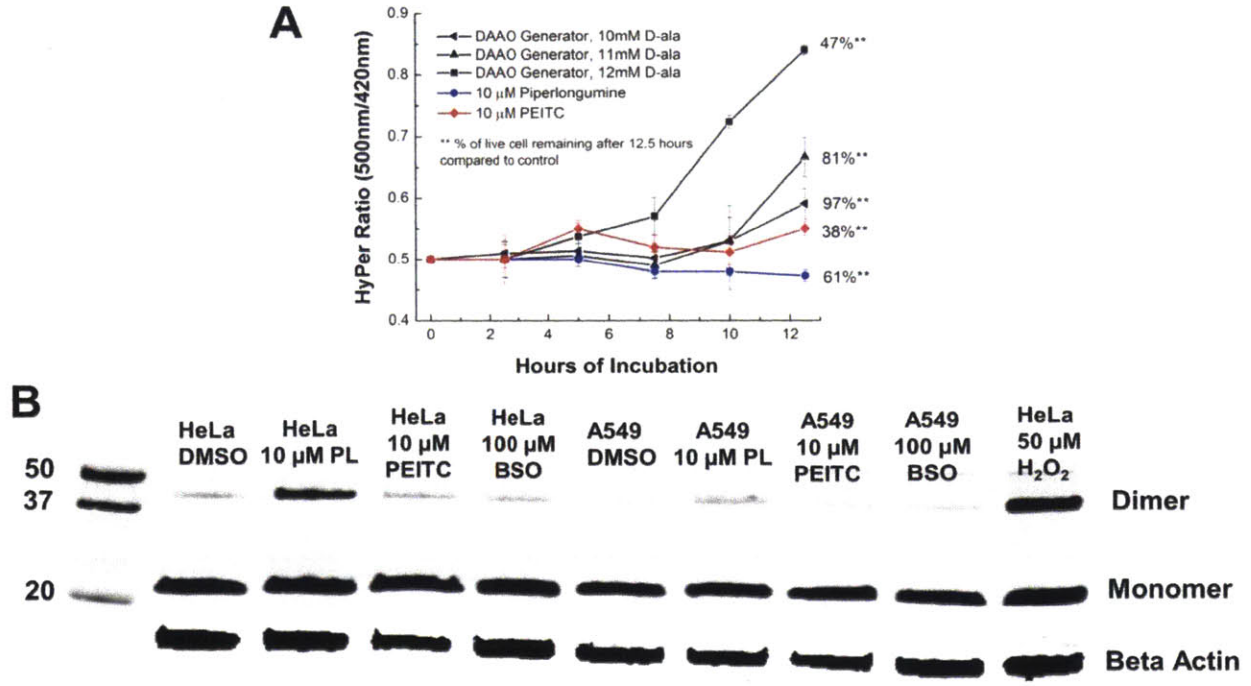

Figure 5.4: Detection and generation of oxidative stress in HeLa and A549 cells treated with PL, PEITC and BSO. A) Measurement of HyPer ratio over a period of 12.5 hours for HeLa cells treated with 10 μM PL, 10 μM PEITC, or virally infected with DAAO generator producing H2O2 with three different kinetic rates. The % of live cells remaining on the dish after 12.5 hours compared to the DMSO control was determined. Incubation with PL and PEITC did not cause a rise in HyPer ratio, while causing significant growth inhibition compared to the DAAO generators, which did cause a rise in HyPer ratio. B) Measuring oxidized peroxiredoxin-2 as an indicator of peroxide elevation below the threshold of HyPer detection. HeLa and A549 cells were incubated with 10 μM PL, 10 μM PEITC or 100 μM BSO for a period of 10 hours. Antibody against Prx-2 was used to detect both the dimer (oxidized) and the monomer form of Prx-2. Only piperlongumine caused a noticeable increase in Prx-2 oxidation compared to the DMSO control. A549 cells show less oxidation in response to PL than the HeLas.

approach allows us to better understand which ROS is being generated by these cancer chemotherapeutics and whether the quantities generated is enough to induce toxicity. In particular, we investigated the role of H_2O_2 in the toxicity mechanism since many ROS-therapies are thought to interfere with the function of antioxidants for peroxide elimination [8].

We expressed HyPer, a ratiometric protein sensor with specificity towards H_2O_2, inside HeLa cells exposed to PL and PEITC. As intracellular H_2O_2 increases, the ratio of excitation spectra peak at 500nm/420nm, also known as the HyPer ratio, should also increase. However, we did not see any increase in HyPer ratio upon incubation of the PL and PEITC tracking over a period of 12.5 hours (Figure 5.4a). At the same time, incubation of the drugs for a period of 12.5 hours cause significant growth inhibition effects, with 61% of live cells remaining after 48 hours for PL and 38% for PEITC. As a control, we co-expressed an intracellular enzymatic generator for peroxide, D-amino acid oxidase (DAAO) with HyPer in the HeLa cells. By adding different substrate concentrations of D-Ala, we can tune the kinetics of intracellular H_2O_2 generation by the enzyme. We found that to cause growth inhibition at the same level as PL or PEITC, the amount of H_2O_2 that is needed is significantly above the detection threshold of the HyPer sensor: a 1.6 fold increase in the ratiometric signal is needed to see close to 50% growth inhibition in the HeLa cells. The combination of generator and sensor for H_2O_2 allows us to conclude that the main toxicity mechanism of these drugs is not via excessive generation of peroxide alone.

While peroxide generation is not the main toxicity mechanism, it can still be produced by these drugs at levels below the detection threshold of the HyPer sensor. To see if any peroxide is produced, we needed a more sensitive detection method. Peroxiredoxin II (Prx-2) is an antioxidant found in the mammalian cytoplasm at hundreds of micromolar abundance and reacts specifically with H_2O_2 at rate constants greater than 10^7 $M^{-1}s^{-1}$.[23,34–36] Thus its reaction with peroxide is much more sensitive than that of HyPer. When Prx-2 comes in contact with H_2O_2, a cysteine on the Prx-2 is oxidized to –SOH, which can then form a disulfide bond with a nearby thiol group of another Prx-2 to form a dimer [37]. Elevated presence of this dimer-form of Prx-2 is indirect evidence of H_2O_2-derived oxidative stress. We treated HeLa cells and A549 cells with

10 μM PL, 10 μM PEITC or 100 μM BSO and immuno-blotted for Prx-2 to detect the monomer and the dimer form of the antioxidant after a period of 10 hours. Treatment with PL resulted in

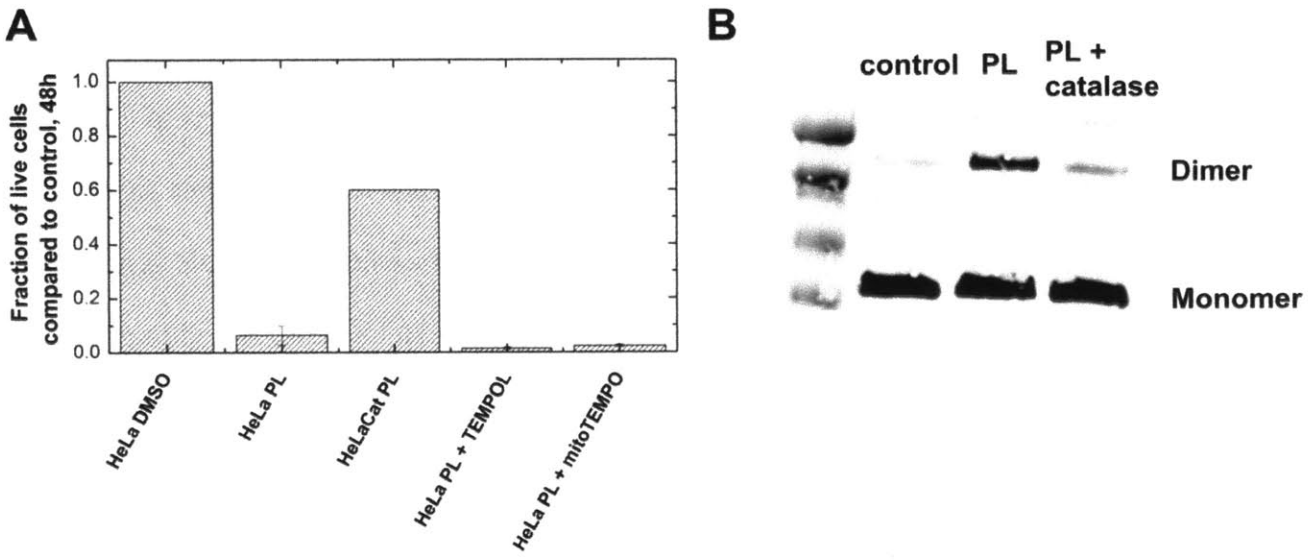

Figure 5.5: Using antioxidants to eliminate peroxide stress elevated by PL. A) HeLa cells treated with PL, PL + TEMPOL, PL + mitoTEMPO and HeLa cells virally infected with human catalase then treated with PL. Cell viability was determined after 48 hours. TEMPOL and mito-TEMPO are super-oxidase dismutase mimetics, and pre-incubation of HeLa cells with these mimetics did not cause significant improvement in cell viability. However, HeLa cells expressing endogenous catalase showed significant improvement in cell viability. B) Prx-2 oxidation for HeLa cells treated with antioxidants and PL. Only the HeLa cells expressing catalase showed decrease in oxidation compared to cells treated with PL only.

an increase in the dimer-form of Prx-2 in both HeLa and A549 (Figure 5.4b). However, treatment with PEITC or BSO did not result in any increase in H_2O_2. Thus, the increase in H_2O_2 in response to PL is not due to glutathione depletion. Interestingly, the HeLa cells have more elevated H_2O_2 in response to PL than the A549 cells.

We want to test if this elevation of H_2O_2 stress in the cytoplasm is important for the increased sensitivity of the HeLa cells to PL versus the A549 cells. By modifying the peroxisome targeting sequence –KANL of human catalase to –KADL, we can re-distribute the catalase we infect the HeLa cells with to the cytoplasm [38]. Immunofluorescence staining and western blot for catalase showed that the HeLa cells transfected with catalase lenti-viral vector have increased expression in the cytoplasm (Appendix). This modified cell line, HeLaCat, is much more resistant to PL

than the HeLa cells (Figure 5.5a). To test to see if PL actually generates superoxide in the cytoplasm or mitochondria, we pre-treated the cells with TEMPOL and mito-TEMPO, two super oxide dismutase mimetics, before addition of PL. Neither TEMPOL or mito-TEMPO improve the survival of the HeLa cells, thus PL generates hydrogen peroxide, but not superoxide inside the cell. We confirmed that the resistant of the HeLaCat cells is due to the decrease in peroxide stress through immuno-blot for Prx-2 dimer (Figure 5.5b). HeLaCat cells have less oxidation of Prx-2 upon PL incubation compared to HeLa, or HeLa cells treated with TEMPOL or mito-TEMPO (Appendix).

Since the presence of this low level H_2O_2 elevation appears to be important to the toxicity mechanism of PL, we looked at an alternative indicator of oxidative stress, the presence of protein s-glutathionylation inside the cell. Protein s-glutathionylation occurs because GSH protects oxidized protein thiols by forming a mix-disulfide with –SOH group, this mixed-disulfide form can then be reduced via glutaredoxin and convert the oxidized thiol back to a sulfhydryl group [39]. We performed immunofluorescence using an antibody that detects GSH-protein conjugation for cells treated with 10 μM PL, 10 μM PEITC or 100 μM BSO for a period of 10 hours. Unsurprisingly, only PL showed elevation of protein-GSH conjugation (Figure 5.6a). Furthermore, the HeLa cells have more elevated protein-GSH conjugation than the A549 cells in response to 10 μM PL treatment (Figure 5.6b). We also tested whether the interaction between the GSH and the oxidized protein is due to the formation of a disulfide bond. By converting all intracellular sulfhydryl groups on cysteine side chains into –S-S-CH3 using MMTS (methyl methanethiosulfonate), we can then use glutaredoxin to convert all the GSH-protein mix-disulfides to sulfhydryl group [28]. Following a biotinylation reaction using maleimide, we can detect the newly converted sulfhydryl groups using a biotin-FITC antibody

(Figure 5.6c). We found that the GSH-protein complexes formed during PL treatment are not reducible via glutaredoxin, since there is no elevation of immunofluorescence signal from reduced disulfide bonds (Figure 5.6d). Therefore, it appears that the interaction of GSH and oxidized thiol groups during to PL treatment is atypical of what traditionally happens during elevated oxidative stress. Finally, we measured the protein-GSH conjugates of HeLa cells producing peroxide via the DAAO generator. Although the generator produced more H_2O_2 than PL as indicated via HyPer, it did not cause the same level of protein oxidation as PL (Appendix). So the presence of oxidative stress alone cannot produce this much protein oxidative damage.

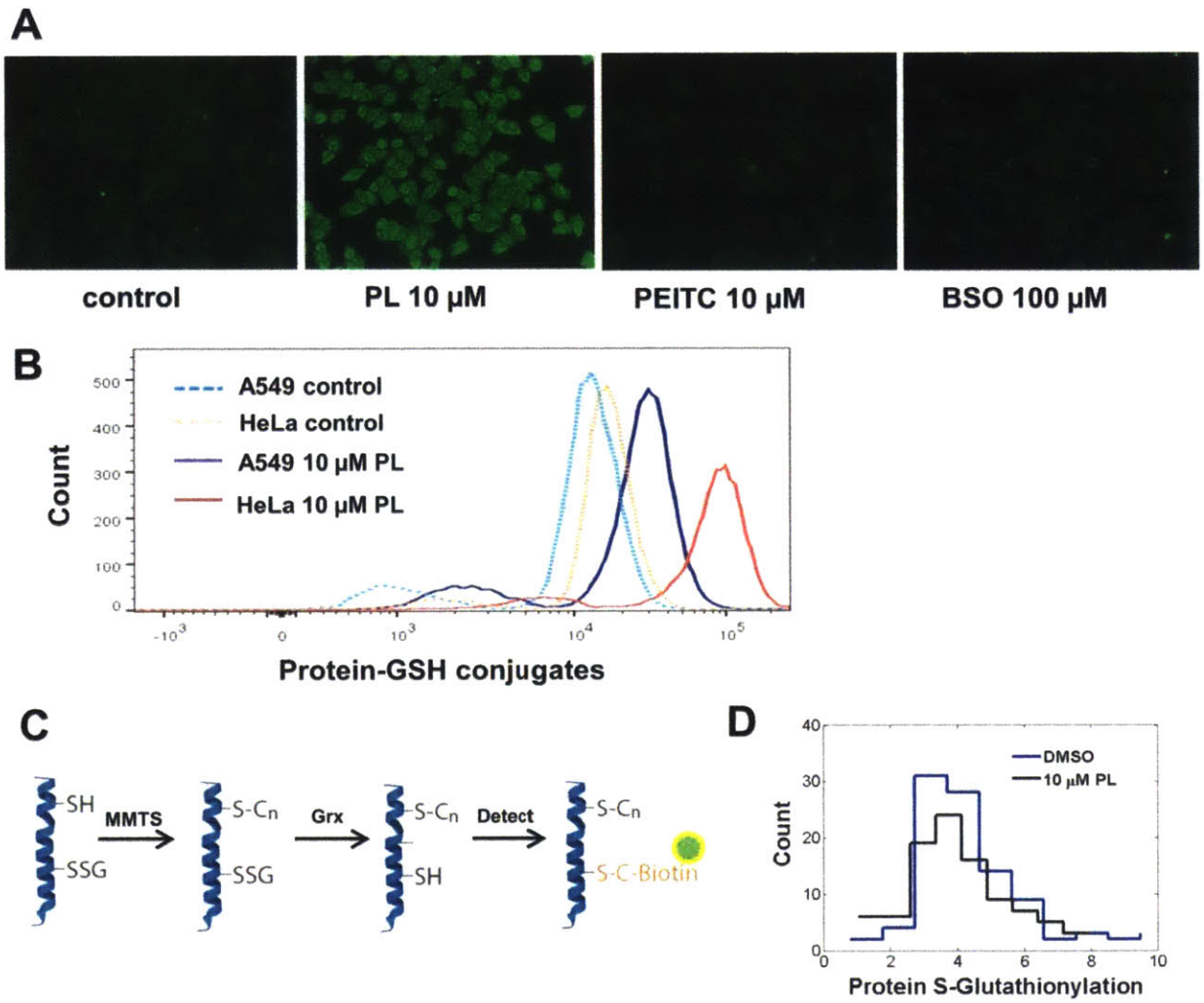

Figure 5.6: Protein-GSH detection as evidence of protein oxidative stress in response to PL and PEITC. A) Immunofluorescence detection of protein-GSH conjugate. HeLa cells were incubated for 10 hours with 10 μM PL, 10 μM PEITC and 100 μM BSO, then protein-GSH conjugates were detected using an antibody raised against GSH. Only PL show increase in in the level of protein-GSH conjugates. B) Flow cytometry quantification of protein-GSH conjugate for A549 and HeLa cells treated with PL. HeLa cells show much greater increase in protein-GSH complexes compared to the A549 cells. C) Schematic of an assay to detect s-glutathionylation. The free thiol groups are blocked using MMTS, then the mix disulfide formed by oxidized protein and GSH is reduced using glutaredoxin. These sulfhydryl groups are then biotinylated and detected using an antibody against biotin. D) Detection of s-glutathionylation for HeLa cells treated with PL. Treatment with 10 μM PL for 10 hours did not result in elevated s-glutathionylation.

5.3.4 The role of NRF-2 in conferring A549 resistance to PL and PEITC

To provide a molecular understanding for the increased resistance of A549 cells to these compounds, we investigated the role of NRF-2, a transcriptional molecule that is a master regulator for many oxidative stress protecting functions inside the cell [40,41]. At basal state in normal cells, NRF-2 is mostly sequestered and bound to KEAP-1 in the cytoplasm. When there is an elevation in oxidative stress, KEAP-1 is oxidized and undergoes conformational change, which releases NRF-2, allowing it to translocate to the nucleus and activate the antioxidant response element (ARE) signaling pathway [42]. The products of the signal pathway allow for modulation the oxidative stress. A549 cells have two different mutations, KRAS and KEAP-1, both of which causes elevation of nuclear NRF-2, activating the transcription of important antioxidants [43]. In particular, the KEAP-1 is important for sequestering NRF-2 in the cytoplasm, and mutations in the molecule will repair its ability to bind and inhibit the nuclear translocation of NRF-2 [44,45]. We used primary cells from a murine lung tumor model, Kras/p53, and created two knockouts cell lines from it: NRF-2 and KEAP-1. The knockout of NRF-2 should severely deplete the nuclear NRF-2 and the knockout of KEAP-1 should cause a significant increase in NRF-2 level. The difference in nuclear NRF-2 between the three cell lines is reflected in the total glutathione level, since translocated NRF-2 regulates activation of GSH synthesis (Appendix).

When we exposed the three cell lines to PL and PEITC, we found that the absence of KEAP-1 is important for conferring resistance to both drugs (Figure 5.7a, b), while the prescence of KRAS mutation does not allow for greater cell survival over NRF-2 knock-out cells. Furthermore, the KEAP-1 knock-out cells show almost no elevation in H_2O_2 during PL treatment as measured by Prx-2 dimerization, while the Kras/p53 and the NRF-2 knock-out cell line shows significant H_2O_2 elevation (Figure 5.7c). As a result, the increase in S-glutathionylation in KEAP-1 knock-outs upon PL treatment is the least amongst the three cell lines, at 5 times less than that of p53/Kras cells (Appendix). Thus, the NRF-2 up-regulation due to KEAP-1 knockout is important for protection of the cells against effects of oxidative stress induced by PL.

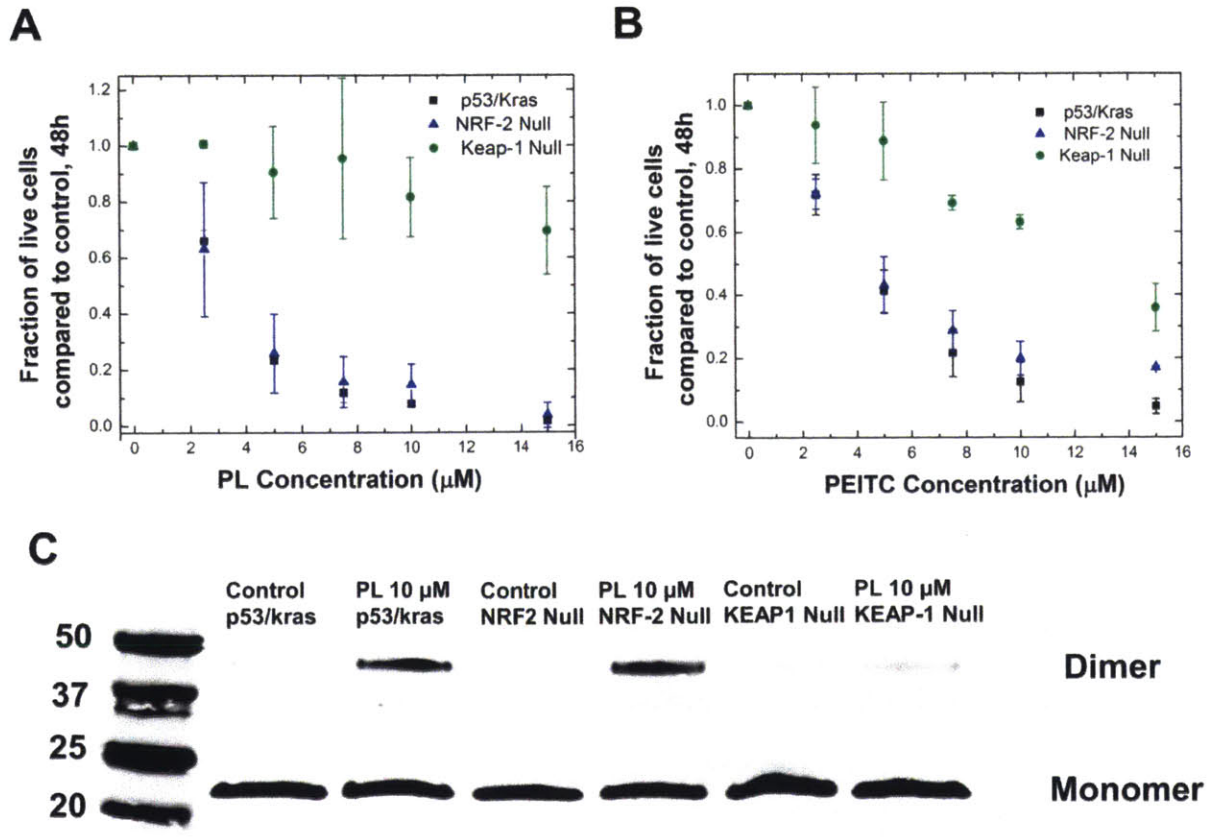

Figure 5.7: Effect of nuclear NRF-2 level on the cell toxicity and oxidative stress induced by PL and PEITC. Three model tumor cell lines, $p53^{fl}$/Kras ^{G12D}, $p53^{fl}$/Kras ^{G12D}/Nrf-2^{-}, $p53^{fl}$/Kras ^{G12D}/Keap-1^{-} were created to give a variety of range of NRF-2 based on specific mutations found in A549 cells. A) & B) The p53/Kras and the knockout cell lines treated with PL or PEITC

concentrations 0 – 15 μM. Number of live cells remaining on the dish after 48 hours were counted and compared to the DMSO control. The Keap-1 null cell lines were the most resistant to both compounds. C) Measurement of Prx-2 oxidation via treatment by 10 μM PL for a period of 10 hours. The Keap-1 cell line show the least amount of oxidation in response to PL treatment, and subsequently it is the most resistant to the drug.

5.4 Discussion and Conclusion

Investigations into the mechanism of ROS-based chemotherapeutics are plagued by a lack of proper controls and tools to achieve a better quantitative understanding of how these molecules induce toxicity in the cancer cells. In relations to PL and PEITC, we found that the depletion of glutathione is not the main mechanism responsible for the toxicity of the drug. By using an appropriate control, BSO, we showed that amount of GSH depletion in HeLa cells due to these compounds is non-toxic. We also showed that the GSH depletion does not act in synergy with the main toxicity mechanism of the compounds to confer selectivity of the drugs for HeLa cells over the A549 cells. Co-incubation of BSO and either chemotherapeutic causes GSH depletion in A549 cells to levels below that of HeLa cells treated with the chemotherapeutics alone, without increasing drug toxicity. It is surprising that we have to deplete almost all of the intracellular GSH in order to see any synergistic effect between BSO and the chemotherapeutic, highlighting the unimportance of GSH as a primary toxicity target and also a secondary protective measure in the mechanism of these two drugs.

The combined use of a species specific sensor and generator demonstrated a unique approach for understanding intracellular oxidative perturbations. Many studies on ROS generated by chemotherapeutics use DCFH, which lacks information about the amount or the type of ROS. Furthermore, it is unclear whether the quantity produced is important for toxicity, without a proper control generator that mimics the amount and kinetics of the generation. We used HyPer, a sensor for H_2O_2, in conjunction with the DAAO enzyme, a tunable generator of H_2O_2, to

conclude that the amount of peroxide generated by either drug cannot induce the growth inhibition effects alone. Going one step further, we employed a new approach for measuring H_2O_2 at levels below the limit of HyPer by immuno-blotting for Prx-2 dimers. We found that the immuno-blotting method is more sensitive and revealed interesting oxidative patterns for PL, PEITC and BSO incubation. Surprisingly, PEITC did not produce any H_2O_2, despite previous literature suggesting that the compound impairs glutathione and glutathione peroxidase activity. We also noted that BSO, which causes the most GSH depletion amongst the three compounds, also did not cause elevation in H_2O_2 level, so GSH depletion at the levels achieved by PL or PEITC cannot contribute to H_2O_2 increase. The only compound that was able to cause an increase in H_2O_2 was PL, and HeLa cells, which are more sensitive to the drug, showed more increase in H_2O_2 compared to the A549 cells.

We demonstrated that the H_2O_2 elevation below the detection limit of HyPer is important to PL toxicity. By adding intracellular catalase to the HeLas, we scavenged the elevated H_2O_2 from PL treatment and made the cell line more resistant to the drug. This is surprising since using the DAAO generator to produce H_2O_2 at levels below the detection limit of HyPer did not result in significant growth inhibition, so the effect of oxidative stress alone at the amount present during PL treatment cannot cause significant toxicity. We investigated the effect of PL on protein s-glutathionylation, a consequence of GSH protecting oxidized thiol groups by forming a mix-sulfide bond with them that can be reduced by glutaredoxin. We found that the s-glutathionylation that happens during PL treatment results in a GSH-protein bond that cannot be reduced, thus trapping thiol groups oxidized by H_2O_2 and keeping the protein in an inactive form. This irreversible protein oxidation is unlike what occurs under normal oxidative stress, in which the oxidation effects can be reversed using glutaredoxin. This irreversibility has been

noted in previous studies on PL, where the use of DTT cannot reduce the protein-GSH bond [46]. It is hypothesized that the two electrophilic sites on the drug help form a covalent interaction between the –SOH, GSH and PL, since absence of either double bond result in a non-toxic variant of the compound [46]. Thus, it is possible that the toxicity effects from PL are due to the small quantity of H_2O_2 elevation that causes irreversible protein-oxidation in synergy with the compound. We should note that this toxic synergy between the PL and oxidative stress is uncovered when we used not only sensitive sensors, but also H_2O_2 generators to test if the amount detected is meaningful by itself in producing any effects, highlighting the importance of this dual approach for studying ROS-induced mechanisms.

Finally, we attempted to understand why certain cancer cells are more resistant to the effects of PL and PEITC than other. In our case, the A549 cells had a greater resistance to both compounds than the HeLa cells. By using model lung tumor cell lines that allow for varying levels of nuclear NRF-2, we demonstrated that NRF-2 level is important in protecting cells from the effects of these compounds. In particular, the KEAP-1 mutation of the A549 cells can cause an up-regulation in protective function of NRF-2, some of which include antioxidant production, drug efflux and heat-shock proteins activation [47]. Thus, it is unsurprising that for the KEAP-1-null cells, the up-regulation in antioxidant can contribute to a lower H_2O_2 elevation in response to PL, which in turn contributes to a much higher resistance to the drug. In fact, NRF-2 has been shown to be up-regulated in many instances of chemo-resistance. For example, cell lines adapted to increasing concentrations doxorubicin often show elevated levels of NRF-2 [48]. More work will need to be done to uncover exactly which antioxidants up-regulated by the NRF-2 confers resistance to PL.

It should be noted that we have not yet discovered the mechanism of action for PEITC in our study. While originally thought to operate by similar mechanisms as PL, we now showed that treatment with PEITC does not produce H_2O_2 or superoxide (Figure 5.4a, Appendix), so oxidative stress is unlikely to play a role in the drug mechanism. However, it is possible that other reactive molecules, such as reactive nitrogen species (RNS) may contribute to the toxicity of the drug, and the current repertoire of tools we have is insufficient to study these molecules in a controlled and rigorous manner [49]. Nevertheless, our combined use of H_2O_2-specific sensors and generator uncovered a surprising toxic synergy between PL and H_2O_2, and demonstrated the need for both tools simultaneously in order to understand the role of oxidative stress in cancer chemotherapeutics. Furthermore, our use of GSH depletion controls such as BSO, help elucidate the lack of importance of GSH in the mechanism of these drugs. Overall, our study highlighted the need for quantification of molecules affected by these drugs, and control experiments to demonstrate that the amount increase or decrease is important to the toxicity mechanism. Only then can we achieve a truly rigorous understanding of these ROS-based cancer chemotherapeutics.

5.5 Bibliography

(1) Lambeth, J. D. (2007) Nox enzymes, ROS, and chronic disease: an example of antagonistic pleiotropy. *Free Radic. Biol. Med. 43*, 332–47.

(2) Murphy, M. P., Holmgren, A., Larsson, N.-G., Halliwell, B., Chang, C. J., Kalyanaraman, B., Rhee, S. G., Thornalley, P. J., Partridge, L., Gems, D., Nyström, T., Belousov, V., Schumacker, P. T., and Winterbourn, C. C. (2011) Unraveling the biological roles of reactive oxygen species. *Cell Metab. 13*, 361–6.

(3) Laurent, A., Nicco, C., Chéreau, C., Goulvestre, C., Alexandre, J., Alves, A., Lévy, E., Goldwasser, F., Panis, Y., Soubrane, O., Weill, B., and Batteux, F. (2005) Controlling tumor growth by modulating endogenous production of reactive oxygen species. *Cancer Res. 65*, 948–956.

(4) Gough, D. R., and Cotter, T. G. (2011) Hydrogen peroxide: a Jekyll and Hyde signalling molecule. *Cell Death Dis. 2*, e213.

(5) Liou, G.-Y., and Storz, P. (2010) Reactive oxygen species in cancer. *Free Radic. Res. 44*, 479–96.

(6) Waris, G., and Ahsan, H. (2006) Reactive oxygen species: role in the development of cancer and various chronic conditions. *J. Carcinog. 5*, 14.

(7) Schumacker, P. T. (2006) Reactive oxygen species in cancer cells: live by the sword, die by the sword. *Cancer Cell 10*, 175–6.

(8) Gorrini, C., Harris, I. S., and Mak, T. W. (2013) Modulation of oxidative stress as an anticancer strategy. *Nat. Rev. Drug Discov. 12*, 931–47.

(9) Trachootham, D., Alexandre, J., and Huang, P. (2009) Targeting cancer cells by ROS-mediated mechanisms: a radical therapeutic approach? *Nat. Rev. Drug Discov. 8*, 579–91.

(10) Trachootham, D., Zhou, Y., Zhang, H., Demizu, Y., Chen, Z., Pelicano, H., Chiao, P. J., Achanta, G., Arlinghaus, R. B., Liu, J., and Huang, P. (2006) Selective killing of oncogenically transformed cells through a ROS-mediated mechanism by beta-phenylethyl isothiocyanate. *Cancer Cell 10*, 241–52.

(11) Raj, L., Ide, T., Gurkar, A. U., Foley, M., Schenone, M., Li, X., Tolliday, N. J., Golub, T. R., Carr, S. A., Shamji, A. F., Stern, A. M., Mandinova, A., Schreiber, S. L., and Lee, S. W. (2011) Selective killing of cancer cells by a small molecule targeting the stress response to ROS. *Nature 475*, 231–4.

(12) Tusskorn, O., Senggunprai, L., Prawan, A., Kukongviriyapan, U., and Kukongviriyapan, V. (2013) Phenethyl isothiocyanate induces calcium mobilization and mitochondrial cell death pathway in cholangiocarcinoma KKU-M214 cells. *BMC Cancer 13*, 571.

(13) Yeh, Y.-T., Yeh, H., Su, S.-H., Lin, J.-S., Lee, K.-J., Shyu, H.-W., Chen, Z.-F., Huang, S.-Y., and Su, S.-J. (2014) Phenethyl isothiocyanate induces DNA damage-associated G2/M arrest and subsequent apoptosis in oral cancer cells with varying p53 mutations. *Free Radic. Biol. Med. 74*, 1–13.

(14) Dhillon, H., Chikara, S., and Reindl, K. M. (2014) Piperlongumine induces pancreatic cancer cell death by enhancing reactive oxygen species and DNA damage. *Toxicol. Reports 1*, 309–318.

(15) Adams, D. J., Boskovic, Z. V, Theriault, J. R., Wang, A. J., Stern, A. M., Wagner, B. K., Shamji, A. F., and Schreiber, S. L. (2013) Discovery of small-molecule enhancers of reactive oxygen species that are nontoxic or cause genotype-selective cell death. *ACS Chem. Biol. 8*, 923–9.

(16) Zhu, C., Hu, W., Wu, H., and Hu, X. (2014) No evident dose-response relationship between cellular ROS level and its cytotoxicity--a paradoxical issue in ROS-based cancer therapy. *Sci. Rep. 4*, 5029.

(17) Winterbourn, C. C. (2014) The challenges of using fluorescent probes to detect and quantify specific reactive oxygen species in living cells. *Biochim. Biophys. Acta 1840*, 730–8.

(18) Tetz, L. M., Kamau, P. W., Cheng, A. A., Meeker, J. D., and Loch-Caruso, R. Troubleshooting the dichlorofluorescein assay to avoid artifacts in measurement of toxicant-stimulated cellular production of reactive oxidant species. *J. Pharmacol. Toxicol. Methods 67*, 56–60.

(19) Belousov, V. V, Fradkov, A. F., Lukyanov, K. A., Staroverov, D. B., Shakhbazov, K. S., Terskikh, A. V, and Lukyanov, S. (2006) Genetically encoded fluorescent indicator for intracellular hydrogen peroxide. *Nat. Methods 3*, 281–6.

(20) Gutscher, M., Sobotta, M. C., Wabnitz, G. H., Ballikaya, S., Meyer, A. J., Samstag, Y., and Dick, T. P. (2009) Proximity-based protein thiol oxidation by H2O2-scavenging peroxidases. *J. Biol. Chem. 284*, 31532–40.

(21) Meyer, A. J., and Dick, T. P. (2010) Fluorescent protein-based redox probes. *Antioxid. Redox Signal. 13*, 621–50.

(22) Malinouski, M., Zhou, Y., Belousov, V. V, Hatfield, D. L., and Gladyshev, V. N. (2011) Hydrogen peroxide probes directed to different cellular compartments. *PLoS One* (Kowaltowski, A. J., Ed.) *6*, e14564.

(23) Huang, B. K., and Sikes, H. D. (2014) Quantifying intracellular hydrogen peroxide perturbations in terms of concentration. *Redox Biol. 2*, 955–962.

(24) Glasauer, A., Sena, L. A., Diebold, L. P., Mazar, A. P., and Chandel, N. S. (2013) Targeting SOD1 reduces experimental non-small-cell lung cancer. *J. Clin. Invest.*

(25) Haskew-Layton, R. E., Payappilly, J. B., Smirnova, N. A., Ma, T. C., Chan, K. K., Murphy, T. H., Guo, H., Langley, B., Sultana, R., Butterfield, D. A., Santagata, S., Alldred, M. J., Gazaryan, I. G., Bell, G. W., Ginsberg, S. D., and Ratan, R. R. (2010) Controlled enzymatic production of astrocytic hydrogen peroxide protects neurons from oxidative stress via an Nrf2-independent pathway. *Proc. Natl. Acad. Sci. U. S. A. 107*, 17385–90.

(26) Halvey, P. J., Hansen, J. M., Johnson, J. M., Go, Y.-M., Samali, A., and Jones, D. P. (2007) Selective oxidative stress in cell nuclei by nuclear-targeted D-amino acid oxidase. *Antioxid. Redox Signal. 9*, 807–16.

(27) Matlashov, M. V, Belousov, V. V, and Enikolopov, G. (2013) How Much H2O2 Is Produced by Recombinant D-Amino Acid Oxidase in Mammalian Cells? *Antioxid. Redox Signal. 00.*

(28) Circu, M. L., and Aw, T. Y. (2012) Glutathione and modulation of cell apoptosis. *Biochim. Biophys. Acta 1823*, 1767–77.

(29) Franco, R., Panayiotidis, M. I., and Cidlowski, J. a. (2007) Glutathione depletion is necessary for apoptosis in lymphoid cells independent of reactive oxygen species formation. *J. Biol. Chem. 282*, 30452–30465.

(30) DuPage, M., Dooley, A. L., and Jacks, T. (2009) Conditional mouse lung cancer models using adenoviral or lentiviral delivery of Cre recombinase. *Nat. Protoc. 4*, 1064–72.

(31) Hartig, S. M. (2013) Basic image analysis and manipulation in imageJ. *Curr. Protoc. Mol. Biol.* 1–12.

(32) Sobotta, M. C., Barata, A. G., Schmidt, U., Mueller, S., Millonig, G., and Dick, T. P. (2013) Exposing cells to H2O2: a quantitative comparison between continuous low-dose and one-time high-dose treatments. *Free Radic. Biol. Med. 60*, 325–35.

(33) Carpenter, A. E., Jones, T. R., Lamprecht, M. R., Clarke, C., Kang, I. H., Friman, O., Guertin, D. a, Chang, J. H., Lindquist, R. a, Moffat, J., Golland, P., and Sabatini, D. M. (2006) CellProfiler: image analysis software for identifying and quantifying cell phenotypes. *Genome Biol. 7*, R100.

(34) Low, F. M., Hampton, M. B., Peskin, A. V, and Winterbourn, C. C. (2007) Peroxiredoxin 2 functions as a noncatalytic scavenger of low-level hydrogen peroxide in the erythrocyte. *Blood 109*, 2611–7.

(35) Marinho, H. S., Real, C., Cyrne, L., Soares, H., and Antunes, F. (2014) Hydrogen peroxide sensing, signaling and regulation of transcription factors. *Redox Biol. 2*, 535–562.

(36) Manta, B., Hugo, M., Ortiz, C., Ferrer-Sueta, G., Trujillo, M., and Denicola, A. (2009) The peroxidase and peroxynitrite reductase activity of human erythrocyte peroxiredoxin 2. *Arch. Biochem. Biophys. 484*, 146–54.

(37) Wood, Z. a, Schröder, E., Robin Harris, J., and Poole, L. B. (2003) Structure, mechanism and regulation of peroxiredoxins. *Trends Biochem. Sci. 28*, 32–40.

(38) Purdue, P. E., and Lazarow, P. B. (1996) Targeting of human catalase to peroxisomes is dependent upon a novel COOH-terminal peroxisomal targeting sequence. *J. Cell Biol. 134*, 849–862.

(39) Grek, C. L., Zhang, J., Manevich, Y., Townsend, D. M., and Tew, K. D. (2013) Causes and consequences of cysteine S-glutathionylation. *J. Biol. Chem. 288*, 26497–504.

(40) DeNicola, G. M., Karreth, F. a, Humpton, T. J., Gopinathan, A., Wei, C., Frese, K., Mangal, D., Yu, K. H., Yeo, C. J., Calhoun, E. S., Scrimieri, F., Winter, J. M., Hruban, R. H., Iacobuzio-Donahue, C., Kern, S. E., Blair, I. a, and Tuveson, D. a. (2011) Oncogene-induced Nrf2 transcription promotes ROS detoxification and tumorigenesis. *Nature 475*, 106–9.

(41) Sporn, M. B., and Liby, K. T. (2012) NRF2 and cancer: the good, the bad and the importance of context. *Nat. Rev. Cancer 12*, 564–71.

(42) Jaramillo, M. C., and Zhang, D. D. (2013) The emerging role of the Nrf2-Keap1 signaling pathway in cancer. *Genes Dev. 27*, 2179–91.

(43) Solis, L. M., Behrens, C., Dong, W., Suraokar, M., Ozburn, N. C., Moran, C. A., Corvalan, A. H., Biswal, S., Swisher, S. G., Bekele, B. N., Minna, J. D., Stewart, D. J., and Wistuba, I. I. (2010) Nrf2 and Keap1 abnormalities in non-small cell lung carcinoma and association with clinicopathologic features. *Clin. Cancer Res. 16*, 3743–53.

(44) Kansanen, E., Kuosmanen, S. M., Leinonen, H., and Levonen, A.-L. (2013) The Keap1-Nrf2 pathway: Mechanisms of activation and dysregulation in cancer. *Redox Biol. 1*, 45–9.

(45) Kobayashi, M., Li, L., Iwamoto, N., Nakajima-Takagi, Y., Kaneko, H., Nakayama, Y., Eguchi, M., Wada, Y., Kumagai, Y., and Yamamoto, M. (2009) The antioxidant defense system Keap1-Nrf2 comprises a multiple sensing mechanism for responding to a wide range of chemical compounds. *Mol. Cell. Biol. 29*, 493–502.

(46) Adams, D. J., Dai, M., Pellegrino, G., Wagner, B. K., Stern, A. M., Shamji, A. F., and Schreiber, S. L. (2012) Synthesis, cellular evaluation, and mechanism of action of piperlongumine analogs. *Proc. Natl. Acad. Sci. U. S. A. 109*, 15115–20.

(47) Ma, Q., and He, X. (2012) Molecular basis of electrophilic and oxidative defense: promises and perils of Nrf2. *Pharmacol. Rev. 64*, 1055–81.

(48) Shim, G., Manandhar, S., Shin, D., Kim, T.-H., and Kwak, M.-K. (2009) Acquisition of doxorubicin resistance in ovarian carcinoma cells accompanies activation of the NRF2 pathway. *Free Radic. Biol. Med. 47*, 1619–31.

(49) Chen, G., Chen, Z., Hu, Y., and Huang, P. (2011) Inhibition of Mitochondrial Respiration and Rapid Depletion of Mitochondrial Glutathione by β-Phenethyl Isothiocyanate: Mechanisms for Anti-Leukemia Activity. *Antioxid. Redox Signal. 15*, 2911–2921.

5.6 Appendix

HeLa cells infected with lenti-viral plasmid containing catalase redirected to the cytoplasm. Immunofluorescence staining of catalase shows that there is up-regulation of the antioxidant in the cytoplasm, this is increased expression is confirmed via western blot for catalase expression.

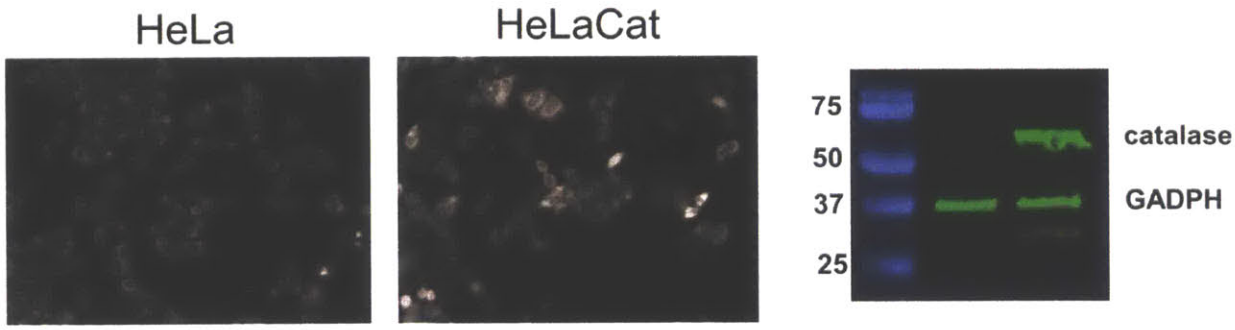

Prx-oxidation for HeLa cells treated with PL, externally added catalase , TEMPOL and Mito-tempo. The Prx-oxidation is not decreased using these antioxidants.

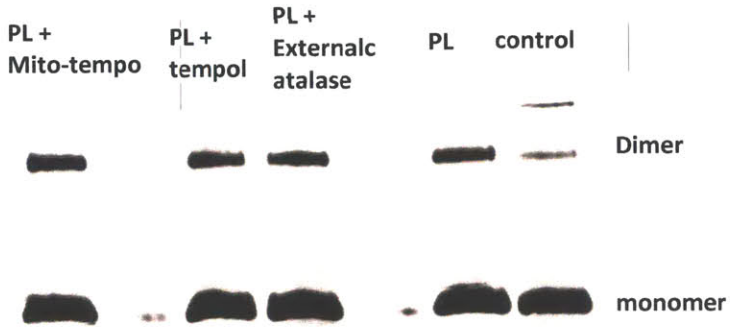

Protein-GSH conjugate comparison between PL and DAAO generated peroxide. While PL produced less peroxide as measured via the HyPer than the DAAO generator, the oxidative stress produced via the DAAO generator did not cause a significant increase in protein oxidation, while PL caused a significant increase in protein-GSH conjugates

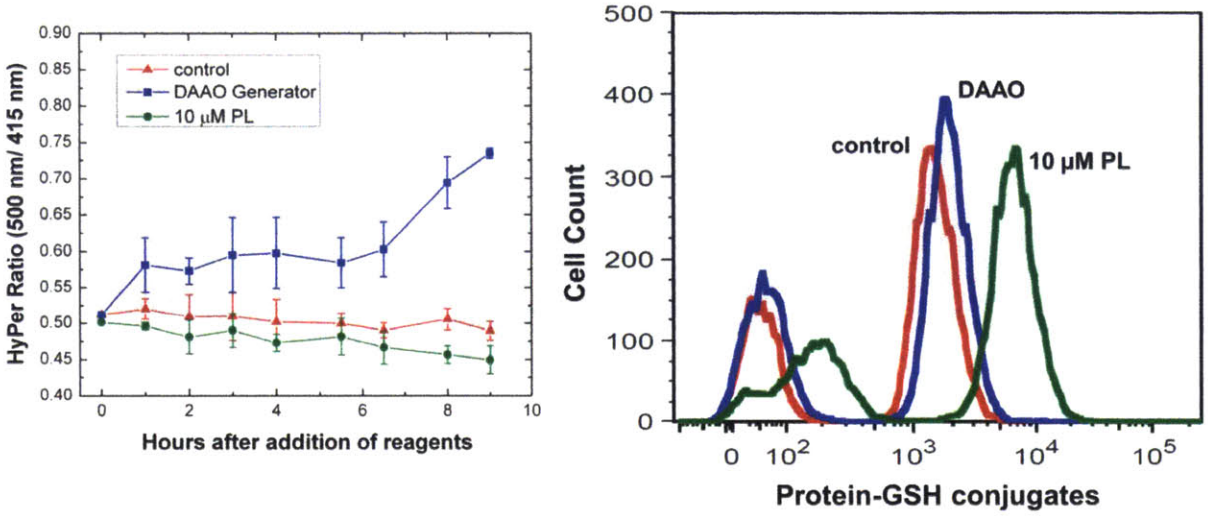

Total glutathione level in the kras/p53, NRF-2 null and Keap-1 null cell lines for control case and upon treatment with 10 µM PL, 10 µM PEITC or 25 µM BSO.

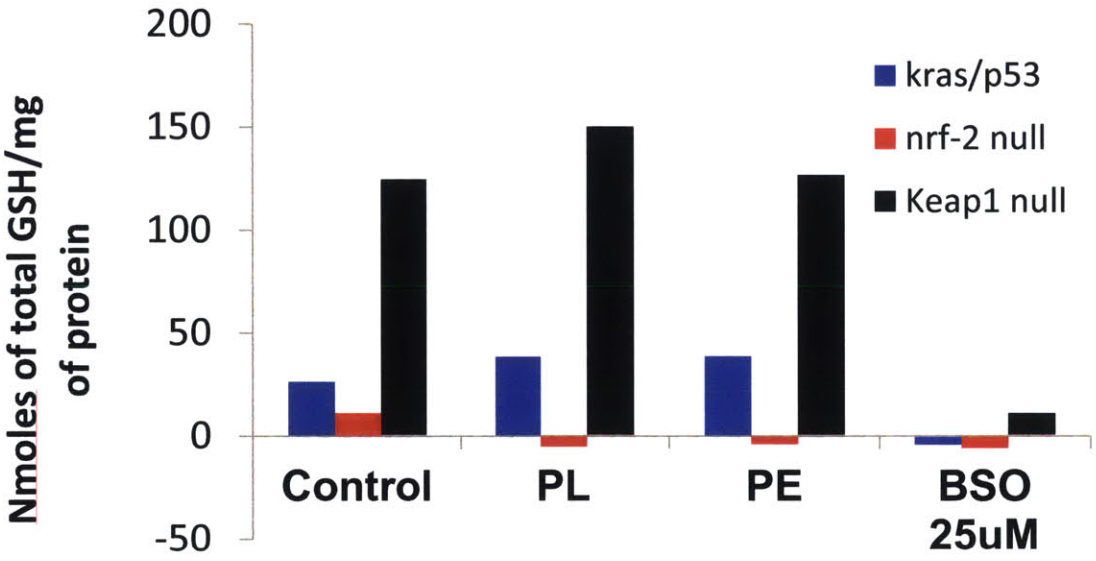

Increase in protein-glutathione conjugates for kras/p53, NRF-2 Null and Keap-1 null cells treated with 10 μM PL as measured via flow cytometry.

Cell Type	Protein oxidation (fold change)
$p53^{fl}/Kras^{G12D}$	6.7
$p53^{fl}/Kras^{G12D}/Nrf\text{-}2^{-}$	3.5
$p53^{fl}/Kras^{G12D}/Keap\text{-}1^{-}$	2.4

HeLa cells pre-treated with catalase, TEMPOL and mito-TEMPOL does not improve viability upon incubation with PEITC

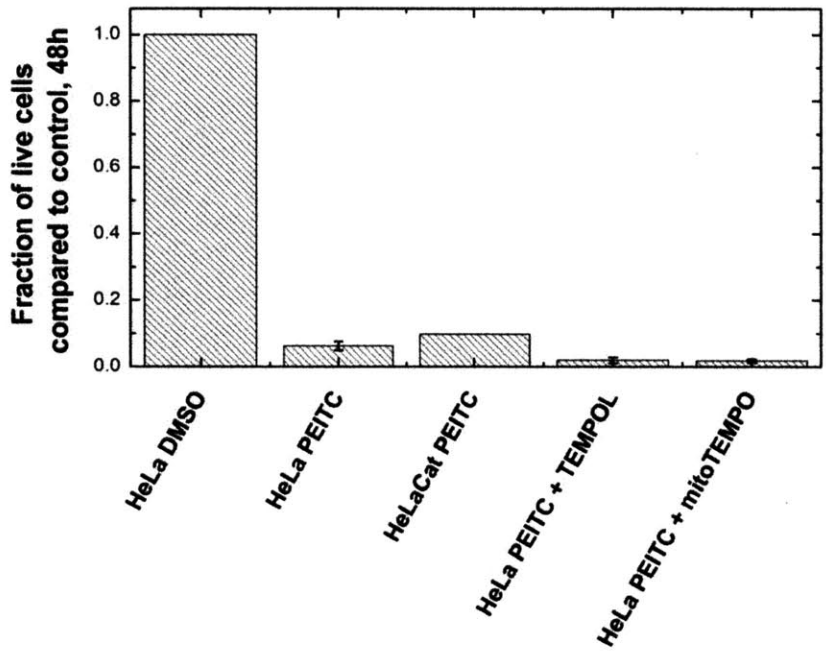

Chapter 6: Exploration of cytochrome P450 BM3 as a next-generation ROS-generator

*This chapter is a collaborative effort with Joseph B. Lim

6.1 Introduction

ROS is a natural byproduct of cellular metabolism that has also been implicated in numerous biological processes, including the respiratory burst, proliferation, apoptosis, and cellular signaling.[1–3] ROS has been studied using methodologies to both measure and perturb ROS levels inside and outside cells. To perturb ROS levels, researchers have historically used bolus addition of H2O2 to cell culture or stimulation and inhibition of nicotinamide adenine dinucleotide phosphate (NADPH) oxidase (NOX).[4,5] However, these methodologies add conflating variables of extracellular H2O2, a gradient between extracellular and intracellular species, and production of superoxide ($O2^{\cdot-}$) as an intermediate, complicating interpretation of resulting biological effects. Furthermore, bolus addition in particular adds H2O2 in non-physiological and kinetics amounts, which may result in effects not seen when H2O2 is produced endogenously during events in which H2O2 has been implicated. [6–8]

To more accurately mimic physiological production of ROS, researchers have recently turned to soluble, localizable enzymes, including glucose oxidase (GO), xanthine oxidase (XO), and D-amino acid oxidase (DAAO). GO, modulated by the H2O2 scavenger catalase, has been primarily used for extracellular generation of H2O2, as has been XO; neither can be used effectively inside the cell because of GO's requirement of a valuable metabolite, glucose, and

XO's promiscuous activity on a variety of substrates and production of both O2- in addition to H2O2.[9–12] DAAO has been genetically encoded and used for intracellular H2O2 production in numerous studies;[13–15] however, its requirement of exogenous substrate, typically D-alanine, and production of byproducts ammonia and α-keto acid may still introduce conflating effects.

Thus far, there is no endogenous generator of ROS that allows controlled production of both superoxide and H2O2, and does not require exogenous co-substrates (limiting the ease of subcellular localization). In this chapter, we explored the use of an enzyme with an established history of being engineered for biotechnological applications (mainly in difficult oxidation processes) and the capability of producing H_2O_2 or superoxide using only nicotinamide adenine dinucleotide phosphate (NADPH) and molecular oxygen.

Cytochrome P450s (CYPs) is a family of heme-containing enzymes that generally perform hydroxylation and are found in almost all organisms. The hydroxylation reaction proceeds as follows:

$$R\text{–}H + O_2 + NADPH + H^+ \rightarrow R\text{–}OH + H_2O + NADP^+$$

where R–H is substrate, O_2 is molecular oxygen, $NADPH/NADP^+$ is nicotinamide adenine dinucleotide phosphate, and R–OH is hydroxylated product. The reaction requires coupling of activities between a reductase, to which NADPH transfers its electrons, and an oxidase, which binds O_2 and R–H and receives electrons from the reductase to perform catalysis (Figure 6.1). While the electron transfer is usually well-coupled with the reaction, uncoupling sometimes occurs, albeit at low frequencies, resulting in production of either H_2O_2 or O_2^-.

One member of the CYP family, P450 BM3, is of particular interest because it captures many of the qualities that define an ideal ROS generator. Unlike membrane-bound mammalian CYPs,

P450 BM3 is water-soluble and is found in the cytosol of *Bacillus megaterium*. While many other CYPs rely on a protein partner for electron transfer, P450 BM3 fuses the reductase and oxidase domains into one polypeptide.[16,17] As a result of this and perhaps other factors, P450 BM3 has the highest reported activity in the CYP family; indeed, its activity is several orders of magnitude higher than those reported for mammalian CYPs, as shown in Table 6.1.

Table 6.1. Maximum velocity rates of CYPs on native substrates.

CYP	Source	Activity (min^{-1})
CYP102A1 (BM3)	*Bacillus megaterium*	17000 [16]
CYP101 (cam)	*Pseudomonas putida*	4200 [18]
CYP4F2	Human liver	7.4 [19]
CYP4A11	Human liver	49.1 [19]
CYP1A1	Human liver	7.25 [20]
CYP1A2	Human liver	3.34 [20]

When in contact with non-native substrate or when certain mutations are introduced, P450 BM3 performs a leakage reaction whereby electrons are transferred from NADPH to reduce O_2, producing either water or the ROS H_2O_2 and O_2^- in a reproducible fashion (Figure 6.1).[21] P450 BM3 is thus of interest because it captures nearly all the qualities of an ideal ROS generator: it is endogenous, does not need exogenous substrates, and it can produce both superoxide and H2O2. The single characteristic that the wild-type (WT) P450 BM3 may be lacking, however, is high enough activity to sustain accumulation of intracellular ROS. While its native activity (Table 6.1) is on par with the activity levels of past enzymes used for H_2O_2 generation (Table 1.3), its reported leak rate ranges from 12 ± 6 [22] to 28 ± 0.7 min^{-1} [23], depending on experimental conditions, making it several orders of magnitude less than the activities of previously used ROS enzyme generators.

Thus, we need to engineering mutant forms of this enzyme that selects for higher production of ROS. By developing a mutant library, we can selectively tune the kinetic activity and the ratio of superoxide to H2O2 output of our generator.

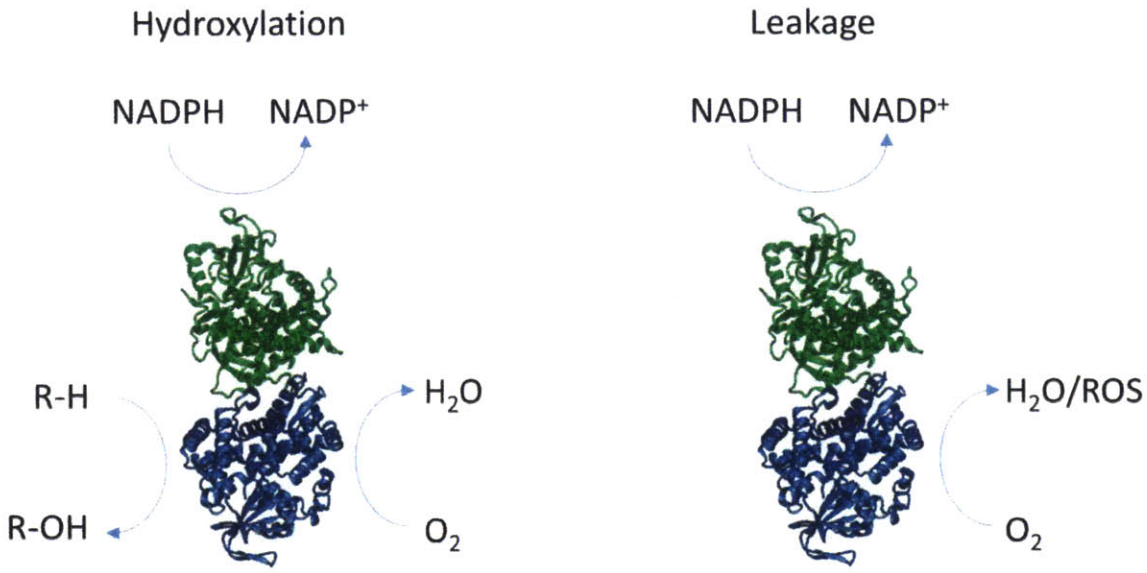

Figure 6.1: Schematic of P450 hydroxylation and leakage. NADPH binds to the reductase domain and donates electrons to the FAD and then FMN cofactors, which then transfer the electrons to the heme in the oxidase domain. In coupled hydroxylation, O2 and R–H bind at distinct sites, and O2 is reduced and activated to hydroxylate R–H, transforming it into R–OH. In leakage, the electrons are still transferred to the heme and used to reduce O2, but this may result in water, H2O2, or O2-. R–H is not involved in the leakage reaction.

We used a two prong approach for the protein engineering efforts of this project. Previous studies demonstrated certain mutations in the protein, i.e. A82W [24], T268N/F393H [22], and I401P

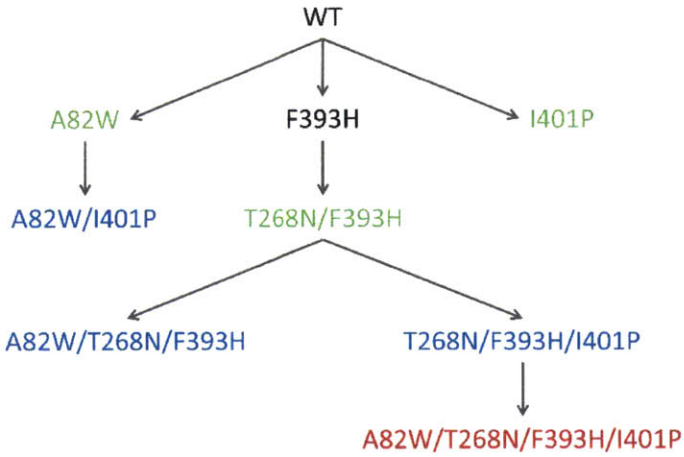

Figure 6.2: Schematic for lineage of variants with enhanced leakage derived from WT P450 BM3. Variants found to exhibit enhanced leakage in previous studies colored in green. Variants directly derived from variants measured in previous studies colored in blue. Variant containing all mutations in this chapter colored in red.

[23], exhibit leakage significantly higher than that of WT. we explored leakage in P450 BM3 and its potential use as a ROS generator by generating and combining past mutations mentioned above and previously shown to induce higher leakage [22–24], resulting in four new variants: A82W/I401P, A82W/T268N/F393H, T268N/F393H/I401P, and A82W/T268N/F393H/I401P (Figure 6.2).

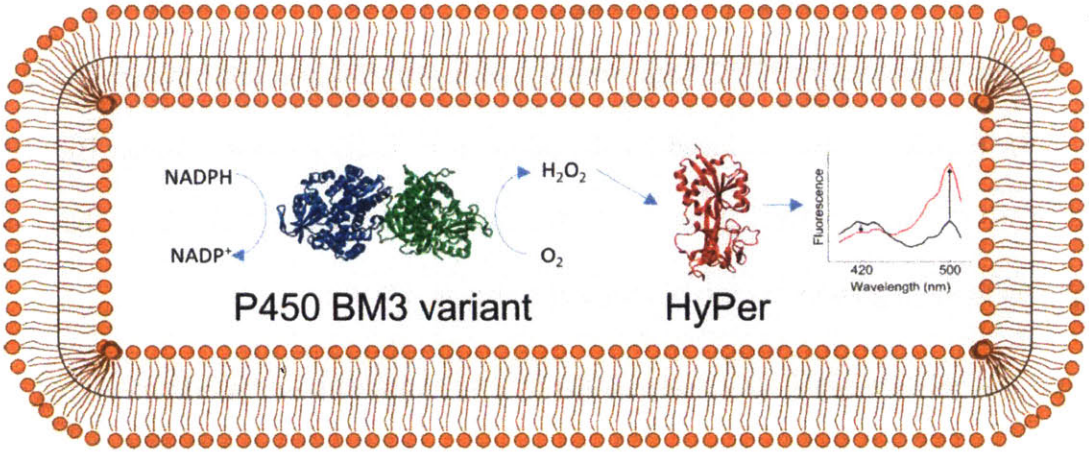

Figure 6.3: Schematic of HyPer-based screen for enhanced enzymatic production of H2O2. P450 BM3 variants from a library generated by error-prone PCR were co-expressed with HyPer. The enzyme used cellular supplies of NADPH and O2 to produce H2O2, which oxidized HyPer, resulting in an increase in its excitation spectrum at 500 nm and a decrease at 420 nm when emission was measured at 545 nm. Oxidized spectrum shown in red and reduced spectrum shown in black.

Secondly, we used a high-throughput screening method, co-expressing a genetically encoded sensor for H2O2, HyPer[25], into the bacteria cell along with the P450-BM3 enzyme. After using error-prone PCR to generate a mutant bacterial population, we can screen for mutants that cause an elevation in bacterial HyPer signal (Figure 6.3). We tested mutants found by these two methods on HeLa and human embryonic kidney (HeK) cells, endogenously expressing them and characterizing the H2O2 outputs from these enzymes.

6.2 Methods and Materials

Protein expression and purification

Reagents for making growth media were obtained from Becton Dickinson. A single colony of *E. coli* DH5α cells harboring the expression plasmid was used to inoculate 5 ml of LB medium (Becton Dickinson) containing ampicillin (100 μg/ml; USB Corporation) in a 14 ml culture tube (17 x 100 mm, VWR) and incubated at 37 °C with orbital shaking of 250 rpm overnight. This overnight culture was then used to inoculate 250 ml of TB medium (Becton Dickinson) containing ampicillin at the same concentration in a non-baffled 1 liter Erlenmeyer flask (VWR). The culture was incubated at 37 °C with orbital shaking of 250 rpm until the end of log phase (OD_{600} ~0.9). Expression was induced by the addition of IPTG (1 mM; Omega Bio-Tek) and occurred at 30 °C with orbital shaking of 200 rpm for 24 hours. Cells were harvested by centrifugation at 4000 g and 4 °C for 10 min and stored at -20 °C.

For purification, the cell pellet was resuspended in Tris buffer (20 ml, 25 mM Tris-HCl, pH 7.9; MP Biomedicals, LLC) and lysed by sonication (7 x 1 min; output control = 5, duty cycle 50%; Sonicator, S-250A analog, Branson). The lysate was centrifuged at 18000 g and 4 °C for 10 min and the supernatant was filtered using a 0.8/0.2 μm Acrodisc syringe filter with Supor membrane (Pall Corporation). The filtrate was loaded onto a 1 ml HiTrap Q Sepharose FF anion exchange column via a superloop; the column and superloop were integrated into an ÄKTApurifier with a UNICORN control system v5.20 and a Frac-950 collector (GE Life Sciences). Non-P450 BM3 proteins (as evidenced by absorbance at 280 nm and lack of absorbance at 417 nm) were eluted in a first step from 0 to 0.2 M NaCl (Mallinckrodt Pharmaceuticals). P450 BM3 and related variants were eluted in a second step to 0.4 M NaCl. Any remaining protein on the column was eluted in a third step to 1 M NaCl. The purification was performed at 1 ml/min and 4 °C. Purified P450 BM3 fractions were centrifuged through an Amicon Ultra-15 Centrifugal Filter Unit with Ultracel-100 membrane with nominal molecular weight limit of 100 kDa (Millipore). After

centrifugation at 4000 g and 4 °C for 10 min, 3 ml of KPi (100 mM, composed of monopotassium phosphate and dipotassium phosphate purchased from VWR, pH 8) was added to the remaining sample and centrifuged again through the filter unit at the same conditions. 3 ml of KPi (100 mM, pH 8) was added to the supernatant and centrifuged through the filter unit at the same conditions, generally resulting in 200-400 µl supernatant of protein solution. The remaining supernatant was diluted by adding 200-400 µl of KPi (100 mM, pH 8) and then dispensed into 20 µl aliquots and stored at -80 °C.

Spectrophotometric analysis of oxidized enzyme and carbon monoxide binding

Purified protein (20-200 µl) stored at -80 °C was thawed on ice and introduced into KPi (100 mM, pH 8) to make a 1 ml solution. Absorption spectra were recorded from 350 to 750 nm at room temperature (22 °C) using a Varian Cary 50 spectrophotometer and a polystyrene cuvette (VWR) with path length of 1 cm. The enzyme was reduced with a spatula tip of sodium dithionite before introducing 30 bubbles of carbon monoxide (CO; Airgas, Inc.) at 1 bubble/s into the assay solution, and absorption spectra were recorded before reduction, after reduction, and after reduction and treatment with CO. Reduced CO-bound difference spectra and the extinction coefficient $\varepsilon_{450\text{-}490}$ = 91 mM^{-1} cm^{-1} were used to calculate the concentration of correctly folded full-length protein. Experiments were carried out in duplicate save for A82W/T268N/F393H/I401P due to prohibitively low expression of correctly folded protein. P450 concentrations were recorded as a mean ± standard deviation save for A82W/T268N/F393H/I401P.

For mammalian lysates, cells were lysed in 200 µL of 1% Triton x-100 (Sigma). 160 µL of cell lysate was mixed with 40 µL of sodium dithionate 10mM in a 96-well microplate, and incubated

with CO for a period of 15 minutes. Absorption spectra were recorded from 400-510 nm before and after the CO binding, and the amount of functional P450 was calculated as above.

Enzyme kinetic measurements for Km and Kcat

Absorbance data was collected using a Varian Cary 50 spectrophotometer. Reactions (1 ml) were carried out at room temperature in KPi (100 mM, pH 8) using enzyme (10-100 nM) and NADPH (1-100 μM; Roche). Absorbance was followed at 340 nm and leak rates were calculated using the initial 12-30 seconds of a reaction and $\varepsilon_{340} = 6.22\ mM^{-1}\ cm^{-1}$. Experiments were carried out in triplicate and each leak rate was reported as a mean ± standard deviation. For each variant, Origin software (Origin Labs) was used to fit the leak rates at different concentrations of NADPH to the Michaelis-Menten equation to obtain $k_{cat,\ leakage}$ and $K_{m,\ leakage}$.

Analysis of H2O2 production via ABTS/HRP assay

The proportion of H_2O_2 production formation was determined by an HRP/ABTS assay. To develop a standard curve, a stock solution of H_2O_2 was quantified based on absorbance at 240 nm ($\varepsilon_{240} = 43.6\ M^{-1}\ cm^{-1}$) and used to prepare serial dilutions of H_2O_2. Purified enzyme (100 nM) was incubated with aliquots of the H_2O_2 dilutions; enzyme was included to account for the possible effects of antioxidants such as catalase and Ahp, which may have been present in the enzyme purifications in at least trace amounts. For trial reactions to measure H_2O_2 formation by P450 BM3, purified enzyme (100 nM) was incubated with NADPH (100 μM).

All reactions, both those to develop a standard curve and those to measure H_2O_2 formation by P450 BM3, were performed at a fixed volume (150 μl) and room temperature (22 °C). Reactions were performed in KPi (100 mM, pH 8) with sodium azide (NaN_3, 10 mM; Sigma-Aldrich Corporation), an inhibitor of catalase activity. Reactions were stopped after an initial incubation

period of 2-6 min using hydrochloric acid (10 µl, 5 N; Mallinckrodt Pharmaceuticals); for each P450 BM3 variant, the incubation period was held constant between trials. The reaction was centrifuged at 14000 g and 4 °C for 10 min. A portion of the supernatant (140 µl) was added to KPi (20 µl, 100 mM, pH 8), more concentrated KPi (50 µl, 1 M, pH 8), ABTS (50 µl, 2.5 mM; Tokyo Chemical Industry, Co., Ltd.), and HRP (10 µl, 3 mg/ml, Thermo Scientific) in a transparent 96-well microtiter plate (Greiner) and mixed. The absorbance at 405 nm was read using a Tecan Infinite M200 plate reader.

Experiments were carried out in triplicate. Absorbances of the standard curve reactions were averaged and standard deviations were calculated. These were then correlated with the initial H_2O_2 concentrations to develop a standard curve via linear regression, which was used to convert the absorbances of the trial reactions to the amount of H_2O_2 produced by each variant of P450 BM3 (Figures B.9-B.13). To calculate the proportion of product comprised by H_2O_2, the amount of H_2O_2 was normalized by the amount of NADPH consumed by P450 BM3 during the incubation period as measured by steady state kinetics assays.

Transfer of P450 gene to mammalian vector

The gene for the WT heme domain codon optimized for mammalian expression using Gene Designer software (DNA 2.0, Menlo Park, CA) and encoded in a pCMV-Sport vector was provided as a kind gift from Professor Mikhail Shapiro, Caltech, Pasadena, CA. The gene was transferred to the pTRE3G-IRES vector (Clontech) by PCR. A Kozak sequence was added immediately upstream of the gene to enhance expression, and a 6X His-tag was added immediately downstream to enable detection by a Western blot. The reductase domain was then codon optimized by GenScript (Piscataway, NJ) and fused with the heme domain by PCR.

Mutations were implemented using site-directed mutagenesis, with codon of the most frequency chosen.

Amplex Red assay for detection of H2O2 production in mammalian cell lysate

Cell lysate was collected as in the case of the CO binding assay, then mixed in 1:1 ratio with a solution containing 100 μM of Amplex Red reagent (Invitrogen) and 0.1 U/mL of horseradish peroxidase. The signal was captured at excitation of 490 nm and emission at 545 nm over a course of 30 minutes at room temperature.

Immunoblot for P450 expression and Prx-2 dimerization

The his-tagged P450 proteins were detected using the Thermo Scientific HisProbe-Hrp Reagent kit. Briefly, the detection probe is a tridentate chelator that binds to Ni^{+2}.The peroxiredoxin-2 dimerization was detected using an antibody against Prx-2 (R&D systems), along with an IR680 secondary antibody (Licor Biosciences) and was described in Ch.4 and 5. The block, primary and secondary buffers were purchased from Licor Biosciences.

HyPer measurement for HeLa cells expressing P450

HeLa cells were seeded on a 6-well plate at $5x10^5$ cells/well. The next day, the Tet3G and the pTRE3G-IRES vectors containing P450 were transfected using Lipofectamine 2000 at a ratio of 1 μg:4 μg:4 μg for a period of 18 hours. The media was replaced with media containing 1 mg/mL of doxycycline and incubated for another 3 days (a media refreshment after 2 days to replace the depleted doxycycline). 5-6 images were taken per condition at that point. The excitation wavelengths of HyPer were captured using a Nikon x81 epi-fluorescence microscope

on 10x objective setting. Images were excited at 415 nm/30 nm and 488 nm/25 nm and emission was recorded at 525 nm/40 nm, on 10% lamp intensity and 300ms exposure.

Construction and transformation of library of P450 BM3 variants for whole cell screening

Using P450 BM3/pRSFDuet-1 as the template plasmid, the primers 5'-AGGAGATATACCATGGCAATTAAAGAAATGCCTCAGCC-3' and 5'-GCGCCGTTCCTTCAGCTGTTCC-3' were used to amplify the part of the gene encoding the oxidase domain of P450 BM3 from the plasmid pRSFDuet-1 containing the gene of P450 BM3 from *Bacillus megaterium*. The reaction mixture for 50 µl error-prone PCR contained 1X Mutazyme II reaction buffer, 0.8 mM dNTP mixture, 125 ng of each primer, 4.7 µg of P450 BM3/pRSFDuet-1, and 2.5 U of Mutazyme II DNA polymerase (Novagen). After denaturation for 2 min at 95 °C, the PCR was run for 30 cycles of 95 °C for 30 seconds, 58.2 °C for 30 seconds, and 72 °C for 2 min, with a final extension step at 72 °C for 10 min. The error-prone PCR products were run on a 1% agarose gel at 100 V for 45 min and purified using a Gel Extraction Kit.

50 µl restriction digest reactions were performed on the purified error-prone PCR products and P450 BM3/pRSFDuet-1. The former contained 2 µg of the error-prone PCR products and the latter contained 5 µg of the vector. Both reactions contained 1X CutSmart Buffer, 20 U of NcoI-HF, and 20 U of SacI-HF. After incubation at 37 °C for 1 hour, reaction products were loaded onto a 1% agarose gel and run at 100 V for 50 min. The digested vector with the original P450 BM3 removed, along with the digested error-prone PCR products, were purified using a Gel Extraction Kit. Ligation of the purified restriction digest products was performed in a reaction with T4 DNA Ligase at 16 °C for 16 hours and purified using a Clean & Concentrate Kit. The

purified ligated product was introduced into electrocompetent cells of *E. coli* BL21 (DE3) Tuner by electroporation; these electrocompetent cells had already been previously transformed with the HyPer/pQE30 plasmid.

Developing the screening culture protocol

To determine the time of measurement optimal for fold difference between the WT and I401P controls, a colony of E. coli BL21 (DE3) Tuner cells harboring HyPer/pQE30 and WT P450 BM3/pRSFDuet-1 and another harboring HyPer/pQE30 and I401P P450 BM3/pRSFDuet-1 were each cultured in a flask, washed, and resuspended as described above in 1X PBS at pH 7.4. Cells were diluted to a concentration of 60 x 106 per 200 µl in three replicate wells in a black 96-well solid plate. Fluorescence emission intensity of each well was measured upon excitation at 500 nm with 9 nm bandwidth (F500) and 420 nm with 9 nm bandwidth (F420) with emission monitored at 545 nm (20 nm bandwidth) at 3 min intervals for 2 hours and 9 min using a Tecan Infinite M200 plate reader. Results indicated that the fold change maximized at approximately 2 hours; hence, all measurements hereafter were performed after 2 hours.

A side-by-side test was also performed to determine the effects on signal when cells are measured at high frequency every 3 min for 2 hours versus measured only once after 2 hours. In a sterile round-bottom 96-deep well microplate with a lid, 8 replicate wells each of WT and I401P co-expressed with HyPer were cultured by inoculation of 500 µl of LB medium supplemented with 50 µg/ml ampicillin and 25 µg/ml kanamycin. The plate was incubated at 37 °C with orbital shaking of 250 rpm overnight. 90 µl from each well in the 96-deep well microplate was then used to inoculate a single well in another sterile round-bottom 96-deep well microplate with a lid containing 1000 µl of TB medium supplemented with 50 µg/ml ampicillin

and 25 μg/ml kanamycin and incubated at 37 °C with orbital shaking of 250 rpm for 3 hours. 0.5 μl of IPTG was then added to each well to a final concentration of 0.05 mM and the cultures were incubated at 20 °C with orbital shaking of 250 rpm for 22 hours. The microplate was centrifuged at 4000 g and 4 °C for 5 min, the supernatant was removed, and each pellet in a well was resuspended in 250 μl of 1X PBS at pH 7.4. This washing step was repeated twice to remove traces of interfering fluorescent components of the growth medium. 100 μl of each well was mixed with 100 μl of 1X PBS at pH 7.4 in a black 96-well solid plate.

To test the effects of buffers with different pH levels and compositions on the signal, a colony of E. coli BL21 (DE3) Tuner cells harboring HyPer/pQE30 and WT P450 BM3/pRSFDuet-1 and another harboring HyPer/pQE30 and I401P P450 BM3/pRSFDuet-1 were each cultured in a flask, washed, and resuspended as described above in either 1X PBS at pH 7.4, 1X PBS at pH 8, or 0.1 M KPi at pH 8. Cells were diluted to a concentration of 480 x 106 per 200 μl in three replicate wells in a black 96-well solid plate.

Screening for variants with elevated H_2O_2 production

Colonies resulting from the mutagenic PCR were each picked and inoculated in individual wells of a sterile round-bottom 96-deep well microplate as described in in previous section. For controls, 8 colonies containing HyPer/pQE30 and WT P450 BM3/pRSFDuet-1 and 8 colonies containing HyPer/pQE30 and I401P P450 BM3/pRSFDuet-1 were each used to inoculate wells. The plate was incubated at 37 °C with orbital shaking of 250 rpm overnight. 150 μl from each well was mixed with 50 μl of 50% v/v glycerol in a sterile Falcon flat-bottom 96-well plate (Corning) with a lid to create a glycerol cell stock and stored at -80 °C. 90 μl from each well in the 96-deep well microplate was then used to inoculate a single well in another sterile round-

bottom 96-deep well microplate (VWR), incubated, induced for protein co-expression using IPTG, and washed and resuspended in assay buffer as described in Section 4.2.3. 100 µl of each well was mixed with 100 µl of 1X PBS at pH 7.4 in a black 96-well solid plate (Corning). Fluorescence was measured at 3 min intervals for 2 hours as described in Section 4.2.3.

Hits were selected based on their final ratiometric signal (F500/F420) relative to the average of those of the WT controls. For each hit, the glycerol cell stock plate was used to inoculate 8 replicate wells of a sterile round-bottom 96-deep well microplate with a lid. Each plate contained 8 replicate wells of WT P450 BM3 and 8 replicate wells of the I401P variant. The procedure described above was repeated except no glycerol cell stock plate was made. Final hits were confirmed by averaging the final ratiometric signals of replicate wells and performing Student's t-test to compare with the averaged final signal of the WT controls.

To isolate the P450 BM3/pRSFDuet-1 plasmid from the HyPer/pQE30 plasmid in selected hits, overnight cultures (5 ml) were started from the glycerol cell stock plate in LB medium supplemented with 50 µg/ml ampicillin and 25 µg/ml kanamycin and incubated at 37 °C and 250 rpm. The plasmids were extracted and purified using a GenCatch Plasmid DNA Mini-Prep Kit. 50 µl restriction digest reactions were performed on 900-1400 ng of the purified plasmids. Each reaction contained 1X CutSmart Buffer, 20 U of BamHI-HF, and 20 U of SbfI-HF. After incubation at 37 °C for 1 hour, reaction products were loaded onto a 1% agarose gel and run at 100 V for 1 hour. The linearized P450 BM3/pRSFDuet-1 plasmid (~7 kb) was separated from the linearized HyPer/pQE30 plasmid (~5 kb) and purified using a Gel Extraction Kit. Ligation of the purified restriction digest products was performed in a reaction with T4 DNA Ligase at 16 °C for 16 hours and purified using a Clean & Concentrate Kit. The purified ligated product was introduced into electrocompetent cells of *E. coli* DH5α by electroporation; we note that these

electrocompetent cells did not contain the HyPer/pQE30 plasmid. Each variant was cultured, and the plasmid was extracted via a DNA miniprep and verified by sequencing.

6.3 Results

6.3.1 Kinetic modeling to establish design criteria for ROS generator

Before our protein engineering efforts, we needed to establish some quantitative design criteria for the ROS generator using kinetic modeling efforts. The information from our analysis will be important for understanding our mutant selection goals. Questions such as how "good" the mutant would need to be, can be answered from knowing how much H2O2 needs to be produced

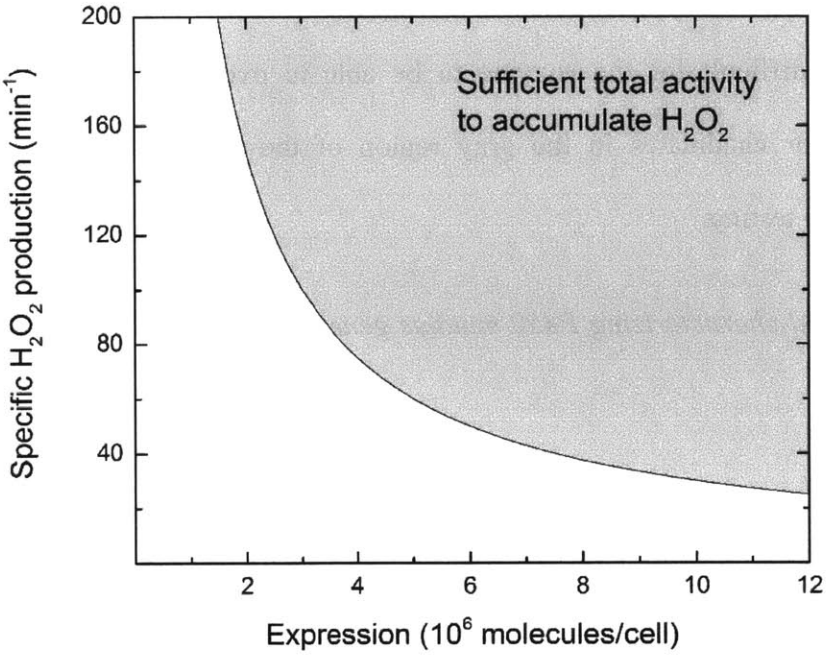

Figure 6.4: Design criterion specifying the total amount of H_2O_2 production required for a generator, as a product of specific production rate and total amount of generator, to overcome cellular antioxidant capacity and sustain generation. The criterion is shown as a contour; any generator in the shaded, grey region surpasses the required threshold. The criterion calculated here is specific to HeLa cells.

in order to overcome the antioxidants inside the cell. We adapted a model from Adimora et al, it included the reactivity of catalase, glutathione peroxidase, peroxiredoxin and glutaredoxin, the

redox reactions of thioredoxin and glutathione, the pseudo-enzymatic oxidative turnover of protein thiols, and the diffusion of H_2O_2 across the plasma membrane [26]. We adjusted the model for HeLa cells using rate constants and other parameters that we measured in previous work [27], the changes in rate constants and initial conditions are listed in Chapter 3 Appendix. Instead of simulating a bolus addition, we instead increased the endogenous production of H2O2 parameter until the intracellular concentration profile begins to rise. We found that an endogenous generator would need to produce 10^8 H2O2 molecules/min in order it to overcome the antioxidant system and be detected. Since the production rate is a function of both expression level of the generator and the specific kinetic activity, we illustrated the design criteria by plotting the two variables against each other in Figure 6.4. As we can see from the plot, when the expression level gets below 10^6 molecules/cell and the specific activity gets below 20 min^{-1}, it becomes extremely difficult for the enzyme to be able to overcome the intracellular H2O2 scavengers. Generator candidates in the gray region of the plot will considered promising candidates for *in vivo* testing.

6.3.2 Producing and characterizing P450 mutants generated via literature reported mutations in vitro

All mutant proteins from the lineage tree in Figure 6.2 were overexpressed and purified. The final preparations of the WT protein and A82W, I401P, T268N/F393H, and A82W/I401P variants had purities in excess of 95% as evidenced by strong single bands in SDS-PAGE analysis (appendix). The A82W/T268N/F393H, T268N/F393H/I401P, and A82W/T268N/F393H/I401P preparations showed a weaker P450 band and a significant band between 50 and 75 kDa. The A82W/T268N/F393H preparation was mostly comprised of P450, but the T268N/F393H/I401P and A82W/T268N/F393H/I401P preparations had purities less than

50%. The decrease in purity may be due to the fact that expression of the protein decreased when leakage-enhancing mutations were introduced, and decreased even further when mutations were combined.

We then kinetically characterized them by measuring their Michaelis-Menten parameters for leakage. All variants studied here exhibited $k_{cat,\ leakage}$ values significantly higher than that of the WT enzyme. Interestingly, variants with two mutations – A82W/I401P and T268N/F393H – did not exhibit $k_{cat,\ leakage}$ values higher than that of single-mutation variants, i.e. A82W and I401P. Moreover, A82W/I401P had a K_m 5-fold greater than that of the next highest (A82W) and more than an order of magnitude greater than those of all other variants measured in this work (Table 6.2).

Table 6.2. Measured $K_{m,\ leakage}$ and proportion of product comprised by H_2O_2.

Variant	**$K_{m,\ leakage}$ (μM)**	**% H_2O_2**
WT	1.3 ± 0.4	-
A82W	4.0 ± 0.9	24 ± 1.7
I401P	1.7 ± 0.3	62 ± 5.7
T268N/F393H	< 1[a]	89 ± 11
A82W/I401P	20.1 ± 4.4	59 ± 15
A82W/T268N/F393H	< 1[a]	53 ± 7.4
T268N/F393H/I401P	< 1[a]	> 0[b]

[a] NADPH absorbance not detectable at concentrations less than 1 μM

[b] positive signal indicated presence of H_2O_2 but was not quantifiable due to inability to generate a standard curve

When three of the four mutations were combined – A82W/T268N/F393H and T268N/F393H/I401P – $k_{cat,\ leakage}$ increased dramatically to several fold higher than the $k_{cat,\ leakage}$ of any of the one- or two-mutation variants. The $K_{m,\ leakage}$ of these three-mutation variants also remained below 1 μM. When combined in numbers greater than two, the mutations in this chapter dramatically increase leakage. The combination of all mutations, A82W/T268N/F393H/I401P, which we do not show in Table 6.2, resulted in a variant that was

the most active with respect to leakage as shown in the table. While the variant was extremely difficult to express and purify, enough active enzyme was obtained to measure the leak rate using 100 μM NADPH: 1198 ± 43 min^{-1}. Given the $K_{m,\ leakage}$ of all other variants, it is likely that A82W/T268N/F393H/I401P was assayed at a saturating level of NADPH, and thus the leak rate can be approximated as the $k_{cat,\ leakage}$.

Each variant other than WT produced different amounts of H_2O_2 as indicated by measurements of H_2O_2 in Table 6.2. No variant produced only H_2O_2; thus, each variant also produced either O_2^-, water, or both, in addition to H_2O_2. Notably, the T268N/F393H variant exhibited the highest percentage, which may be due to its particular conformation. In the structure of the T268N variant, the amine on N268 points into the active site and is able to donate a hydrogen bond to the ferrous dioxygen species, but cannot accept a hydrogen bond from the hydroperoxy ferric species [22]. This makes the hydroperoxy ferric species less stable, increasing the chance that H_2O_2 will be released as a product, which is consistent with the percentage obtained for T268N/F393H.

6.3.3 Expressing and characterizing P450 mutants generated via literature reported mutations in mammalian cells

The WT P450-BM3 with a his-tag was codon optimized using a proprietary algorithm and encoded in the pTRE3G-IRES inducible vector for expression in mammalian cells. The mutations in Figure 6.2 were then introduced by site-directed mutagenesis. Vectors encoding each variant were transfected into HyPer-HeLa cells, which stably contained a pHyPer-cyto vector that encoded the HyPer sensor. A histidine western blot showed visible bands for both the

WT and mutant expressed inside the cell (Figure 6.5), although the band for WT is much stronger than the mutants.

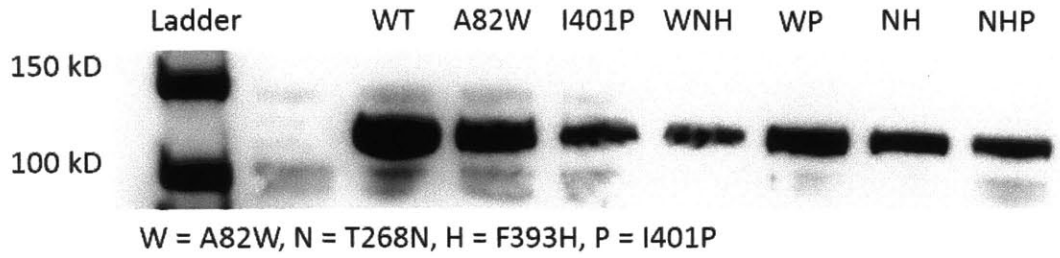

Figure 6.5: Western blot of P450 BM3 variants encoded in a pTRE3G-IRES vector and expressed in HyPer-HeLa cells. The unlabeled lane was sourced from cells transfected with an empty vector. NH = T268N/F393H, WNH = A82W/T268N/F393H, WP = A82W/I401P, NHP = T268N/F393H/I401P.

However, the western blot only promised the presence of the protein, not whether it is functional or correctly folded. We performed a spectrophotometric analysis of oxidized enzyme and carbon monoxide binding to determine whether the protein is functional. A cell lysate consisted of HeLa cells expressing P450 BM3 was incubated with carbon monoxide, with function P450s showing a spectra shift at an absorbance of 450nm upon incubation with CO (sample figure in Appendix). only WT was detectable by a CO binding assay, indicating that the variants suffered severe decreases in their expression of active enzyme relative to their general expression levels and suggesting disruptions in their protein folds. WT was detected at an active expression level of 6.7 x 10^6 molecules/cell. Coupled with its H_2O_2 production rate, it falls short of the threshold for overcoming the antioxidants inside the cell. For the variants, we are unable to determine the expression level of the active protein such it was inaccessible by the CO binding assay.

Since it was still possible that the variants in this chapter might have sufficient active expression levels and H_2O_2 production rates to meet the criteria posed in Figure 1.2, we used measured the H2O2 production in the cell lysate expressing P450s using Amplex Red horseradish peroxidase based assay (Figure 6.6). Incubation of Amplex Red, a chemical probe that is oxidized to resorfin

upon oxidation by H2O2, with the cell lysates expressing P450, showed many that many P450 variants, including the WT, were producing H2O2 well above the empty vector control. This rise in signal was not due artifacts such as P450 protein, cell lysate or buffer interacting with Amplex Red (Appendix).

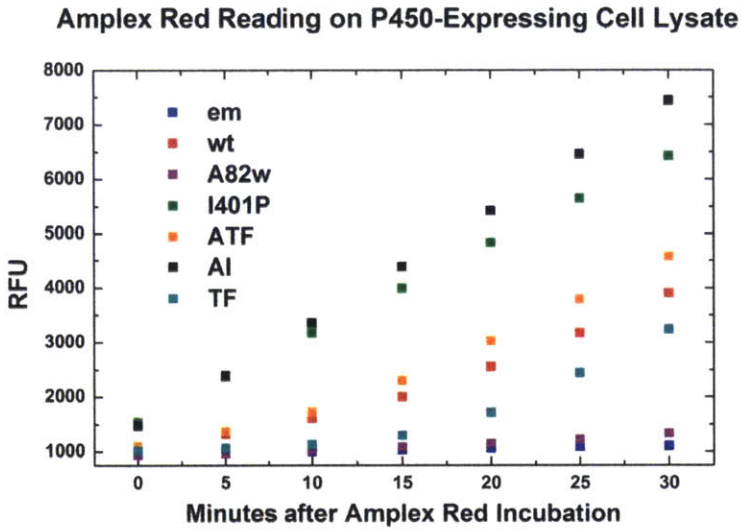

Figure 6.6: Amplex red reading on cell lysates expressing different variants of P450-BM3. HeLa cells expressing P450-BM3 were lysed in 200 µL of 1% triton buffer. 50µL samples of the lysate were incubated with 50 µL of Amplex Red/Hrp reagent and fluorescence was recorded on the plate reader at ex. 490 nm emission. 545 nm for a period of 30 minutes.

While this initial result was promising, a definitive test would be to use these enzymes in a live cell setting. We developed a stable HeLa cell line expressing HyPer, then introduced the P450-BM3 to measure their H2O2 production (Figure 6.7). However, the signal was not significantly different between the empty vector and all P450 BM3 variants expressed. In an effort to amplify the signal, a mCherry protein was introduced at the second site of the expression vector as a fluorescence tag for P450. Cells expressing both the HyPer sensor and the P450 protein were sorted and collected on the flow cytometer. The sorting induced unwanted stress and artificial elevation of HyPer signal on the HeLa cells (Appendix); these elevations in signals went away

within 10 minutes of sorting completion and there was no elevation in HyPer signal in any of the cell samples expressing P450.

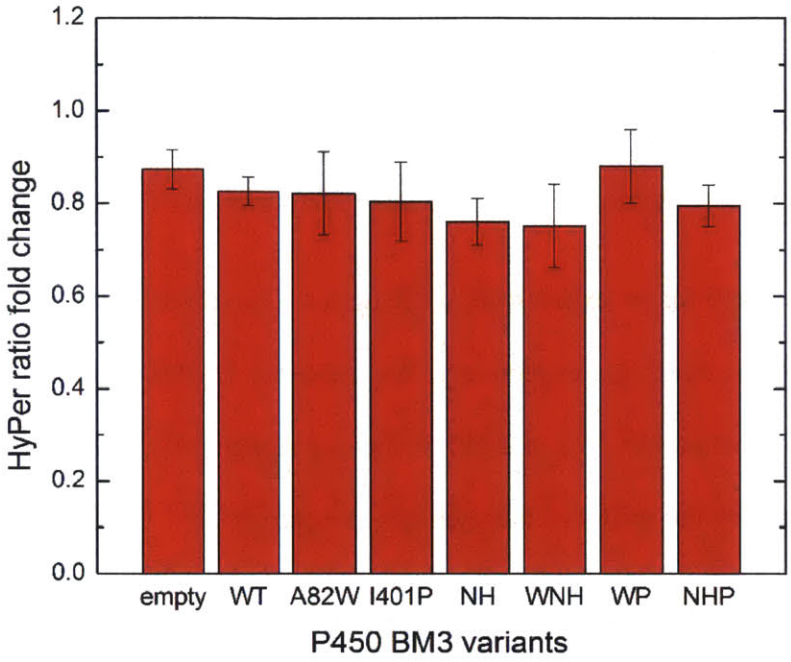

Figure 6.7: Signal of HyPer when co-expressed with P450 BM3 variants in HyPer-HeLa cells. Signal measured 4 days after transfection was normalized by signal at the time of transfection; signals were measured using microscopy and adherent cells. NH = T268N/F393H, WNH = A82W/T268N/F393H, WP = A82W/I401P, NHP = T268N/F393H/I401P.

6.3.4 Optimization for the whole-cell H2O2 screen

We first evaluated two schemes for co-expression by determining the effects of placing the gene for HyPer in the second cloning site of pRSFDuet-1 with P450 BM3 (either WT or I401P) in the first versus placing the genes in two separate vectors, P450 BM3 (either WT or I401P) in pRSFDuet-1 and HyPer in pQE30 (Appendix). While both the enzyme and HyPer are expressed when encoded in the same vector, HyPer's expression level appeared to dramatically increase by more than two-fold when co-expressed with I401P versus WT. In contrast, HyPer's expression levels were nearly identical when co-expressed with I401P and WT with HyPer encoded in the pQE30 vector. Because HyPer's expression level was better controlled when co-expressed from

a separate plasmid with a different origin of replication, we implemented the screen with the two proteins expressed from two separate plasmids rather than from a single plasmid. We also devised a new electrocompetent screening strain by transforming only HyPer/pQE30 into BL21 (DE3) Tuner cells. For future transformations with the pRSFDuet-1 vector, this new strain eliminated the need for co-transformation with HyPer/pQE30 and the consequent decreased transformation efficiency known to occur with co-transformation of multiple plasmids.

After choosing a scheme for co-expression, we sought to determine if WT and I401P could serve as baseline and positive controls, respectively. We measured HyPer's signal for the two samples at the end of protein expression. WT and I401P showed signals of 0.93 ± 0.02 and 1.12 ± 0.02, respectively, confirming the utility of these clones as controls.

We measured the temporal behavior of the signal after resuspension and dilution of the cells and found that the signal (F500/F420) for I401P monotonically increased and plateaued, while the signal for WT decreased and flattened, with the fold difference maximizing at ~2 hours as WT and I401P showed final signals of 0.792 ± 0.002 and 1.812 ± 0.004, respectively (Appendix). We thus measured the signal after 2 hours in all following screening experiments.

After validating the controls and determining the optimal time for measurement, we performed a side-by-side test of the controls comparing signal fold change when fluorescence measurements were performed at 3 min intervals for 2 hours as was shown in Appendix versus one fluorescence measurement after a 2 hour incubation period. In the former case, WT and I401P had signals of 0.96 ± 0.05 and 1.81 ± 0.05, respectively; in the latter case, WT and I401P had signals of 0.85 ± 0.02 and 1.12 ± 0.08, respectively. Since cells analyzed using these two alternative procedures were taken from the same source, the samples measured at 3 min intervals can be directly

compared with the samples that were measured only once. The comparison shows that the former method maximizes the fold change between the baseline and positive controls.

To investigate whether the choice of buffer impacts the magnitude of the observed fold change between the baseline and positive controls, we tested the effects of buffer pH and composition by resuspending *E. coli* co-expressing HyPer and either WT P450 BM3 or the I401P variant in three different buffers: 1X PBS at pH 7.4, 1X PBS at pH 8, and 0.1 M KPi at pH 8. Previous work has established that the external buffer can induce changes in *E. coli*'s cytosolic pH [28] and it is also known that HyPer's signal is quite sensitive to pH changes in this range [25]. Although the F500/F420 values differed in each buffer as expected, the fold change between signals induced by WT and I401P remained consistently high and did not change significantly across the buffers tested (Appendix). We thus decided to use our initial choice of buffer, 1X PBS at pH 7.4, to implement the screen.

6.3.5 Producing and characterizing P450 mutants generated via high-throughput, whole cell screening method in vitro

We proceeded to engineer WT via directed evolution by performing error-prone PCR to introduce random mutations into the oxidase domain of the enzyme encoded in pRSFDuet-1 using primers described in Section 6.2. After transformation of the library into the screening strain, DNA sequence analysis of 10 randomly picked variants showed an average mutation frequency of 2.1 base pairs per P450 gene, indicating one amino acid per enzyme was changed on average. We co-expressed variants with HyPer in 96-well microplates with eight wells dedicated each to WT and I401P to provide a measure of the variability expected from clones bearing the same constructs.

One round of evolution was sufficient to increase the enzyme's H_2O_2 production. We screened 400 clones and found 10 variants with higher signals than that induced by the WT control, as measured by fold change (appendix) and confirmed by Student's t-test ($p < 10^{-9}$). To confirm these initial hits, we used the glycerol cell stock of each to inoculate eight wells in a separate microplate and cultured and assayed these hits again (appendix). In this re-screening with multiple replicates for each hit, 9 of the 10 original hits had statistically higher final signals than that of the WT control ($p < 10^{-6}$).

To confirm whether the nine hits had elevated levels of H_2O_2 production, we extracted and transformed their plasmids into BL21 (DE3) Tuner cells. Each variant was expressed, purified, and assayed for leakage activity and H_2O_2 production (Appendix). All nine had leak rates higher than that of WT to varying extents, from 2- to 30-fold greater ($p < 0.05$). The proportion of product comprised by H_2O_2 was measured using an HRP/ABTS assay. When the proportion was multiplied by leak rate to determine the H_2O_2 production rate, three of the hits – P142S/V216A, W90L/R255C/T427I, and D222N/E247D – had higher production rates than WT with $p < 0.05$, and two others – T152A/A184V/T269A/R296Q and L249H – had higher rates with $p < 0.1$, demonstrating the screen's efficacy in finding novel variants with higher H_2O_2 production than the parent enzyme. Overall, 5 of the original 10 hits had higher H_2O_2 production, indicating a percentage of confirmed hits of 50%.

After verifying the efficacy of the screen, we screened an additional 640 clones from the library and found 18 more hits with signals significantly higher than that of the WT control. We chose the variants with the 11 highest signals, including those previously screened in the first 400 clones, and expressed them side-by-side along with WT in a 96-well microplate, with eight wells dedicated to each variant. After expression, we lysed the cells with lysozyme and performed a

CO binding assay to measure the amount of active P450 in the lysate (Appendix). Simultaneously, we also measured the leak rate of the lysate by adding NADPH and following absorbance at 340 nm over time (Figure 6.8). Although measurement in lysate is obscured by the effects of the lysis procedure and other intracellular contents, we chose this method for an efficient side-by-side comparison of variants, to avoid having to purify them separately for *in vitro* assays.

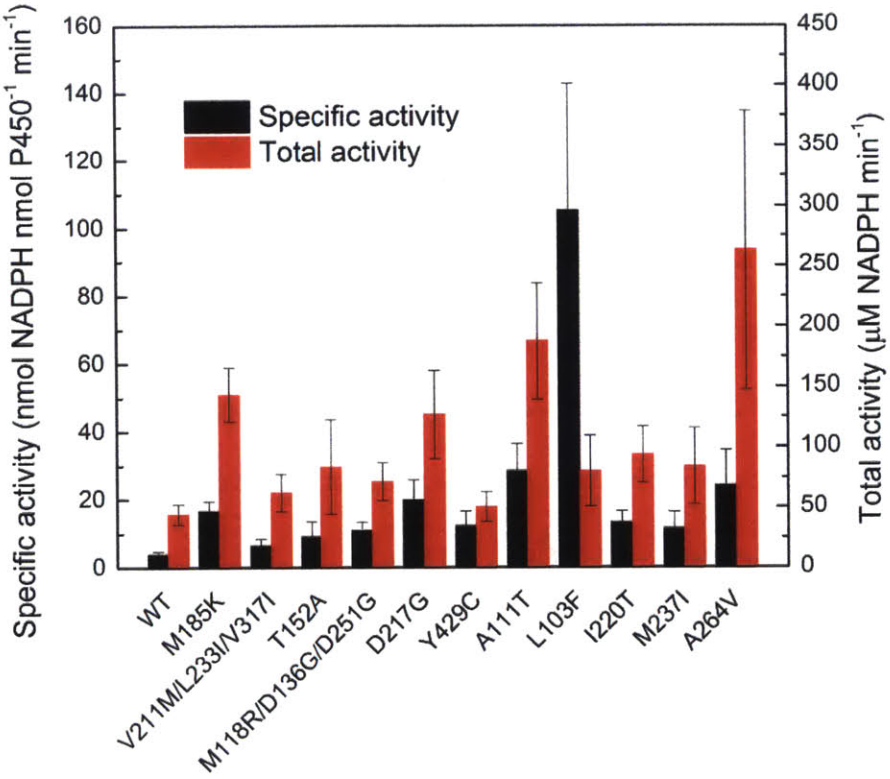

Figure 6.8: Specific and total leak rates of P450 BM3 variants measured in lysate and expressed in a 96-well microplate. Cultures were grown on three different days, with 8 wells dedicated to each variant each day (n = 24). Total leak rate was calculated without taking into consideration the concentration of active P450 as measured by a CO binding assay, specific leak rate was calculated by normalizing the total leak rate by the concentration of active P450. Error bars represent a single standard deviation.

Although the data contains wide variability likely due to the measurements having been performed in lysate, they still offer insights into the variants as they compare with each other in terms of bacterial expression and leakage. All variants experienced decreased expression relative

to WT, though several – namely, M185K, V211M/L23I/V317I, T152A, A111T, I220T, and A264V – had expressions that could not be statistically distinguished from that of WT ($p > 0.05$). We also found that several variants – M185K, D217G, A111T, I220T, and A264V – had both statistically higher total and specific leak rates ($p < 0.05$).

6.3.6 Expressing and characterizing P450 mutants generated via high-throughput, whole cell screening method in mammalian cells

We took the set of variants that had expression statistically comparable with that of WT and total and specific leakage statistically higher than that of WT – M185K, A111T, I220T, and A264V – and introduced each by site-directed mutagenesis into the WT gene codon optimized for mammalian expression and encoded in the pTRE3G-IRES vector. Indeed, we found that each variant expressed to levels detectable by a CO binding assay, something not achieved by the variants in Chapter 3. M185K, A111T, I220T, and A264V had expression levels of 3.3, 6.5, 5.5, and 3 x 10^6 molecules/cell, respectively; for comparison, WT expression amounted to 9.1 x 10^6 molecules/cell. It is important to consider, however, that the plasmids were transfected into HEK293 cells rather than HeLa cells, for improvement of expression level of the protein.

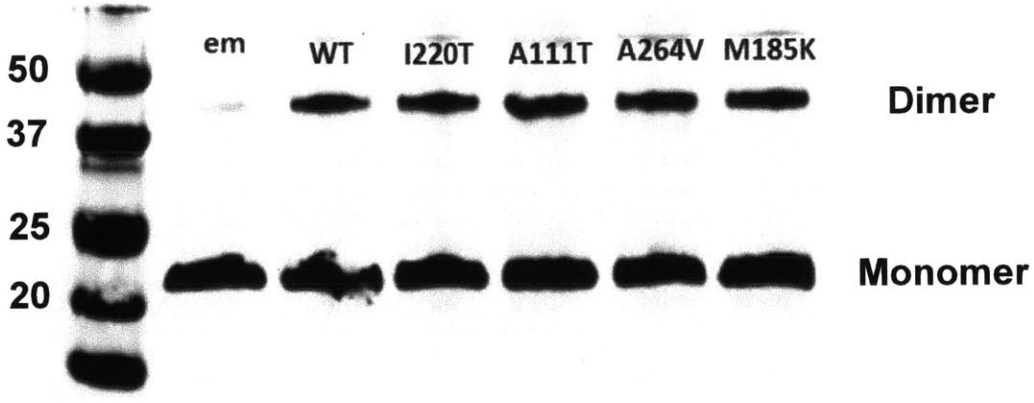

Figure 6.9: Detection of peroxiredoxin-2 oxidation in HeK cells expressing P450 variants obtained from a whole-cell screen. Mutants of P450 that are potential candidates for expressing high levels of H2O2 were found using a whole cell screen. The

candidates were expressed inside HeK cells for a period of 4 days using the inducible vector. At end of 4 days, the cells were lysed and an antibody against peroxiredoxin-2 was used.

To improve our chances for detection of H2O2 elevation, we decided to employ a detection method more sensitive than HyPer, discussed in Chapter 4 and 5. Peroxiredoxin II (Prx-2) is an antioxidant found in the mammalian cytoplasm at hundreds of micromolar abundance and reacts specifically with H_2O_2 at rate constants greater than 10^7 $M^{-1}s^{-1}$.[27,29–31] Thus its reaction with peroxide is much more sensitive than that of HyPer. When Prx-2 comes in contact with H_2O_2, a cysteine on the Prx-2 is oxidized to –SOH, which can then form a disulfide bond with a nearby thiol group of another Prx-2 to form a dimer [32]. Elevated presence of this dimer-form of Prx-2 is indirect evidence of H_2O_2-derived oxidative stress. When we immunoblot for the presence the dimeric Prx-2, we found that the expression of P450 in general causes an elevation in H2O2 level. However, there was no difference in elevation between the WT protein and the mutant candidates from the whole cell screen.

6.4 Discussion and Conclusion

In this chapter, we presented two different protein engineering approaches for discovering P450 mutants that exhibit higher generation of ROS, specifically H2O2. We then characterized the mutants both *in vitro* and *in vivo* to determine whether they will be good candidates to use as an endogenous ROS generator in mammalian cells. The combination of mutations previously found to enhance leakage in P450 BM3 resulted in increased leakage, and consequently, H_2O_2 production *in vitro*. However, these mutations were also associated with sharp decreases in bacterial expression. These decreases may be linked to the lack of active expression observed in mammalian cells, which hinder the ability of P450 BM3 and related variants to be powerful enough generator to overcome antioxidants inside the cell. We were therefore surprised to find

increase in Amplex Red signal in response to cell lysate expressing P450 for both WT and the mutants, indicating that there were correctly folded and functionally active mutants expressed inside the cells taking NADPH from the cell lysate and converting it to H2O2. However, when we measured H2O2 elevation via HyPer in a live cell, we were unable to detect any changes between cells expressing the empty vector and the cells expressing the library of P450s.

Two items might contribute the discrepancy in results between the Amplex Red measurement and the live cell measurement. First of all, it is well-known that cell lysis induce oxidation of antioxidants, especially peroxiredoxins, a powerful scavenger that consumes 99% of H2O2 generated.[8,33] The lowered antioxidant defenses in cell lysate may contribute to the ability for the P450 expressed to overcome the defenses and cause a rise in H2O2 elevation. In this case, doing measurements on the cell lysate does not yield information about whether the generator will be useful for studying biological phenotype, which requires live cells. Another possibility, one that has been highlighted in previous chapters, is that HyPer is simply not sensitive enough for detection of low level H2O2 produced by P450s, and those low levels could still be interesting for further studies.

We must also consider that we have not fully explored P450 BM3's sequence space, as it is comprised of 1049 amino acids; there may exist variants with both sufficient H_2O_2 production and active mammalian expression to satisfy the quantitative criteria and fulfill the requirements of an ideal generator. To address all of the above points, we continued investigating P450 BM3 as a possible H_2O_2 generator by targeting it for engineering in a whole-cell screen for enzymatic H_2O_2 production, and we used a new method of detection H2O2 increase by using a technique that is informative for live cell oxidation state and is much more sensitive than HyPer.

Our new whole-cell screen method by co-expressing P450 mutants with HyPer in live bacterial cell, and selecting for the population that has elevated signal allowed facile identification of novel P450 BM3 variants with elevated H_2O_2 production and leakage. The methodology proved advantageous in comparison with other methods for screening for H_2O_2 production because of its lack of any time-consuming lysis, purification and characterization with ABTS assay, allowing for rapid, high-throughput screening for generator candidates. Furthermore, since we are screening for H2O2 elevation rather than looking at specific activity, so both the robustness of the expression along with the catalytic kinetic parameter are being selected for. The screening generated four promising generator candidates that we tested in HeK cells. We found much higher expression of functional protein of these generator candidates than the ones from the first protein engineering approach. We also tested for H2O2 elevation in these candidates by looking for dimerization of Prx-2. Surprisingly, we found that just by expressing P450 causes an elevation of oxidative stress, as evidenced by the elevation of dimer Prx for WT protein. It is unclear whether this elevation occurs because of the stress of overexpressing a foreign protein, or if the WT P450 was actually generating H2O2 via NADPH and O_2 catalysis. Furthermore, we did not see an increase in dimerization in the mutants compared to the controls, therefore the screening effort did not yield mutants with higher endogenous ROS generation ability than the WT.

The results from our demonstrated that the whole-cell screening method might be a potential technique for discovering new ROS generators based on the NADPH and O_2 catalytic ability of the P450 enzyme to produce hydrogen peroxide and superoxide. While the candidates from the first two screening rounds were unsuccessful in generating an array of mutants with a variety of H2O2 production kinetics, the mutants found were in general more stable and expressed more

abundantly in the mammalian system. Any of these mutants can be a parent species for further rounds of directed evolution to find other, more suitable candidates. All in all, our engineering efforts with the P450-BM3 protein for generators of ROS represent an unlikely intersection of two very separate fields, and an unique application of an enzyme that has traditionally been used in relationship to traditional chemical engineering industries.

6.5 Bibliography

(1) D'Autréaux, B., and Toledano, M. B. (2007) ROS as signalling molecules: mechanisms that generate specificity in ROS homeostasis. *Nat. Rev. Mol. Cell Biol. 8*, 813–24.

(2) Sies, H. (2014) Role of metabolic H2O2 generation: redox signaling and oxidative stress. *J. Biol. Chem. 289*, 8735–41.

(3) Gough, D. R., and Cotter, T. G. (2011) Hydrogen peroxide: a Jekyll and Hyde signalling molecule. *Cell Death Dis. 2*, e213.

(4) Mueller, S., Millonig, G., and Waite, G. N. (2009) The GOX/CAT system: a novel enzymatic method to independently control hydrogen peroxide and hypoxia in cell culture. *Adv. Med. Sci. 54*, 121–35.

(5) Antunes, F., and Cadenas, E. (2001) Cellular titration of apoptosis with steady state concentrations of H(2)O(2): submicromolar levels of H(2)O(2) induce apoptosis through Fenton chemistry independent of the cellular thiol state. *Free Radic. Biol. Med. 30*, 1008–18.

(6) Son, Y.-O., Jang, Y.-S., Heo, J.-S., Chung, W.-T., Choi, K.-C., and Lee, J.-C. (2009) Apoptosis-inducing factor plays a critical role in caspase-independent, pyknotic cell death in hydrogen peroxide-exposed cells. *Apoptosis 14*, 796–808.

(7) Barbouti, A., Amorgianiotis, C., Kolettas, E., Kanavaros, P., and Galaris, D. (2007) Hydrogen peroxide inhibits caspase-dependent apoptosis by inactivating procaspase-9 in an iron-dependent manner. *Free Radic. Biol. Med. 43*, 1377–87.

(8) Sobotta, M. C., Barata, A. G., Schmidt, U., Mueller, S., Millonig, G., and Dick, T. P. (2013) Exposing cells to H2O2: a quantitative comparison between continuous low-dose and one-time high-dose treatments. *Free Radic. Biol. Med. 60*, 325–35.

(9) Van Stroe-Biezen, S. A. M., Janssen, A. P. M., and Janssen, L. J. J. (1994) A kinetic study of soluble glucose oxidase using a rotating-disc electrode. *Bioelectrochemistry Bioenerg. 33*, 55–60.

(10) Gao, L., and Mann, G. E. (2009) Vascular NAD(P)H oxidase activation in diabetes: a double-edged sword in redox signalling. *Cardiovasc. Res. 82*, 9–20.

(11) Aitken, R., Buckinham, D., and Harkiss, D. (1993) Use of a xanthine-oxidase free-radical generating-system to investigate the cytotoxic effects of reactive oxygen species on human spermatozoa. *J. Reprod. Fertil. 97*, 441–450.

(12) Kelley, E. E., Khoo, N. K. H., Hundley, N. J., Malik, U. Z., Freeman, B. A., and Tarpey, M. M. (2010) Hydrogen peroxide is the major oxidant product of xanthine oxidase. *Free Radic. Biol. Med. 48*, 493–8.

(13) Haskew-Layton, R. E., Payappilly, J. B., Smirnova, N. A., Ma, T. C., Chan, K. K., Murphy, T. H., Guo, H., Langley, B., Sultana, R., Butterfield, D. A., Santagata, S., Alldred, M. J., Gazaryan, I. G., Bell, G. W., Ginsberg, S. D., and Ratan, R. R. (2010) Controlled enzymatic production of astrocytic hydrogen peroxide protects neurons from oxidative stress via an Nrf2-independent pathway. *Proc. Natl. Acad. Sci. U. S. A. 107*, 17385–90.

(14) Matlashov, M. E., Belousov, V. V, and Enikolopov, G. (2014) How much H(2)O(2) is produced by recombinant D-amino acid oxidase in mammalian cells? *Antioxid. Redox Signal. 20*, 1039–44.

(15) Stegman, L. D., Zheng, H., Neal, E. R., Ben-Yoseph, O., Pollegioni, L., Pilone, M. S., and Ross, B. D. (1998) Induction of cytotoxic oxidative stress by D-alanine in brain tumor cells expressing Rhodotorula gracilis D-amino acid oxidase: a cancer gene therapy strategy. *Hum. Gene Ther. 9*, 185–93.

(16) Noble, M. A., Miles, C. S., Chapman, S. K., Lysek, D. A., MacKay, A. C., Reid, G. A., Hanzlik, R. P., and Munro, A. W. (1999) Roles of key active-site residues in flavocytochrome P450 BM3. *Biochem. J. 339*, 371–9.

(17) Munro, A. W., Leys, D. G., McLean, K. J., Marshall, K. R., Ost, T. W. B., Daff, S., Miles, C. S., Chapman, S. K., Lysek, D. A., Moser, C. C., Page, C. C., and Dutton, P. L. (2002) P450 BM3: the very model of a modern flavocytochrome. *Trends Biochem. Sci. 27*, 250–7.

(18) Brewer, C., and Peterson, J. (1988) Single turnover kinetics of the reaction between oxycytochrome P-450cam and reduced putidaredoxin. *J. Biol. Chem. 263*, 791–798.

(19) Powell, P. K., Wolf, I., Jin, R., and Lasker, J. M. (1998) Metabolism of Arachidonic Acid to 20-Hydroxy-5,8,11,14-eicosatetraenoic Acid by P450 Enzymes in Human Liver: Involvement of CYP4F2 and CYP4A11. *J. Pharmacol. Exp. Ther. 285*, 1327–1336.

(20) Tsyrlov, I. B., Goldfarb, I. S., and Gelboin, H. V. (1993) Enzyme-kinetic and immunochemical characteristics of mouse cDNA-expressed, microsomal, and purified CYP1A1 and CYP1A2. *Arch. Biochem. Biophys. 307*, 259–66.

(21) Jung, C. (2007) Leakage in Cytochrome P450 Reactions in relation to Protein Structural Properties, in *The Ubiquitous Roles of Cytochrome P450 Proteins* (Sigel, A., Sigel, H., and Sigel, R. K. O., Eds.), pp 187–234. John Wiley & Sons Ltd, Chichester, England.

(22) Clark, J. P., Miles, C. S., Mowat, C. G., Walkinshaw, M. D., Reid, G. A., Daff, S. N., and Chapman, S. K. (2006) The role of Thr268 and Phe393 in cytochrome P450 BM3. *J. Inorg. Biochem. 100*, 1075–90.

(23) Whitehouse, C. J. C., Bell, S. G., Yang, W., Yorke, J. A., Blanford, C. F., Strong, A. J. F., Morse, E. J., Bartlam, M., Rao, Z., and Wong, L.-L. (2009) A highly active single-mutation variant of P450BM3 (CYP102A1). *Chembiochem 10*, 1654–6.

(24) Huang, W.-C., Westlake, A. C. G., Maréchal, J.-D., Joyce, M. G., Moody, P. C. E., and Roberts, G. C. K. (2007) Filling a hole in cytochrome P450 BM3 improves substrate binding and catalytic efficiency. *J. Mol. Biol. 373*, 633–51.

(25) Belousov, V. V, Fradkov, A. F., Lukyanov, K. A., Staroverov, D. B., Shakhbazov, K. S., Terskikh, A. V, and Lukyanov, S. (2006) Genetically encoded fluorescent indicator for intracellular hydrogen peroxide. *Nat. Methods 3*, 281–6.

(26) Adimora, N. J., Jones, D. P., and Kemp, M. L. (2010) A Model of Redox Kinetics Implicates the Thiol Proteome in Cellular Hydrogen Peroxide Responses. *Antioxid. Redox Signal. 13*, 731–743.

(27) Huang, B. K., and Sikes, H. D. (2014) Quantifying intracellular hydrogen peroxide perturbations in terms of concentration. *Redox Biol. 2*, 955–962.

(28) Wilks, J. C., and Slonczewski, J. L. (2007) pH of the cytoplasm and periplasm of Escherichia coli: rapid measurement by green fluorescent protein fluorimetry. *J. Bacteriol. 189*, 5601–7.

(29) Low, F. M., Hampton, M. B., Peskin, A. V, and Winterbourn, C. C. (2007) Peroxiredoxin 2 functions as a noncatalytic scavenger of low-level hydrogen peroxide in the erythrocyte. *Blood 109*, 2611–7.

(30) Marinho, H. S., Real, C., Cyrne, L., Soares, H., and Antunes, F. (2014) Hydrogen peroxide sensing, signaling and regulation of transcription factors. *Redox Biol. 2*, 535–562.

(31) Manta, B., Hugo, M., Ortiz, C., Ferrer-Sueta, G., Trujillo, M., and Denicola, A. (2009) The peroxidase and peroxynitrite reductase activity of human erythrocyte peroxiredoxin 2. *Arch. Biochem. Biophys. 484*, 146–54.

(32) Wood, Z. a, Schröder, E., Robin Harris, J., and Poole, L. B. (2003) Structure, mechanism and regulation of peroxiredoxins. *Trends Biochem. Sci. 28*, 32–40.

(33) Winterbourn, C. C. (2008) Reconciling the chemistry and biology of reactive oxygen species. *Nat. Chem. Biol. 4*, 278–86.

6.6 Appendix

Example protein purification result of WT and NH, as done on SDS-page gel comassie staining.

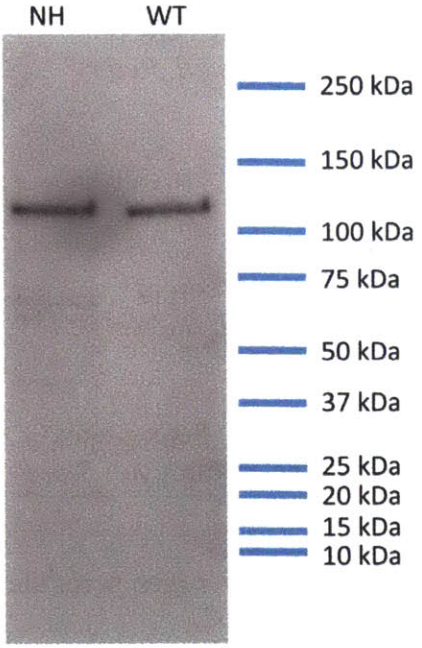

Example of absorption spectra for CO binding assay on the P450-BM3 proteins. This spectra example is from bacterial lysates expressing P450

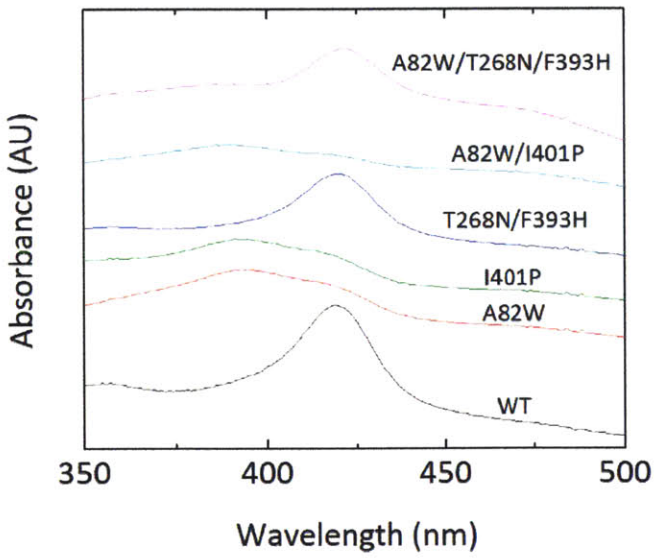

Controls for the Amplex red experiment involving cell lysates expressing P450-BM3 variants. The buffer, cell lysate and P450 protein does not interfere with the Amplex Red signal.

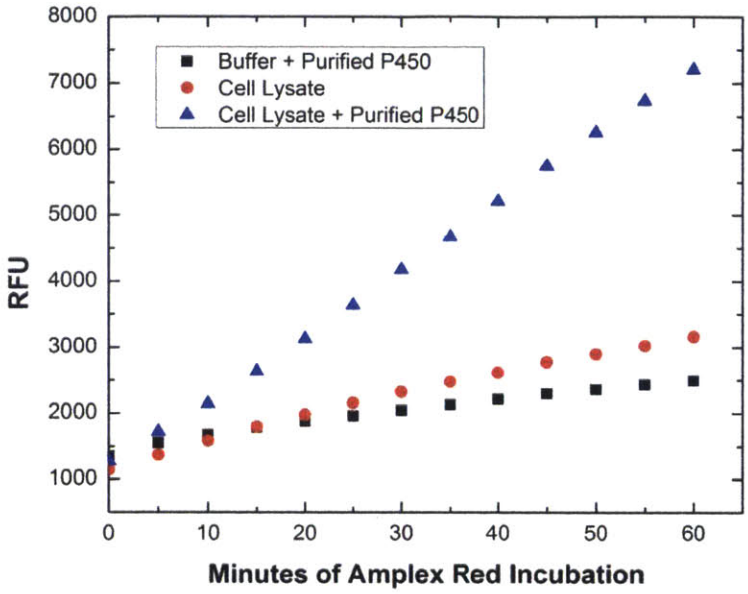

Enriching population of HeLa cells co-expressing P450 and HyPer via flow cytometry. The sorted cells double positive for mcherry and GFP were read immediately on the fluorescent plate reader

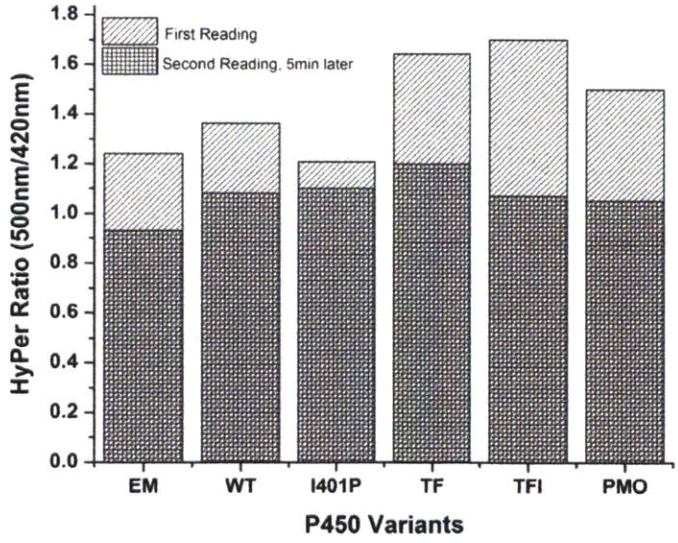

Fluorescence spectra of HyPer co-expressed with WT (black) or the I401P variant (red), encoded in either the second cloning site of pRSFDuet-1 (solid) or pQE30 (dashed). In all cases, WT or I401P was encoded in the first cloning site of pRSFDuet-1.

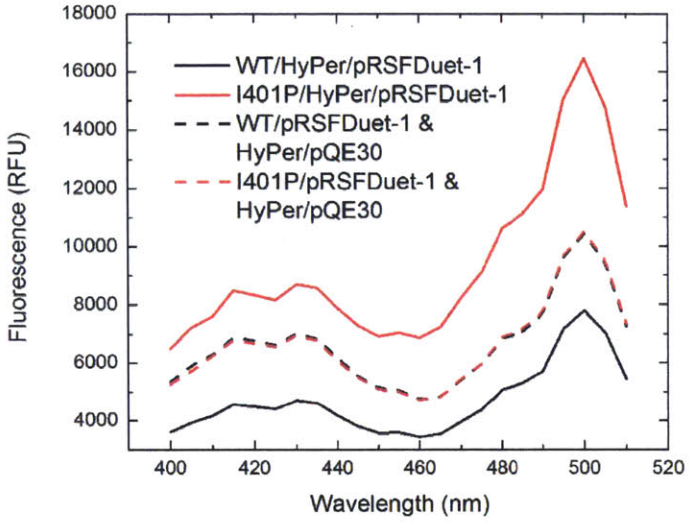

Temporal behavior of HyPer's signal (F500/F420) measured from intact *E. coli* cells co-expressing the sensor and either WT P450 BM3 or the I401P variant

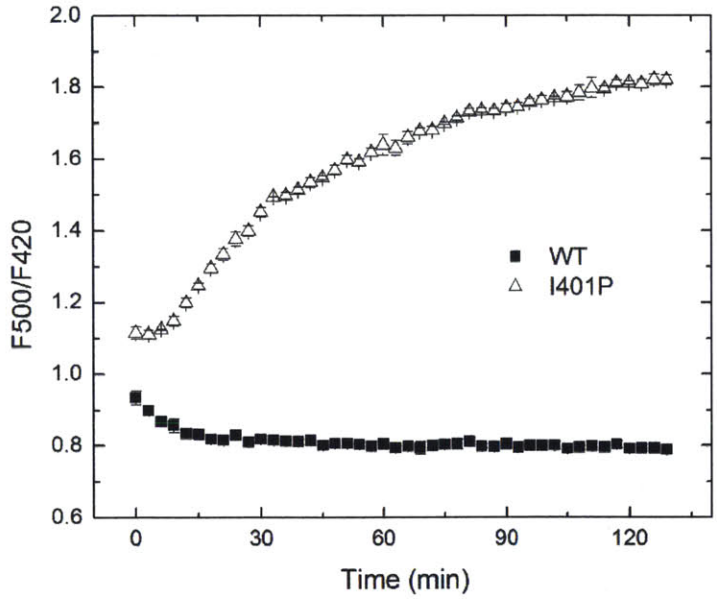

HyPer's signal when co-expressed with WT or the I401P variant after resuspension in three different buffers: 1X PBS at pH 7.4, 1X PBS at pH 8, and 0.1 M KPi at pH 8.

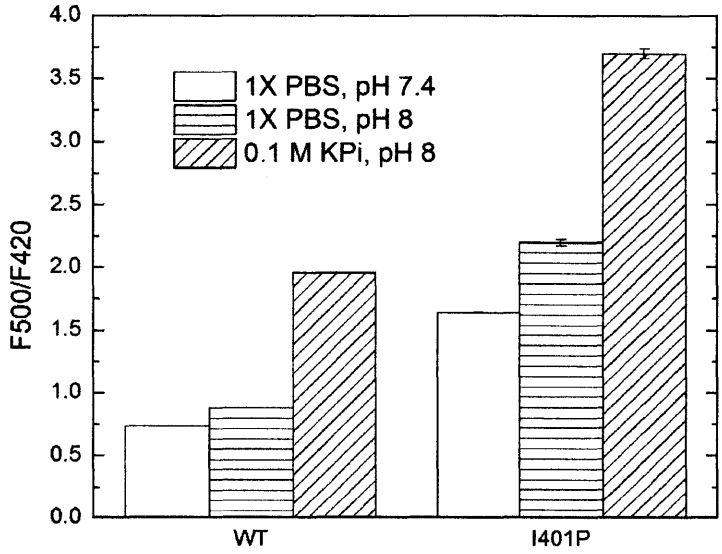

Upon co-expression with a library of P450 BM3 variants, HyPer's fluorescent signal from intact *E. coli* cells revealed several putative H_2O_2 generators in an initial screen (n = 1) and in re-screening (n = 8).

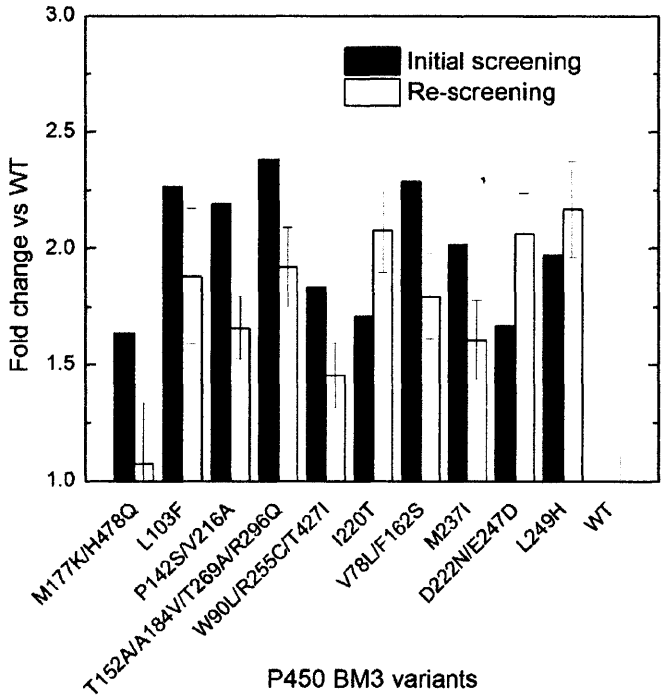

In vitro evaluation of putative H_2O_2 generators identified using the HyPer-based screen of intact cells. Measurements were performed using purified enzymes and well-established analytical methods. Leak rates were determined by monitoring absorbance at 340 nm as a function of time to measure NADPH oxidation by each variant. The percentage of leakage product comprised by H_2O_2 for each variant was measured using an HRP/ABTS assay.

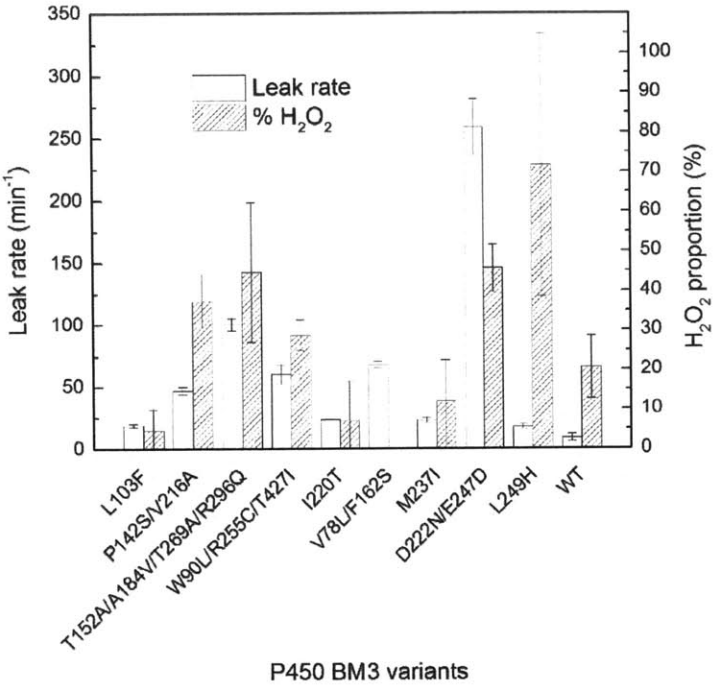

Expression levels of P450 BM3 variants measured in lysate and expressed in a 96-well microplate.

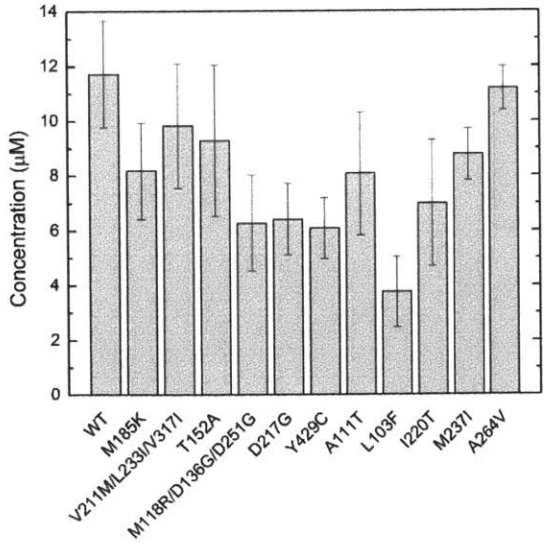

Chapter 7: Conclusions and Outlook

7.1 Summary of thesis

This thesis has developed an analysis of reactive oxidative species and its effects on cell toxicity, with applications for designing better ROS-based chemotherapeutics. To achieve this goal, we demonstrated how to use and interpret signals from genetically encoded sensors for H_2O_2 in a quantitative manner. Then, using these sensors in combination with H_2O_2 generators, we were able to mimic and measure physiological H_2O_2 generation in a spatially and kinetically controlled manner for our phenotypic and mechanistic investigations. Finally, in an ongoing effort to provide alternative ROS generators that can produce other species in a simplified manner, we explored the use of P450-BM3 enzyme by engineering them to generate ROS with regulated species output.

Hydrogen peroxide is an often studied molecule since its longer lifetime allows it to selectively interact with intracellular biological targets to confer the desired phenotypic outcome. While many studies have suggested the importance of intracellular concentration and localization to predicting the downstream effects of these molecules, these studies are often done under non-physiological conditions, so there are little consensus on on what those concentrations are supposed to be. The first step to a better quantitative analysis of H_2O_2 is to thoroughly understand how to use intracellular sensors for these molecules. Genetically encoded protein sensors such as HyPer have been in existence for about 10 years now, but little has been done to really interpret the signal from these sensors in a meaningful way. We developed a method of converting the fluorescence ratiometric outputs from these sensors into intracellular peroxide

concentrations. We did so by titrating known external addition of H_2O_2 against sensor signal, then measuring the gradient across the plasmid membrane of the cell to get the corresponding internal concentration. This way, the sensor output is now indirectly calibrated with internal concentrations. Using this calibration method, we can look at both data from existing literature, or perform our own experimental analysis to correlate signaling activation or phenotypic response with intracellular H_2O_2 levels.

We also explored the caveats of using these protein sensors in response to H_2O_2 elevation. One interesting phenomena we frequently observed was the large heterogeneity in cellular response to an identical H_2O_2 stimulation. We found that 70% of the heterogeneity in HyPer response was due to the expression level differences of the sensor inside the cell. This was a surprising result, since one of the advantages touted of the sensor was that by looking at two spectra features changes instead one, the ratiometric output from the sensor controls for variability in expression level. Using a kinetic model, we looked at the interplay of H_2O_2, sensor and antioxidant network in H_2O_2 scavenging, and the evolution of sensor oxidative states over time. The model predicted the same correlation between expression level and HyPer signal response, and showed that this was due to the slow reduction kinetics of HyPer, leaving more and more kinetically trapped oxidized form of the sensor as the expression level increases. We then used these sensors in conjunction with continuous generators of H_2O_2 to explore the interesting kinetic features of HyPer ratio over time. We found that using the probe beyond the maximum possible signal, or when cells are undergoing apoptosis, causes the output reading to become unreliable.

With a better understanding of how to use H_2O_2 sensors and generators, we conducted a systematic study of how localization and concentration of H_2O_2 generation affects cell toxicity. We discovered that the traditional view of intracellular concentration predicting H_2O_2 toxicity

was too simplified. Two toxicity thresholds exist for H_2O_2-mediated apoptosis: a total cumulative amount, defined by concentration x time is needed, and a certain concentration level has to be achieved for the onset of apoptosis. Furthermore, generating H_2O_2 outside the cell was much less toxic than generating H_2O_2 inside the cell, even when there were comparative rise in intracellular concentration, highlighting the importance of localization to specificity of phenotypic response. Finally, we showed that HyPer was insufficient if we wanted to study phenotypic effects of low, chronic oxidative stress, since these concentrations, while still providing interesting effects, were below the detection limit of the sensor.

We applied these tools to investigating the mechanism of ROS-generating chemotherapeutics PEITC and Piperlongumine. Previous studies suggest that the depletion of glutathione was central the toxicity mechanism of these compounds, inducing H_2O_2 elevation and subsequent apoptosis. We found instead that the depletion of glutathione was unimportant to the toxicity mechanism of the drugs and the amount of oxidative stress generated by these compounds was not enough to induce significant toxicity by itself. In the case of piperlongumine, there was a synergy between oxidative stress generated and the chemical compound that caused irreversible protein oxidation and subsequent cell death. We also used NRF-2 mouse models to understand chemo-resistance certain tumor cell lines to these drugs. The antioxidant protective function of elevated NRF-2 via KEAP-1 was important for conferring chemo-resistance to piperlongumine.

Finally, we explored the use of P450-BM3, an enzyme that can generate superoxide and hydrogen peroxide through a reaction that requires only NADPH and oxygen, termed leakage. While this leakage reaction is slow in wild-type P450-BM3 proteins, it can be engineered to have much higher catalytic rates. We demonstrate through various protein engineering approaches that we can create P450-BM3 proteins with higher catalytic leak rates, and generation of H_2O_2. We

were able to express correctly folded, active enzymes inside mammalian cells that utilize intracellular NADPH and oxygen to produce H_2O_2. Ongoing efforts involve finding examples of P450 mutants that can generate detectable levels of H_2O_2 in live mammalian cells and creating a library of mutants with different kinetic and H_2O_2 to superoxide ratios.

7.2 Outlook

This thesis highlights the importance of a quantitative understanding of ROS-mediated phenotypic effects. While many chemotherapeutics were thought to kill tumor cells by inducing excessive oxidative stress, our analysis using a sensor to measure, and a generator to mimic the ROS generation showed that the oxidative stress alone was not enough to induce toxicity in tumor cells. This might account for why many high-throughput screenings to find more of these ROS-based chemotherapeutics are failing in the recent years. To improve this screening effort, we would need information on the quantity, duration and level of ROS needed to actually see the desired effect. These studies can be done by employing the sensor and generator system, along with our analysis process to establish design criteria for selective tumor toxicity. Secondly, our experience working with these ROS tools allowed us to develop a deeper understanding of how to use genetically encoded peroxide sensors in a quantitative manner and to appreciate the nuances of using the probe. These findings will be important for future studies involve use of these sensors as researchers are more informed of the caveats, and are able to extract more meaningful concentration information from the signal output.

The beauty of using genetically encoded sensors and generators is that they can be localized to subcellular compartments using targeting sequences. It is becoming more realized that these sub-cellular localizations of ROS generation can be vastly important in driving distinct, specific

responses. While our thesis primarily deals with cytoplasmic generation of ROS, these tools can be easily adapted to studies in the mitochondria, peroxisome and we have even done some work in the centrosome that were not included as part of this thesis work.

Our thesis findings can also enable future technology development for better H_2O_2 sensors. We've demonstrated many times that we can detect H_2O_2 elevation below the detection limit of HyPer using cytoplasmic peroxide oxidation. Furthermore, we've found that the levels detectable by Prx-2 can have significant and interesting phenotypic effects. Therefore, creating a H_2O_2 sensor using peroxiredoxin as the detection agent is a worthwhile investment. Efforts utilizing the disulfide formation that occurs during peroxiredoxin oxidation (ie FRET) can be potential avenue for linking oxidation with detectable response.

Finally, while many studies on ROS have been focused on H_2O_2 due to their stability, H_2O_2 itself does not react with relevant biological proteins, lipids and DNAs directly, but through secondary species or antioxidants. Also, very little has been done to understand the impact of superoxide generation, which can lead to nitric oxide species. It will be interesting to explore kinetically and spatially the entire ROS network, understanding the conversion between all the species and their respective lifetimes inside the cell. These modeling analyses will be interesting for understanding which species are most important for conveying the biological effects. We can also being to explore the interplay between ROS and RNS networks through these kinetic models to better understanding the impact of the full spectrum of reactive species.